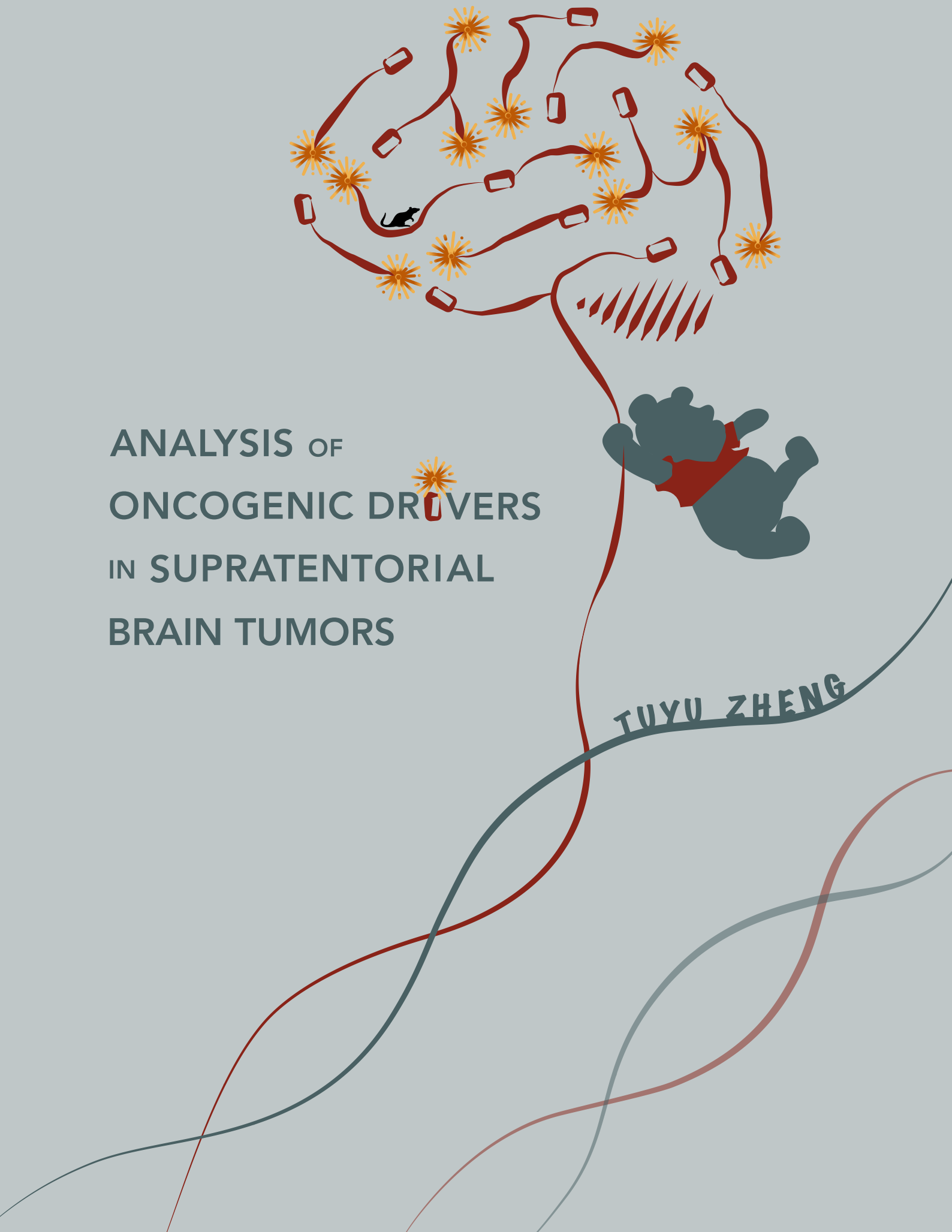

ANALYSIS OF ONCOGENIC DRIVERS IN SUPRATENTORIAL BRAIN TUMORS

TUYU ZHENG

Dissertation

submitted to the

Combined Faculty of Natural Sciences and Mathematics

of the Ruperto Carola University Heidelberg, Germany

for the degree of

Doctor of Natural Sciences

Presented by

M.Sc. & M.Eng. Tuyu Zheng 鄭途昱

Born in: Shanghai, China

Oral examination: May 8th 2023

Analysis of Oncogenic Drivers in Supratentorial Brain Tumors

Referees:

Prof. Dr. Peter Angel

Dr. Hai-Kun Liu

Declaration

This thesis is composed of my original work, and contains no material written by another person except where due reference has been made in the text. I have clearly stated the contribution by others who jointly authored works that I have included in my thesis. This was confirmed by the plagiarism checker iThenticate[1].

Section 1.4.2, the results and discussion of Chapter 2 are partially adapted from the publication "Cross-species genomics reveals oncogenic dependencies in C11orf95/ZFTA fusion-positive supratentorial ependymomas" from Cancer Discovery in 2021 and the abstract submitted for the 19th International Symposium on Pediatric Neuro-Oncology Conference (ISPNO) in 2020, which were originally written by myself and co-authors (Zheng et al., 2020; Zheng et al., 2021). The summary of Chapter 4 is partially adapted from the abstract submitted for the 20th International Symposium on Pediatric Neuro-Oncology Conference (ISPNO) in 2022, which were originally written by myself and co-authors (Zheng et al., 2022).

Tuyu Zheng

[1] https://www.ithenticate.com

Abstract

Pediatric brain tumors are a leading cause of cancer mortality among children and adolescents (age 0-19) because of the paucity of effective treatment regimens. Especially for ependymoma, surgical intervention combined with focal radiotherapy is the current standard of care in routine clinical practice while this regimen very often induces irreversible damage on the developing brain and patients frequently still suffer from tumor recurrence. Thus, generating *de novo* representative tumor models to decipher the underlying molecular mechanisms of tumorigenesis is imminent and crucial to provide more precise and mechanism-of-action based treatment plans. In my thesis, I applied various techniques to create *in vivo* models for several brain tumor types and identified potential therapeutic vulnerabilities.

Chapter 2 focuses on dissecting the role of oncogenic fusion genes in *C11orf95* fusion-positive supratentorial ependymoma (ST-EPN), a type of pediatric brain tumor with poor prognosis. C11orf95 is a zinc finger protein that binds to DNA but has not yet been well characterized. I performed *in-utero* electroporation in mouse embryos and found all tested *C11orf95* fusion genes were able to drive malignant transformation in the cerebral cortex. The tumors faithfully recapitulated molecular characteristics of their human counterparts. The zinc finger domain and the fusion partners were essential for tumor formation. Cross-species genomic analyses demonstrated that C11orf95-related fusions can increase the expression of a sonic hedgehog mediator gene, *GLI2*. Targeting GLI2 with arsenic trioxide prolonged survival in mouse models, providing a basis for further preclinical studies for *C11orf95* fusion-positive tumors. Based on these findings, *C11orf95* is now officially designated as *zinc finger translocation associated* (*ZFTA*) by the HUGO Gene Nomenclature Committee. In the latest edition of the WHO classification of central nervous tumors, the group of ST-EPN with *ZFTA* fusion genes is now named as Supratentorial ependymoma, *ZFTA* fusion-positive (ST-EPN-ZFTA).

In Chapter 3, I investigated on a novel group of neuroepithelial tumors harboring *PLAGL1* fusion (NET_PLAGL1) that has been identified in 2021 only. Mouse model generation via *in-utero* electroporation unfortunately failed. However, after I had performed substantial methodological optimization, overexpression of *PLAGL1* fusion gene through a doxycycline-mediated system in human induced pluripotent stem cell-derived neural stem cells, followed by *in vivo* orthotopic transplantation successfully led to brain tumor formation in mice. This inducible *in vivo* system offers a reliable model to study NET_PLAGL1 tumors as well as a versatile tool to answer various biological questions behind brain tumorigenesis.

Array-based DNA methylation analysis to accurately classify tumors has been developed as a routine diagnostic tool for brain tumors and sarcomas. Since mouse models are the most widely used *in vivo* systems in pediatric cancer research, it is important to assess the molecular similarity across species based on the methylome. In Chapter 4, I describe the approach of generating a mouse model biobank for pediatric cancers. I collected and profiled 86 murine tumor models and 40 normal tissue controls. DNA methylation-based clustering showed that samples from the same model clustered together and the copy number alteration pattern of ependymoma and glioma (e.g TFG-MET fusion-driven) mouse models recapitulate their human counterparts. This validated biobank will serve as a beneficial resource for future developmental studies such as identifying cellular origin of the tumor and decoding the composition of tumor immune microenvironment.

Zusammenfassung

Pädiatrische Hirntumoren sind die häufigste Ursache für Krebssterblichkeit bei Kindern und Jugendlichen (0-19 Jahre), da es nur wenige wirksame Behandlungsmethoden gibt. Vor allem bei Ependymomen ist ein chirurgischer Eingriff in Kombination mit einer fokalen Strahlentherapie der derzeitige Therapiestandard, obwohl diese Behandlung sehr oft irreversible Schäden am sich entwickelnden Gehirn verursacht und die Patienten häufig immer noch unter Tumorrezidiven leiden. Daher ist die Erstellung repräsentativer Tumormodelle zur Entschlüsselung der zugrunde liegenden molekularen Mechanismen der Tumorentstehung dringend erforderlich, um präzisere und am Wirkmechanismus orientierte Behandlungskonzepte zu erstellen. In meiner Dissertation habe ich verschiedene Techniken angewandt, um *in-vivo*-Modelle für verschiedene Hirntumorarten zu erstellen und mögliche therapeutische Angriffspunkte zu identifizieren.

Kapitel 2 befasst sich mit der Untersuchung der Rolle onkogener Fusionsgene beim *C11orf95*-Fusions-positiven supratentoriellen Ependymom (ST-EPN), einem pädiatrischen Hirntumor mit schlechter Prognose. C11orf95 ist ein Zinkfingerprotein, das an die DNA bindet, aber noch nicht gut charakterisiert wurde. Ich führte *in-utero* Elektroporations-Experimente in Mausembryonen durch und stellte fest, dass alle getesteten *C11orf95*-Fusionsgene in der Lage waren, eine bösartige Transformation in der Großhirnrinde auszulösen. Die Tumore rekapitulierten die molekularen Merkmale der humanen Tumoren dieser molekularen Subgruppe. Die Zinkfinger-Domäne und die Fusionspartner waren für die Tumorbildung essentiell. Speziesübergreifende Genomanalysen zeigten, dass *C11orf95*-Fusionen die Expression eines Sonic-Hedgehog-Vermittlergens, GLI2, erhöhen können. Die gezielte Inhibition von GLI2 mit Arsentrioxid verlängerte das Überleben in Mausmodellen, was eine Grundlage für weitere präklinische Studien zu *C11orf95*-positiven Tumoren bildet. Auf der Grundlage dieser Ergebnisse wird *C11orf95* nun vom HUGO-Gen-Nomenklaturausschuss offiziell als Zinkfingertranslokations-assoziiert (ZFTA) bezeichnet. In der neuesten Ausgabe der WHO-Klassifikation von Tumoren des Zentralnervensystems (5. Edition) wird die Gruppe der ST-EPN mit ZFTA-Fusionsgenen nun als supratentorielles Ependymom, ZFTA-Fusions-positiv bezeichnet.

In Kapitel 3 untersuchte ich eine neue Gruppe von neuroepithelialen Tumoren, die eine *PLAGL1*-Fusion (NET_PLAGL1) aufweisen, die erst 2021 identifiziert wurde. Die Erzeugung von Mausmodellen mittels *in-utero*-Elektroporationstechnik schlug in diesem Fall leider fehl. Nachdem ich jedoch erhebliche methodische Optimierungen vorgenommen hatte, führte die Überexpression des *PLAGL1*-Fusionsgens durch ein Doxycyclin-vermitteltes System in aus menschlichen induzierten pluripotenten Stammzellen abgeleiteten neuralen Stammzellen und die anschließende orthotope *in-vivo*-Transplantation

erfolgreich zur Bildung von Hirntumoren in Mäusen. Dieses induzierbare *in-vivo*-System bietet ein zuverlässiges Modell zur Untersuchung von NET_PLAGL1-Tumoren sowie ein vielseitiges Instrument zur Beantwortung verschiedener biologischer Fragen der Hirntumorentstehung.

Array-basierte DNA-Methylierungsanalysen zur molekularen Tumorklassifikation wurden als diagnostisches Routineinstrument für Hirntumore und Sarkome entwickelt. Da Mausmodelle die am häufigsten verwendeten In-vivo-Systeme in der pädiatrischen Krebsforschung sind, ist es wichtig, die molekulare Ähnlichkeit zwischen verschiedenen Spezies auf der Grundlage des Methyloms zu bewerten. In Kapitel 4 beschreibe ich den Ansatz zur Erstellung einer Mausmodell-Biobank für pädiatrische Krebserkrankungen. Ich sammelte und profilierte 86 Maustumormodelle und 40 Normalgewebekontrollen. Die auf DNA-Methylierung basierende Clusterbildung zeigte, dass Tumorproben desselben Modells zusammen clustern und das Muster der Kopienzahlveränderungen von Ependymom- und Gliom- (z.B. TFG-MET-fusionsgesteuerten) Mausmodellen diejenigen in humanen Tumoren derselben Gruppe rekapituliert. Diese validierte Biobank wird als nützliche Ressource für künftige Entwicklungsstudien dienen, z. B. zur Identifizierung des zellulären Ursprungs des Tumors und zur Entschlüsselung der Zusammensetzung der immunen Mikroumgebung des Tumors.

In Loving Memory of My Dearest Grandfathers

鄭德賢 & 耿正榮

Acknowledgement

To head of department, Stefan Pfister. Thank you for having me in this amazing KiTZ family. I really appreciate that a successful person like you were approachable and humble, and your passion for science and your kind heart always inspired me. I am very grateful as well for all the constructive suggestions you gave during our meetings.

To my direct PhD supervisor, Kristian Pajtler. Thank you for providing me with the opportunity to carry out my PhD project in the lab. It is hard to find words to describe how lucky I am to have you as my supervisor. My mom always says that my straightforward character is most likely undesirable at workplace, however, it is not the case here and I feel I can be myself in front of you. Although I did not communicate with you as often as with Daisuke or Marc, every meeting we had was efficacious and triggered magical effect to motivate me. I am highly impressed by the multi-tasking skill you have, and acknowledge for the time you spent on helping me moving forward the projects. I appreciate the freedom you gave me as well as the guidance. Your enthusiasm and support made working with you the most enjoyable experience.

To my co-supervisor, Daisuke Kawauchi. Although we only spent time together for the first year of my PhD, you cannot imagine how much you influenced me on both hard and soft skills. To be honest, summer 2019 was a hard time for me with the pressure from the project and the misunderstanding between us. However, I feel extremely grateful looking back on that period because it forced me to grow up rapidly. Working with you was always at fast pace and efficient. Not only lab techniques, I learnt how to think critically as a scientist from you as well. I am deeply thankful for the continuous help with a wide range of knowledge you have, even after you left the lab.

To my co-supervisor, Marc Zuckermann. Thank you for providing guidance after Daisuke's leave. You were always very responsive and spent time for me whenever I have questions. I am also grateful for the liberty you gave me and help me become a more independent researcher.

To my thesis advisory committee: Peter Angel and Sevin Turcan. Thank you for all the discussions and constructive advice for my projects.

To my close collaborators: David Ghasemi, Konstantin Okonechnikov, Martin Sill and Stephen Mack. It was such pleasant moments to discuss about science with you. Your passion for research always amazed me and new ideas continuously came out after our meetings. I owe eternal gratitude for your hard work and dedication to our projects.

To my S2 roommates, Patricia Benites and Aylin Camgöz. I was so lucky to share time with both of you inside and outside the lab. Working until midnight, during weekends and on holidays were never boring because of you. Despite the difference in hobbies and food preference, we still organized parties together and had lots of fun. Thank you for having taken good care of me and creating such wonderful memories throughout the time.

To Chun Ho (Ken) Chan. It was such a great time sharing the office with you, chatting about food and games, life and experience, and of course science and experiments. Thank you for the prettiest yearly Christmas cards and lively conversations about anything including gossips.

To my lab sisters, Lena Kutscher, Laura Sieber and Lisa Spänig. Thank you for your kindness and everlasting mental support whenever I need.

To our best helpers, Nina Hofmann and Britta Statz. I am extraordinarily thankful for your sense of responsibility and hard work in supporting the experiments.

To all the friends and colleagues at DKFZ (past and current):

To B062 members: Kendra Maaß, Tatjana Wedig, Lukas Schmitt, Norman Mack, Benjamin Schwalm, Eric Konrath, Natalie Stumpf, Franziska Hertel, Daniel Gimenes, Agnes Finster, Julia Benzel, Sophie Henneken, Sema Hamurcu, Paulina Schad, Julia Sundheimer, Nathalie Schwarz, Tom Fischer, Clara Gade, Nike Simon, Johanna Rettenmeier, Paula Ertel, Asta Försti, Beiping Miao, Yasmeen Niazi, Alessia Cais, Marta Cook. Karla Catacora, Stefanie Volz, Jens-Martin Hübner, Anne Jenseit, Sonja Krausert, Aniello Federico, Shanzheng Wang, Felix Schmitt-Hoffner, Joudi Khal, Monika Mauermann, Marcel Kool, Pengbo Beck and Apurva Gopisetty.

To B360 members: Laura von Soosten, Kati Ernst, Michaela-Kristina Keck, Karam Al Halabi, Andrea Wittmann and David Jones.

To B430 members: Frederik Manz, Chiara Lukasch, Piyush Joshi, Jan Vaillant and Daniel Haag.

To B060/1 members: Ka Hou (Matthew) Man, Pavle Boskovic, Mona Göttmann, Tolga Lokumcu and Michael Persicke.

To our short-term but fondly remembered visitors: Mackenna Schuow, Mieke Roosen, Toma Adachi, Magdalena Radoš, Selin Özdurmus and Cornelia Gansert.

To members outside of TP3, Roland Imle, Florencia Cidre-Aranaz, Thomas Grünewald, Mirco Friedrich, Niklas Kehl, Fuwei Shang, Dominik Vonficht, Laura Dörner and Felix Sahm.

It was such a fulfilling experience having worked with all of you. I cannot list the uncountable wonderful moments we created together. Thank you for making my PhD life colorful and unforgettable.

To other national and international collaborators, Robert Kupp, Richard Gilbertson and Alaide Morcavallo from the UK, Amir Arabzade and Kelsey Bertrand from the US, Ryo Shiraishi and Wanchen Wang from Japan, Olivier Ayrault from France, Melanie Schoof and Ulrich Schüller from Germany. Without your help my thesis work would not have been carried out efficiently.

To animal core facility, light microscopy core facility, genomics and proteomics core facility, cytometry core facility and IT core facility at DKFZ, particularly Kerstin Dell, Damir Krunic and Matthias Schick. Thank you for providing outstanding support in all circumstance. In addition, thank all the animals that have been sacrificed for the research work.

To those who offered great help in administration, Jasmin Müller, Ines Hofmann, Iris Oezen, Nicola Herrmann-Wichmann and Heike Langloz. Thank you for helping a non-German speaker cope with all the administrative tasks in order to work in Germany.

To DKFZ international PhD program office, particularly Heike Riehm-Geier and Lindsay Murrells. Thank you for organizing the PhD selection events, helping me apply for the scholarship and settle down in Heidelberg. In addition, I express deep thank to the German Academic Exchange Service (DAAD) who provided a 4-year full scholarship for me to carry out my thesis.

To my PhD defense committee, Peter Angel, Hai-Kun Liu, Hilmar Bading and Christian Schaaf. Thank you for your time to evaluate my thesis.

To sel et poivre family, Veerle Geurts, Sandy Joaquina and Tasneem Cheytan. I am very surprised how well we get along with each other and I will never forget the fun time we spent together in Portugal.

To my dearest past and current flatmates: Jing Sun, Lasse Meyer and Luc Weihermüller. Thank you for welcoming me in a new household, always cheering me up and sharing sweet moments at home. I am very grateful that we have been through the pandemic together.

To my friends in Heidelberg, Siddharth Tourani, Maximilian Stein and Kaarjel Narayanasamy. Thank you for spending time with me playing boardgames, watching animes, hiking, bouldering and discovering restaurants in Heidelberg region. The relaxing atmosphere you created really supported me through the tough moments in my PhD.

To my first teacher who introduced me to the wonderful world of academic research, Anne-Clémence Vion. You are still the benchmark for me to choose a mentor. I owe you everlasting thank for trusting me and encouraging me to pursue this path.

To my best friends who have supported me over 10 years: Rong Yi, Wenqian Sun, Mengge Wang, Zongqi Li and Xiaotong Zhang. You are without doubt the most precious treasure I found in my life. Thank you so much for being there.

To Yuzu. 私の心の支えになってくれて本当にありがとう。

À la famille de Richaud de Lyon à Versailles : merci pour votre soutien malgré la distance.

To my family, especially mom and dad. 謝謝你們無條件的支持，我愛你們。

Table of Contents

List of Figures and Tables

List of Abbreviations

ALL	Acute lymphoblastic leukemia
ATAC-seq	Assay for transposase-accessible chromatin using sequencing
ATO	Arsenic trioxide
AT/RT	Atypical teratoid rhabdoid tumor
BBB	Blood-brain barrier
C11orf95	Chromosome 11 open reading frame 95
CAG	Cytomegalovirus early enhancer/chicken beta-actin hybrid
Cas9	CRISPR associated protein 9
CBTRUS	Central Brain Tumor Registry of the United States
ChIP-seq	Chromatin immunoprecipitation followed by DNA sequencing
CMV	cytomegalovirus
CNS	Central nervous system
CNV	Copy number variation
CRISPR	Clustered regularly interspaced short palindromic repeats
CSF	Cerebrospinal fluid
CUT&RUN	Cleavage under targets and release using nuclease
DBD	DNA binding domain
DIPG	Diffuse intrinsic pontine glioma
E11.5	Embryonic day 11.5 after conception
EAD	Ewing sarcoma activation domain
EdU	Ethinyldesoxyuridin
EF1a	Human elongation factor-1alpha
EPN	Ependymoma
ESC	Embryonic stem cell
EV	Extracellular vesicles
EWSR1	Ewing sarcoma RNA binding protein 1
FFPE	Formalin-fixed paraffin-embedded
FISH	Fluorescence *in situ* hybridization
forNSC	Forebrain neural stem cell
FrFr	Fresh-frozen
GBM	Glioblastoma
GEMM	Genetically engineered mouse models
HA	Human influenza hemagglutinin surface glycoprotein
H&E	Hematoxylin and eosin
HGG	High-grade glioma
hinNSC	Hindbrain neural stem cell

IF	Immunofluorescence
IHC	Immunohistocheminstry
i.p.	Intraperitoneal
iPSC	Induced pluripotent stem cell
IRES	Internal ribosome entry site
ITCC-P4	Innovative Therapies for Children with Cancer Pediatric Preclinical Proof-of-Concept Platform
IUE	*In utero* electroporation
IVIS	*In vivo* imaging system
kbp	Thousand base pairs
KD	Knockdown
MB	Medulloblastoma
NCM	NeuroCult medium
NGS	Next generation sequencing
NLS	Nuclear localization signal
NPM	Neural progenitor medium
NSC	Neural stem cell
NSCMM	Neural stem cell maintenance medium
NSG	Non-obese diabetic/Severe combined immunodeficient (NOD/SCID)/Gamma
OPC	Oligodendrocyte progenitor cell
PB	PiggyBac
PDX	Patient-derived xenograft
PF	Posterior fossa
PGK	Phosphoglycerate kinase
PLAGL1	Pleomorphic adenoma gene-like 1
RCAS/TVA	Replication-competent avian sarcoma-leukosis virus long terminal repeat with splice acceptor/tumor virus A
RNA-seq	RNA-sequencing
SB	Sleeping Beauty
scRNA-seq	Single-cell RNA-sequencing
SHH	Sonic hedgehog
SP	Spinal
ST	Supratentorial
TAD	Transactivation domain
T2TP	Tol2 transposase
TF	Transcription factor
TIR	Terminal inverted repeats
TME	Tumor microenvironment
Tol2	Transposable element of *Oryzias latipes*, number 2

TPase	Transposase
TRE	Tetracycline-dependent promoter
TSM	Tumor sphere media
t-SNE	t-distributed stochastic neighbor embedding
WHO	World health organization
ZF	Zinc finger domain
ZFTA	Zinc finger translocation associated

Chapter 1

Introduction

1.1 A brief introduction to cancer genomics

As a disease of genome, cancer originated from DNA sequence changes in oncogenes and/or tumor suppressor genes (Stratton et al., 2009). In 2011, Hanahan and Weinberg proposed 8 processes as hallmarks of cancer which include maintaining proliferative signaling, evading growth suppressors, allowing replicative immortality, resisting cell death, inducing angiogenesis, activating invasion and metastasis, reprogramming of energy metabolism and evading immune destruction. Across all these hallmarks, genome instability is the underlying basis that engenders the genetic diversity through which multiple hallmark functions were fostered (Hanahan & Weinberg, 2000, 2011).

Cancer genomics is a relatively new field of research that emerged alongside the evolution of sequencing technology in the end of the 20th century to study the human genome. By sequencing the genetic material of tumor cells and comparing the sequences to healthy tissue, cancer genomics allow scientists to discover genetic differences at molecular level that contribute to the uncontrolled cell growth which lead to cancer. A substantial amount of information can be retrieved from the genomics data, such as single nucleotide variants, chromosomal rearrangements, insertions or deletions, alternatively spliced transcripts, gene fusions and chromosomal copy number variations (Garraway & Lander, 2013).

The completion of Human Genome Project at the turn of the millennium provides a basis for the design of high-density microarrays to detect genomic alterations through hybridization of nucleic acids (Lander et al., 2001; Lipshutz et al., 1999; Venter et al., 2001). In the context of cancer genomics, microarrays have a broad range of prominent applications including but not limited to gene expression monitoring (Lockhart et al., 1996), detection of single nucleotide polymorphisms (Cutler et al., 2001), detection of foreign DNA (such as from virus; Wang et al., 2002) and aberrations in DNA methylation patterns (Yan et al., 2001).

1.2 Brain tumor classification

According to the previous WHO guidelines, the classification of CNS tumors was mainly performed by the neuropathologists based on the morphological similarity of tumor cells to their presumed cellular origin. This was evaluated mostly by hematoxylin and eosin (H&E) staining and in certain cases by immunohistochemical (IHC) staining of molecular signatures of the tumors (Louis et al., 2007). Using this information, tumors have been subclassified based on their aggressiveness into four grades, from grade I (benign) to grade IV (very aggressive) (Louis et al., 2016). However, CNS tumors are histologically highly diverse and were reported for considerable inter-observer viability in histopathological diagnosis in previous studies, for instance, in ependymomas (EPN), CNS primitive neuroectodermal tumors and diffuse gliomas (Ellison et al., 2011; Sturm et al., 2016; van den Bent, 2010).

During the last decade, the revolution in molecular biology dramatically changed the way to stratify pediatric CNS tumor, which has yielded progressively more detailed insights into the genetic basis for each type of tumor (Louis et al., 2017). In the updated WHO classification in 2021, an increasing number of pediatric CNS tumor is classified using their genetic information which has been recognized by the WHO (Brat et al., 2020; Brat et al., 2018; Ellison et al., 2020; Ellison et al., 2019; Louis et al., 2019; Louis et al., 2016; Louis et al., 2021; Louis et al., 2020; Louis et al., 2018). Some molecular stratification was introduced such as WNT medulloblastoma and Sonic Hedgehog medulloblastoma (Kijima & Kanemura, 2016). Additionally, several fluorescence *in situ* hybridization (FISH) as well as DNA methylation analyses for single gene evaluation were implemented in clinical diagnoses. However, standardization of various diagnostic methods remained difficult and the discordance of these methods might lead to confusion in clinical decision-making and misinterpretation of results from clinical trials.

DNA methylation is described as the methylation of the 5-carbon on cytosine residues in CpG dinucleotides (CpG island), which is an extensively characterized modification of chromatin. CpG islands are primarily concentrated in the transcription starting sites, gene body and enhancer regions which indicates the central role of DNA methylation in regulating gene expression. Mapping of DNA methylation profile between normal and cancer genomes reveals that around 5% to 10% of typically unmethylated CpG islands located in promoter regions become aberrantly methylated in diverse cancer genomes (Bird, 2002). With the advances of technology in genomics, genome-wide and single-base resolution DNA methylation profiles or 'methylomes' can be achieved (Lister et al., 2009). In cancer, methylome profiling is a highly robust and reproducible method which

provides not only information on somatically acquired alterations in DNA methylation, but also traits that reflect the cellular origin of the tumor (Fernandez et al., 2012; Hovestadt et al., 2014; Hovestadt et al., 2013). In the past decade, DNA methylation profiling has been extensively used for classification of brain tumors as well as identification of new tumor entities (Capper et al., 2018; Johann et al., 2016; Koelsche et al., 2015; Korshunov et al., 2016; Korshunov et al., 2014; Lambert et al., 2013; Mack et al., 2014; Pajtler et al., 2015; Reuss et al., 2015; Sturm et al., 2016; Sturm et al., 2012; Thomas et al., 2016). A massive joint effort from an international collaboration profiled 2801 brain tumors and non-neoplastic brain tissues with DNA methylation microarray, resulting in a reference cohort consisting of 82 brain tumor classes (Capper et al., 2018). Using this reference cohort, a classifier tool was developed to automatically classify new samples and is available online for free[2]. This tool might change the diagnosis in up to 12% of the cases, compared to the standard methods, that has a significant impact on clinical decision-making (Capper et al., 2018).

1.3 Gene fusion in tumor

In the early 2000, the emergence of next-generation (NGS) revolutionized the field in the way that sequencing became high-throughput, less laborious, faster and cheaper (Garraway & Lander, 2013). As an important member of NGS family, RNA sequencing (RNA-seq) enlarges the research spectrum in oncology, which includes investigations on differential gene expression analysis and cancer-specific biomarkers, tumor microenvironment (TME) and immunotherapy, tumor heterogeneity and drug resistance, fusion gene detection and so forth (Hong et al., 2020; Mortazavi et al., 2008).

Chromosomal rearrangements bringing to the fusion of two genes can lead to aberrant expression of oncogenic fusion proteins driving tumor formation, such as *BCR-ABL*, the first onco-fusion gene discovered in chronic myeloid leukemia patients in 1973 (Rowley, 1973). In clinical practice, the conventional method for detection of fusion genes is FISH and IHC. To utilize the biopsies more efficiently, combining multiple investigations in one single assay is demanded. Thus, several computational tools were developed to identify gene fusions from RNA-seq data, for instance, FusionSeq (Sboner et al., 2010), deFuse (McPherson et al., 2011), InFusion (Okonechnikov et al., 2016) and Arriba (Uhrig et al., 2021). As the tools

[2] https://www.molecularneuropathology.org/mnp/

turn into more accurate and efficient, fusion detection from RNA-seq data becomes a routine task in cancer research and genomic-guided precision oncology (Heydt et al., 2021).

Many fusion proteins involve receptor tyrosine kinase that aberrantly activates signaling pathways for cell survival, such as ALK fusions in non-small cell lung carcinoma (Devarakonda et al., 2015; Gainor et al., 2013; Wong et al., 2009). In some circumstance, transcription factors (TF) are fused with a partner gene that triggers undesirable gene expression like *EWSR1* fusions in Ewing sarcoma (Downing et al., 1993). A systematic review in 2022 greatly recapitulated 110 reported unique fusion genes in pediatric central nervous system (CNS) neoplasms, including 65% kinase fusions and 33% of TF fusions (Roosen et al., 2022). TF is a family of protein that primarily binds to DNA to regulate the expression of target genes. The common shared features among all TFs are DNA-binding domain and transactivation domain (TAD). In numerous cancer types, the alteration of TF activity leads directly to the dysregulation of gene expression pattern resulting in uncontrolled proliferation (Bushweller, 2019). To survey the interactions between TFs and DNA, chromatin immunoprecipitation followed by DNA sequencing (ChIP-seq) is an essential technique, that can also be used to determine TF localization on a specific genomic locus (Solomon et al., 1988; Staynov & Crane-Robinson, 1988). An alternative novel method to study protein-DNA relation is cleavage under targets and release using nuclease (CUT&RUN) sequencing, which provides higher resolution and less background signal compared to ChIP-seq (Bushweller, 2019).

1.4 Pediatric central nervous system tumors

1.4.1 Overview

Cancer is the second most common cause of death among children and adolescents (age under 20) in the United States, surpassed only by injuries, based on the latest cancer statistics from 2022 (Cunningham et al., 2018; Siegel et al., 2020). Leukemia is the most common cancer in children (age 0-14), accounting for 28%, followed by CNS tumors (26%; Figure 1-1a). Cancer types and their distribution differ in adolescents (age 15-19): CNS tumors are most common (21%), followed closely by lymphoma (19%; Figure 1-1b). Overall, pediatric CNS tumors are the most common solid tumor and the most frequent cause of cancer-related mortality and morbidity in children age 0-19 years in the United States (Ostrom et al., 2021; Ostrom et al., 2015).

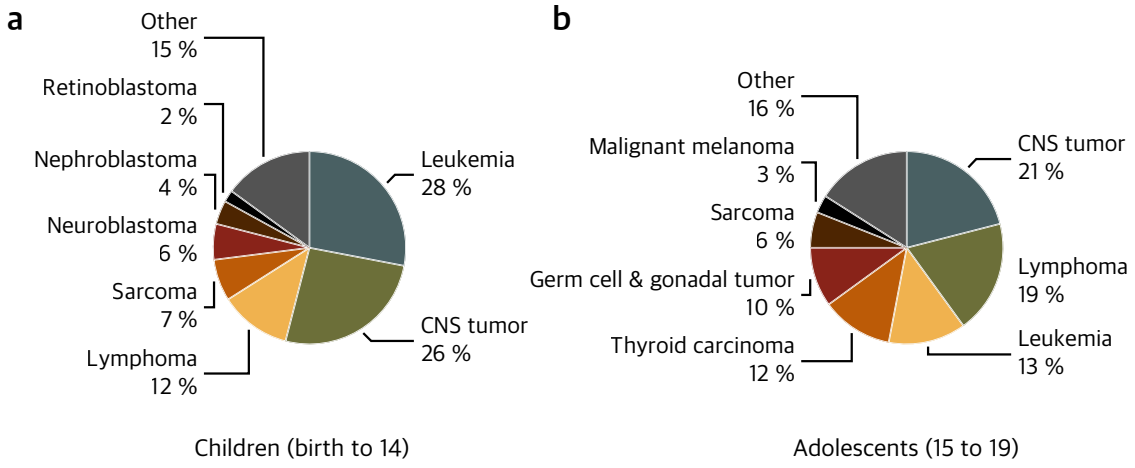

Figure 1-1 | Case distribution and international classification of childhood cancer type in the United States

Case distribution for (a) children (age 0-14) and (b) adolescents (age 15-19). CNS: central nervous system. Data derived from Siegel et al., 2020.

According to the latest statistics from Central Brain Tumor Registry of the United States (CBTRUS), pediatric gliomas account for circa 42.8% of brain tumors in children and adolescents ages 0-19 years (I will refer to pediatric hereafter). Pilocytic astrocytoma is the most common glioma (15.3%), followed by other gliomas (12.6%), diffuse & anaplastic astrocytoma (4.8%) and ependymoma (EPN, 4.7%). Embryonal tumors are the second largest category for malignant pediatric CNS tumors (9.2%), in which medulloblastoma (MB) is the most frequent (6.4%; Figure 1-2; Ostrom et al., 2022).

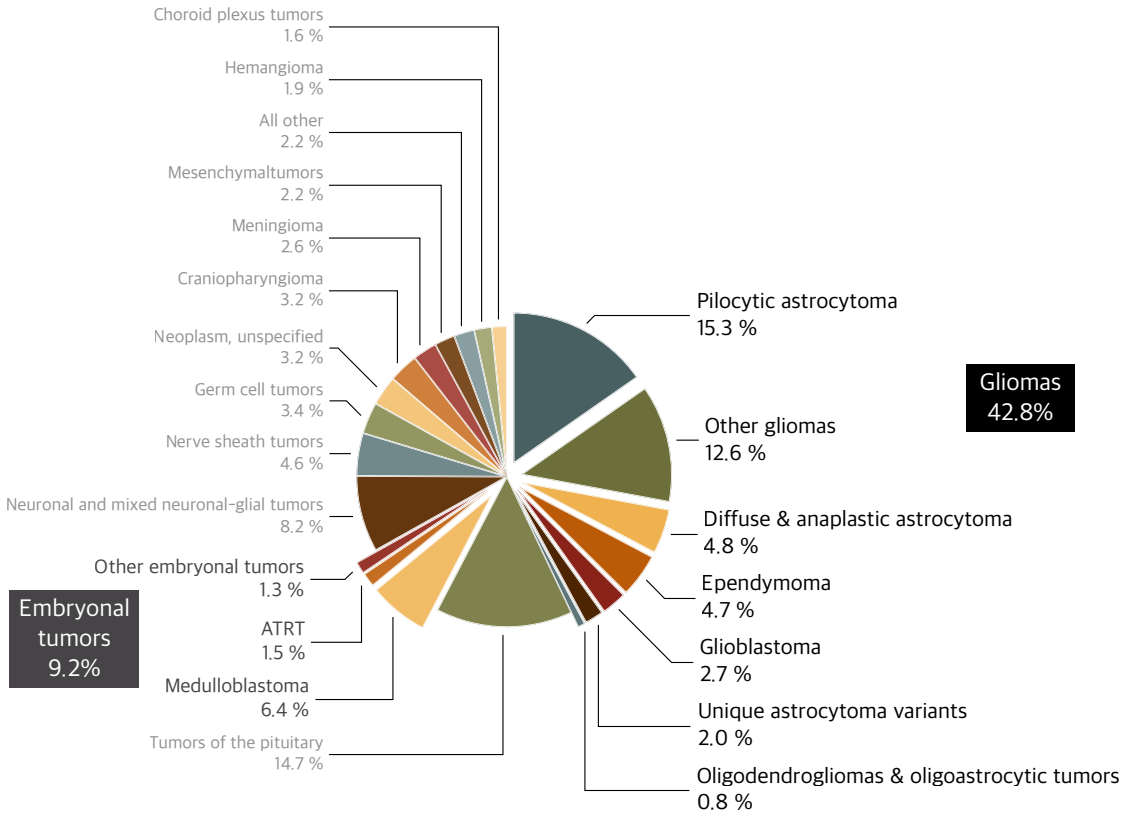

Figure 1-2 | Distribution of all primary CNS tumors by histopathology in children and adolescents (ages 0-19 years).

5-year total = 25,340; annual average cases = 5,068; CBTRUS Statistical Report: US Cancer Statistics – NPCR and SEER, 2015-2019. Figure adapted from Ostrom et al., 2022 Fig. 19b.

The overall outlook for pediatric cancers has improved enormously over the last 50 years. In the mid-1970s, the 5-year survival rate for children under 14-year-old was only 58% and for adolescents aged between 15 and 19-year-old was 68% (Siegel et al., 2021). In the past decade, the 5-year survival rate has been increased to 84.7% for children and 85.9% for adolescents diagnosed with cancer (Howlader N, 2021).

Although survival rate for most pediatric cancers have improved, the progress was particularly dramatic for a few cancers, for instance the most common pediatric cancer, acute lymphoblastic leukemia (ALL). After introducing the ameliorated treatments in the 1960s, the 5-year survival rate for children under 14 diagnosed with ALL increased from 57% (in 1975) to 92% (in 2012) and with non-Hodgkin lymphoma also raised drastically from 43% to 91% (Jemal et al., 2017). With the improvements of survival for these tumors, brain cancer

has recently overtaken leukemia as the leading cause of cancer fatalities among children (Curtin et al., 2016).

Of note, compared to adult cancers, pediatric malignancies are fundamentally different in many aspects. The former is often associated with an extended exposure to carcinogens while tumors in childhood predominantly result from an aberrant development at early stage or due to cancer predisposition syndrome in approximately 10% of patients (Pfister et al., 2022). In contrast to adult tumors, pediatric tumors typically bear a much lower somatic mutational burden and are generally caused by a single driver event, such as an onco-fusion caused by a gene translocation or driving mutations (e.g. BRAFV600E in gliomas; (Gröbner et al., 2018; Ma et al., 2018). Another typical feature in childhood tumors that could directly affect the treatment outcome, especially immunotherapy, is the limited level of infiltrated immune cell (Y. Grabovska et al., 2020; Wienke et al., 2021; Wu et al., 2020). Therefore, assessing pediatric patients based on the criteria from adult tumors is not appropriate and the discrepancy between the two categories need to be taken into account during the treatment planning. In fact, single-agent chemotherapy trials of seven different chemical compounds on high-grade glioma (HGG, WHO grade III and IV) showed a distinct and relatively dismal outcome on pediatric patients compared to the adult patients, despite the similarity in tumor morphology (Jones et al., 2012). With a worldwide effort of numerous international laboratories and consortia, for the first time, pediatric tumors are listed in the new 5th edition of the WHO classification of tumors as a separate section, while previously they were classified with adult tumors the respective organ systems (Louis et al., 2021; Pfister et al., 2022).

In most cases, neurosurgical procedures remain the first-line treatment procedure for pediatric brain tumors. Depending on the tumor type, surgical interventions allow to obtain tumor tissue for diagnostic procedures, to re-establish normal cerebrospinal fluid (CSF) pathways, sometimes through diversion of CSF, tumor debulking and/or complete tumor resection (Heuer et al., 2007). A frequent therapeutic modality after surgery is radiotherapy, followed by chemotherapy either as an adjuvant treatment in case of removable tumors or as first-line treatment when the tumor is unresectable (Pollack et al., 2019). Although advances in therapeutics have generally improved survival rates, there have been growing concerns regarding a considerable morbidity generated by the cancer treatment in childhood, including organ failure, neurodisability, subfertility, other endocrinopathies, or second malignancies (Behjati et al., 2021). More precise and targeted treatment regimens need to be applied to cure the young patients by reducing the sequelae. To achieve this goal, deeper understanding of the molecular biology and the underlying mechanisms of the tumorigenesis in pediatric brain tumors is urgently needed.

1.4.2 Ependymoma

Ependymomas (EPN) are CNS tumors that can occur both in children and in adults. EPNs most commonly arise in the fourth ventricle but can be observed throughout the entire neuraxis (Katrin Scheinemann, 2015; Pajtler et al., 2015). EPNs account for 4.7% of all CNS tumors among all pediatric patients (Figure 1-2). Pediatric EPNs have poor prognoses and high tumor recurrence. Most childhood cancer patients who survived 5 years after the diagnosis of the primary tumor can subsequently survive up to 15 years with a high probability, while in the case of EPNs, a tremendous decline in survival was observed (Ward et al., 2014). Overall, pediatric patients diagnosed with EPNs have a 5-year and a 10-year survival rate of 70% and 52%, respectively (De et al., 2018; Marinoff et al., 2017).

The unfavorable clinical outcome is associated with the limited treatment regimens. The current standard-of-care for pediatric EPN patients includes maximal safe surgical resection, followed by focal radiotherapy which mostly will cause long-term sequalae in children (Kilday et al., 2009; Merchant et al., 2009). As there is no convincing role for conventional chemotherapeutic procedures in the treatment of EPNs, targeted treatment is urgently needed for the pediatric patients with aggressive EPNs (Katrin Scheinemann, 2015).

EPNs have long being classified solely based on histopathology into four subtypes: subependymomas (WHO grade I), myxopapillary ependymomas (WHO grade I), classic ependymomas (WHO grade II) and anaplastic ependymomas (WHO grade III; Figure 1-3a; Louis et al., 2017). However, the utility of histologic grading of EPN for risk stratification has been discussed controversially, with no consistent associations of tumor grade and patient outcome (Ellison et al., 2011). Recent genomic studies have allowed for subdivision, based on the anatomical area, of supratentorial (ST), posterior fossa (PF), and spinal (SP) EPN into 10 molecularly distinct groups with biologically homogenous features and clearly distinct clinical outcome (Figure 1-3a; Ghasemi et al., 2019; Johnson et al., 2010; Pajtler et al., 2015; Parker et al., 2014; Taylor et al., 2005; Witt et al., 2011).

Within the ST compartment, underlying molecular signatures including DNA methylation and transcriptome analysis define three major groups: ST-SE, ST-EPN-YAP1, and ST-EPN-ZFTA (formally ST-EPN-RELA; Figure 1-3a; Pajtler et al., 2015). ST-SE are fusion-negative molecularly classified subependymoma that are mostly observed in adults. ST-EPN-YAP1 tumors are enriched for gene fusions involving the Hippo effector YAP1 and primarily affect infants (median age of 1.5 years). More than 70% of the ST-EPN account for ST-EPN-ZFTA, which are associated with a worse prognosis than the other two groups (Figure 1-3a and b; (Pollack et al., 2019). ST-EPN-ZFTA predominantly contain oncogenic fusions between *RELA*, the transcription factor involved in the canonical NF-κB signaling,

and ZFTA, a less well-characterized neighboring gene on chromosome (chr.) 11 (Malgulwar et al., 2018; Pajtler et al., 2015; Parker et al., 2014). The ST-EPN-ZFTA is the first molecular group among pediatric CNS tumors that has been included in the 2016 WHO classification and all 10 groups were finally integrated into WHO classification in 2021 (Louis et al., 2016; Louis et al., 2021).

Apart from chromothriptic events on chr. 11 surrounding the fusion, the genome of human ST-EPN-ZFTA is generally stable, and additional recurrent alterations other than focal *CDKN2A/B* deletions have not yet been identified (Pajtler et al., 2015). The tumor formation by transplantation of mouse neural stem cells overexpressing *ZFTA-RELA* fusion in *Cdkn2a* null background clearly prove the transforming capacity of the fusion gene (Parker et al., 2014). A more recent study using RCAS/TVA system (principle explained in section 1.5.3) illustrates that *ZFTA-RELA* serves as a single driver in tumor formation *in vivo* (Ozawa et al., 2018). However, the role of the *RELA* fusion partner *ZFTA* in ST-EPN-ZFTA, is not yet fully understood. Further characterization of *ZFTA* and its fusions in ependymal tumorigenesis is the key event to find relevant molecular targets to provide more therapeutic options to save our patients in the future.

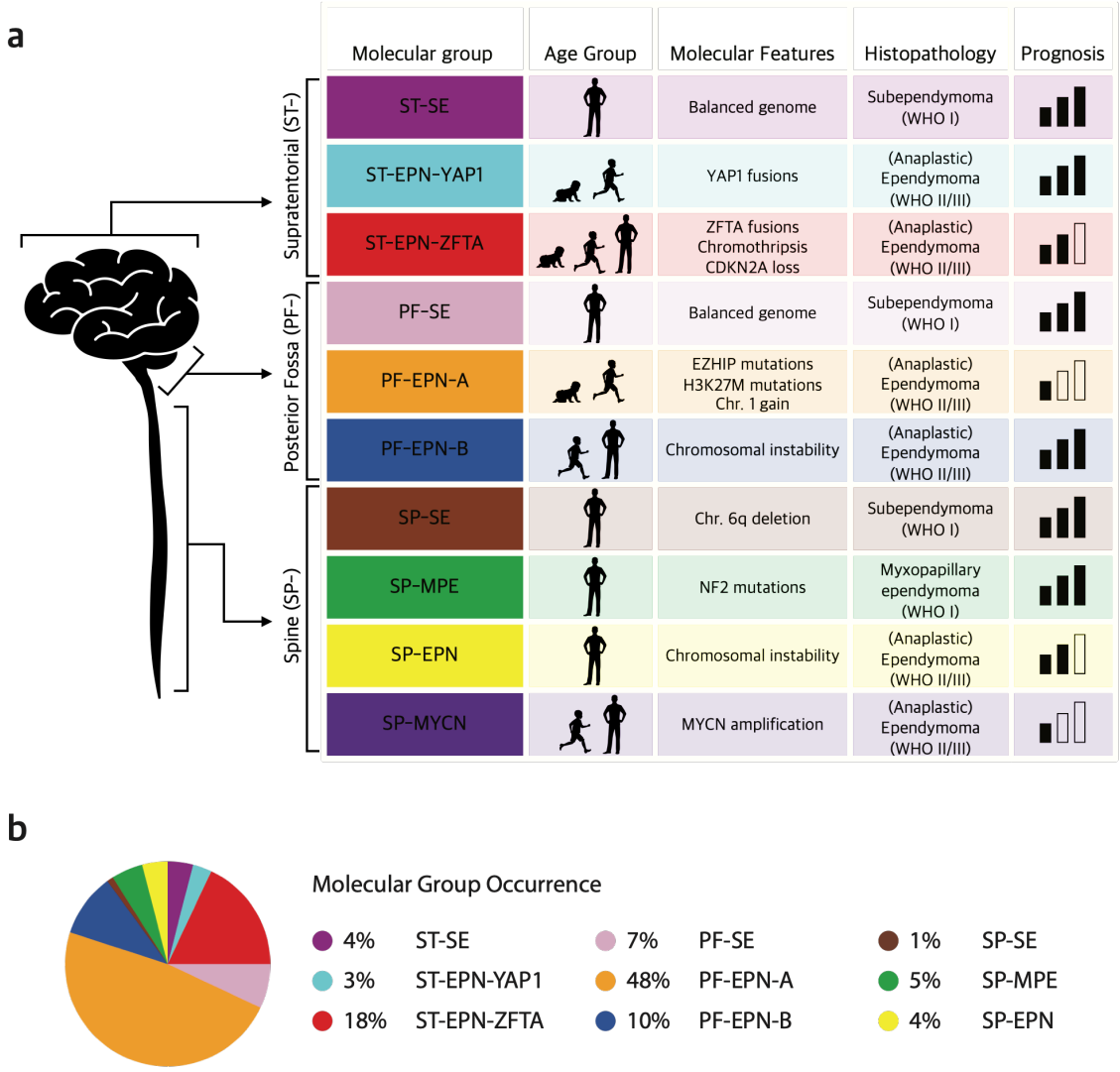

Figure 1-3 | Illustration of the 10 recognized groups of ependymomas.

a, Graphical illustration of key genetic and epigenetic findings in the 10 molecular groups of ependymomas classified by DNA methylation profiling. **b**, Estimate of the overall frequency of the different groups of ependymomas. Figure adapted from Ghasemi et al., 2019; Pajtler et al., 2015; Pollack et al., 2019.

1.4.3 NET_PLAGL1

Apart from the 10 molecular groups of EPNs presented in Figure 1-3a, there is still a proportion of tumors, which does not match with one of these groups although being histopathologically diagnosed as EPNs. Recent collaborative efforts have identified a novel highly distinct cluster based on DNA methylation profiling with a relatively wide spectrum of histopathological diagnoses, including 60% of tumors designated as EPN (Figure 1-4a; Sievers et al., 2021). RNA sequencing unveiled recurrent fusions harboring the *pleomorphic*

adenoma gene-like 1 (*PLAGL1*) gene in 95% of the analyzed samples, among which the most common fusion was *EWSR1-PLAGL1* followed by *PLAGL1-FOXO1* fusion and *PLAGL1-EP300* fusion. At the time of diagnosis, median age of the patients was 6.2 years (Figure 1-4b) and the sex distribution was relatively balanced (Figure 1-4c). All tumors in the cohort were located in the ST compartment (Figure 1-4d). Median progression-free survival was 35 months (Figure 1-4e). To gain further insights into the molecular biology of this novel cluster in the interest of finding potential therapeutic targets, models are urgently needed.

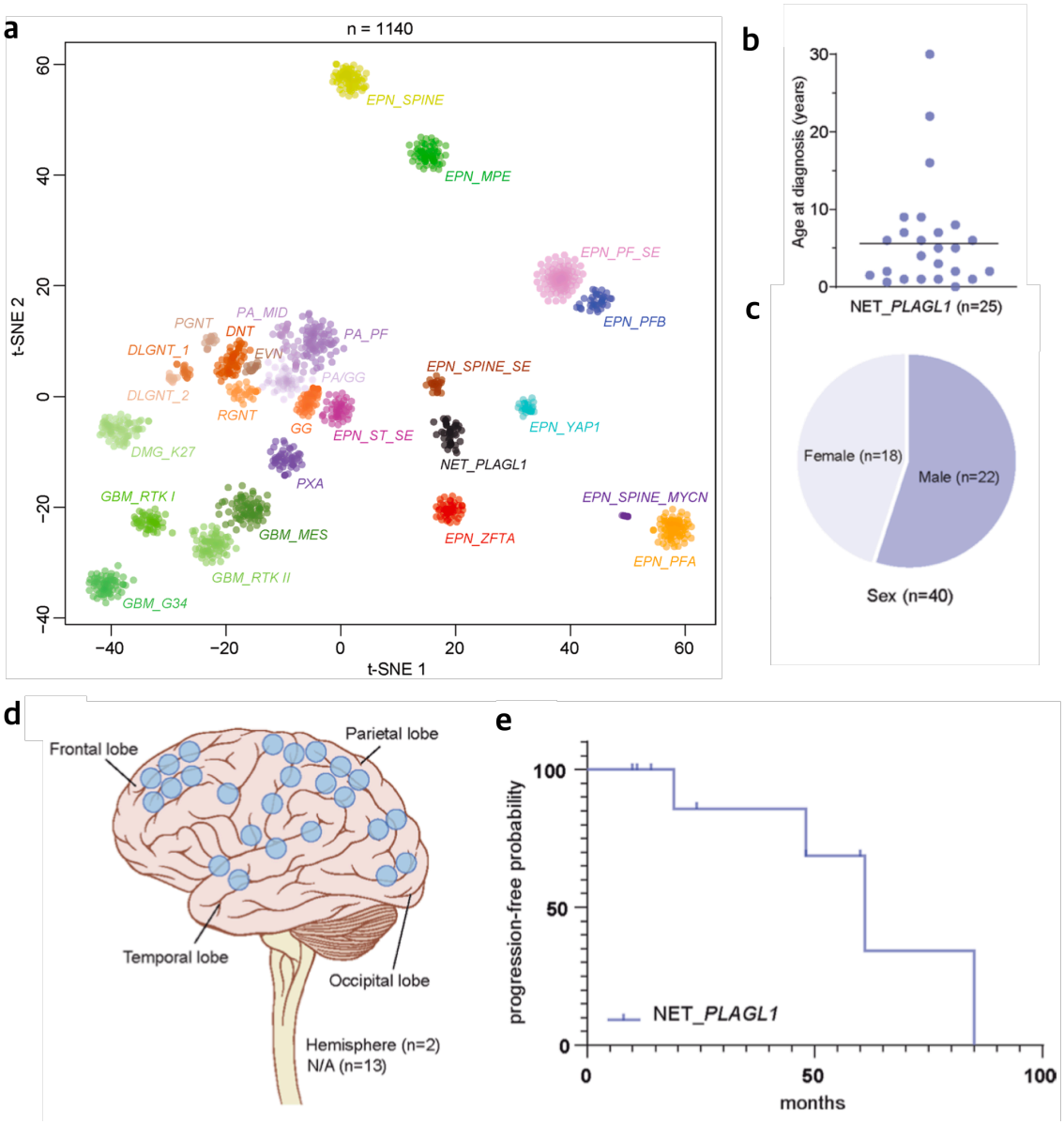

Figure 1-4 | DNA methylation profiling identifies a molecularly distinct group of neuroepithelial tumors.

a, t-distributed stochastic neighbor embedding (t-SNE) analysis of DNA methylation profiles of the 40 tumors of NET-PLAGL1 investigated together with 1100 reference brain tumor samples. **b**, At time of diagnosis with the median age of 6.2 years; **c**, Patient sex distribution; **d**, Tumor location distribution; **e**, Time to progression or recurrence of NET_PLAGL1 cohort for whom follow-up data were available (n = 11). Figure adapted from Sievers et al., 2021.

1.5 Brain tumor modeling

1.5.1 Overview

On average, it takes 10.5 years and 1.1 billion US dollar to develop one successful drug (Wouters et al., 2020). Only around 10% of drugs make it all the way from Phase I clinical trial to approval and the success rate in oncology trials is the lowest among major diseases, with a depressing 3.4% (Mullard, 2016; Wong et al., 2018). Extensive endeavor has been made on the side of basic and translational research, while only few outcomes can be beneficial to the patients. Generating tumor models that efficiently transfer the knowledge from bench to bedside plays a key role in filling this gap.

About 80 years ago, scientists successfully generated a carcinogen-induced model for studying brain malignancies (Seligman et al., 1939). 40 years later, the first pediatric brain tumor models were created in 1980s by transplanting cancer cells into immunodeficient mice, resulting in brain tumors histologically similar to high-grade glioma (HGG), medulloblastoma (MB) and atypical teratoid rhabdoid tumor (AT/RT; Friedman et al., 1988; Friedman et al., 1985; Jacobsen et al., 1985; Keles et al., 1995; Pietsch et al., 1994; Wasson et al., 1990; Yachnis et al., 1998).

To date, a decent amount of *in vitro* and *in vivo* models has been developed using various techniques specifically for pediatric brain tumors. Both methods are used to investigate molecular characteristics behind tumorigenesis as well as to determine whether a new therapeutic strategy meets the requirement for clinical success (Huszthy et al., 2012). The current guidelines to describe a good animal model is: short latency, high incidence rate, presenting histopathological and molecular features of human disease, as well as ability to predict treatment response in patient (Perrin, 2014). While faithfully recapitulating tumor biology, *in vitro* culture conditions of brain tumor models should be suitable for high-throughput screenings as well (Li, 2005). Every system is individually limited; no single model can fully reflect the complexity, advancement and drug responsiveness of a human tumor. Therefore, attention should be placed on understanding the benefits and barriers of

the model and choice should be made according to the purpose of the study. It is critical to use a strategic combination of approaches to translate effectively any findings to the clinic to benefit the patients (Dobson & Gopalakrishnan, 2018; Huszthy et al., 2012; Neumann, Swartling, et al., 2017). In the following sections, commonly used *in vitro* and *in vivo* models for pediatric brain tumor research will be introduced.

1.5.2 *In vitro* models

In vitro models were utilized for decades to identify the genetic and epigenetic alterations in tumor cells contributing to the underlying biological mechanisms of tumorigenesis (Goodspeed et al., 2016; Hemmati et al., 2003; Singh et al., 2003; Suslov et al., 2002; J. Xu et al., 2012). Cultured cells also play a prominent role in predicting drug response and resistance in a high-throughput manner to evaluate potential treatment efficacy (Goodspeed et al., 2016; Houghton et al., 2007; Li, 2005; Morfouace et al., 2016; Rubinstein et al., 1990; Sewing et al., 2017).

Model systems for neuro-oncology research include tumor cell lines, cultured in monolayer or as neurospheres, and an emerging potent technology, brain organoids (Ballabio et al., 2020; Bez et al., 2003; Lovett et al., 2020). *In vitro* cultures are relatively uncomplicated to handle because they are robust, low-cost, grow fast, can be engineered easily and be stored long-term (Neumann, Swartling, et al., 2017). Another important feature for these models is that the culture conditions are well-defined, which provides a controlled environment for studying specific molecular functions.

Over 60 pediatric cancer cell lines have been established including MB, EPN, HGG and AT/RT, both primary culture and continuous cell lines (Xu et al., 2015). Primary culture refers to the culture of tumor cells directly harvested from patients, which shows high resemblance to the original tumor and are usually heterogenous mixture of different cell populations. After the first passage, cells are increasingly put under a selective pressure in the culture media until they either stop growing or become a continuous cell line. Cell lines are often cultured in serum-containing media that can trigger cell differentiation, gradually leading to a genetic and phenotypic drift from the original tumor over time and eventually becomes a homogenous population (Ivanov et al., 2016; Ledur et al., 2017; Lee et al., 2006; Jingying Xu et al., 2012).

The challenge was addressed after the establishment of neurosphere models, that are cultured in serum-free media and maintain tumor heterogeneity, making them an attractive

alternative to serum cultured cells (Sandén, 2016; Wenger et al., 2017; Zhou et al., 2017). However, neurosphere culture does not overcome the general limitations shared among the *in vitro* models such as lack of tumor microenvironment (TME), which can lead to biased interpretation of tumor cell behavior (Hanahan & Weinberg, 2011; Lilienblum et al., 2008). For instance, glioblastoma (GBM) cells cultured without TME highly enriches a subpopulation called glioma stem cell-like cells, which represent solely a relatively small portion of the original tumors (Caragher et al., 2019; Xiao et al., 2017).

This drawback can be, to some extent, addressed using a more complex *in vitro* modeling system, brain organoid. Organoids are embryonic stem cell (ESC)- or induced pluripotent stem cell (iPSC)-derived 3-dimentional structures that bear some level of self-organization and mimic, at least partially, *in vivo* organs (Di Lullo & Kriegstein, 2017). Up till now, a variety of protocols for generating brain organoid have been established, aiming to model the development of cortical (Birey et al., 2017; Kadoshima et al., 2013; Lancaster et al., 2013; Qian et al., 2016), hippocampus (Sakaguchi et al., 2015), midbrain (Jo et al., 2016; Monzel et al., 2017; Qian et al., 2016), hypothalamus (Qian et al., 2016), cerebellum (Muguruma et al., 2015; Qian et al., 2016) and anterior pituitary (Suga et al., 2011). Not only as models of development, but also can these organoids be used as a platform to study brain tumorigenesis in a more robust and accurate way (Sakaguchi et al., 2015). Several pediatric CNS tumor organoid models for MB and GBM were generated very recently that recapitulate their human counterparts (Ballabio et al., 2020; Hubert et al., 2016; Linkous et al., 2019; Ogawa et al., 2018). It is a versatile *in vitro* model that forms distinct, complex, biologically relevant structures, making it a promising tool to unveil the complexity of tumor network and as drug screening platforms. Despite the advantages, the absence of stroma cells, tissue-resident immune cells, and in particular, vasculature, a key role in blood-brain barrier (BBB) which is a unique network in the brain and has notably a huge impact on drug delivery (Pardridge, 2002; Sarkaria et al., 2018; Stamatovic et al., 2016; Sweeney et al., 2018). Recently, a protocol for generating blood vessel organoid was released and a vascularized brain organoids began to emerge, while mimicking a BBB effect remains challenging (Sun et al., 2022; Wimmer et al., 2019).

1.5.3 *In vivo* – Genetically engineered mouse models

Only 1% of genes are not shared between mouse and human, and on average, 85% of the genome is identical across the two species (Waterston et al., 2002). With the advantages of their natural properties, such as short life span (1-2 years), fast reproduction cycle (19-21 days), small body size (20-60 grammes), and fully characterized genome information (Smith

et al., 2017), mice gained their place as the most widely used experimental animals in biomedical research as well as the gold standard for drug safety and efficacy testing in the pharmaceutical industry (Hickman et al., 2017; Monaco et al., 2015; Polli, 2008). Highly conserved molecular and cellular mechanisms in the CNS of human and mouse made the latter the most prevalent model organism in pediatric brain tumor research (Chan et al., 2009; Dobson & Gopalakrishnan, 2018; Liao & Zhang, 2006; Miller et al., 2010; Monaco et al., 2015).

With increased understanding of genomic alterations in CNS tumors and considerable progress in gene editing technologies, the use of genetically engineered mouse models (GEMM) in studying pediatric brain diseases drastically augmented (Huszthy et al., 2012). GEMMs, in many instances, recapitulate tumor initiation and progression in an integrated organism with an intact immune system, functional BBB and undisrupted microenvironment, making them particularly attractive models for investigating tumor-host interactions and testing new therapeutic strategies (Niclou et al., 2008; Simeonova & Huillard, 2014). The alterations of genes in GEMMs may be conventional or conditional to control the expression in a spatial and temporal manner, using systems like Cre-LoxP, tamoxifen or tetracycline/doxycycline-controlled transcription activation (Kim et al., 2018; Robertson et al., 2019; Simeonova & Huillard, 2014). Over the past 30 years, a substantial amount of GEMMs were generated for pediatric CNS tumors, notably MB and gliomas (extensively reviewed by (Li & Langhans, 2021).

The germline GEMMs are generated via *ex vivo* genome editing of ESCs followed by injection of successfully genetically modified ESCs into blastocysts and subsequently transplanted into foster mice (Day et al., 2015; Koller et al., 1989; Thompson et al., 1989). This technique requires extensive breeding scheme, which is laborious, time-consuming and pricy. One of the biggest intrinsic drawbacks is the difficulty of studying multiple genes involved in tumorigenesis at the same time (Zuckermann, 2016).

A somatic gene transfer technology was developed using replication-competent avian sarcoma-leukosis virus long terminal repeat with splice acceptor/tumor virus A (RCAS/TVA) system that can bypass the shortcomings from the germline GEMMs (Orsulic, 2002). Since RCAS retrovirus can exclusively transduce genetically engineered mammalian cells that express the cognate avian retroviral receptor TVA, the RCAS/TVA gene delivery system can be applied in various germline TVA-expression GEMMs (Orsulic, 2002). The application spectrum can be extended by crossing a GEMM in which Cre-activatable conditional TVA-expression is under the control of ubiquitous promoter *Rosa26* with a large number of available Cre-expressing mouse lines (von Werder et al., 2012). Furthermore, the TVA-expressing cells are susceptible to multiple RCAS infections simultaneously or

sequentially, which render this model system possible to evaluate tumor etiology in the situation of synergistic effect of multiple altered genes (von Werder et al., 2012). Various pediatric CNS mouse models established with RCAS/TVA system were already published and present high resemblance to their human counterparts, including MB, EPN and gliomas (Gronych et al., 2011; Li & Langhans, 2021). This system allows to identify putative cellular origin of the tumor. It was shown using a RCAS/TVA system that *NES*, *GFAP* and *BLBP*-positive neural stem/progenitor cells in the ventricular zone can give rise to ST-EPN-RELA/ZFTA (Ozawa et al., 2018). However, as emphasized in the overview section, there is no perfect model; the transduction efficiency is low (<20%) *in vivo*, the RCAS viral packaging capacity is limited to 2.8 thousand base pairs (kbp) thus larger cancer-related genes of interest cannot be investigated, and only mitotic cells can be infected *in vivo* due to the natural property of retroviruses (von Werder et al., 2012). Moreover, the RCAS/TVA system can be applied exclusively on cells at neonatal or postnatal stage, where many neural stem and progenitor cells are already committed to various lineages, thus it is not suitable for studying pediatric tumors that occur at prenatal stage (Meyer, 2007; Stiles & Jernigan, 2010).

To circumvent these difficulties, another somatic gene transfer technique, *in utero* electroporation (IUE), was introduced into the field of pediatric brain tumor modeling. The IUE technique was developed in 2001 by two Japanese labs, intending for gene analyses through gain- or loss-of-function approaches in the developing mouse brain (Saito & Nakatsuji, 2001; Tabata & Nakajima, 2001). To achieve this, DNA is microinjected into the ventricular zones of the mouse brain between embryonic days 11.5 after conception (E11.5) and E16.5, followed by applying repetitive square pulses from outside the uterus using forceps-type electrodes (Arabzade et al., 2021; Saito, 2006, 2010; Saito & Nakatsuji, 2001). To date, genes have been successfully transfected to diverse CNS areas including telencephalon (Borrell et al., 2005; Mizutani & Saito, 2005; Saito & Nakatsuji, 2001), diencephalon (Saito & Nakatsuji, 2001), midbrain (Saito & Nakatsuji, 2001), hindbrain (Kawauchi et al., 2006) and spinal cord (Ding et al., 2004; Saba et al., 2005; Saba et al., 2003). In 2015, Zuckermann et al. generated the first mouse models for sonic hedgehog (SHH) MB and GBM using IUE (Zuckermann et al., 2015). Two years later, Kawauchi et al. constitutively overexpressed *Myc* together with dominant-negative form of *Trp53* in mouse cerebellum, via the combination of IUE and transposon system, successfully leading to a novel Group 3 MB mouse model (Kawauchi et al., 2017). Pajtler et al. established as well a mouse model for ST-EPN-YAP1 using IUE and transposon by overexpressing *YAP1-MAMLD1* fusion gene in mouse cerebral cortex (Pajtler et al., 2019).

Transposons are genetic elements allowing gene shifting from one location of the genome to another, which are found throughout all kingdoms of life (Ni et al., 2008). This

natural gene transfer machinery is utilized as experimental tools for shipping a variety of external DNA sequences into the genomes of target cells, to overexpress the oncogenic driver genes, impair tumor suppressor genes and introduce reporter genes. The mechanism of these systems is dependent on a cut-and-paste mode, during which an enzyme called transposase (TPase) excises the transposon flanked by terminal inverted repeats (TIR) from the donor vector, and reintegrates into a new chromosomal locus (Figure 1-5; Sandoval-Villegas et al., 2021). The most widely used transposon systems are Sleeping Beauty (SB; Ivics et al., 1997; Ivics et al., 1996), PiggyBac (PB; Cary et al., 1989; Fraser et al., 1996) and Transposable element of *Oryzias latipes*, number 2 (Tol2; Koga et al., 1995; Koga et al., 1996). Their benefits and barriers are thoroughly reviewed by (Sandoval-Villegas et al., 2021). Of note, Tol2 system, compared to the other two, can deliver up to 12 kbp to mammalian cells without decreased integration efficiency and has lower overproduction inhibition effect (Balciunas et al., 2006; Grabundzija et al., 2010).

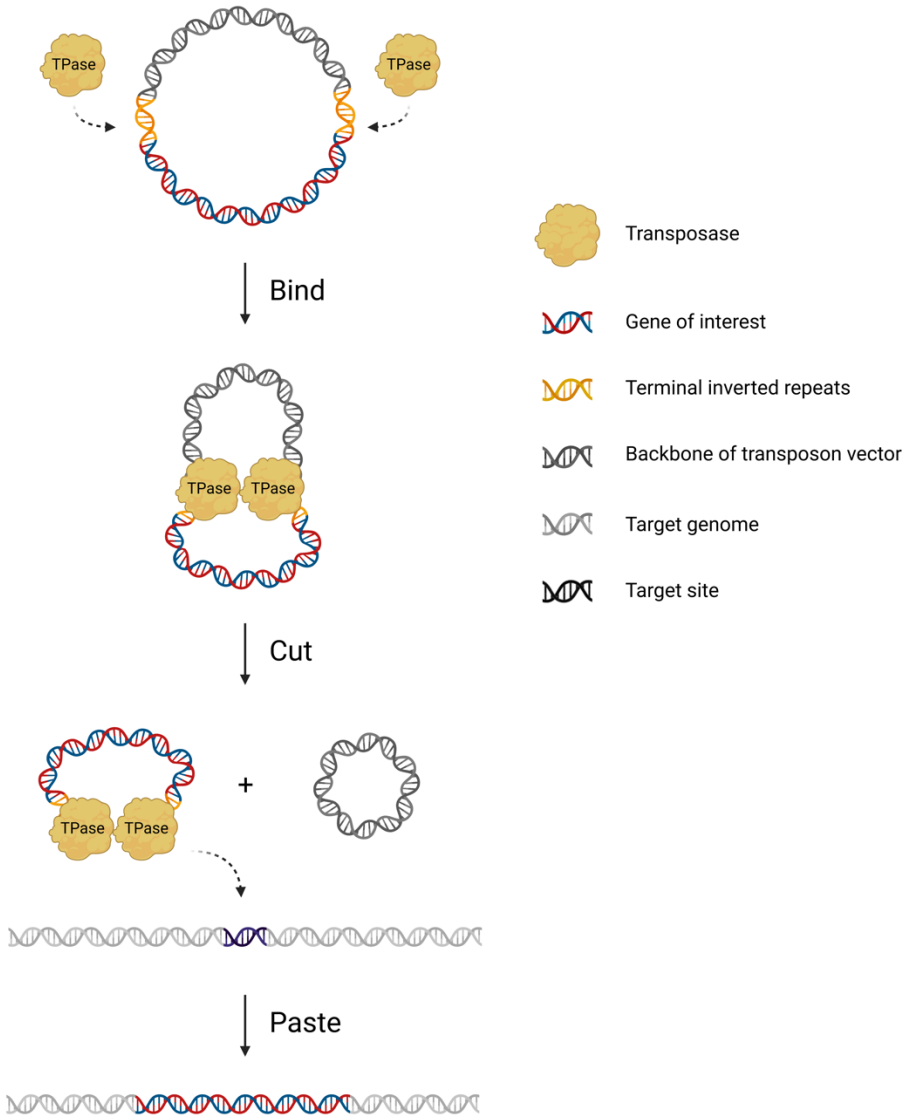

Figure 1-5 | Illustration of transposase-mediated cut-and-paste principle.

The transposase (TPase) recognizes and binds to the terminal inverted repeats (DNA in yellow), subsequently induces double-stranded DNA break and excises the gene of interest (DNA in blue-red) from the donor vector (DNA in dark grey). The transposon-TPase complex encounters its target site (DNA in black) and eventually integrates into the target genome (DNA in light grey). Figure created with BioRender.com

While traditional methods for constructing locus-specific genetic modifications are tedious and expensive, the recently developed groundbreaking gene editing approach, clustered regularly interspaced short palindromic repeats (CRISPR)/CRISPR associated protein 9 (Cas9) technology, has significantly reduced the time for engineering (Mou et al.,

2015; Yang et al., 2014). Its efficiency and versatility accelerate germline engineering and also facilitate somatic engineering, which dramatically broadens the application of GEMM in oncology (Weber & Rad, 2019). With the help of single-strand guide RNA, endonuclease Cas9 is recruited to the recognized DNA sequence and induces the double-stranded DNA break at the target site. Subsequently, gene editing can be attained via DNA repair, including high-fidelity homology directed repair pathways and error-prone non-homologous end joining (Jinek et al., 2012). CRISPR/Cas9-mediated *in vivo* somatic gene editing can be used to create chromosomal rearrangements at endogenous level, which mimic the situation in human diseases (Heyer et al., 2010). The adaptability of the CRISPR system to the scientific question and the possibility to broaden the experimental design has opened up to high-throughput screenings *in vivo* to identify, for instance, a functional landscape of suppressors in GBM within the native microenvironment of the mouse brain (Chow et al., 2017).

The above-described autochthonous GEMMs have great utility, most are not fitting the scheme of large-scale first-line drug screening because of high cost, long timelines, and in certain cases difficulties in obtaining synchronous tumorigenesis (Day et al., 2015). A GEM-derived allograft model has been developed to reduce price and to obtain a low variance in tumor latency/synchronicity for better uniformity of the model (Heyer et al., 2010). To generate allograft models, tissue fragments are harvested from GEMM tumors and expanded, without *in vitro* manipulation, by orthotopic or subcutaneous transplantation into syngeneic hosts. Therefore, GEMM tumor cells can be banked to facilitate large-scale production, allowing for high-throughput *in vivo* drug efficacy screenings in preclinical studies (Heyer et al., 2010). Allograft models are also amenable for evaluating metastatic disease and understanding stromal-tumor interactions (Day et al., 2012; Sreedharan et al., 2017; Wang et al., 2011). However, *in vivo* serial passaging increases the growth rate and deviate the tumor characteristics from primary tumors due to further evolution and/or clonal selection of certain aggressive populations, depleting heterogeneity (Huszthy et al., 2012; Mak et al., 2014; Wang et al., 2011). Therefore, tumor models based on transplantation should be monitored for molecular and histological similarity to original tumors.

With the rapid advances in genome engineering, the size of the tool box for creating specific GEMMs to address complex and precise scientific questions is magnified. Nevertheless, species discrepancy remains an unsurmountable impediment.

1.5.4 *In vivo* – Xenograft models

A way to circumvent this problem is xenograft modeling, which refers to the engraftment of human cells, subcutaneously or orthotopically into a host animal. In oncology, xenograft models essentially refer to patient-derived xenografts (PDX) which highly mimic the original tumor histologically and molecularly as well as stromal-tumor interactions (Day et al., 2015; Hermans & Hulleman, 2019; Huszthy et al., 2012; Zarzosa et al., 2017). Early in the 1980s, PDX models were already implemented in preclinical trials and showed high correlation to their patient counterpart in response of chemotherapy (Fiebig et al., 1984; Houghton et al., 1982; Mattern et al., 1988). In most cases, the host animals used for PDX generation are immunodeficient mice, for instance, the most frequently used Non-obese diabetic/Severe combined immunodeficient (NOD/SCID)/Gamma (NSG). Human bone marrow engrafting into immunodeficient mice can reconstitute a human immune response, which provides an avenue to study the involvement of the immune system in CNS tumorigenesis, and to assess the effect of immunotherapies (Sengupta et al., 2018).

Undoubtedly, there are some downsides to work with PDX, like with any model. Similar to allografts, multiple passages select the most aggressive cells, tumor lag time decreases with increasing passage, and the cell–matrix interactions and BBB can be disrupted (Huszthy et al., 2012; Leten et al., 2014; Mak et al., 2014; Neely et al., 1983; Neumann, Swartling, et al., 2017). PDX models are restricted by the amount of available patient material as well as the fluctuating engraftment rates (tumors with poor prognosis often present high engraftment rates). In addition, results may only reflect individual samples; thus, typically a large cohort size is needed to obtain unbiased outcome especially for tumors with significant heterogeneity, coming with high cost and high effort (Dobson & Gopalakrishnan, 2018). To establish a sufficient repertoire of robust and representative preclinical models accurately reflecting human disease and providing efficient platforms for preclinical drug testing, an international Innovative Therapies for Children with Cancer Pediatric Preclinical Proof-of-Concept Platform (ITCC-P4)[3] is currently undergoing the development, which encompasses 400 PDXs as well as around 15 GEMMs.

By nature of the technique, implementing the original tumor material directly into the host animal does not allow to investigate tumor initiation. Fortunately, this limitation can be bypassed using human induced-pluripotent stem cell (hiPSC)-derived xenograft models. hiPSC-derived xenograft models marry the versatility and flexibility of the stem cell

[3] https://www.itccp4.eu

technology with all the advantages of PDX setting such as the microenvironment provided by the host animal and no species difference between the original disease and engrafted cells. Basically, desired cell types were differentiated from hiPSCs and genetically modified *in vitro*, subsequently injected into immunodeficient mice. Stem cell technology allows iPSCs to differentiate into theoretically any kind of neural and glial cell lineages *in vitro*, namely neural stem cells (NSC), oligodendrocyte progenitor cells (OPC), Purkinje cells, astrocytes and neurons (Danjo et al., 2011; David Gordon, 2009; Douvaras et al., 2014; Eiraku & Sasai, 2012; Krencik & Zhang, 2011; Muguruma et al., 2010; Wichterle et al., 2002). Key factors for neural induction from iPSCs were reported such as inhibition of TGFβ and BMP signaling pathways. To date, a large variety of NSC differentiation protocols are available on the market among which monolayer method and embryoid body formation are the most prevalent (Hong & Do, 2019). Among pediatric CNS tumors, only few of them have clear trace of cellular origin, for instance, SHH MB was proved to be driven by aberrant activation of SHH pathway in granule neuron progenitors during cerebellar development (Kool et al., 2008; Schüller et al., 2008; Yang et al., 2008). Several sutdies suggested that EPN were likely originated from radial glia cells which are NSCs giving rise to both neuronal and glial lineage (Campbell & Götz, 2002; Dwyer et al., 2016; Taylor et al., 2005). Downregulation of *NANOG* and *OCT3/4* with upregulation of *NES* and *PAX6* are commonly used biomarkers to characterize NSCs (Chambers et al., 2003; Dahlstrand et al., 1995; Mitsui et al., 2003; Morshead et al., 1994; Ng & Surani, 2011; Reynolds & Weiss, 1992; Sansom et al., 2009). A recent study successfully created a low-grade glioma model by intracranial injection of *NF1*-null and *KIAA1549-BRAF*-expressing hiPSC-derived neural stem cells (iNSC) into immunodeficient mice (Anastasaki et al., 2022). Haag et al. demonstrated that identical genome mutations in distinct iPSC-derived cell types (iNSC vs. iOPC) may behave differently; diffuse intrinsic pontine glioma (DIPG) formation in mice engrafted with H3K27M and *TP53* altered iNSCs but not with iOPCs suggested the cellular origin property of NSCs in DIPG tumorigenesis (Haag et al., 2021). HiPSC-derived xenografts are gaining increasing attention as a great potential to generate *de novo* models for previously hard-to-engraft less aggressive brain tumors, and to advance our understanding of the cellular origin of these malignancies.

1.6 Objective of the study

With the rapid advances in cancer genomics, DNA methylation-based molecular classification is changing the perspective of clinical diagnosis for pediatric CNS tumors

(Capper et al., 2018). According to the molecular classification, several histologically EPN-like tumors formed discrete clusters apart from the defined 10 groups of EPN. Some clusters harbor *ZFTA* fusion genes including canonical *ZFTA-RELA* and other new fusion genes (e.g., *ZFTA-MAML2*). Another distinct cluster NET_PLAGL1 was named after the recurrent *PLAGL1* fusions found in the tumors. These fusion genes show high likelihood as oncogenic drivers in tumorigenesis. The objective of my thesis was to establish new models for these newly identified tumor entities by employing various brain tumor modeling strategies described above. Thereafter, I used the models that faithfully recapitulate their human counterparts to unravel the decode molecular mechanisms of tumorigenesis and explore the potential therapeutic vulnerabilities.

Chapter 2

Cross-species analysis identifies *GLI2* as oncogene in *ZFTA/C11orf95* fusion-positive supratentorial ependymomas

2.1 Summary

This project focused on dissecting the role of tumor-driving fusion genes in supratentorial ependymoma (ST-EPN), a rare type of pediatric brain tumor with a poor prognosis. *C11orf95-RELA* fusions are frequently found in ST-EPN and were proven to be the oncogenic drivers in these tumors (ST-EPN-RELA; Ozawa et al., 2018; Parker et al., 2014). Recently, our lab identified *de novo* fusions of *C11orf95* to numerous fusion partners different from *RELA*, e.g., *MAML2*, *MAML3*, *NCOA2* and *SS18*, suggesting a general role of *C11orf95* in tumorigenesis of ST-EPN. Using *in vivo* mouse models and *in utero* electroporation-based gene transfer technology, I found that both, the partner gene and the zinc finger (ZF) DNA binding domain of C11orf95, were essential to exert tumorigenesis. Applying cross-species comparative analyses, I showed that C11orf95-related fusions alter the expression of several specific transcriptional activators, such as the transcription factor GLI2, a sonic hedgehog signaling mediator gene. Targeting GLI2 with arsenic trioxide caused extended survival of tumor-bearing animals, identifying a potential therapeutic vulnerability in *C11orf95* fusion-positive tumors. Based on these findings, *C11orf95* is now officially designated as *zinc finger translocation associated (ZFTA)* by the HUGO Gene Nomenclature Committee. In addition, the WHO has accepted based on our work to call the group of supratentorial ependymoma carrying a fusion containing the ZFTA fusion gene Supratentorial ependymoma, ZFTA fusion-positive (ST-EPN-ZFTA; Louis et al., 2021; Zheng et al., 2021).

2.2 Various *ZFTA*-positive fusion genes were identified and formed separate clusters from the canonical ST-EPN-RELA cluster

Based on the DNA methylation profiling, our lab previously identified new clusters in addition to the three conventional ST-EPN groups, named Clusters 1-4. These clusters contain samples with partly calibrated scores < 0.9 for ST-EPN-RELA (Capper et al., 2018). Within these clusters, RNA-sequencing revealed fusions of *ZFTA* with different partner genes, including *MAML2* (n = 15), *MAML3* (n = 2), *SS18* (n = 2), *NCOA2* (n = 9) and a new type of *ZFTA-RELA* (Type 8; n = 2; Figure 2-1b).

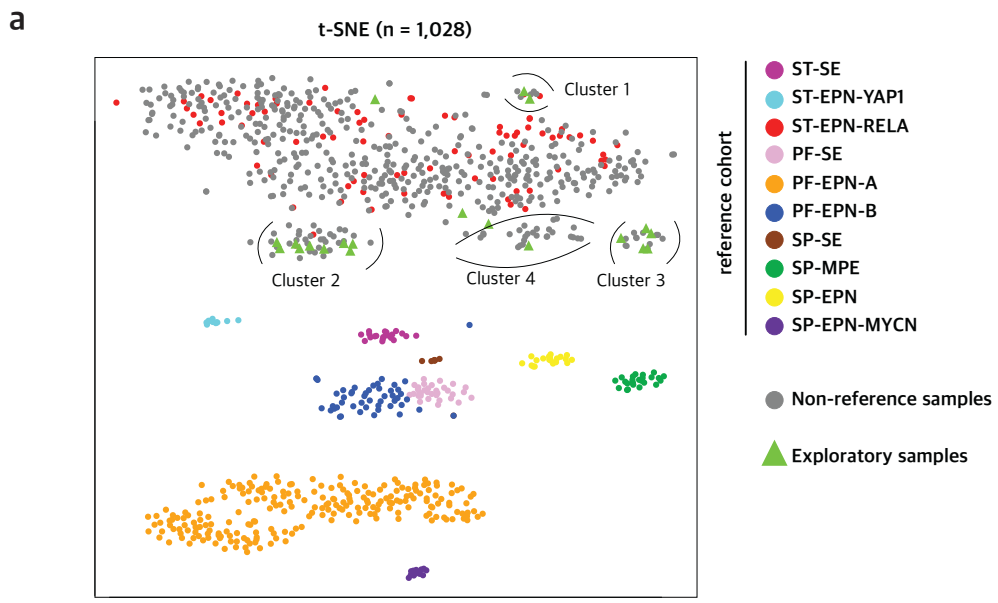

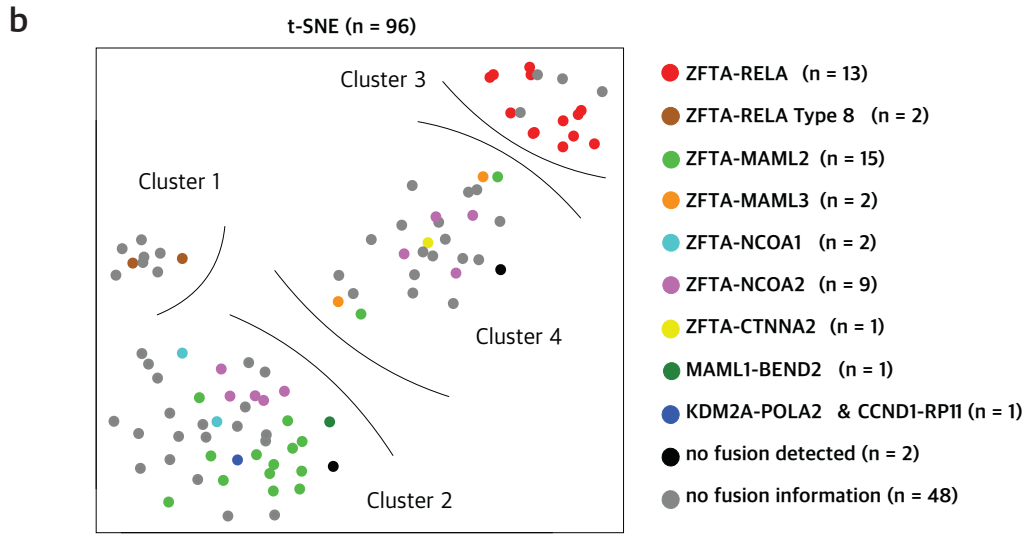

Figure 2-1 | New fusion genes and genetic heterogeneity in ST-EPN tumors.

a, Unsupervised clustering based on DNA methylation of ependymoma samples (n = 1028) using t-SNE dimensionality reduction. **b**, t-SNE analysis based on DNA-methylation profiling depicting fusions detected in each novel clusters. Cluster 2 and 4 show fusions of *ZFTA* with genes other than *RELA*, while cluster 1 and 3 depict different variants of *ZFTA-RELA*-fusions. Figure provided by David Ghasemi.

In order to validate the fusion breakpoints detected *in silico*, I performed the reverse transcription followed by PCR (RT-PCR). I amplified the region that covers the fusion breakpoint and extracted and sequenced the PCR fragment (Figure 2-2a). Various new fusion breakpoints sharing the common partner *ZFTA* were validated: *ZFTA-MAML2*, *ZFTA-MAML3*, *ZFTA-NCOA2* and *ZFTA-SS18*. All validated fusion genes were in frame, leading to the expression of the corresponding fusion proteins (Figure 2-2b).

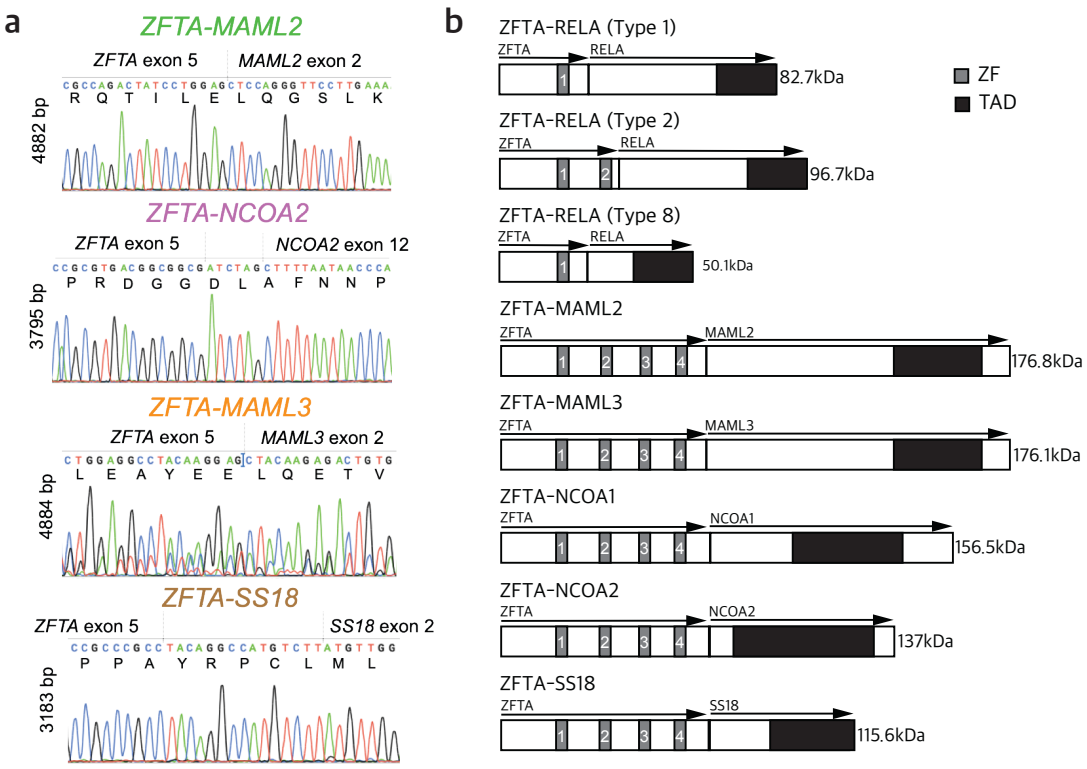

Figure 2-2 | New fusions genes are validated by RT-PCR and subsequent Sanger sequencing.

a, Sanger sequencing confirmed fusion constructs detected by RNA-sequencing. **b**, Illustration of the different fusion protein constructs containing ZFTA that were detected in the Clusters 1-4 (c.f. Figure 2-1b). ZF: zinc finger domain, TAD: transactivation domain.

2.3 The most N-terminal ZF domain from ZFTA is indispensable for tumor formation *in vivo*

The *ZFTA-RELA* fusion gene has been proven to drive tumor formation, when delivered to neonatal forebrain cells positive for either NESTIN, GFAP or BLBP using the RCAS/TVA system (Ozawa et al., 2018), suggesting that canonical ST-EPN-RELA formation may result from single-hit oncogenesis in cells at an early stage during development. This prompted me to test whether the respective fusions detected in Clusters 1-4 are sufficient to cause tumor formation as well.

2.3.1 ZFTA fusion proteins induce tumor formation in mouse model by IUE

To investigate this, I cloned the recurrently identified fusion genes (*ZFTA-RELA*, *ZFTA-MAML2*, *ZFTA-MAML3*, and *ZFTA-NCOA2*) into the Tol2-based doner vector (pT2K) that allows the expression of fusion genes together with the luciferase reporter in the target cells (c.f. section 1.5.3 and Figure 1-5 for principles of Tol2 transposon system). All the fusion genes were tagged with the human influenza hemagglutinin surface glycoprotein (HA) allowing further detection for the fusion proteins via immunostainings. The reporter gene luciferase was co-expressed through the internal ribosome entry site (IRES) which allowed to follow the tumor development *in vivo* via injection of luciferin, a substrate of luciferase enzyme (Hastings, 1996). Bioluminescence is produced during the catalytic reaction of luciferase-luciferin which can be easily detected through a non-invasive in vivo imaging system (IVIS®) in the living mice. To generate a stable expression of the fusion gene in the cell of interest in the mouse brain, I used the *in-utero* electroporation (IUE) gene transfer technology combined with Tol2 transposon system (Tabata & Nakajima, 2001). In short, I injected the mixture of pT2K plasmid with the Tol2 transposase (T2TP) into the cells of the cortical ventricular zone via a microinjector at embryonic day 13.5 (E13.5) and applied an electric pulse immediately after the injection to deliver the plasmids into the cells (Figure 2-3).

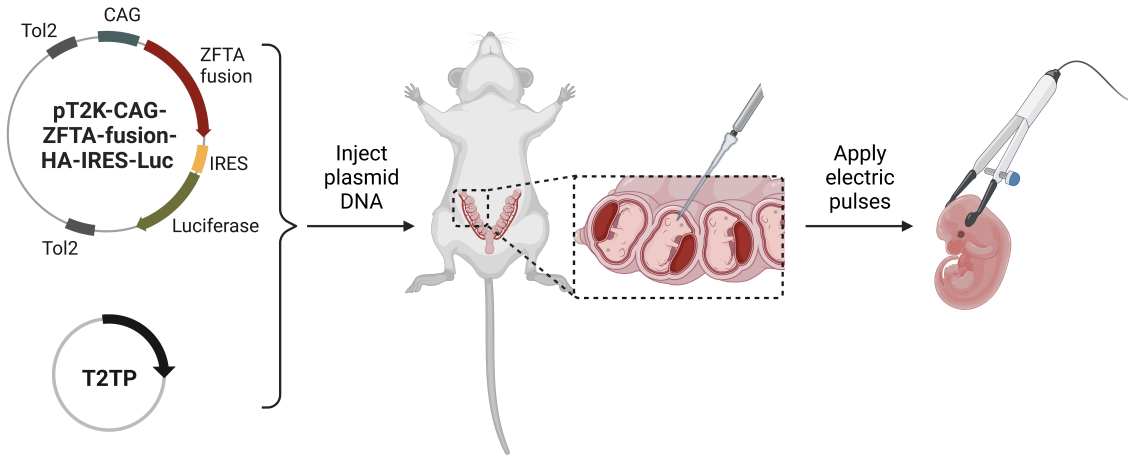

Figure 2-3 | Graphical illustration of the *in-utero* electroporation technique.

All plasmid constructs are tagged with the human influenza hemagglutinin surface glycoprotein (HA). *ZFTA* or *ZFTA*-fusion constructs were cloned into the pT2K transposable vector and injected with the Tol2 transposase (T2TP) into the lateral ventricle of E13.5 wild-type mice followed by transfection using an electroporation-based *in vivo* gene transfer approach. CAG: CMV early enhancer/chicken beta actin promotor, IRES: internal ribosomal entry site, Tol2: Tol2 terminal inverted repeats sequence recognized by T2TP. Figure created with BioRender.com.

As expected based on the results from our previous study (Pajtler et al., 2019), when we electroporated canonical *ZFTA–RELA* or *YAP1–MAMLD1*, the fusion proteins induced tumor formation in the cerebral cortex with a median survival of 44 and 29.5 days (n = 11/11 for *ZFTA–RELA* and n = 30/30 for *YAP1–MAMLD1*), respectively, whereas no tumors were formed by overexpression of wild-type *ZFTA* (n = 0/13; Figure 2-4a). When I overexpressed *ZFTA–MAML2* (n = 11/11), *ZFTA–MAML3* (n = 5/11), and *ZFTA–NCOA2* (n = 5/5) fusion genes, they induced tumors with a median survival of 29, 142, and 36 days, respectively, with 100% penetrance except for *ZFTA-MAML3* (Figure 2-4a). Histopathological assessment using H&E staining the *ZFTA* fusion–driven mouse tumors showed 3 common features that share with human tumors: 1) high density of small round cells, 2) highly vascularized and 3) sharp demarcation from the surrounding healthy brain regions (Figure 2-4b, c, d and e). Together, all the newly identified recurrent *ZFTA* fusion genes were able to drive tumorigenesis *in vivo* and displayed common histological features.

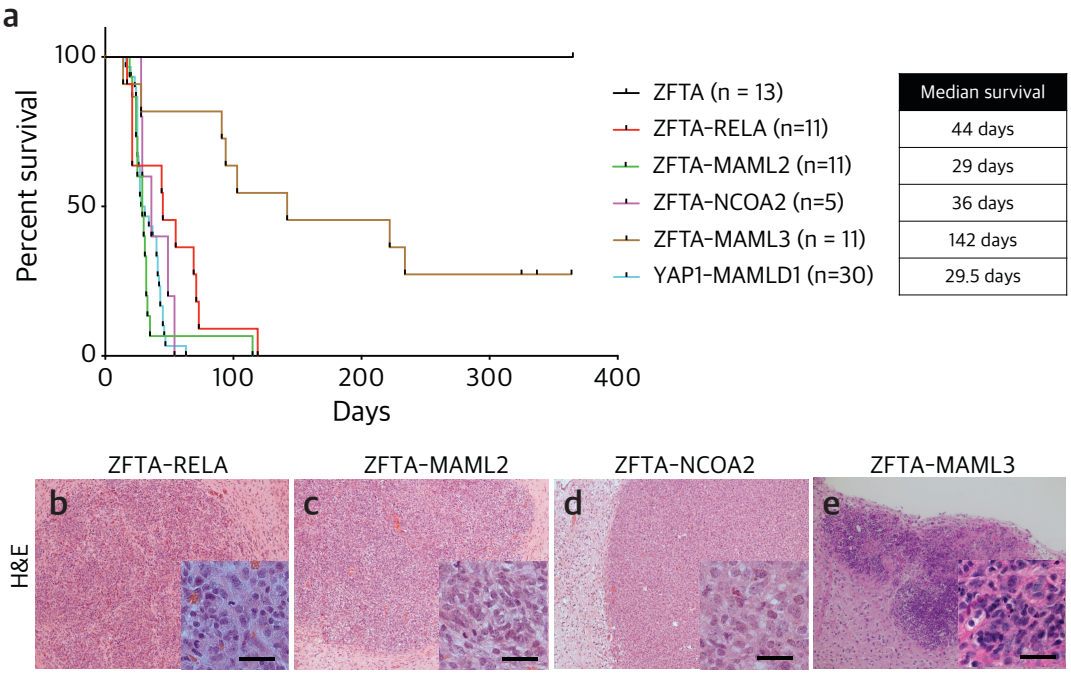

Figure 2-4 | *ZFTA* fusion-driven mouse models generated by IUE displayed similar features.

a, Kaplan-Meier survival curves of the animals electroporated with *ZFTA* or indicated *ZFTA* fusion genes. Note that *YAP1-MAMLD1* was used as a positive control. **b-e**, Micrographs (H&E) of *ZFTA* fusion-driven tumors in mice. (Scale bar = 300 μm and 50 μm for insets).

2.3.2 A shared ZFTA DNA binding domain is essential for tumor formation

Based on the fact that 1) ZFTA contains four ZF domains which function as DNA binding domain (Figure 2-2b) and 2) nuclear localization signal (NLS) mapper detected several NLS regions across the ZF domains (Kosugi et al., 2008; Kosugi, Hasebe, Matsumura, et al., 2009; Kosugi, Hasebe, Tomita, et al., 2009), I decided to investigate the role of ZF1 (most N-terminal ZF DNA binding domain) as this domain is the only ZF shared by all of ZFTA in tumorigenesis. I first applied immunohistochemistry staining on the mouse ZFTA fusion-driven tumors using an antibody against HA-tagged fusion proteins. Results showed a nuclear localization of the ZFTA fusion proteins in all tumors (Figure 2-5a, b and c). I subsequently deleted the ZF1 (ΔZF1) from all the fusions and overexpressed these in human HEK293T cells (Figure 2-5d, e, f, g, h and i). Staining against the fusion proteins (anti-HA, in red) and cell nuclei (DAPI, in blue) revealed the shuttling of the ZFTA(ΔZF1)-RELA fusion from the nucleus to the cytoplasm (Figure 2-5d and g), while the nuclear localization capacity retained in the ZFTA(ΔZF1)-MAML2 and ZFTA(ΔZF1)-NCOA2 fusion in HEK293T cells (Figure 2-5e, h, f and i). The result also implied that ZF1 is part of a NLS in the canonical ZFTA-RELA fusion. The fact that alternative ZFTA fusion proteins can still shift to the

nucleus suggested the potential NLS located in the other ZF domains of ZFTA and/or fusion partners.

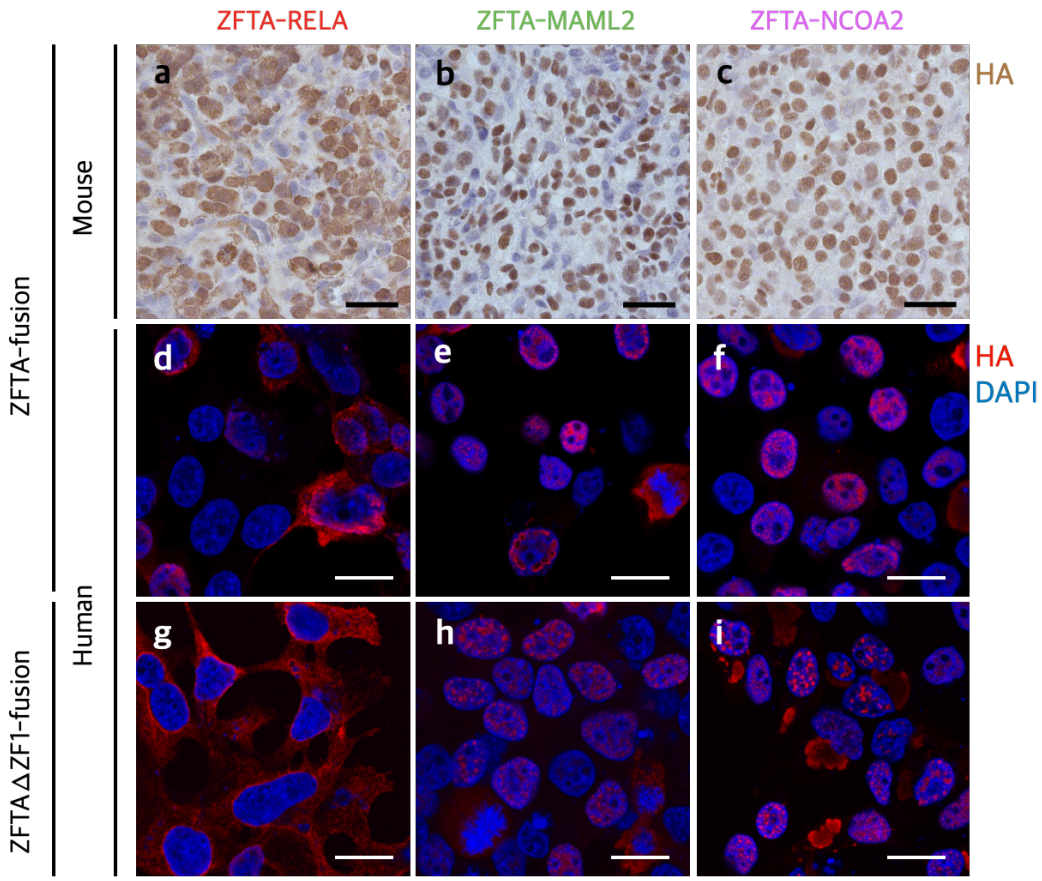

Figure 2-5 | Localization of ZFTA-related proteins in mouse and human cells.

a-c, IHC staining using an anti-HA antibody on respective ZFTA-RELA/MAML2/NCOA2-driven tumors in mice (Scale bar = 50 μm). **d-f**, Immunofluorescence (IF) staining against HA for ZFTA fusions overexpressed in HEK293T cells. **g-i**, IF staining against HA for ZFTA(ΔZF1)-RELA/MAML2/NCOA2 overexpressed in HEK293T cells. (Scale bar = 10 μm).

Since ZFTA-RELA serves very likely as a transcription factor (TF), the fact that it was excluded from the nucleus by deleting the ZF1 might cause the loss of function of the fusion protein subsequently hamper the tumor formation. Indeed, *in-utero* electroporation of the *ZFTAΔZF1* fusion genes failed to develop tumors in mouse (Figure 2-6). On the other hand, nuclear translocation still took place without ZF1 in the other ZFTA fusions which lost the tumorigenesis capacity *in vivo* as well, strongly indicating the importance of the DNA-binding ability of ZF1 in tumor formation.

Taken together, most common alternative *ZFTA* associated fusion types identified in human supratentorial tumors invariably lead to brain tumor formation *in vivo*. This result strongly suggested that a ZF domain shared among all fusion types was found to be essential for tumorigenesis and may function as a transcriptional regulator.

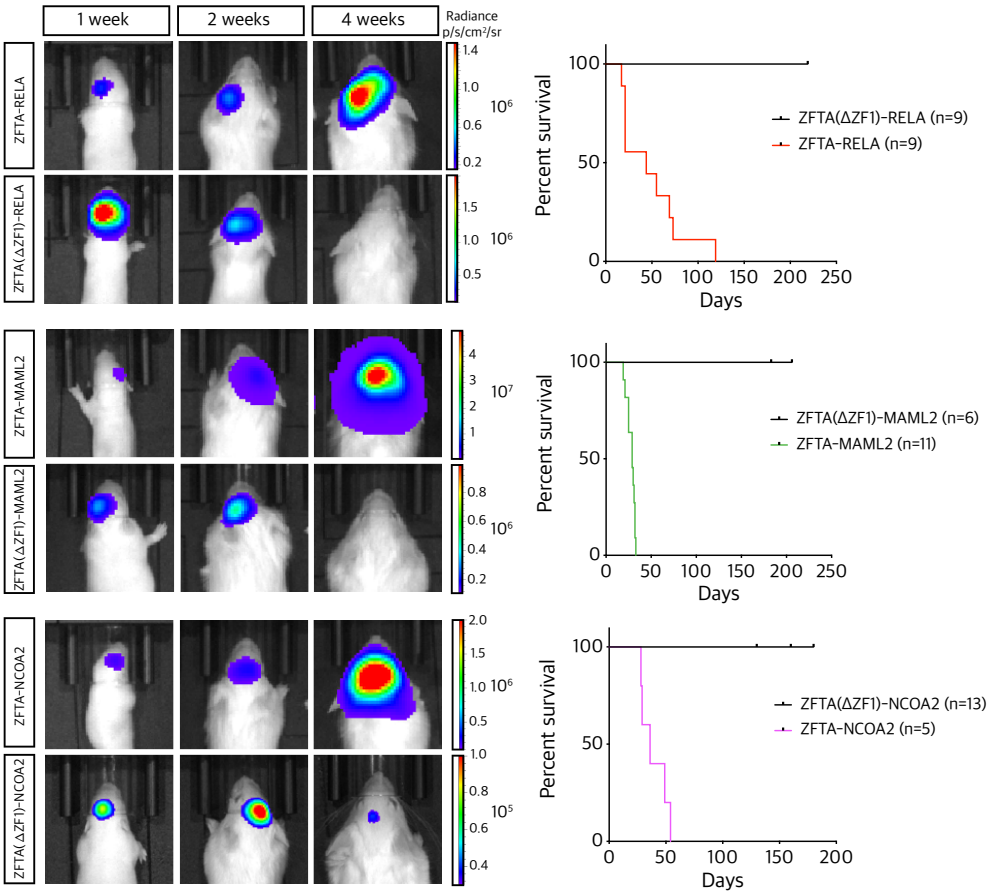

Figure 2-6 | ZF1 shared between all ZFTA fusions is essential for tumor formation *in vivo*.

In vivo bioluminescence images at weeks 1, 2 and 4 after birth of the electroporated animals with the respective Kaplan-Meier survival curves of mice electroporated with ZFTA-RELA and ZFTA(ΔZF1)-RELA/MAML2/NCOA2 constructs.

2.3.3 ZFTA fused with potent transactivation domains do not demonstrate transformation capacity *in vivo*

Transactivation domains (TAD) represented another shared element among oncogenic fusion proteins which located at the C-terminal of the proteins (Figure 2-2b). To further investigate the role of TADs for tumor formation, I generated artificial fusions that consisted of ZFTA and potent TADs, VP64 (Beerli et al., 1998), or EP300 (Eckner et al., 1994)

instead of fusion gene partners (Figure 2-7a). None of the animals electroporated with *ZFTA–VP64* or *ZFTA–EP300* developed tumors during surveillance over 12 months (Figure 2-7b, n = 0/6). These findings suggest that in addition to ZF1 further oncogenic mechanisms are associated with domains of the respective fusion partners. Importantly, this does not preclude an oncogenic role for the TAD within ZFTA–RELA and alternative fusion types, as Kupp et al. demonstrated that the TAD of RELA also contributes to the fusion-associated transcriptional program through recruitment of transcriptional coregulators (Kupp et al., 2021).

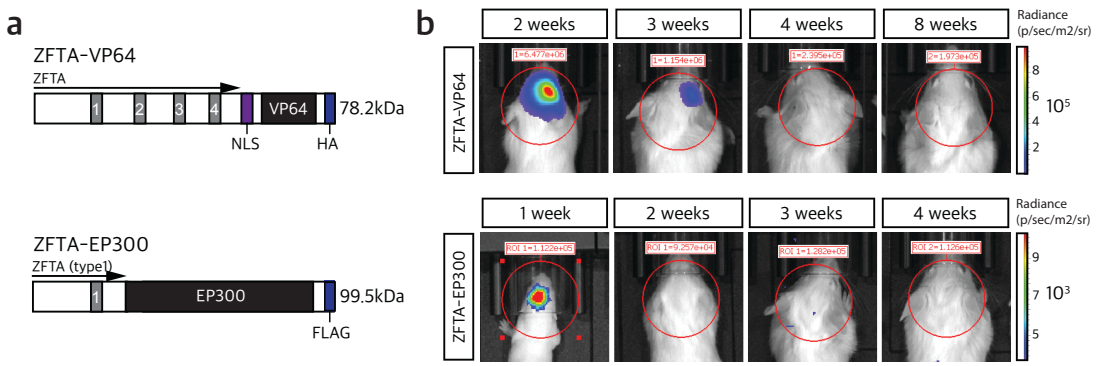

Figure 2-7 | ZFTA fused with potent transactivation domains do not demonstrate transformation capacity in vivo.

a, Illustration of artificial ZFTA-VP64 and ZFTA-EP300 fusion protein structures. HA: Human influenza hemagglutinin surface glycoprotein, NLS: nuclear localization signal (originally designed as part of VP64 in Beerli et al., 1998). **b**, *In vivo* bioluminescence images at indicated age of animals electroporated with ZFTA-VP64 and ZFTA-EP300.

2.3.4 Mouse models recapitulate human ST-EPN-ZFTA tumors at molecular level

Next, with the help of Konstantin Okonechnikov, I investigated the molecular characteristics of mouse tumors with *ZFTA* fusion genes. Total RNA was extracted from the snap-frozen mouse tumor chunk followed by Affymetrix microarray expression profiling. In order to integrate the human data, Konstantin and I first selected top 5000 most differentially expressed orthologous genes between the canonical ST-EPN-RELA and ST-EPN-YAP1. Principal component analysis of these selected genes demonstrated global differences at the transcriptome level between mouse tumors driven by *ZFTA* fusion genes and*YAP1-MAMLD1* fusion gene (Figure 2-8a; Pajtler et al., 2019). Unsupervised hierarchical clustering of the same gene set revealed distinct molecular signatures from the *ZFTA-RELA*, *ZFTA-MAML2* and *ZFTA-NCOA2*-driven mouse tumors. These ZFTA fusion-positive mouse tumors clustered together with human ST-EPN-RELA but not with human ST-EPN-YAP1

tumors (Figure 2-8b). Provided that the activation of *L1CAM* and *CCND1* as well as the activation of the NF-kB signaling pathway are striking molecular characteristics of ST-EPN-RELA (Parker et al., 2014), we examined these characteristics in the *ZFTA* fusion-driven murine tumors. *CCND1* but not *L1CAM* was highly expressed across all types of the fusion-driven tumors (Figure 2-8c and d).

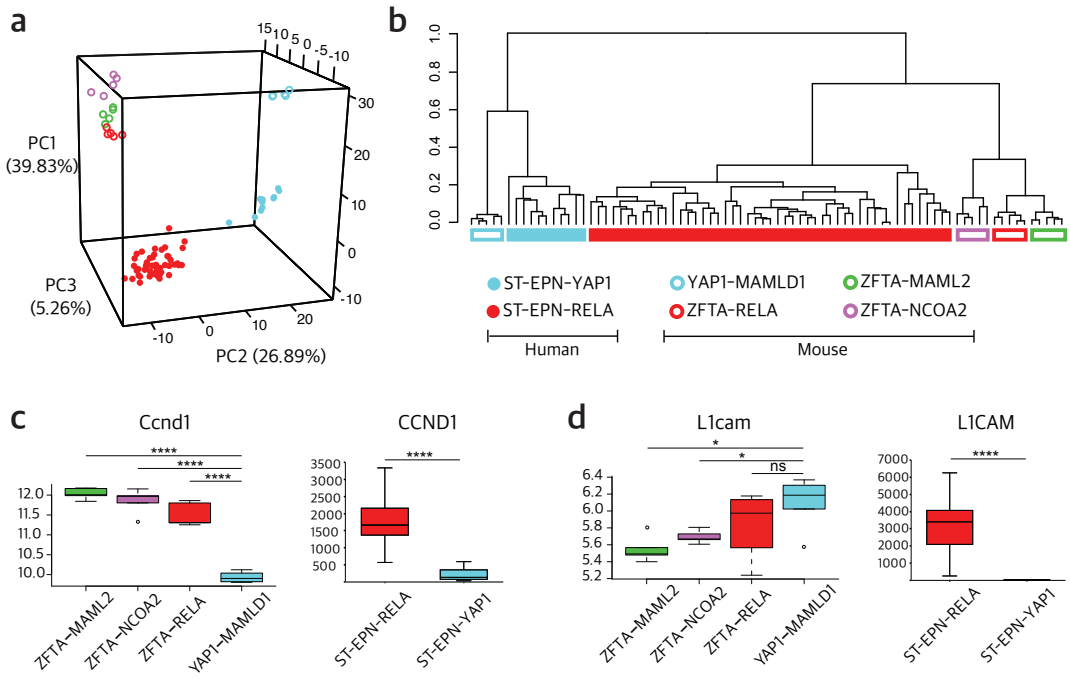

Figure 2-8 | *ZFTA* fusion-associated murine tumor models share molecular characteristics with human ST-EPN-RELA.

a-b, Principal component analysis in **a** and hierarchical clustering in **b** based on orthologous genes expressed in human ST-EPN-RELA (solid red) and ST-EPN-YAP1 (solid cyan) tumors and murine *ZFTA-RELA* (hollow red), *ZFTA-MAML2* (hollow green), *ZFTA-NCOA2* (hollow purple) and *YAP1-MAMLD1*-driven (hollow cyan) tumors. Each dot represents one tumor. **c**, Expression level of Ccnd1/CCND1 in mouse (left) and in human (right); ****P < 0.0001. **d**, Expression level of L1cam/L1CAM in mouse (left) and in human (right); ns, nonsignificant; *P < 0.0332; ****P < 0.0001.

However, I did not observe any global activation of the NF-κB pathway in the *ZFTA* fusion-driven models, indicating that aberrant activity of this pathway is not contributing to tumorigenesis in mice (Figure 2-9). In line with these findings, Kupp et al. observed that altering the Rel-homology domain in *ZFTA-RELA* fusions, which represents the DNA binding domain shared by the NF-κB family proteins for their signal transduction, did not result in loss of oncogenicity in mice (Kupp et al., 2021). As a direct transcriptional target of NF-κB pathway, *CCND1* was still upregulated without the global activation of this pathway (Guttridge et al., 1999; Hinz et al., 1999), suggesting that abnormal expression of CCND1 in

ST-EPN-ZFTA was attributed to other signaling pathways or ZFTA fusion proteins per se since they are very likely transcription regulators (Figure 2-8c).

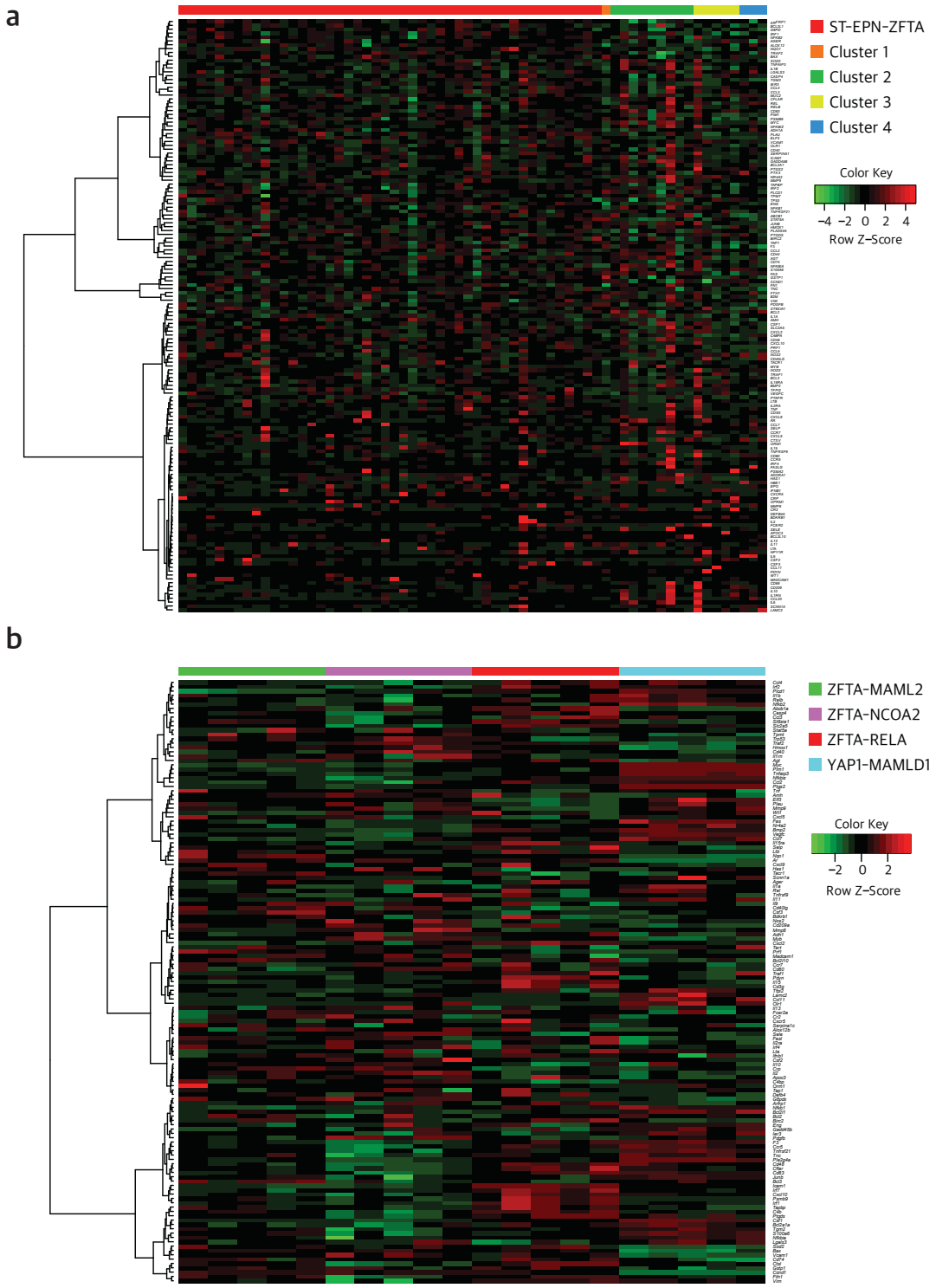

Figure 2-9 | The NF-kB signaling pathway is not activated in newly identified ZFTA fusion-driven tumors.

Heatmap showing expression of NF-kB pathway target genes in human ST- EPN-RELA and Cluster 1-4 (**a,** n = 66) and indicated mouse models (**b,** n = 20).

2.4 Cross-species analysis identifies putative oncogenes downstream of ZFTA-fusions

Since there was evidence that the same DNA binding domain of ZFTA is required for oncogenicity, I further explored common downstream effectors induced by transactivation of the *ZFTA*-associated fusion genes (Figure 2-2b). To this end, we chose a cross-species approach to concisely match signaling pathways between human tumors and mouse models. To exclude the ependymoma cell identity signature genes across molecular groups that we had observed previously (Mack et al., 2018), we selected differentially expressed genes for human primary ST-EPN-RELAs significantly upregulated compared to all other molecular groups of EPNs (n = 3825 genes; Figure 2-10a). We used a similar approach to compare gene expression data from *ZFTA*-driven mouse tumors against data from murine *YAP1-MAMLD1* tumors representing the only available alternative faithful model system (Pajtler et al., 2019). We found that 2637 genes shared by *ZFTA* fusion-driven murine tumors are significantly higher expressed in comparison to *YAP1-MAMLD1* tumors (Figure 2-10b). Filtering for orthologues in both mouse and human data resulted in 535 genes commonly upregulated in *ZFTA* fusion-related tumors across species (Figure 2-10).

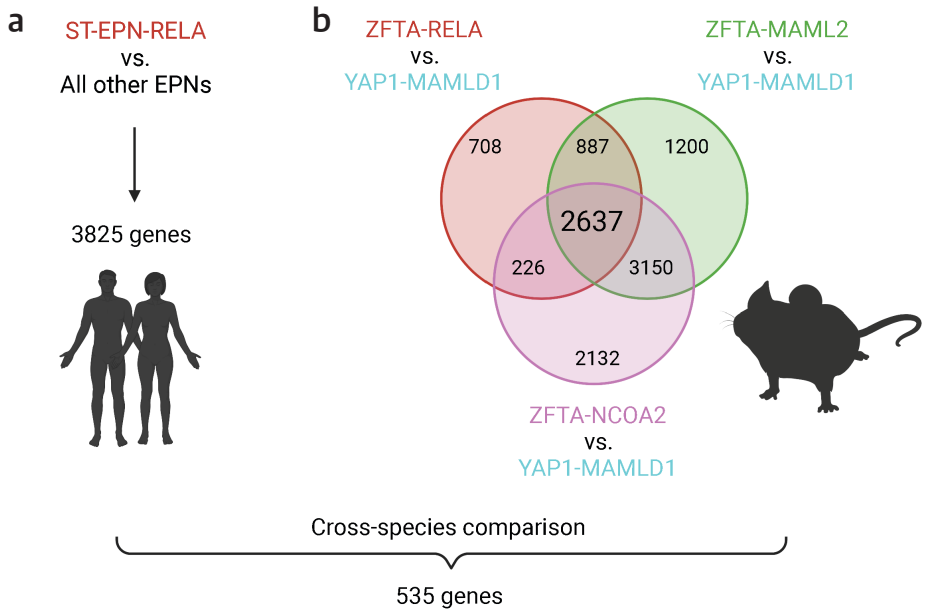

Figure 2-10 | Cross-species comparison narrowed down the putative downstream candidate oncogenes.

a, Differential expression analysis on Affymetrix microarray data of ST-EPN-RELA vs. all other EPNs human samples and **b**, on Affymetrix microarray data of *ZFTA*-fusion-driven murine models vs. *YAP1-MAMLD1*-driven murine. Integrated analysis resulted in 535 differentially expressed orthologous genes shared between human and mouse tumors. The Affymetrix data for human EPNs were generated using Affymetrix GeneChip Human Genome U133 Plus 2.0 Array and published in Pajtler et al., 2015.

A gene ontology analysis on the list of 535 genes revealed enrichment for cancer-related signaling pathways and partly convergence into known ST-EPN-RELA group-associated pathways, e.g., MAPK signaling (Figure 2-11a). I also found several well-known oncogenes, such as the sonic hedgehog (SHH) mediator gene *GLI2*, the WNT-mediator gene *LEF1* and the EPN oncogene *EPHB2* shared by *ZFTA* fusion-driven tumors (Figure 2-11a). Moreover, I found all three genes were specifically upregulated among the genes with highest expression in human ST-EPN-RELA as compared to other molecular groups of EPNs based on transcriptomics (Figure 2-11b).

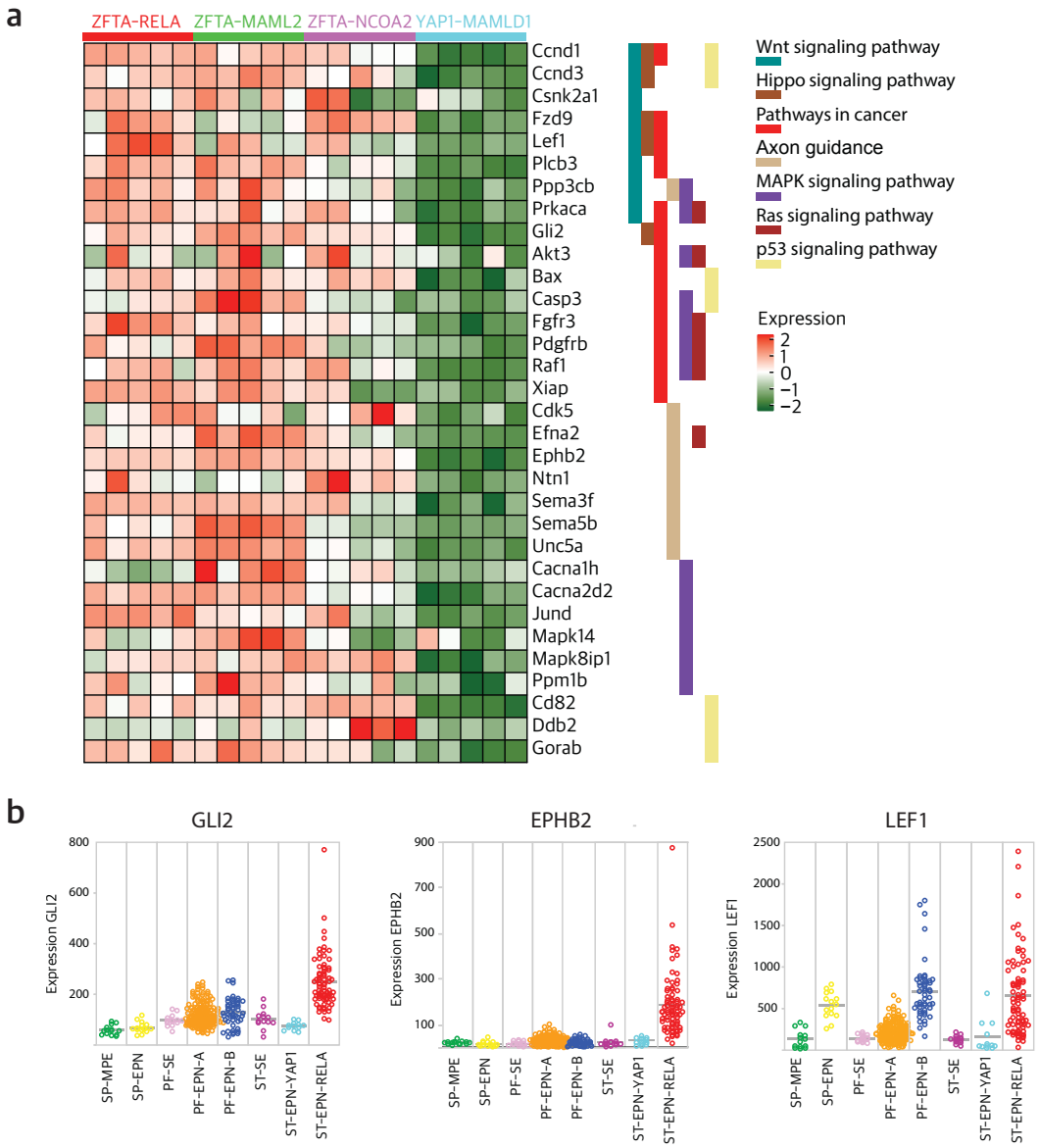

Figure 2-11 | Gene Ontology analysis indicates numerous upregulated genes implicated in cancer-related pathways.

a, Heat map reporting 32 genes implicated in cancer-related signaling pathways, which were extracted from a gene ontology analysis of 535 genes after human-mouse orthologous selection. **b**, Comparison of mRNA expression levels for *GLI2*, *EPHB2* and *LEF1* among different molecular groups of human EPNs based on Affymetrix gene expression data.

"To further explore potential direct interactions of *ZFTA* fusions with *Gli2*, *Lef1* and *Ephb2* gene loci, in collaboration with Stephen Mack's lab, we performed chromatin immunoprecipitation sequencing (ChIP-seq) with antibodies against HA and H3K27ac as well as assay for transposase-accessible chromatin using sequencing (ATAC-seq) analyses

on *ZFTA– RELA*-driven murine tumor cells. Indeed, the *ZFTA–RELA* fusion was found to directly bind to H3K27ac-marked open chromatin regions of *Gli2*, *Lef1*, and *Ephb2* (Figure 2-12)."

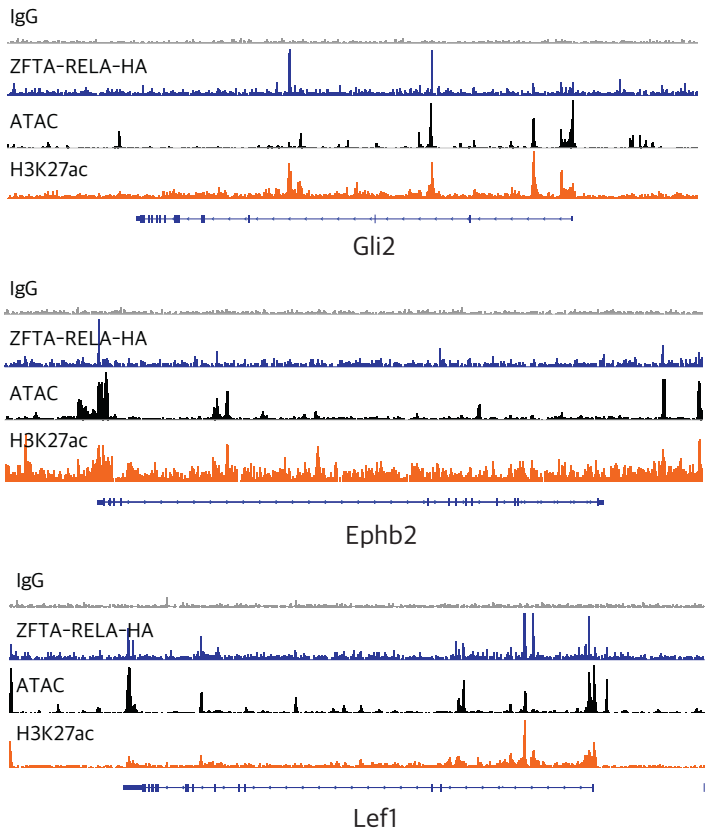

Figure 2-12 | Chromatin immunoprecipitation sequencing on IUE-derived ZFTA-RELA mouse tumors.

Plots of normalized and scaled ZFTA-RELA-HA, ATAC and H3K27ac RPKM profiles for candidate genes *Gli2*, *Ephb2* and *Lef1* in IUE-based ZFTA-RELA mouse tumor. Signals derived from ChIP-seq (peaks shown on the figures) showed interactions between ZFTA-RELA/ATAC/H3K27ac and the gene loci of *Gli2*/*Lef1*/*Ephb2*. Figure generated in collaboration with Stephen Mack.

In addition, we reanalyzed the ChIP-seq against H3K27ac and RELA on human canonical ST-EPN-RELA and -YAP1 tumors generated previously in our lab in collaboration with Stephen Mack (Figure 2-13; Mack et al., 2018). In ST-EPN-RELA, the peaks presented on *GLI2*, *EPHB2* and *LEF1* gene loci partially overlapped with the RELA-subgroup-specific enhancers indicated as red lines in the figure. Consistent with the mouse data, this result showed that *GLI2*, *EPHB2* and *LEF1* are ST-EPN-RELA tumor-specific enhancer genes in human (Figure 2-13).

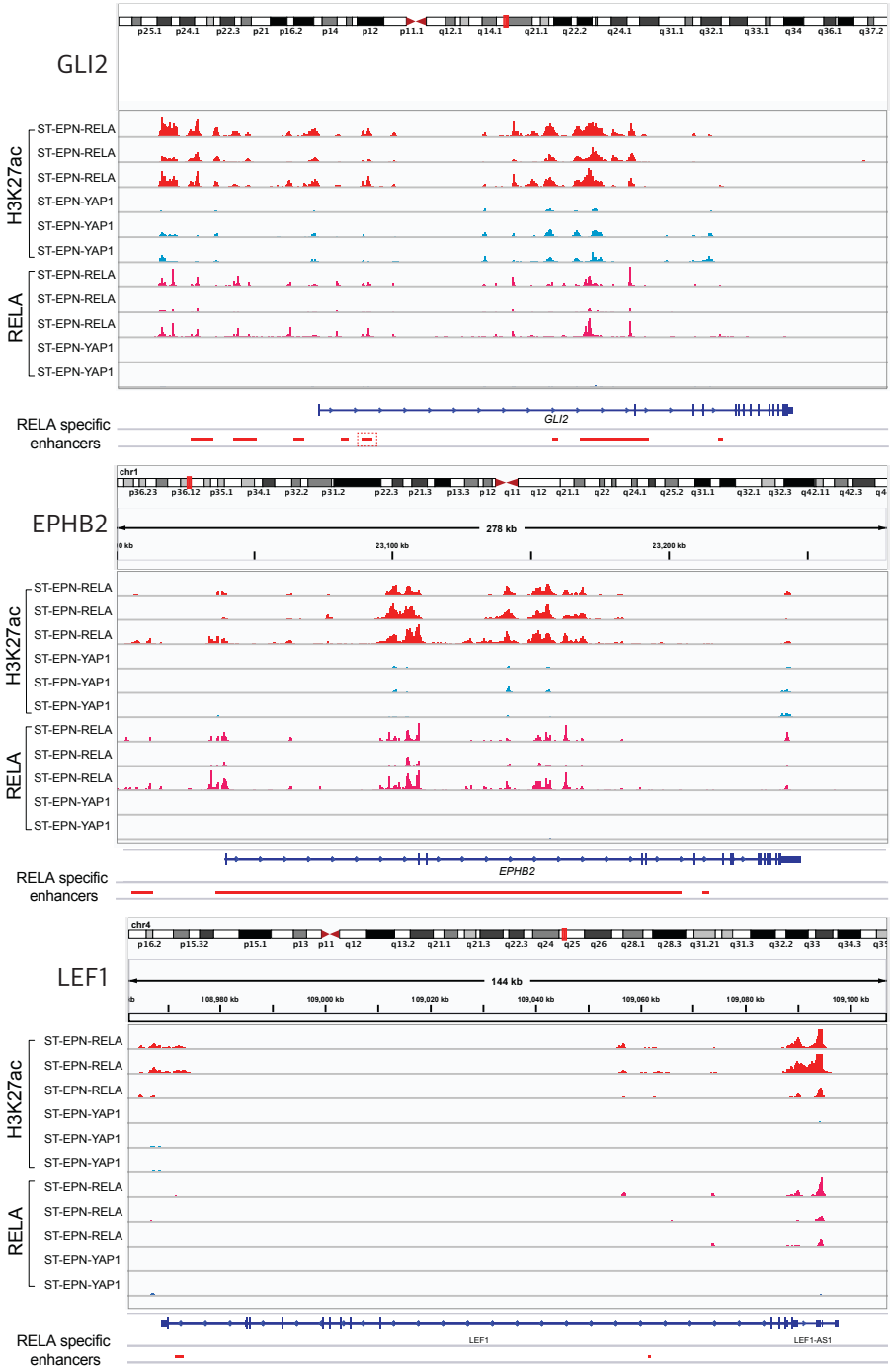

Figure 2-13 | Chromatin immunoprecipitation sequencing on human ST-EPN-RELA and -YAP1.

Plots of normalized and scaled H3K27ac and RELA RPKM profiles for candidate genes *GLI2*, *EPHB2* and *LEF1* in human ST-EPN-RELA (n = 3) and ST-EPN-YAP1 (n = 3). ST-EPN-RELA-specific enhancer regions are given as red lines. Data generated in collaboration with Stephen Mack and published in Mack et al., 2018.

2.5 *GLI2* represents a candidate downstream target of *ZFTA* fusion-associated tumorigenesis *in vivo*

To examine a potential functional implication of the revealed genes for *ZFTA*-driven tumorigenesis, I subsequently generated plasmids harboring *ZFTA-RELA* together with genes encoding a dominant-negative form of *Gli2*, *Lef1 and Ephb2*, respectively (Figure 2-14). A dominant-negative mutation adversely affects the normal, wild-type gene function competitively within the same cell. The plasmids were then delivered into the mouse brain at E13.5 stage using the same IUE technique as described above.

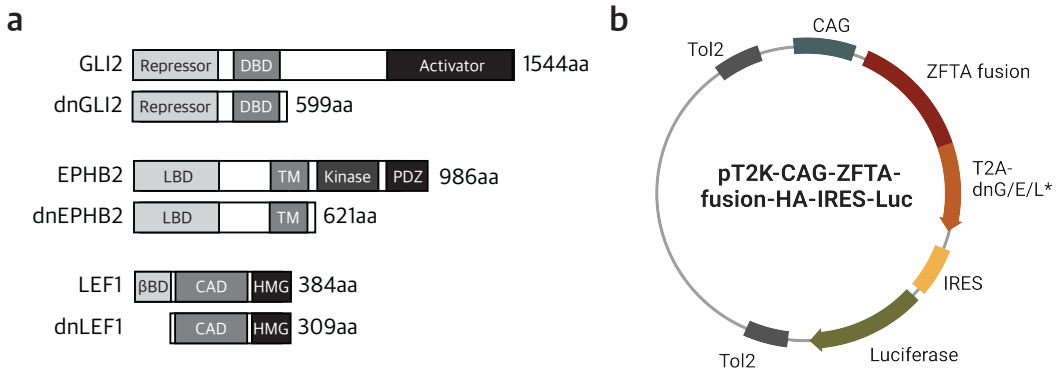

Figure 2-14 | Graphical illustration of the dominant-negative forms of the candidate genes.

a, Illustration of the proteins GLI2, EPHB2, LEF1 and their respective dominant-negative forms. DBD: DNA binding domain, LBD: ligand binding domain, TM: transmembrane domain, PDZ: beta-catenin-binding domain, CAD: context-dependent activation domain, HMG: high-mobility group DNA-binding domain, aa: amino acid. **b**, Illustration of the plasmid vector carrying *ZFTA-RELA* fused to the genes encoding a dominant-negative form of indicated oncoproteins with T2A self-cleaving peptides.

2.5.1 A dominant-negative form of GLI2 hampers tumor initiation in the ZFTA-RELA IUE model

While the genes encoding the C-terminal portion of LEF1 and the ectodomain of EPHB2 did not prevent tumor development, the N-terminal portion of GLI2 (dnGLI2) that competitively inhibits GLI2 transactivation hampered the tumor initiation (Figure 2-15a and b). The result indicated the requirement of *GLI2* function for *ZFTA* fusion-associated tumorigenesis. Moreover, we found that *GLI2* transcription factor binding sites were highly enriched in histone H3K27ac-marked enhancers and super-enhancers of human ST-EPN-RELAs reported in the previous study from our lab (Mack et al., 2018), further suggesting a decisive role of this oncogene.

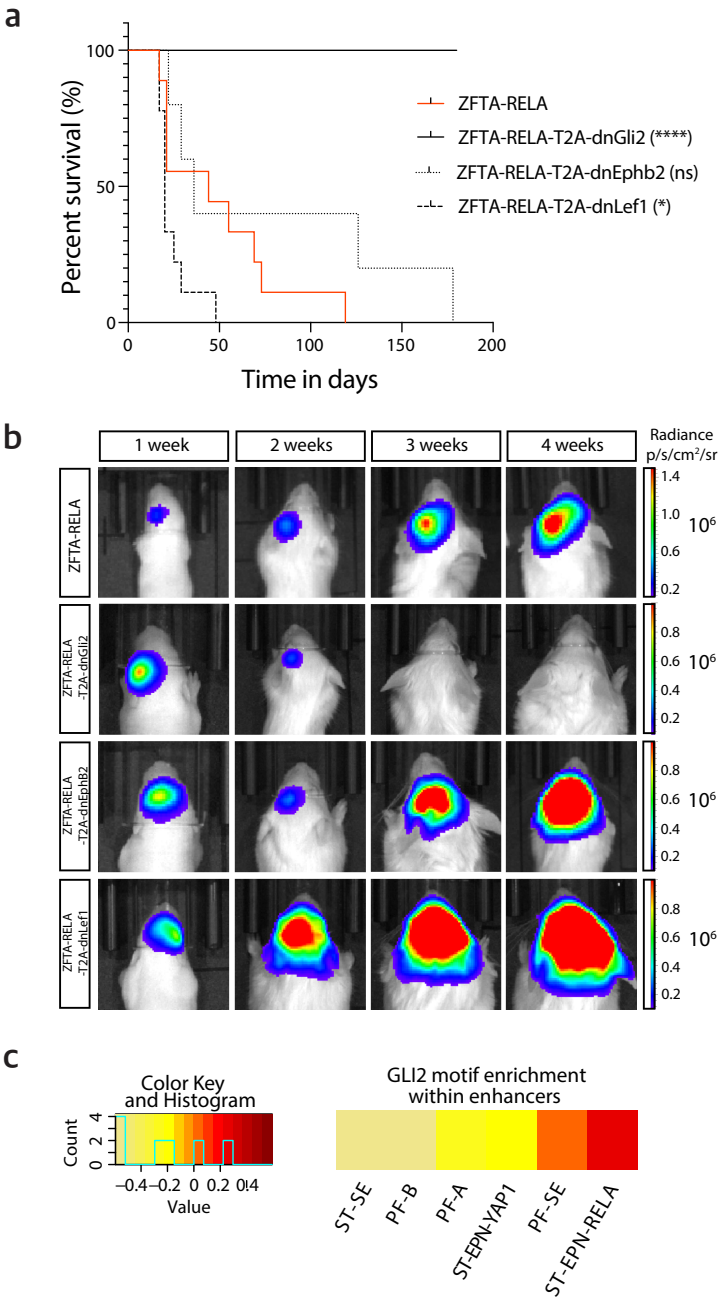

Figure 2-15 | Co-expressing dnGli2 together with ZFTA-RELA *in vivo* suppresses the tumor formation.

a, Kaplan-Meier survival curves of mice electroporated with ZFTA-RELA (median survival = 44 days) or ZFTA-RELA-T2A-dnGli2 (solid line), -dnEphb2 (dashed line, median survival = 36 days), -dnLef1 (dotted line, median survival = 20 days) constructs. ****P < 0.0001, *P = 0.0201, ns: non-significant. **b**, *In vivo* bioluminescence images at week 1-4 after birth of animals electroporated with indicated constructs. **c**, Transcription factor enrichment analysis of GLI2 within histone H3K27Ac-marked enhancers across human primary ST-EPNs and PF-EPNs.

2.5.2 *GLI2* knockdown *in vitro* induces a decrease in cell proliferation and increase in cell apoptosis

To investigate whether *GLI2* contributes to progression of ST-EPN-RELA tumors, I decided to analyze tumor cell behavior upon *GLI2* knockdown (KD) *in vitro* using cell proliferation and cell apoptosis as readout. For this purpose, I used a characterized ST-EPN cell line, EP1NS, which expresses *ZFTA-RELA* fusion. I created two doxycycline (dox)-inducible shRNAs targeting two different locations of the coding region of human *GLI2* (shGLI2_1 and shGLI2_2; Figure 2-16a) as well as a non-targeting control shRNA (shControl). EP1NS cells were infected with a lentivirus containing either shGLI2_1 or shGLI2_2 and selected positive cells with puromycin. I observed approximately 40% reduction of *GLI2* at the transcriptional level 48h after administration of doxycycline (2 µg/mL; Figure 2-16b).

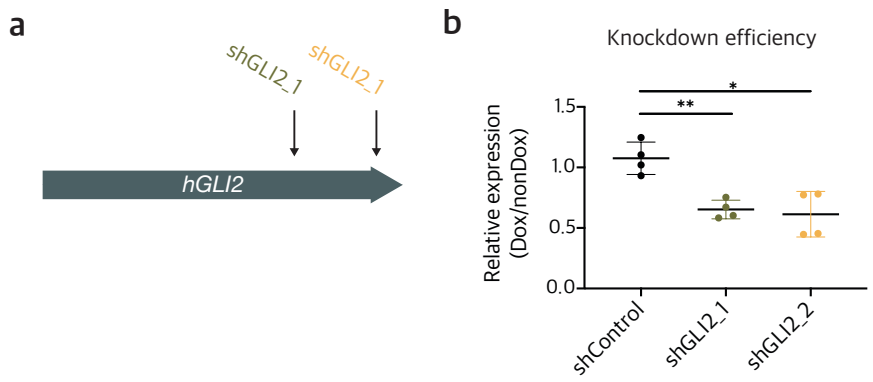

Figure 2-16 | Inducible *GLI2* knockdown system *in vitro*.

a, Illustration of the shRNAs targeting indicated regions on the human *GLI2* transcript. **b**, Relative expression of *GLI2* at mRNA level in the EP1NS cell line 48h after dox-treatment inducing shGLI2 expression. P value determined by paired t test. shGLI2_1: n = 4, mean = 0.6529, SD = 0.07702, P = 0.0041; shGLI2_2: n = 4, mean = 0.6137, SD = 0.1887, P = 0.0465. shControl: n = 4, mean = 1.076, SD = 0.134. **P < 0.005, *P < 0.05

In order to analyze the cell proliferation upon *GLI2* KD, I labelled the cells with a DNA intercalator ethinyldesoxyuridin (EdU) 96h after shRNA induction. Cell number, labelling time, and EdU concentration might affect the readout and these parameters vary depending on the cell type. Therefore, I assessed the readout using various conditions and prior to the experiment. It is better to assess the readout when 30-50% of the cells are proliferating because when more cells are labelled with EdU, it is very likely that some cells are already entering the second cell cycle which makes the result hard to interpret. In the end, 6 hours EdU labelling time matched the requirement (Figure 2-17a). Regarding the seeding number of the cells, I observed an over-confluence with 200 thousand (200K) seeding number by the end of 96h dox treatment, which could inhibit cell growth and subsequently

affects the result. In contrast, no over-confluence was perceived with 100K seeding number which presented a more reliable result. Within the 6 hour - 100K cells settings, the EdU concentration did not seem to be an influential factor (Figure 2-17a). The shGLI2-expressing cells showed a significant decrease in cell proliferation as compared to the shControl-expressing cells (Figure 2-17b). In addition, I stained the cells with Annexin V, a cell marker for early apoptosis, to explore a potential effect of *GLI2* KD on this cellular process. I observed significantly increased apoptotic events in the KD cells when compared to the control cells (Figure 2-17c). These results indicate that the inhibition of *GLI2* expression in ST-EPN cell line leads to a reduced proliferation and increased cell death, which may contribute the slowdown of ST-EPN tumor progression *in vivo*.

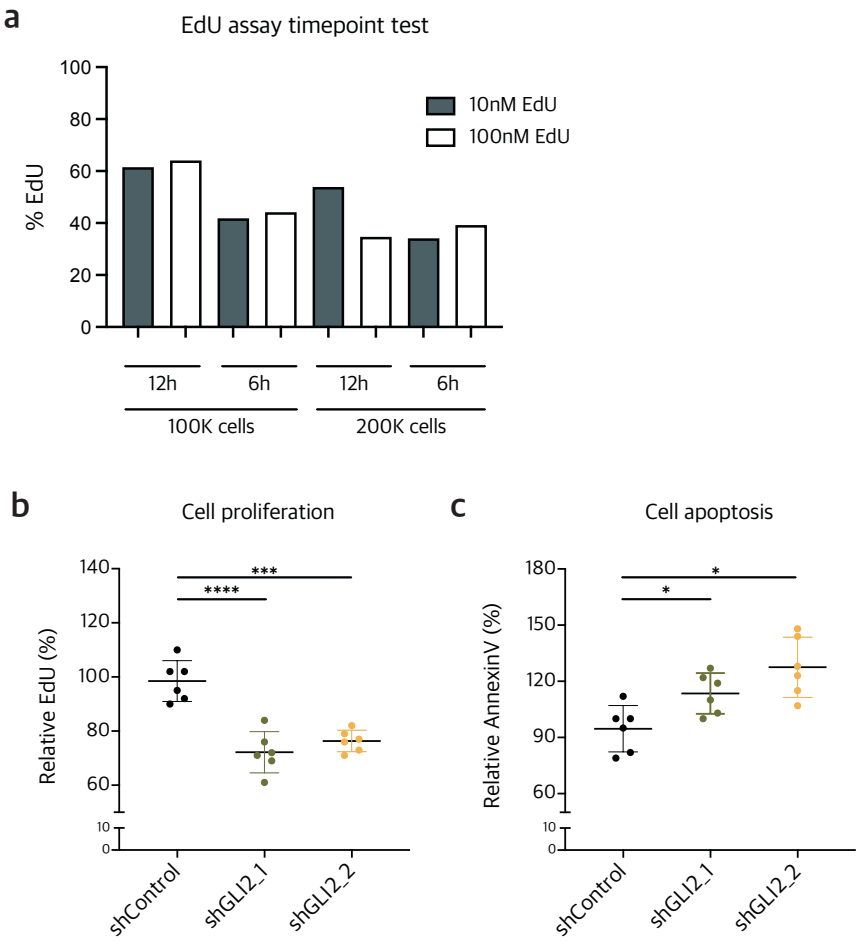

Figure 2-17 | Change in cell proliferation and cell apoptosis in a ST-EPN-RELA cell line upon *GLI2* knockdown.

a, Determination of the optimal parameters for the EdU assay in the EP1NS cell line. **b-c**, Relative level of EdU (**b**) and Annexin V (**c**) in the EP1NS cell line 96h after dox-treatment normalized to the ones without dox-treatment. P value determined by paired t test. For EdU: shGLI2_1: n = 6, mean = 72.17%, SD = 7.627, P < 0.0001; shGLI2_2: n = 6, mean = 76.33%, SD = 3.983, P = 0.0009; shControl: n = 6, mean = 98.5%, SD = 7.530.

For Annexin V: shGLI2_1: n = 6, mean = 113.5%, SD = 10.86, P = 0.0251; shGLI2_2: n = 6, mean = 127.5%, SD = 16.06, P = 0.0223; shControl: n = 6, mean = 94.67%, SD = 12.36. ****P < 0.0001, ***P < 0.001, *P < 0.05

2.5.3 *Gli2* knockout *in vivo* hampers ZFTA-RELA-driven tumorigenesis

To understand the importance of *Gli2* in tumor initiation, I generated an "All-in-one" plasmid which allows the overexpression of *ZFTA-RELA* fusion together with the knockout of *Gli2* via CRISPR/Cas9 system (Figure 2-18a). This vector was based on a PiggyBac transposon system (PB), which integrates the gene of interest specifically at TTAA tetranucleotides in the genome (Cary et al., 1989; Chen et al., 2020). The mice electroporated with sgRNA targeting *Gli2* (sgGli2) completely hampered tumor formation while with control sgRNA (sgCtl), mice developed tumor with 70% of penetrance (Figure 2-18b and c). The median survival of mice carrying ZFTA-RELA-sgCtl (297 days) is much longer than the one of overexpression of *ZFTA-RELA* alone (77 days) in the PB system (Figure 2-18b). This could be attributed to the low integrity efficiency of the gene of interest into the genome due to the nearly tripled size of the gene.

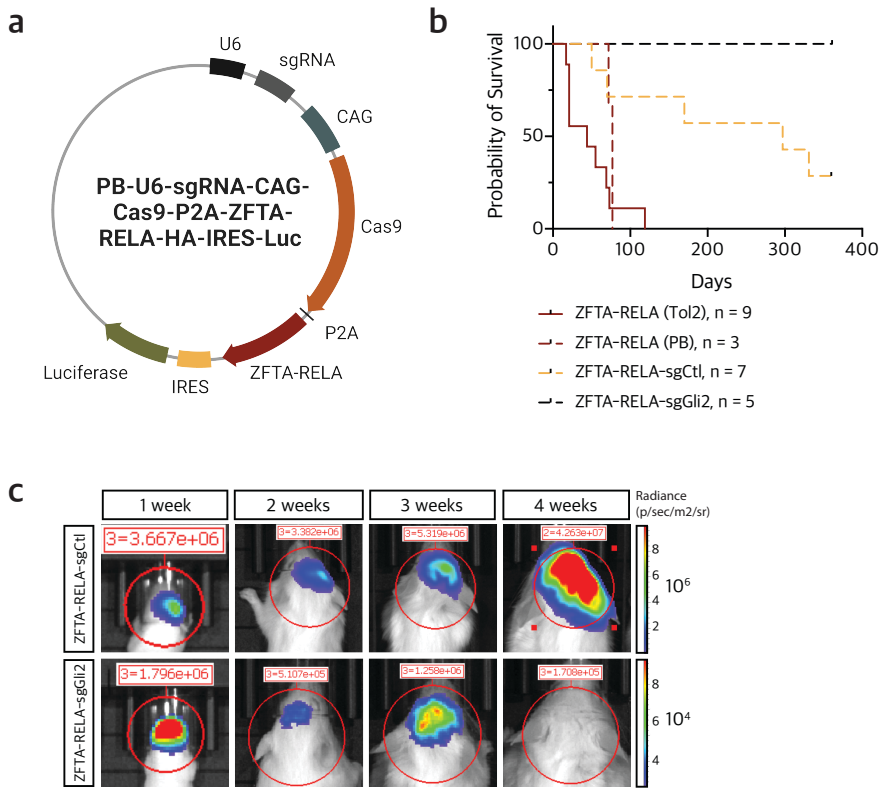

Figure 2-18 | *Gli2* knockout *in vivo* hampers ZFTA-RELA-driven tumorigenesis

a, Graphical illustration of "All-in-one" plasmid expressing ZFTA-RELA and knockout gene of interest via CRISPR/Cas9 system. **b**, Kaplan-Meier curves of the electroporated mice with ZFTA-RELA with Tol2 system (red line) and PB system (red dashed line); all-in-one construct with ZFTA-RELA and sgGli2 (yellow dashed line) or sgCtl (black dashed line). **c**, *In vivo* bioluminescence images 1-4 weeks after birth of animals electroporated with indicated constructs.

2.5.4 Arsenic trioxide treatment *in vivo* extends the survival

To further evaluate the functional role of GLI2 for tumor progression *in vivo*, I treated the IUE-based ZFTA-RELA-expressing mice with arsenic trioxide (ATO). ATO is a blood brain barrier-penetrating drug which includes GLI2 in its target spectrum (Neumann, Wefers, et al., 2017). The mice were treated with either 2.5 mg/kg ATO or vehicle 5 times per week via intraperitoneal injection as soon as the luciferase signal reached ca. $5x10^6$ photons/sec. I measured the luciferase signal weekly for tracking the tumor evolution (Figure 2-19a). The ATO-treated animals demonstrated extended survival when compared to vehicle-treated controls (Figure 2-19b and c). Together, both *in vitro* and *in vivo* data suggest GLI2 as a potential therapeutic target in *ZFTA* fusion-positive ST-EPN tumors.

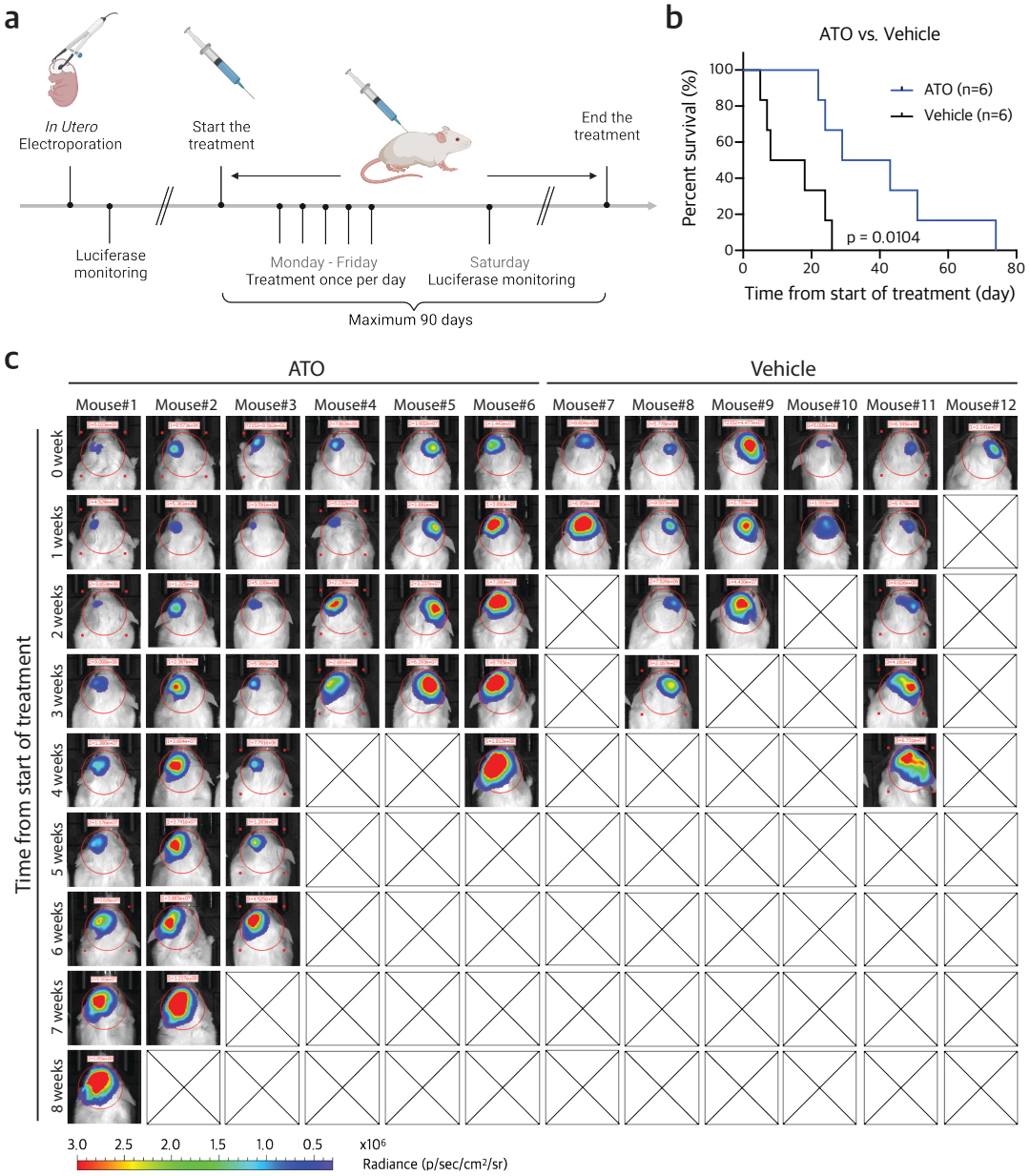

Figure 2-19 | ATO treatment in IUE-based ZFTA-RELA mouse model.

a, Graphical illustration of the ATO drug treatment plan. **b**, Kaplan-Meier curves of the electroporated mice treated with ATO (blue curve, median survival = 36 days) or vehicle (black curve, median survival = 13 days). P value determined by Log-rank test (P = 0.0104). All error bars represent standard deviation (SD) **c**, *In vivo* bioluminescence images post-treatment of ATO or vehicle on *ZFTA-RELA* fusion-driven mouse models over 8 weeks. Figure 2-19a created with BioRender.com

2.6 Establishment of ZFTA-RELA-driven allograft model

During the treatment of IUE-based ZFTA-RELA mouse models with ATO, I realized that the intra-strain variability of tumor occurrence presented in CD-1 outbred mouse line caused a significant difference in the starting time points of the treatment, which subsequently prolonged the time of the experiment and led to a considerable number of single treatments. Therefore, I engrafted the same pre-defined number of tumor cells from IUE-generated primary tumors into NSG mice to create a reliable allograft mouse model with synchronized tumor onset for future preclinical studies.

For the allograft models, I injected freshly prepared mouse tumor cells (1 Mo cells/mouse) intracranially into the cerebral cortex of the recipient mice and retransplanted the tumor cells *in vivo* for up to 3 passages (Allograft P1, P2 and P3). Detailed experimental procedure is described in Chapter 6 section 6.4.2. Tumors developed in all mice and at passage 3 the latency was significantly reduced albeit less cells were inoculated (0.5 Mo cells; Figure 2-20a). The survival curve of passage 3 is steeper which implies that tumors of this model have a more homogenous and aggressive growth pattern, and thus might be more suitable treatment studies (Figure 2-20a). Assessment of histopathology showed similar tumor morphology during the *in vivo* passaging (Figure 2-20b). Clustering based on DNA methylation profiling was performed in section 4.4), which showed molecular resemblance of the allograft models to the primary mouse tumors (Figure 4-2a and c). Analysis of expression profile is still ongoing.

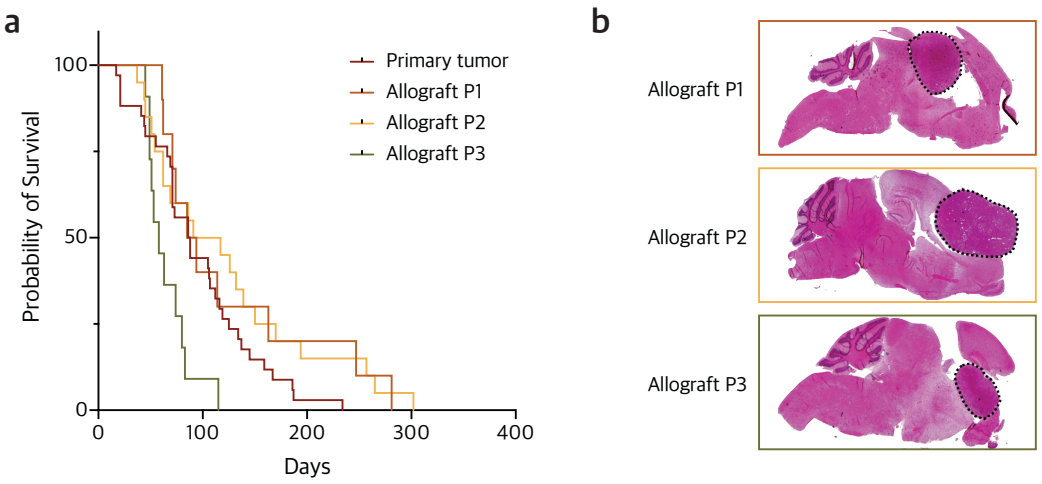

Figure 2-20 | ZFTA-RELA allograft model

a, Kaplan-Meier curves of the ZFTA-RELA IUE-based mouse model (red) and the respective allograft models in passage 1, 2 and 3 (orange, yellow and green). **b,** Representative images of H&E staining for

ZFTA-RELA allograft P1, P2 and P3. Dashed lines indicate the tumor area. H&E staining from b, was performed by Nina Hofmann.

2.7 Establishment of IUE mouse tumor cells cultured *in vitro*

One of the bottlenecks of studying ST-EPN is that only very few models are available. To my knowledge, besides the limited number of human cell lines and *in vivo* models such as IUE-based and RCAS/TVA-based mouse models mentioned in the beginning of this chapter, there are no human or mouse ST-EPN tumor cells that can be reliably long-term cultured *in vitro*. The largest advantage of an *in vitro* model is the strictly controlled environment and relatively easy manipulation and read-out. Therefore, in addition to the allograft model, I decided to culture the IUE-based mouse tumor cells in a dish. I tested several published neural sphere cultural media and commercialized neural progenitor media listed below (Table 2-1).

Media	Recipe		Reference
Neural stem cell maintenance media (NSCMM)	DMEM/F12, B27 (minus VitaminA, 1x), GlutaMAX, Non-essential amino acid (1/2x), CHIR-99021 (1.5 μM),	SB-525334 (2.5 μM), bFGF (40 ng/mL), EGF (40 ng/mL), hLIF (5 ng/mL), Heparin (2 μg/mL)	Haag et al. 2021
Tumor sphere media (TSM)	Neurobasal-A Medium (1X), D-MEM/F-12 (1X), HEPES Buffer (1M), MEM Sodium Pyruvate (1mM), Non-essential amino acid (0.1mM), GlutaMAX,	Antibiotic-Antimycotic (1X), B27 (minus VitaminA, 1x), bFGF (20 ng/mL), EGF (20 ng/mL), PDGF-AA (20 ng/mL), Heparin (2 μg/mL)	Lin & Monje 2017
NeuroCult™ NS-A proliferation media for human (hNCM)	Catalog # 05751		STEMCELL
NeuroCult™ proliferation media for mouse and rat (mNCM)	Catalog # 05702		STEMCELL

Table 2-1 | Overview of neurosphere culture media

Recipe for neural stem cell maintenance media (NSCMM) was provided by Daniel Haag which were designed for culturing iPSC-derived NSCs. Rcipe for tumor sphere media (TSM) was established by Monje's lab, initially used for mouse NSC culture and DIPG primary tumor cell culture (Lin & Monje, 2017). NeuroCult™ proliferation media for human and rodent cells are commercially available from StemCell and the recipes are proprietary.

I found that only in NeuroCult™ proliferation media for mouse & rat (mNCM), ZFTA-RELA-expressing mouse tumor cells can steadily expand. I performed immunofluorescence staining against the HA-tagged ZFTA-RELA fusion to validate the fusion gene expression in the cultured mouse tumor spheres (Figure 2-21). Consistent with the previous observation in the IUE mouse tumor (Figure 2-5), only a portion of the cells expressed the fusion gene (Figure 2-21). Intriguingly, fusion-harboring cells (HA-positive) did not overlap with the proliferating cells (Ki67-positive), which suggested a complex cell-cell communication across the fusion-positive and -negative cells (Figure 2-21). At molecular level, DNA methylation profiling of these *in vitro* cultured cells was investigated (results shown in Chapter 4 section 4.4) and their expression profile need to be further explored which is not part of this thesis. In the future, this model can serve as a robust complementary tool to study the underlying molecular mechanism of ST-EPN-ZFTA as well as various drug screenings *in vitro*.

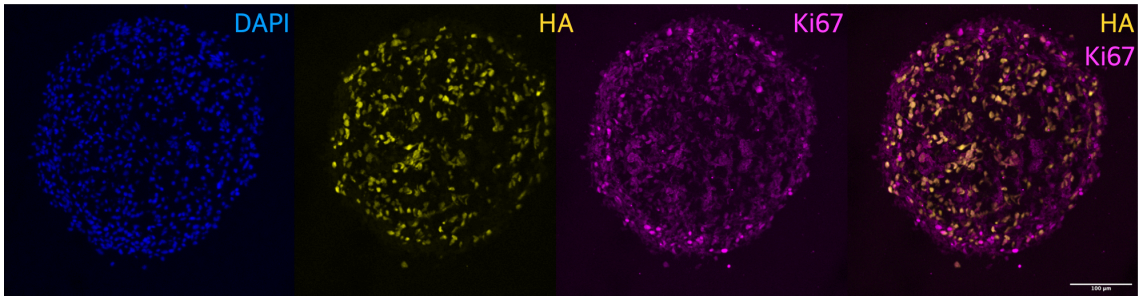

Figure 2-21 | Mouse tumor spheres cultured *in vitro*

Representative images of immunofluorescence staining against HA (yellow) and Ki67 (magenta). Cell nuclei were labelled with DAPI (blue). Scale bar = 100 μm.

2.8 Discussion

In this Chapter, a comprehensive molecular analysis of ST-EPN that identified additional satellite clusters related to ST-EPN-RELA was first introduced. The *RELA* fusion partner *ZFTA* was found to be a recurrent partner in alternative translocations within tumors that constituted these satellite clusters. These clusters are now included in the latest version of the Heidelberg Brain Tumor Methylation Classifier as part of the novel molecular family of ZFTA fusion-positive ST tumors (Capper et al., 2018; Hemmati et al.). The aim of this part of my thesis was to further investigate the biological heterogeneity of ST-EPN as a basis for identifying potential therapeutic vulnerabilities.

To this end, I first validated the expression of various ZFTA fusion proteins in ST tumors. Each of these fusion proteins caused tumor formation as single-hit in the cerebral cortex of mice, implying that they share oncogenic mechanisms. In line with the study from Kupp et al., I indeed identified a zinc finger DNA-binding domain of the fusion partner *ZFTA* as an essential element for tumorigenesis. This also resulted in the new official designation *zinc finger translocation associated (ZFTA)* by HUGO for the gene formerly known as *C11orf95*. In addition, protein structural comparison of all ZFTA fusion partners identified the presence of a shared transactivation domain (TAD), raising the possibility that ZFTA fusion oncoproteins activate oncogenes through recruitment of TAD to its targets.

Interestingly, the newly identified *ZFTA* fusion genes induced tumors with different penetrance and latency. This may be attributed to variable effects of the fusion partners on the transcriptional machinery in neural stem/progenitor cells (NSC). For instance, MAML2 and MAML3 are known to be cofactors of NOTCH, which is responsible for clonal expansion of cortical progenitors in the ventricular zone. However, MAML2 shows much stronger transcriptional activation of *Hes* genes than MAML3 (Wu et al., 2002). Therefore, *ZFTA-MAML2*- mediated enhancement of oncogenic signaling is likely to expand the fusion bearing NSCs more efficiently. In line with this speculation, I observed reduced survival in mice electroporated with *ZFTA-MAML2* compared to *ZFTA- MAML3*. Considering that NF-κB signaling is involved in NSC proliferation in the cerebral cortex (Widera et al., 2006; Young et al., 2006), *ZFTA-RELA* is also likely to expand the progenitor pool of the transfected cells, thus shortening the latency of tumor formation. Since the *ZFTA* fusion-positive ST tumors are characterized by distinct methylation profiles, it could also be hypothesized that each fusion oncoprotein may exert transformation activity in different NSC subtypes already committed to specific progenitors, as was reported for medulloblastoma (Schuller et al., 2008; Yang et al., 2008).

In addition, single cell RNA-sequencing on a cohort of ST-EPN-RELA and posterior fossa group A ependymoma (PF-EPN-A) revealed a larger inter-tumoral heterogeneity for *ZFTA-RELA*-positive tumors compared to PF-EPN-A (Gojo et al., 2020). Future single cell studies coupled with technologies for profiling the chromatin landscape may enable the inference of developmental lineages.

Notably, the ZFTA-positive oncoproteins were not detectable in all cells within the tumor area in mouse models, which underpinned the heterogeneity of these tumors. Partial expression of the fusion proteins in the tumor region strongly suggested the potential transformation capacity of the fusion proteins on the surrounding cells. This may serve as a basis to investigate the dependency of fusion protein expression during tumor development

and progression. It could be that the fusion protein simply acts as a trigger of the tumor initiation. In this case, identifying the way of communication between fusion bearing cells and surrounding cells as well as factors driving progression and proliferation of fusion-negative cells are critical to find out further therapeutic approaches. On the other hand, if both the tumor development and progression are reliant on the fusion gene expression, targeting the fusion genes using gene therapies or fusion proteins via vaccination would be an interesting therapeutic approach.

A previous animal study revealed the NF-κB- and non-NF-κB-related impact of *ZFTA-RELA* fusions on tumor formation by mutagenesis (Ozawa et al., 2018). In our study, we did not observe NF-κB pathway activation in tumors using IUE-based models. Consistent with this result, Arabzade et al. demonstrated that a major component of the fusion binding is tumor-specific and not observed in canonical NF-κB-related gene expression. In addition, Kupp et al. found that the Rel-homology domain is not required for fusion-driven gene expression. It remains to be further elucidated if at least transactivation domains that represent a shared pattern between fusions that cluster together and lack the Rel-homology domain, such as *ZFTA-NCOA1*, *ZFTA-NCOA2* and *ZFTA-MAML2*, may contribute to tumorigenesis through binding of transcriptional cofactors. Indeed, integrated cross-species analyses identified downstream targets shared by ST tumors with *ZFTA* fusions suggesting similar transcriptional activation processes. The results stress that *GLI2* functions as a relevant downstream oncogene in *ZFTA* fusion-driven ST tumors and pharmacological inhibition could significantly reduce tumor growth.

This study showed that GLI2 expression was modulated directly by ZFTA-RELA fusion protein via ChIP-seq and motif enrichment analysis. In addition to the modulation at transcriptional level, activation of numerous signaling pathways as well as protein stabilization processes may result in GLI2 upregulation. Although expression of canonical SHH signaling-related genes were not affected in *ZFTA* fusion-positive tumors, e.g., *PTCH1*, *SMO*, *SUFU*, the other non-canonical signaling pathways such as MAPK/Ras that has been proven to be involved in *GLI2* regulation appeared on the list using GO-term analysis (Kasper et al., 2006; McCleary-Wheeler, 2014). Strikingly, *FGFR3* is highly upregulated in ST-EPN-RELA and all *ZFTA* fusion-positive tumor models, which is one of the ligands that activates MAPK/Ras pathway, subsequently stabilizing GLI2 and preventing its degradation by the proteosome, thus resulting in upregulation of GLI2 activity independent of SHH signaling. *In vitro* evaluation of mouse basal cell carcinoma cells treated with an EGFR inhibitor gefitinib, another activator of the MAPK/Ras pathway, and the GLI inhibitor GANT1 demonstrated a synergistic effect in reducing cellular proliferation (Schnidar et al.,

2009). Therefore, we have planned to study the effect of a combined treatment with FGFR3 inhibitor and GLI2 inhibitor in *ZFTA* fusion-positive tumor models in the future.

Among the non-canonical SHH pathways altering *GLI2* expression, TGFβ is probably the most well-characterized, which allows a rapid induction of transcription of *GLI2* through the binding of SMAD3 on the *GLI2* promoter region (Dennler et al., 2009). Intriguingly, this region also includes TCF/LEF-binding site whereby Wnt signaling can participate through the binding of β-catenin region (Dennler et al., 2009). It implies that potentially the upregulation of LEF1 in *ZFTA* fusion positive tumors does not contribute directly to cell proliferation/survival but rather indirectly through the transcriptional activation of *GLI2*. This mode of action could very well explain the reason why overexpression of dominant-negative LEF1 did not diminish tumor formation *in vivo*.

With regard to EPHB2 that was previously described as ependymoma-associated oncogene and found to have transformation capacity when overexpressed in Blbp positive NSCs extracted from Cdkn2a$^{-/-}$ mice (Johnson et al., 2010). I found downstream effectors of EPHB2-mediated signaling, e.g., ABL1, CCND1 and CDC42 were also upregulated in ST-EPN-RELA. However, in our ZFTA-RELA mouse model the presence of a dominant-negative EPHB2 (dnEPHB2) did not attenuate tumor formation (Jørgensen et al., 2009). EPHB2 is member of ephrin receptor family (Eph). The ligands of Eph are called ephrins. Eph/ephrin signaling is a considerably complex pathway which is involved in development, homeostasis and pathogenesis and interplay with numerous cancer-related signaling pathways such as Wnt and MAPK (Gucciardo et al., 2014). Interestingly, Eph/ephrin pathway has been shown to both induce and suppress tumor cell proliferation depending on cell types, tumor categories and stages. On one hand, activation of EPH signaling presents a tumor-suppressive effect in, for example, glioblastoma, breast, colorectal, prostate and skin cancer (Chiu et al., 2009; Miao et al., 2009; Noblitt et al., 2004; Noren et al., 2006; Teng et al., 2013; Wykosky et al., 2005; Wykosky et al., 2008). EPHA signaling negatively regulates ERK activation in fibroblasts, endothelial cells as well as in tumor cells (Fu et al., 2010; Herath et al., 2009; Kuang et al., 2010). One comprehensive study demonstrated the cross-phosphorylation effect between EPHA and EPHB receptors in HEK293 and COS7 cells *in vitro*. Notably, in presence of EPHB2, EPHA signaling was successfully stimulated and the activation depends on the ratio of EPHA and EPHB (Janes et al., 2011). High-level of EPHB inhibited EPHA phosphorylation thus might increase tumor cell proliferation via ERK phosphorylation (Guo et al., 2006; Janes et al., 2011). Therefore, when overexpressing dnEPHB2 in mouse, it is possible that the tumor-suppressive EPHA signaling was disturbed therefore compensated the inactivation of EPHB2 oncosignaling in ZFTA fusion-positive tumors (Figure 2-23a). However, on the other hand, a reverse pattern has also been observed:

overexpression of EPHA/B in several cancers is associated with tumor higher grades and aggressiveness (Brantley-Sieders et al., 2011). In line with this report, Janes et al. also confirmed that EPH signaling cascade can be triggered by the recruitment of EPHA to dnEPHB2/ephrin complex. Therefore, although dnEPHB2 inhibited EPHB/ephrin coupling-mediated pathway in a competitive manner, the effect can still be by-passed by the EPHA/EPHB association and cross-activation (Figure 2-23b). CRISPR/Cas9-mediated inducible EPHB2 knockout could potentially better evaluate its functional role in tumor initiation and progression.

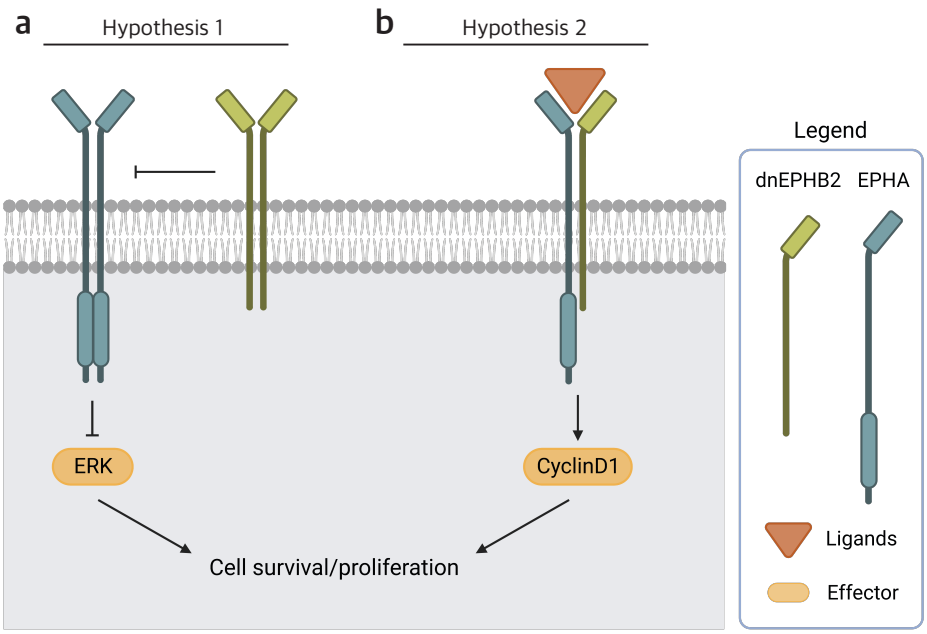

Figure 2-22 | Graphical illustration of two potential mechanisms on dnEPHB2 and EPHA cross-activation. Figure created with BioRender.com.

In summary, the first part of my thesis demonstrated the transforming capacity of *ZFTA*-containing fusions, provided representative mouse models, and presented a rationale for further preclinical studies blocking central molecular dependencies of these fusions. As a consequence from this work, tumors containing a canonical or alternative *ZFTA* fusion are now classified as supratentorial ependymoma, *ZFTA* fusion-positive in the 5th edition of the WHO Classification of Central Nervous System Tumours.

Chapter 3

Modeling a newly identified supratentorial brain tumor driven by *PLAGL1* fusion genes

3.1 Summary

In recent years, DNA methylation profiling has been used to define molecular groups of EPN amongst different anatomical sites in the CNS with distinct pathological characteristics and molecular alterations (Pajtler et al., 2015). Within the supratentorial compartment, in addition to the previously described *ZFTA* fusion-positive and *YAP1* fusion-positive molecular groups, our lab identified rearrangements involving *PLAGL1*, particularly *EWSR1-PLAGL1* fusion, as a molecular hallmark of a novel group of supratentorial neuroepithelial tumors (NET_PLAGL1; Sievers et al., 2021). Modeling these tumors according to previously established protocols (Zheng et al., 2021) with *in utero* electroporation in mice has failed, which was probably associated with species-related difference in microsatellite sequences involved in EWSR1 function. However, after I had performed numerous methodological optimizations, overexpression of *EWSR1-PLAGL1* fusion gene via a doxycycline-mediated system in human induced pluripotent stem cells (iPSCs)-derived neural stem cells (iNSCs) followed by *in vivo* orthotopic transplantation successfully led to supratentorial brain tumor formation in mice. DNA methylation profiling followed by an unbiased clustering approach located these tumor models closely to teratoma, potentially due to the strong stem cell-associated methylation signature pattern of iNSCs. Although not part of this thesis, using expression profiling and/or biomarker validation (e.g., immunohistochemistry staining against H19 and IGF2) may provide better insights into these models. In the future, further validation and refinement of this inducible modeling system will provide not only a reliable *in vivo* model to study *PLAGL1* fusion-positive supratentorial neuroepithelial tumors, but also a general tool to unravel molecular mechanisms behind the tumor development of these brain malignancies, e.g., to answer the question whether distinct fusions are needed for tumor initiation only or also drive progression.

3.2 A new neuroepithelial tumor cluster was identified with *PLAGL1* fusion

By investigating a large cohort of DNA methylation data, our group recently identified a molecularly discrete groups of supratentorial neoplasms with partly ependymal appearance (Sievers et al., 2021). These neuroepithelial tumors reveal recurrent fusions involving the pleomorphic adenoma gene-like 1 (*PLAGL1*) gene, and were named NET_PLAGL1 accordingly (Figure 1-4a). Within the NET_PLAGL1 cluster, *EWSR1-PLAGL1* is the most common fusion gene (n = 13/19) based on RNA-sequencing results, followed by *PLAGL1-FOXO1* (5/19) and *PLAGL1-EP300* (1/19) (Figure 3-1).

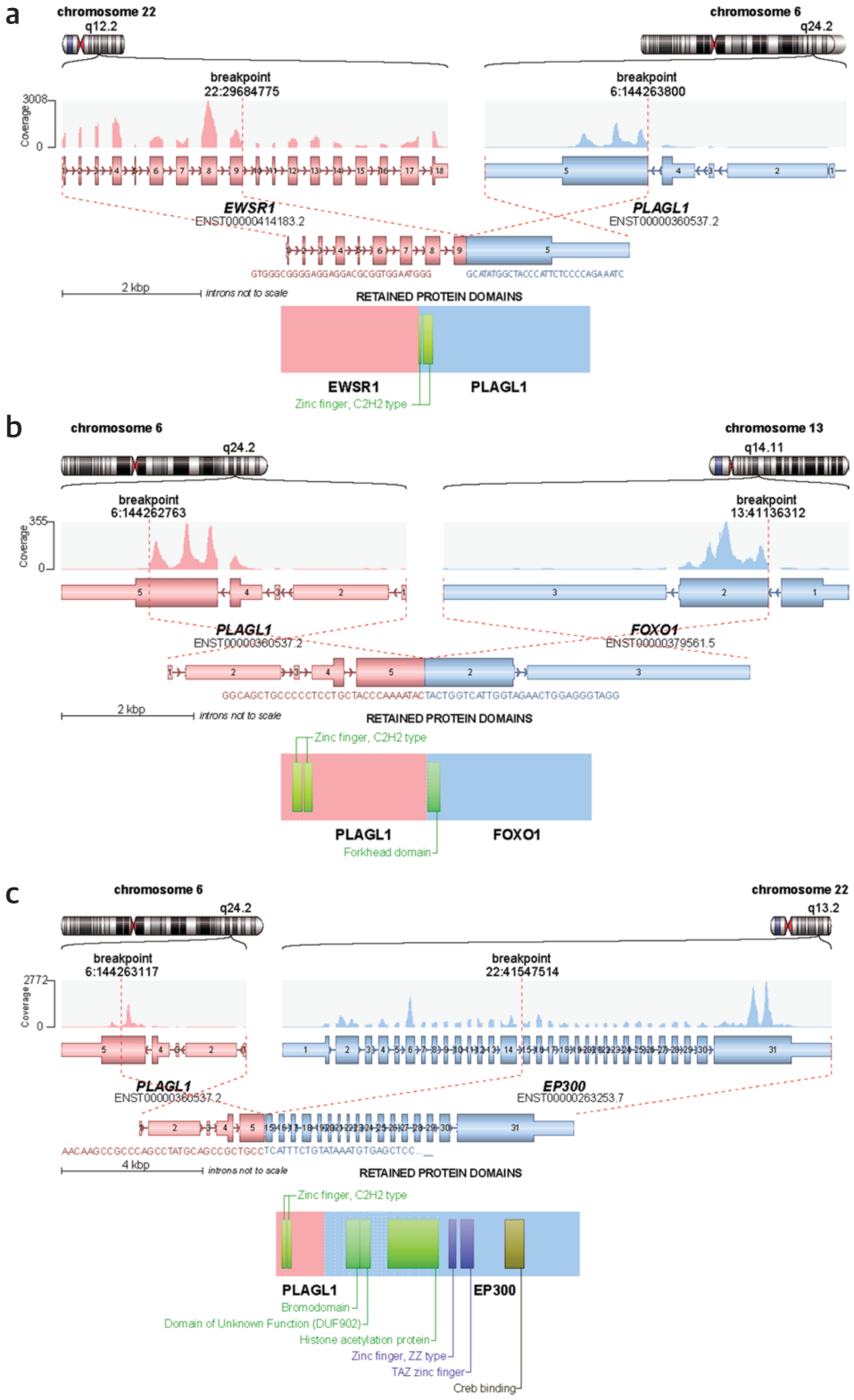

Figure 3-1 | Illustration of PLAGL1 fusion genes and respective protein structures

Fusion status of samples within the *PLAGL1* cluster was assessed by RNA-seq (n = 20): *EWSR1-PLAGL1* (n = 13), *PLAGL1-FOXO1* (n = 5), *PLAGL1-EP300* (n = 1), fusion negative (n = 1). NET: neuroepithelial tumor. **a**, In the *EWSR1-PLAGL1* fusion, exons 1–9 of *EWSR1*, as the 5′ partner, are fused to exon 5 of *PLAGL1*. **b**, In *PLAGL1-FOXO1* fusion, exons 1–5 of *PLAGL1* are fused to exons 2–3 of *FOXO1* as the 3′ partner. **c**, In *PLAGL1-EP300* fusion, exons 1–5 of *PLAGL1* are fused to exons 15–31 of *EP300* as the 3′ partner. All fusions conserve the zinc finger structure (C2H2 type) of PLAGL1 as part of the fusion products. Figure adapted from Sievers et al., 2021.

I first validated the fusion breakpoint by RT-PCR on patient-derived tumor RNA in the same way as described in the section 2.2 (Figure 3-2). All validated fusion genes (n = 3) resulted in in-frame expression of the fusion proteins EWSR1-PLAGL1 or PLAGL1-FOXO1. Based on the RNA-seq data, the fusion protein contains the N-terminal Ewing sarcoma activation domain (EAD) from EWSR1, the DNA binding domain (DBD) as well as the C-terminal transactivation domain (TAD) from the PLAGL1 (Figure 3-2). The intact DBD and TAD of PLAGL1 indicated that the gene transcription function was retained in the fusion gene, strongly suggesting an oncogenic implication of this fusion gene via aberrant activation of gene transcription.

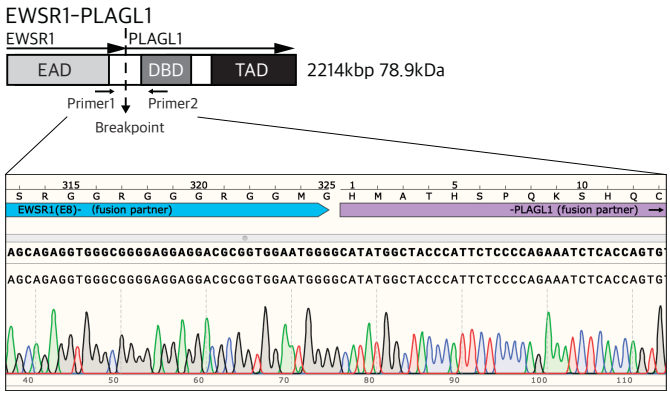

Figure 3-2 | Validation of *EWSR1-PLAGL1* fusion breakpoint by RT-PCR

Fusion breakpoint validation with RT-PCR followed by Sanger sequencing. N-terminal part of EWSR1 is fused with C-terminal part of PLAGL1. EAD: EWS activation domain, DBD: DNA binding domain, TAD: Transactivation domain.

3.3 *EWSR1-PLAGL1* fusion did not lead to malignant transformation applying established *in utero* electroporation protocols

3.3.1 IUE approach using *EWSR1-PLAGL1* at E13.5 time point

To understand the role of *EWSR1-PLAGL1* fusion gene for brain tumor development, I first attempted to overexpress the fusion gene in the developing supratentorial mouse brain using the well-established method *in utero* electroporation (IUE), as described in Chapter 2 (Figure 2-3). When the fusion gene was successfully delivered into the cortical ventricular zone at embryonic day 13.5 (E13.5), I could not observe any tumor formation in the mouse brain during a follow-up period of 1 year (n = 6; Figure 3-3).

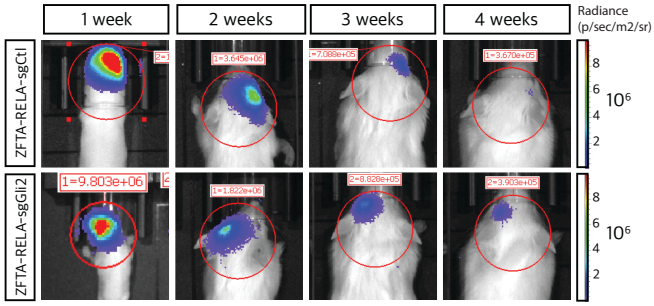

Figure 3-3 | IUE approach using *EWSR1-PLAGL1* at E13.5 time point

Representative figures of *in vivo* bioluminescence images of mice from postnatal age week 1 to week 4 electroporated with the *EWSR1-PLAGL1* fusion.

3.3.2 IUE approach using *EWSR1-PLAGL1* at different time points

In addition, I also delivered the fusion gene at E14.5 and E16.5 to also target different cell stages of the apical progenitors lining the ventricular zone during the mouse brain development (Di Bella et al., 2021). However, it did not result in tumor formation following IUE at any of the indicated time points (Figure 3-4).

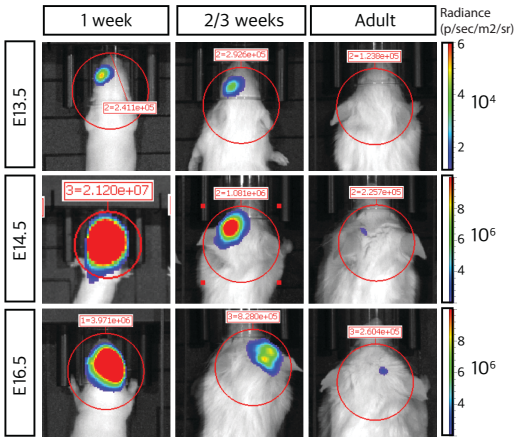

Figure 3-4 | IUE approach using *EWSR1-PLAGL1* at different time points

Representative *in vivo* bioluminescence images of mice electroporated *EWSR1-PLAGL1* fusion at E13.5, E14.5 and E16.5 time point.

3.3.3 IUE approach using murine *Ewsr1* fused to human *PLAGL1* at E13.5

Following negative results of all experiments described above, I assumed a species-related issue regarding EWSR1 that has been revealed and discussed among researchers in the Ewing sarcoma field for many years. In fact, there is a difference between species in the distribution of the microsatellite GGAA repeats. These microsatellite GGAA repeats interact with the EWSR1 transcription factor and play an essential role for EWSR1 transcriptional function (Riggi et al., 2014). For that reason, I next created an artificial chimeric fusion protein containing the mouse Ewsr1 (mEwsr1) N-terminal EAD region and the DBD as well as the TAD of human PLAGL1 (Figure 3-5a). The intent was to investigate whether the mEwsr1 could recapitulate the human counterpart by activating the corresponding set of downstream oncogenes in mice in a species-specific manner. However, I did not observe any tumor in mice electroporated with the *mEwsr1-PLAGL1* fusion gene (Figure 3-5b).

Taken together, I tried to model *EWSR1-PLAGL1* fusion-driven brain tumors *in vivo* using the IUE technique but none of the attempts led to tumor formation. The fact that also other groups have not been able to generate a mouse model for EWSR1 fusion-driven sarcomas yet is most probably associated with a species-specific microsatellite repertoire.

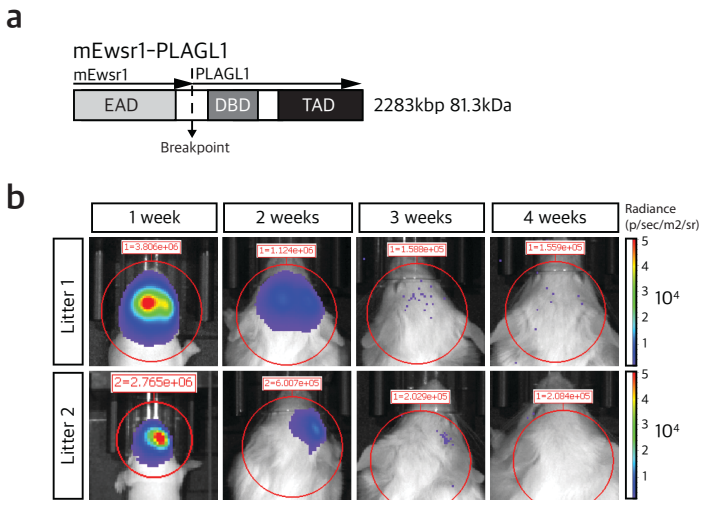

Figure 3-5 | IUE approach using mouse *Ewsr1* fused with human *PLAGL1* at E13.5

Representative *in vivo* bioluminescence images of mice electroporated with the m*Ewsr1-PLAGL1* fusion in postnatal age week 1 to week 4.

3.4 *In vitro* modeling of *EWSR1-PLAGL1* fusion-driven tumors using iPSC-derived iNSCs

Based on the results above, I decided to use human iPSCs (hiPSCs) to overcome species-related hurdles. HiPSC can be derived into a variety of cell types *in vitro* to facilitate model generation of tumors with different cellular origins, as mentioned in the introduction (Chapter 1). Since NET_PLAGL1 cohort shows high similarity to neuroepithelial cell, which is a type of neural stem cell; thus, I decided to use hiPSC-derived neural stem cells (iNSC) as a model system to analyze the *EWSR1-PLAGL1* fusion gene function *in vitro*.

3.4.1 Forebrain neural stem cells derived from hiPSCs were used for tumor modeling

Numerous neural stem/progenitor cell (NSC) differentiation protocols are available based on the literature. Given that all the reported human *PLAGL1* fusion-driven CNS tumors are located in the cerebral cortex (Sievers et al., 2021), I decided to use the monolayer neural induction protocol from StemCell Technologies to generate forebrain NSCs (forNSC). This protocol is relatively simple to conduct and time-saving compared to most other protocols (Figure 3-6).

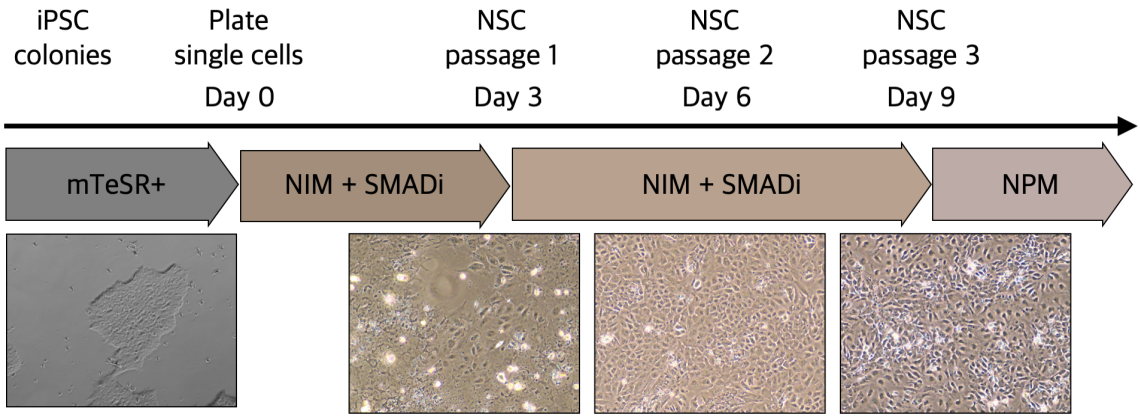

Figure 3-6 Timeline for StemCell monolayer neural induction protocol.

iPSC: induced pluripotent stem cell, NSC: Neural stem cell, mTeSR+: iPSC culture medium from StemCell Technologies, NIM: Neural induction medium, SMADi: SMAD inhibitor, NPM: Neural Progenitor Medium.

After generating iNSC with the monolayer protocol, I performed qPCR to validate expression of a set of marker genes for forNSCs. I used previously generated hindbrain NSCs (hinNSC) published in (Haag et al., 2021) and a commercialized human embryonic stem cell derived NSCs (H9NSC) as control. As expected, *NANOG* and *OCT3/4*, being iPSC marker genes, were significantly downregulated in all NSCs (Figure 3-7). *SOX2*, as a general stem cell marker, maintained a stable expression level across the differentiation process. The NSC markers *NES* and *PAX6* were upregulated in NSCs compared to iPSCs. *OTX2*, *FOXG1*, *SIX3* and *NKX2*.1 as forNSC markers showed expression levels that were decreased in hinNSCs and increased in forNSCs, respectively (Figure 3-7). In contrast, hindbrain markers, such as *GBX2* and *NKX6.1*, presented a reversed pattern (Figure 3-7). Interestingly, the H9NSCs showed a hindbrain biomarker spectrum as well. In addition, expression level of the glial marker *GFAP* did not change during neural induction (Figure 3-7).

The mRNA level of *NES* did not show a tremendous increase from iPSCs to forNSCs but when I performed the immunofluorescence staining against NESTIN protein on forNSCs, it was clearly more expressed than in iPSCs. Probably the translational level of NES is largely increased with a relatively less pronounced increase at transcriptional level.

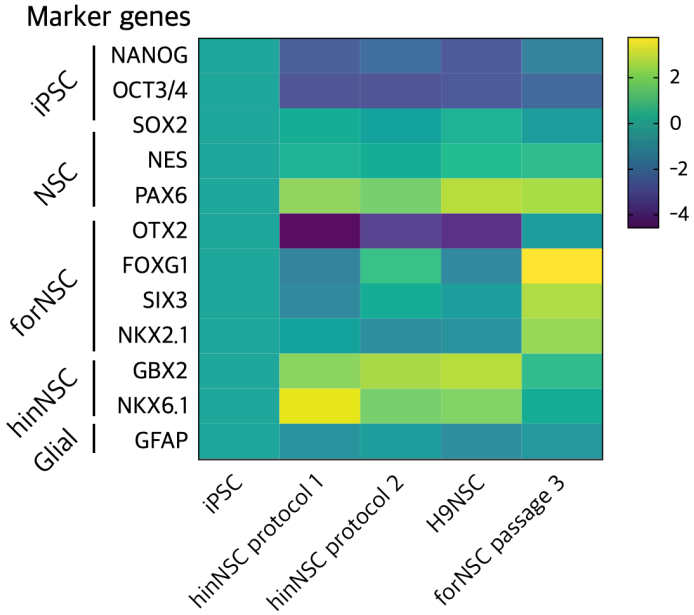

Figure 3-7 | Marker gene expression in iNSCs

RT-qPCR was used to validate the marker gene expression in iPSC, hinNSC with 2 different differentiation protocols, H9NSC and forNSC (n = 2)

3.4.2 Neural stem cell maintenance media was optimal for growth of forNSC

By the end of the neural induction process, I cultured the differentiated iNSCs in the neural progenitor medium (NPM) recommended by the StemCell Technologies. However, after 2 passages I found the iNSCs were proliferating surprisingly slowly in NPM. For this reason, I cultured the iNSCs derived from 2 iPSC lines (771-3G and NH50191) in 3 distinct media in order to test which one provides the best supporting environment for cell growth. INSCs from both lines showed heterogenous morphology when cultured in NPM or in NeuroCult media (NCM). Three days after seeding the cells, they were still not confluent (Figure 3-8a, b, c and d). While in the neural stem cell maintenance media (NSCMM) created by my colleague Daniel Haag adapted from (Palm et al., 2015), the iNSCs nicely formed neural rosettes with homogenous cell morphology and higher cell density (Figure 3-8e and f). The NSCMM was clearly more suitable for iNSC growth with both cell lines compared to the other media tested.

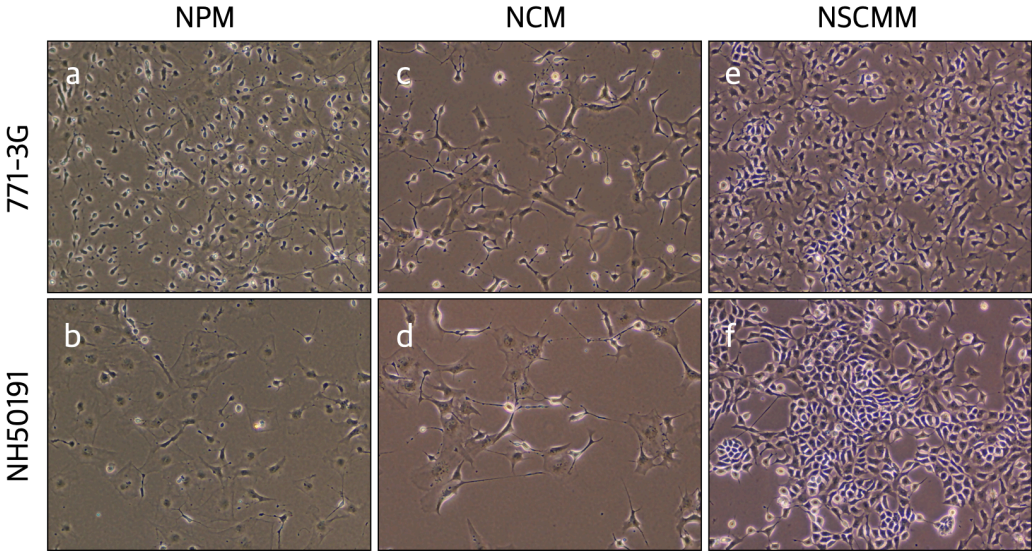

Figure 3-8 | Media comparison for iNSC

Passage 6 of iNSCs derived from 2 iPSC lines (771-3G and NH50191). Cells cultured in Neural progenitor medium (NPM) (**a**, **b**), in NeuroCult medium (NCM) (**c**, **d**) and in Neural stem cell maintenance medium (NSCMM) (**e**, **f**).

3.4.3 Comparison of transfection methods for gene delivery in iNSCs

To deliver the fusion genes into iNSCs, there are several transfection/transduction methods available, for instance electroporation- or liposome-based transfection (lipofection) as well as viral transduction. Here, I briefly list the advantages and disadvantages of these 3 methods (Table 3-1).

	Advantages	Disadvantages
Electroporation 	1. Can be applied for a broad range of cell types 2. High efficiency 3. Low DNA amount required 4. Easy to use	1. Not suitable for some primary cells / low proliferation cells 2. Low cell viability 3. High cost
Lipofection 	1. Simple and fast 2. High cell viability	1. Low efficiency in NSCs 2. Cell-type specific 3. Might be toxic to sensitive cells
Viral transduction 	1. Can be applied for a broad range of cell types 2. High efficiency	1. Biosafety concerns 2. More laborious 3. Low packaging capacity

Table 3-1 | Comparison of the advantages and disadvantages of 3 transfection methods.

In the beginning, I chose to use the electroporation method because it is the most widely used transfection technique in stem cell research and was also proven to be very efficient and less laborious compared to the other methods.

The electroporation method is a physical transfection technique which relies on the temporal destabilization of the cell membrane caused by its exposure to high-intensity electric pulses. The destabilized cell membrane becomes permeable and allows exogenous DNA to enter into the cell. The most critical parameter in this technique is the intensity and duration of the electrical pulse.

The Neon™ electroporation transfection system is an easy-to-use device that can transfect various cell types with high efficiencies. However, this method can cause huge amount of cell death if the transfection is not performed under optimal conditions. The optimal conditions depend largely on the cell type. Therefore, I tested different parameters that were recommended by the manufacturer and/or previously used in the lab for iNSCs (Figure 3-9). I was performing the test while I was generating the iNSCs in section 3.4.1. For that reason, all preliminary tests were carried out on the commercialized NSC line H9NSCs.

To test the electroporation conditions, I simply delivered a plasmid pT2K-CAG-IRES-GreenFire that expresses the fluorescent protein GFP into the NSCs and then assessed the GFP-positive cell proportion by fluorescent-activated cell sorting (FACS). Applying 1400V for 20ms with 2 sequential pulses showed the highest transfection efficiency (55.8%) among the 3 programs I tested (Figure 3-9) despite slightly higher cell death rate (data not shown).

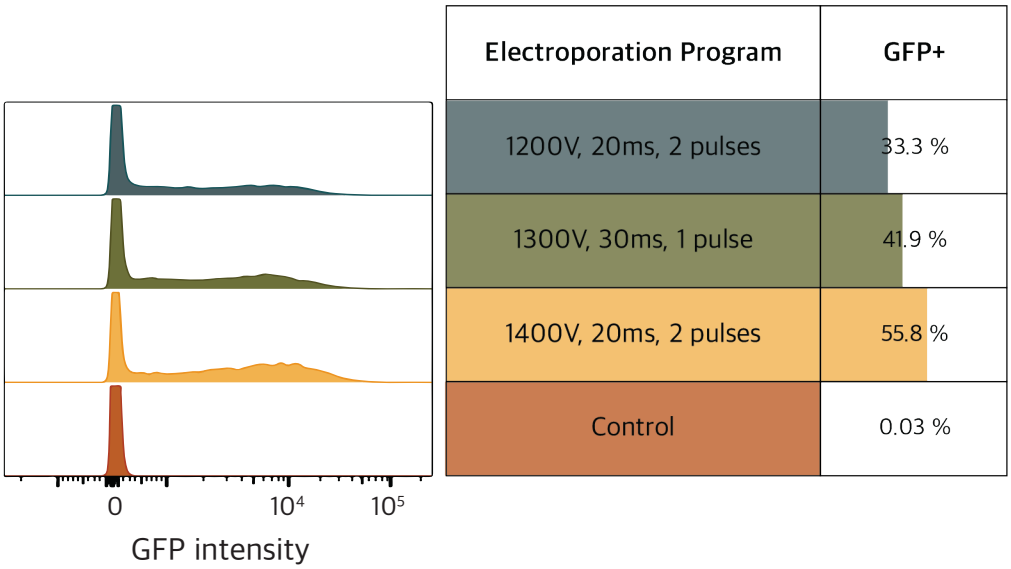

Figure 3-9 | Optimization of the electroporation program for transfection of NSCs

However, even a transfection efficiency of 55.8% is relatively low for the electroporation technique. Therefore, I was asking myself what if this outcome was not due to the transfection per se, rather an issue of plasmid expression in the cells. One of the well-known features, but with unclear mechanism, of stem cells is promoter silencing and previous studies showed that this phenomenon was frequently observed in neural stem cells in which some promoters overcome this issue better than the others (Chung et al., 2002). This prompted me to test the expression level of different constitutive promoters in iNSCs to identify the most suitable one for generating a stable cell line. Four different commonly used constitutive promoters were available in our lab: phosphoglycerate kinase (PGK), human elongation factor-1alpha (EF1α), cytomegalovirus (CMV) and cytomegalovirus early enhancer/chicken beta-actin hybrid (CAG). GFP was used as reporter gene and the optimal electroporation program tested above was applied for the transfection in H9NSCs. It turned out that EF1α promoter was the most efficient resulting in 99.6% of GFP positive cells, followed by CAG (75.8%) and PGK (44.2%). The CMV promoter was not suitable as it

resulted in 2.81% GFP-positive cells only. In addition, the EF1α promoter showed a higher fluorescence intensity than all other promotors tested (Figure 3-10).

The reason for the higher transfection efficiency of CAG driven GFP in this experiment (75.8%) compared to the previous one (55.8%) was most likely due to the type of GFP. In the program test (Figure 3-9) I was using a plasmid expressing GreenFire that has a destabilized GFP (half-life: 2 hours) while in the promoter test (Figure 3-10), all the constructs carry copGFP (aka ppluGFP2), which is a more stable and superbright green fluorescent protein from copepod *Pontellina plumate* (Shagin et al., 2004).

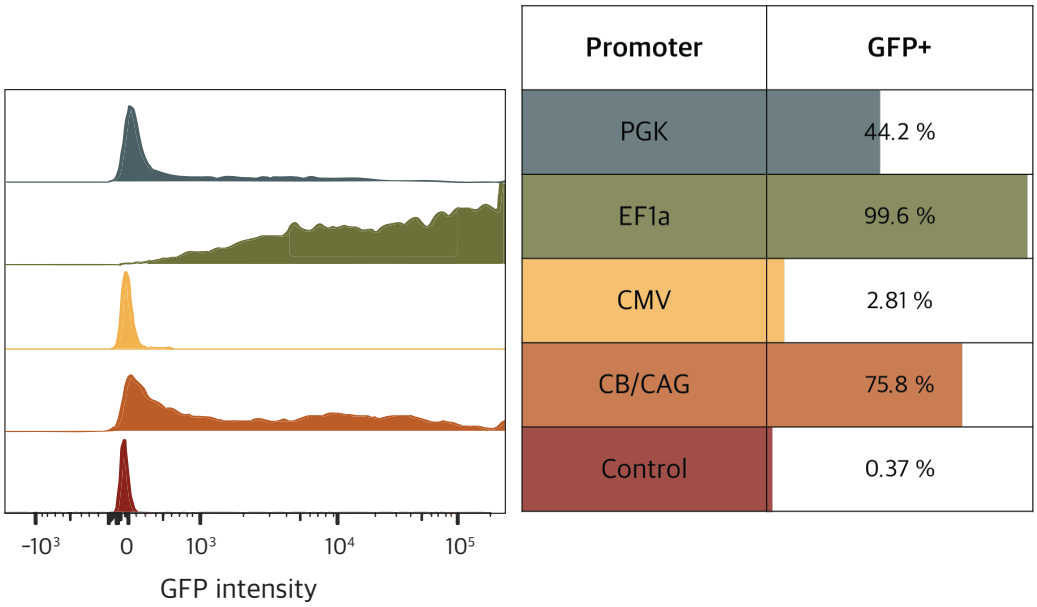

Figure 3-10 | Comparison of promoter expression levels in iNSCs

Although the results from the optimization with the Neon™ electroporation system were exciting, I had to test another transfection method due to lack of material. I ran out of the Neon™ pipette tip for the Neon™ device and COVID pandemic-related supply chain issues resulted in significant delays of placed orders. I subsequently decided to try out the liposome-based transfection technique.

Liposome-based transfection techniques involve the use of liposomes forming a complex with DNA which is overall positively charged, allowing the interaction with negatively charged cell membrane and in consequence facilitate the uptake by endocytosis. Fugene® (Promega) and TransIT® (Mirus) are both liposome-based transfection reagents and were routinely used in our lab. Since the NSCs are considered as a hard-to-transfect cell

type, I tested different DNA/reagent ratio (1:3, 1:4 and 2:6) according to recommendations from both the manufacturer and peers. Results were astonishing, since using the EF1α promoter expressing GFP, I observed around 90% GFP positive cells with both Fugene® and TransIT®, which is extremely high for NSC transfection (Figure 3-11). For the CAG promoter, efficiency was still about 60% for Fugene® and 50% for TransIT®, respectively. While the difference in DNA/reagent ratio did not affect the transfection efficiency with TransIT®, it did increase 10-15% with Fugene® (Figure 3-11).

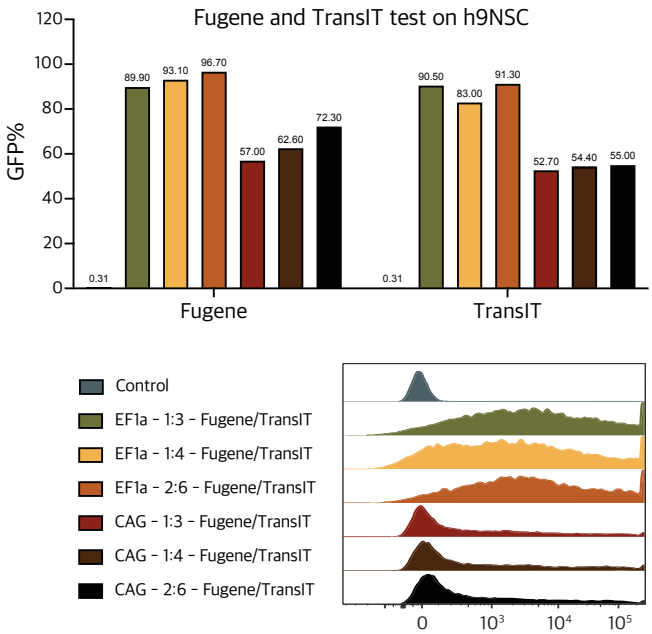

Figure 3-11 | Optimization of Liposome-based transfection in H9NSCs

Based on the previous test, I used the 1:3 ratio to infect the iNSC that I generated in section 3.4.1 with the StemCell monolayer protocol. Unexpectedly, the transfection efficiency was largely lower in iNSC compared to H9NSC with both Fugene® (19.5% vs. 89.9% with EF1α promoter, 6.15% vs. 57% with CAG promoter) and TransIT® (33.8% vs. 90.5% with EF1α promoter, 10.1% vs. 52.7% with CAG promoter) transfection reagents. However, TransIT® seemed to be relatively more efficient than Fugene® in this context (33.8% vs. 19.5% with EF1α promoter, 10.1% vs. 6.15% with CAG promoter) and also EF1α was still more efficient that CAG (19.5% vs. 6.15% with Fugene®, 33.8% vs. 10.1% with TransIT®, Figure 3-12).

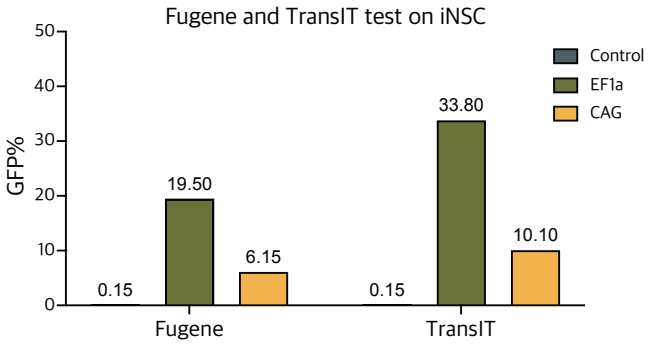

Figure 3-12 | Liposome-based transfection in iNSCs

3.4.4 Establishment of dox-inducible fusion gene expression in iNSCs

Following extensive optimizations of the transfection method including identification of the most suitable promoter, I decided to use TransIT with the Tol2 system to generate an iNSC line stably expressing the *PLAGL1* fusion gene. I cloned the fusion genes *EWSR1-PLAGL1* and *ZFTA-RELA* (as control) into the pT2K vector under the EF1α promoter, which carries GreenFire as reporter gene. Unfortunately, after delivering the plasmids into iNSCs, I observed a high rate of cell death in GFP positive cells with both fusion constructs but not when using the empty control vector. This result suggested that either the fusion proteins are toxic for the iNSCs or the iNSCs are too sensitive to handle both the transfection and the overexpression of the fusion genes at the same time. Based on the successful transformation of mouse NSCs using the *ZFTA-RELA* fusion gene by (Parker et al., 2014), I assumed timing to be the limiting factor. Therefore, I used a dox-inducible vector TLCV2 as backbone, in which Cas9 expression was controlled by a tetracycline-dependent promoter (TRE). I replaced the *Cas9* gene with the fusion genes *EWSR1-PLAGL1*, *ZFTA-RELA* or *YAP1-MAMLD1* (Figure 3-13). The other two fusion genes were proven to be oncogenic drivers in several studies and were used as positive controls here (Ozawa et al., 2018; Pajtler et al., 2019; Parker et al., 2014).

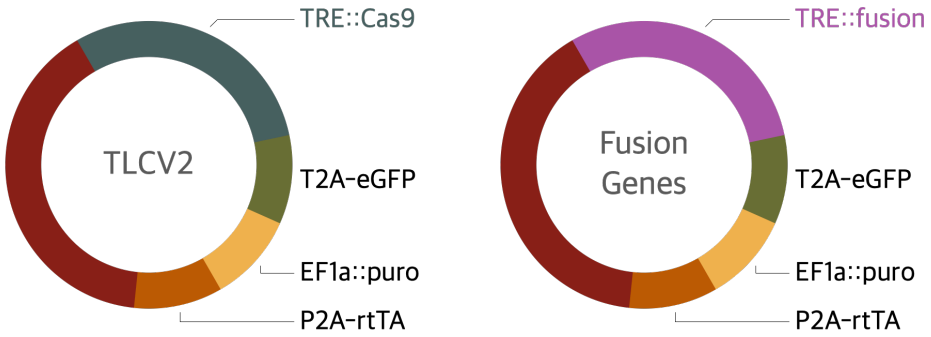

Figure 3-13 | Graphical illustration of the dox-inducible constructs.

TLCV2: Addgene plasmid #87360 (Barger et al., 2019), TRE: tetracycline-dependent promoter, puro: puromycin, rtTA: reverse tetracycline-controlled transactivator.

TLCV2 is a lentiviral-based vector which requires co-delivery of the packaging vectors into the target cells in order to produce a lentivirus carrying our gene of interest. Viral transduction as a transfection method has the advantage of being highly efficient as well as having a broad range of targetable cell types (Table 3-1). However, it is more laborious than the other methods, including additional experiments such as virus production and titration.

After virus production and titration, I infected HEK293T cells to determine the dox concentration and validate the protein expression of the fusion genes upon dox induction. Infected cells went through a 4-day puromycin selection (5 µg/mL) after the infection to eliminate non-infected cells. All fusion proteins were tagged with HA. Western blot against HA or GFP clearly showed that the increment of fusion protein expression or GFP was proportional to the increase of dox concentrations for all 3 constructs (Figure 3-14).

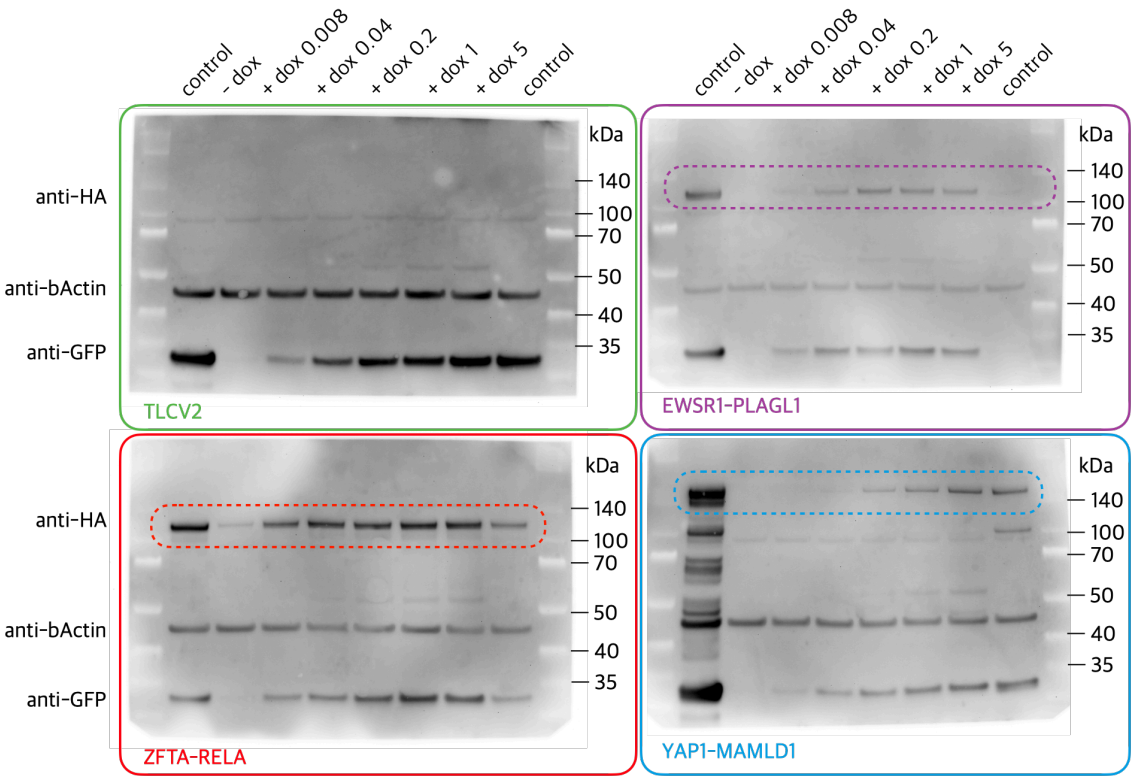

Figure 3-14 | Protein expression validation in HEK293T cells via Western blotting

However, when I performed the same experiment in iNSCs, I could barely detect any fusion protein expression even with high dox concentrations (5 µg/mL). Only GFP protein expression could be detected by WB (Figure 3-15). I repeated the experiment with a double amount of the protein input and obtained a similar result. Knowing that the fusion gene and GFP are separated by a 2A system under the same TRE promoter, the protein ratio of fusion to GFP is theoretically 1 : 1, as presented in the HEK293T cells (Figure 3-14). These results indicated that there was a potential degradation preference for the fusion proteins in iNSCs.

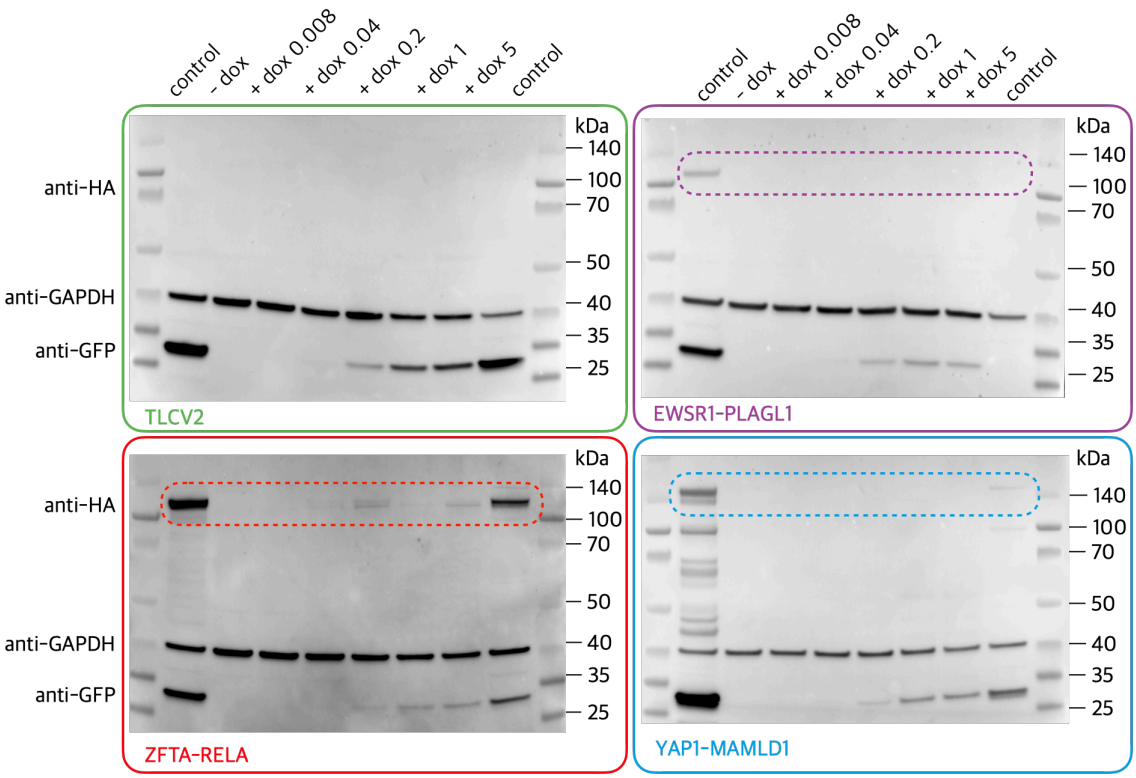

Figure 3-15 | Protein expression validation in iNSCs via Western blotting

Not only via WB, but also under the fluorescent microscope I noticed an increase of GFP positive cells upon dox induction in iNSCs harboring the control construct (Figure 3-16a-f). Similar results were observed with EWSR1-PLAGL1 as well as YAP1-MAMLD1 fusion. However, as soon as dox was added to the media of cells transfected with ZFTA-RELA, these cells started to die. And this cell death was shown mainly in GFP positive cells (Figure 3-16g). This result strongly suggested that the cell death observed previously with the constitutive promoter was essentially due to the double stress from the transfection procedure and the overexpression of the oncoprotein. By using the dox-inducible system, I managed to overcome this issue for EWSR1-PLAGL1 and YAP1-MAMLD1 fusion. However, the problem with ZFTA-RELA fusion still remained.

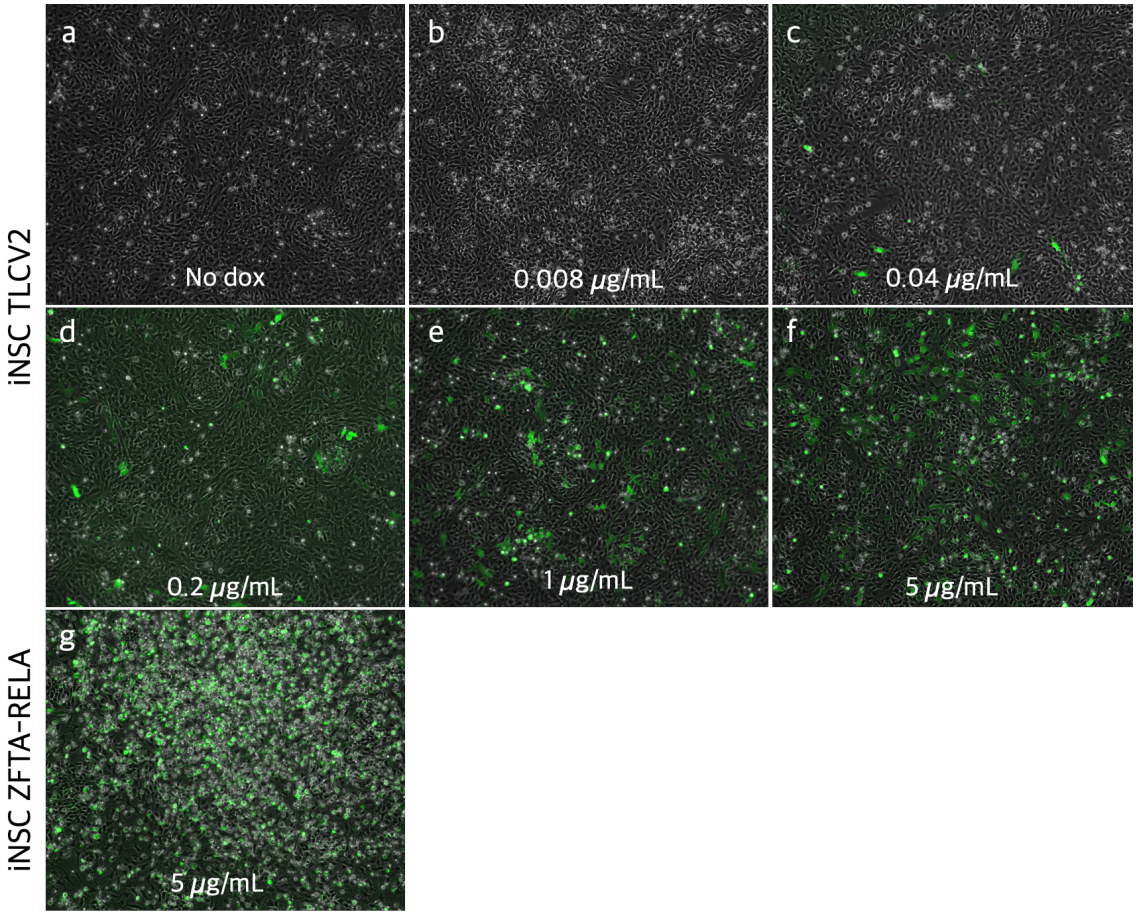

Figure 3-16 | iNSCs express GFP upon dox induction.

Live cell fluorescence image of control iNSCs without dox (**a**) and with 0.008 μg/mL (**b**), 0.04 μg/mL (**c**), 0.2 μg/mL (**d**), 1 μg/mL (**e**) and 5 μg/mL (**f**). **g**, Live cell fluorescence image of iNSC expressing ZFTA-RELA fusion upon 5 μg/mL dox.

When adding high dose of dox on the iNSCs, I could not trigger the fusion gene expression in a considerable fraction of the cell population. Although YAP1-MAMLD1 showed the highest GFP positivity (50% with 5 μg/mL dox), all other constructs did not even reach 35% including the control (Figure 3-17a). While in HEK293T cells, the activation was a lot stronger and in a larger fraction of cell population (Figure 3-17b). Perhaps the non-responsive cells suffered from an impaired drug-uptake capacity or an insufficient sensitivity against dox.

To evaluate this possibility, I added a higher concentration of dox (10 μg/mL) to the cells. However, cells died within a day after the treatment, suggesting that dox became cytotoxic for these cells at 10 μg/mL. To further explore the potential causes for the

heterogenous gene expression, I made use of the puromycin (puro) resistance gene which is part of the viral genome that was integrated into the target cells (Figure 3-13). Instead of a 4-day puro selection (2 µg/mL), I applied a prolonged selection (7 days) to eliminate the non-infected cells. Despite the extended selection, it was still possible that some cells lose their resistance during the expansion of the population. To address this issue, I employed a second round of puro selection for 2 days right before the dox administration. However, the result was not distinguishable from the first attempt (Figure 3-17a). Together, these findings revealed that in iNSCs, there is a preference in protein degradation for fusions over the reporter; the prolonged or additional round of puro selection did not improve the transgene inducibility in these cells.

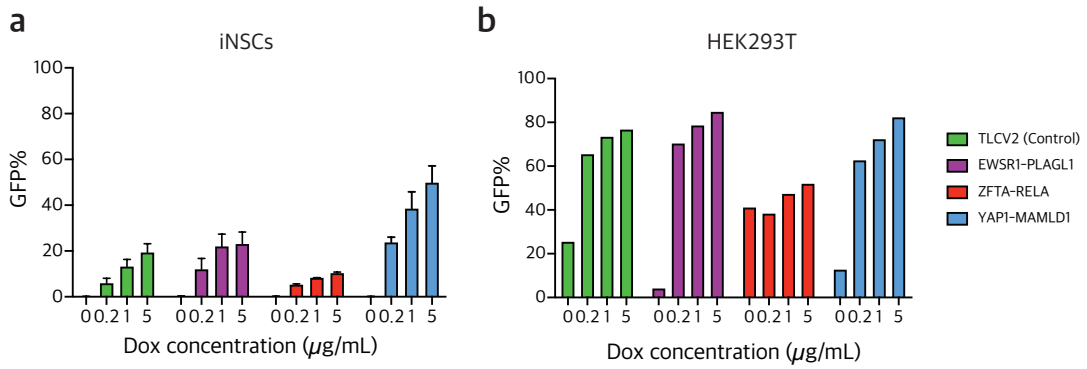

Figure 3-17 | Protein expression upon dox induction in iNSCs and HEK293T

Percentage of GFP positive cells in iNSCs (n = 2, **a**) and HEK293T (**b**) upon dox induction with different concentration.

3.4.5 Cell proliferation did not increase upon dox induction

In spite of the dox-responsiveness issue, an obvious change in phenotype was present, for example, the enormous cell death events with ZFTA-RELA expression in NSCs (Figure 3-16g). I decided to investigate the effect of dox-induced fusion gene expression on cell proliferation. To address this question, I employed the same EdU assay as described in section 2.5.2 and determined the best EdU incubation time as 2 hours (Figure 3-18a). Only EWSR1-PLAGL1 expression resulted in a decreased cell proliferation while other fusion genes did not show significant changes (Figure 3-18b). This result suggested that EWSR1-PLAGL1 fusion gene might play an inhibitory role in cell growth in iNSC in an *in vitro* environment.

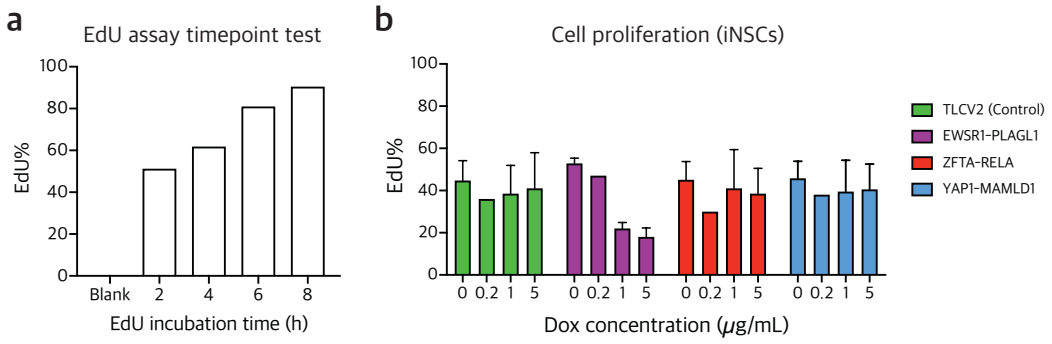

Figure 3-18 | Cell proliferation did not increase upon dox induction *in vitro*.

a, Test of best EdU incubation time for iNSCs. **b,** iNSCs expressing control construct (TLCV2) and fusion genes (EWSR1-PLAGL1, ZFTA-RELA, YAP1-MAMLD1). The percentage of proliferating cells indicated as EdU positive population.

3.5 Orthotopic transplantation of iNSCs into immunodeficient mice

Studies repeatedly demonstrated that cells could behave very differently depending whether exposed to an *in vitro* or an *in vivo* environment (Sugai et al., 2016). Especially in cancer, tumor cells interact extensively with the surrounding cells where the tumor microenvironment plays a huge role in supporting survival and development of the tumor cells (Hanahan & Weinberg, 2011). To assess effects of dox-based fusion gene induction *in vivo*, I labelled the dox-inducible fusion-expressing iNSCs from section 3.4.4 with GreenFire reporter gene to allow for tracking of cell growth in living mice through the detection of bioluminescence. One week after injecting labelled cells orthotopically into the cerebral cortex region of immunodeficient mice (NSG), I fed the mice with food pellets containing 200 mg/kg dox in order to activate the fusion gene expression (Figure 3-19).

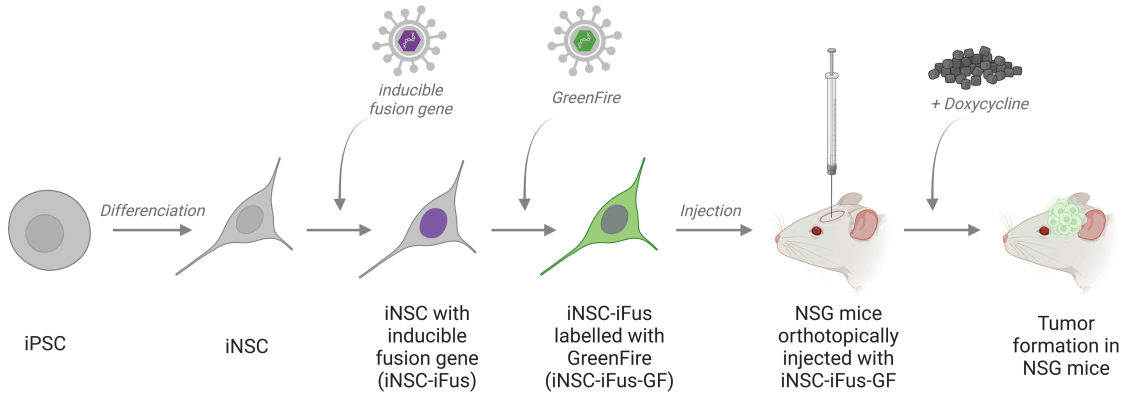

Figure 3-19 | Graphical illustration of the strategy to activate fusion gene expression in immunodeficient mice.

Human induced pluripotent stem cells (iPSC) were first differentiated into neural stem cells (iNSC) using monolayer protocol. INSCs were infected by lentivirus carrying dox-inducible fusion gene and selected using puromycin (iNSC-iFus). Prior to injection, iNSC-iFus were labelled with GreenFire to allow *in vivo* cell tracking (iNSC-iFus-GF). Subsequently, these cells were orthotopically inoculated into cerebral cortex of NSG mice. Mice were fed with dox-containing food pellet to induce fusion gene expression.

Within a month after starting dox food administration, 3 mice already showed symptoms related to neurological disorders. At day 72, 92% (22/24) of mice with or without dox diet displayed neurological symptoms and approximately 4 months after starting dox, regardless of the fusion genes and diet, all 24 mice were sacrificed due to hydrocephalus with comparable time of median survival (Figure 3-20).

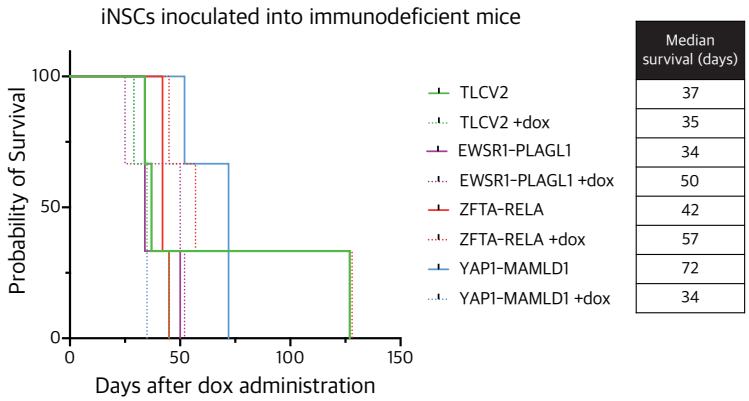

	Median survival (days)
TLCV2	37
TLCV2 +dox	35
EWSR1-PLAGL1	34
EWSR1-PLAGL1 +dox	50
ZFTA-RELA	42
ZFTA-RELA +dox	57
YAP1-MAMLD1	72
YAP1-MAMLD1 +dox	34

Figure 3-20 | Kaplan-Meier curves of NSC mice inoculated with different fusion gene-expressing iNSCs.

To further investigate the potential causes of hydrocephalus in mice, I first tried to localize the previously injected cells. The GFP reporter allowed me to spot these cells in freshly dissected brains. The iNSCs without dox induction migrated towards the olfactory bulb following the rostral migratory stream in most cases (Figure 3-21a, b, c and d, c.f. Figure 3-21i). Similar as in the olfactory bulb, GFP-positive cells were also identified in the sub-granular zone of the dentate gyrus in the hippocampus (Figure 2-21a, b and c). In some brains, GFP-positive cells were also detected around the hypothalamus region (Figure 2-21a, c, d and e). Excitingly, the EWSR1-PLAGL1-expressing (dox-induced) cells did not show the migratory behavior but formed a tumor-like structure in the cerebral cortex near the cortical ventricular zone instead (Figure 3-21f). ZFTA-RELA-expressing cells presented both migratory behavior and tumor-like structure (Figure 3-21g). On the contrary, cells expressing YAP1-MAMLD1 migrated towards the olfactory bulb only and did not form any tumor-like lump (Figure 3-21h). This result indicated that human iNSCs derived from iPSC recapitulate the general NSC migratory features in the mouse brain while expression of the fusion genes could alter the migration behavior. The migration behavior of non-dox exogenous iNSCs caused neurological disorders comparable to the ones with dox induction in a short time period rendering these not suitable as controls (Figure 3-20). It is also possible that the number of inoculated cells was too high (1x 10^6 cells/mouse) and therefore resulted in elevated pressure inside the mouse brain.

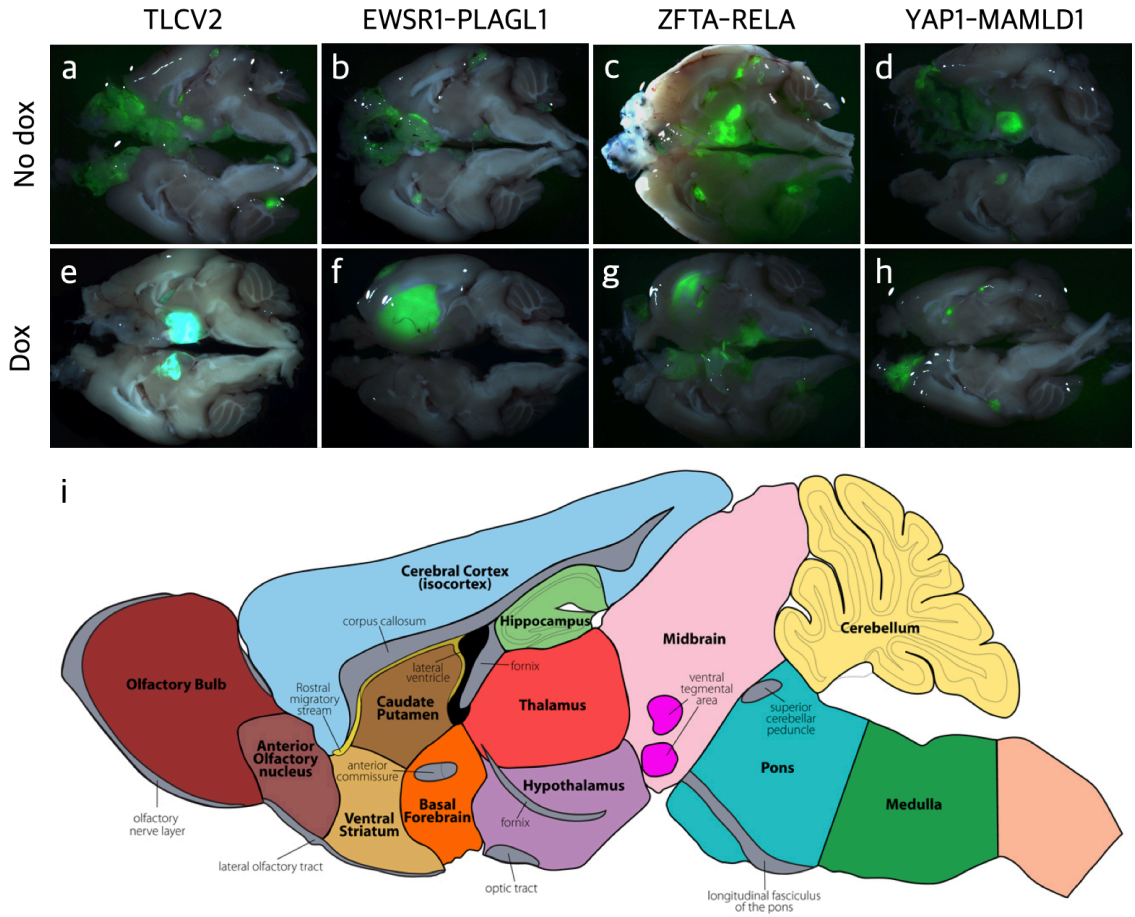

Figure 3-21 | Sagittal plane of the mouse brains showing the location of GFP positive iNSCs.

The upper row represents the mice without dox food (**a-d**). The lower row represents the mice with dox food (**e-h**). Each column represents the indicated control/fusion construct. **i**, Mouse sagittal brain illustration taken from gensat.org

A previous study from our lab had shown that no symptoms were observed in mice after injection of 4 x 10^5 cells into the brain around the pons region (Haag et al., 2021). I therefore decided to inject 2 x 10^5 cells instead of 1 x 10^6. With 5 times less injected cells, mice carrying dox-inducible EWSR1-PLAGL1 fusion survived longer with or without dox administration (Figure 3-22a). Although the mice with lower injected cell number showed a moderate level of bioluminescence signal at the beginning of the dox induction, the signal increased at a comparable speed between the mice with and without dox (Figure 3-22b).

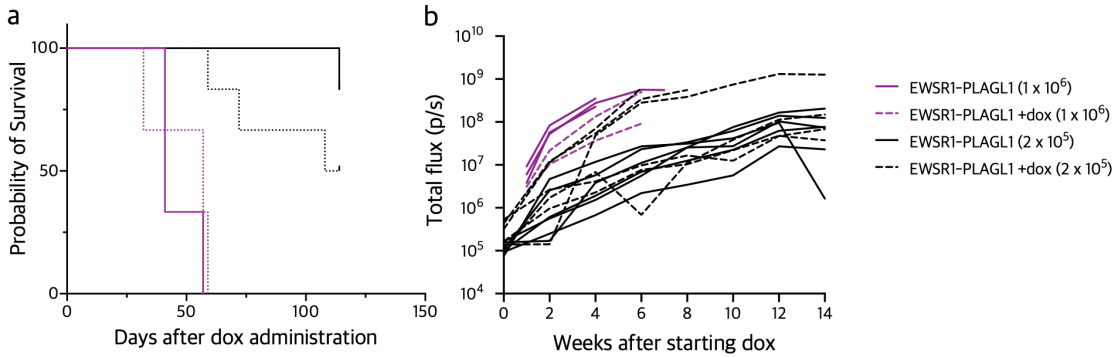

Figure 3-22 | Comparison of inoculated cell number for iNSCs carrying EWSR1-PLAGL1.

a, Kaplan-Meier curves of the mice with different inoculated cell number (purple vs. black) and with or without dox food (dashed line vs. solid line). **b,** The development of the bioluminescence signal of mice inoculated with iNSC over time.

To further examine histology of these mice, I performed H&E staining on the brains injected with iNSCs carrying the *EWSR1-PLAGL1* fusion of mice fed with or without dox, respectively. Histopathology showed low cell density in mice without dox and high cell density in those with dox (Figure 3-23a, b and c). Successful activation of the fusion protein expression upon dox was proven by the positive signal of HA tag via immunohistochemistry staining (Figure 3-23d, e and f). The expression of the proliferation marker Ki67 also indicated the high proliferative characteristic of the tumor cells (Figure 3-23g, h and i). In summary, these results demonstrated feasibility of using the dox-inducible system to induce tumors in immunodeficient mice inoculated with human iNSCs carrying the *EWSR1-PLAGL1* fusion. In addition, these findings further underlined differences in growth behavior of iNSCs between *in vivo* and *in vitro* settings.

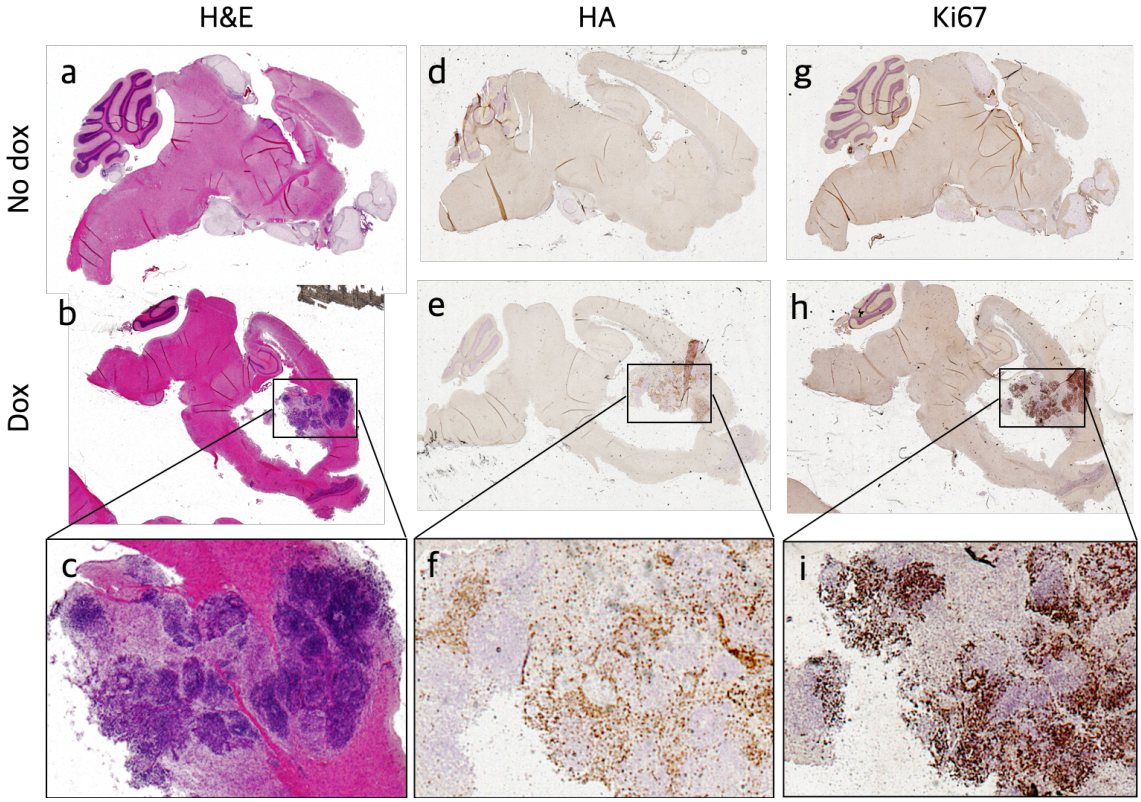

Figure 3-23 | Histopathology of the *EWSR1-PLAGL1* fusion-carrying mice.

H&E staining of the mice inoculated with *EWSR1-PLAGL1*-carrying iNSCs, without dox (**a**), with dox (**b**) and a zoom-in of a tumor formed after induction with dox (**c**). Immunohistochemistry staining against HA of the mice inoculated with *EWSR1-PLAGL1*-expressing iNSCs, without dox (**d**), with dox (**e**) and a zoom-in of with dox (**f**). Immunohistochemistry staining against Ki67 of the mice inoculated with *EWSR1-PLAGL1*-expressing iNSCs, without dox (**g**), with dox (**h**) and a zoom-in of with dox (**i**).

3.6 Tumor classification based on DNA methylation

Next, I characterized the EWSR1-PLAGL1-positive tumors at the molecular level. As control, I took the GFP-positive cell bulk from the mice without dox diet as well. To this end, I assessed whether the mouse samples clustered together with their human counterparts at the DNA methylation level. After the profiling on DNA methylation microarray, Martin Sill helped to analyze and integrate the data into the published DNA methylation classifier (version 12.5), which contains the human data from NET-PLAGL1 cohort (Capper et al., 2018). According to the classifier, EWSR1-PLAGL1-positive (dox-induced) mouse tumors were predicted as embryonal tumor with multilayered rosettes (ETMR) and samples without dox induction were identified as teratoma.

3.7 Discussion

Based on DNA-methylation and expression profiling a previous study from our lab identified a rare group of pediatric supratentorial brain tumors with often ependymoma-like histology. This newly defined entity shows recurrent gene fusions involving the *PLAGL1* gene, among which *EWSR1-PLAGL1* most frequently occurs (n = 13/19; Sievers et al., 2021).

The unsuccessful modeling of *EWSR1-PLAGL1* fusion positive tumors in mice using *in utero* electroporation was most probably related to the lack of relevant species-specific microsatellite GGAA repeats, which are essential for oncogenic function of *EWSR1* fusion in human tumors (Riggi et al., 2014).

To overcome the species barrier, I used human iNSCs derived from iPSC as host cells to model the *PLAGL1* fusion-driven tumor. Following a monolayer NSC differentiation protocol, I successfully obtained iNSCs expressing forebrain marker genes. The media comparison showed that these cells proliferate very well when cultured in the NSCMM while it is not the case in NPM and NCM. To efficiently incorporate genes of interest into the genome of iPSC-derived NSC (iNSC), I optimized several transfection methods (Table 3-2). An interesting remark regarding the media is that NSCs are not prone to be transfected using liposome method in NSCMM and other than in NPM NSCs cannot be successfully transfected. It is possible that some molecules in the NSCMM inhibit the liposome-DNA complex formation. Therefore, using NPM on the day of transfection could solve this problem meanwhile keep cells growing.

	Optimal setting	Advantages	Disadvantages	Notes
Electroporation	1400V, 20ms, 2 pulses	Fast High efficiency	Expensive High cell death	Try 1300V, 30ms, 1 pulse if too much cell death
Lipofection	Fugene 1:3 or 1:4 DNA TransIT 1:3 DNA	Fast Cheap	Low efficiency	Avoid the transfection in NSCMM
Viral transduction	/	Generating a stable line	Laborious Safety concern	/

Table 3-2 | Overview of transfection settings for NSCs.

Numerous studies have been carried out to prove that individual promoter systems have different abilities to trigger transgene expression in embryonic stem cells (ESCs) *in vitro*

and *in vivo* (Chung et al., 2002; Norrman et al., 2010; Xia et al., 2007). Consistent with the results from ESCs, EF1α promoter followed by PGK promoter showed a considerably higher efficiency for gene expression in NSCs. It was also shown that in contrast to human promoters (e.g., EF1α), viral-derived promoters (e.g., SFFV) are strongly methylated during differentiation independent of the transgene, resulting in promoter silencing (Herbst et al., 2012). EF1α was also found to be the most stable promoter during differentiation (Norrman et al., 2010).

Due to the massive cell death after delivering the fusion genes *in vitro*, I finally generated stable NSC lines expressing fusion genes solely upon dox induction. However, a large proportion of the cells were non-responsive to dox even with two rounds of puro selection. The genetic heterogeneity (e.g., copy number of transgene) and/or epigenetic silencing (e.g., DNA methylation) can be responsible for the compromised fusion gene induction (Bencsik et al., 2016). To assess heterogeneity, copy numbers of the transgene in selected and sorted NSCs could be measured via qPCR to determine the minimum copy number needed for transgene expression. As epigenetic silencing by DNA methylation and/or histone acetylation might be another reason causing repression of the fusion gene, treating cells with a DNA hypomethylating agent (e.g., decitabine) or a histone deacetylase inhibitor (e.g., sodium butyrate) might overcome this phenomenon (Kantarjian et al., 2003; Mariani et al., 2003).

The fact that about 40-60% of the NSCs after puro selection did not respond to dox induction might also have caused heterogenous tumor formation *in vivo*. Applying a FACS could largely eliminate the non-responsive cells and resulted in a more homogenous population prior to the transplantation (Bencsik et al., 2016).

While the NSCs harboring *EWSR1-PLAGL1* fusion displayed a decrease in cell proliferation upon dox induction *in vitro*, they formed proliferating tumors in the cerebral cortex *in vivo* with increased Ki67. Although *PLAGL1* has long been considered as tumor suppressor gene (Jarmalaite et al., 2011; Kowalczyk et al., 2015; Lemeta et al., 2007; Vega-Benedetti et al., 2017), more and more evidence showed its oncogenic role in certain type of tumors, e.g., glioma and clear cell renal cell carcinoma (Keck et al., 2023; Kowalczyk et al., 2015; Vega-Benedetti et al., 2017). Given that cancer cells behave differently *in vitro*, *in vivo* and *ex vivo* (Hum et al., 2020) and distinct pathways can be triggered leading to changes in cell behavior (Ahmadiankia, 2020), the differential behaviors *in vitro* and *in vivo* may also be related to the dual role of *PLAGL1* in tumor suppressor and oncogenic signaling pathways.

One hypothesis for the discrepancy of cancer cell behavior between *in vivo* and *in vitro* environment is that the surrounding non-malignant cells plays an indispensable role in

supporting the tumor growth. Given that PLAGL1-associated tumor induction and growth was observed *in vivo* within this thesis, it might be interesting to decipher the essential signaling pathways and/or molecules that impact *PLAGL1* function. For instance, we intended to perform single-cell RNA-seq on human NET_PLAGL1 tumors to decode the complex network of tumor microenvironment (TME). However, we were limited by the lack of fresh-frozen material of PLAGL1 tumors. An alternative would be using a co-culture of glial cells (astrocytes, microglia, oligodendrocyte etc.) or neurons together with the fusion-bearing cells to understand the role of tumor-associated cells in tumorigenesis. In addition, I observed that not all the cells in tumor area showed expression of the fusion gene (HA-negative in IHC), suggesting that these might be cells from TME that play a supporting role for tumor growth. Using a human tissue specific antibody (e.g., anti-human nuclear antigen) could identify whether these HA-negative cells in the TME are from the host or the dox non-responsive human NSCs (Zhang et al., 2021).

I assumed that NSCs are the cells-of-origin of the *PLAGL1* fusion-positive tumors. However, it is also possible that tumors derive from another progenitor cell type (e.g., radial glial cells). A model of Ewing sarcoma carrying *EWSR1-FLI1* fusion was able to be established via overexpressing the fusion gene in specific progenitor cells while it was not successful in other cell types (Tanaka et al., 2014). Similarly, in diffuse intrinsic pontine glioma carrying the H3.3-K27M mutation only iNSCs gave rise to tumors in mice but not iOPCs (Haag et al., 2021). Since various differentiation protocols are available for generating different neural progenitor cells, such as neural epithelial stem cell (NESC; Huang et al., 2019)) or radial glial cell (RGC; Duan et al., 2015)), a strategy to further explore progenitor cell dependency could be to generate iPSCs carrying dox-inducible fusion genes being differentiated into NESCs or RGCs (Figure 3-24).

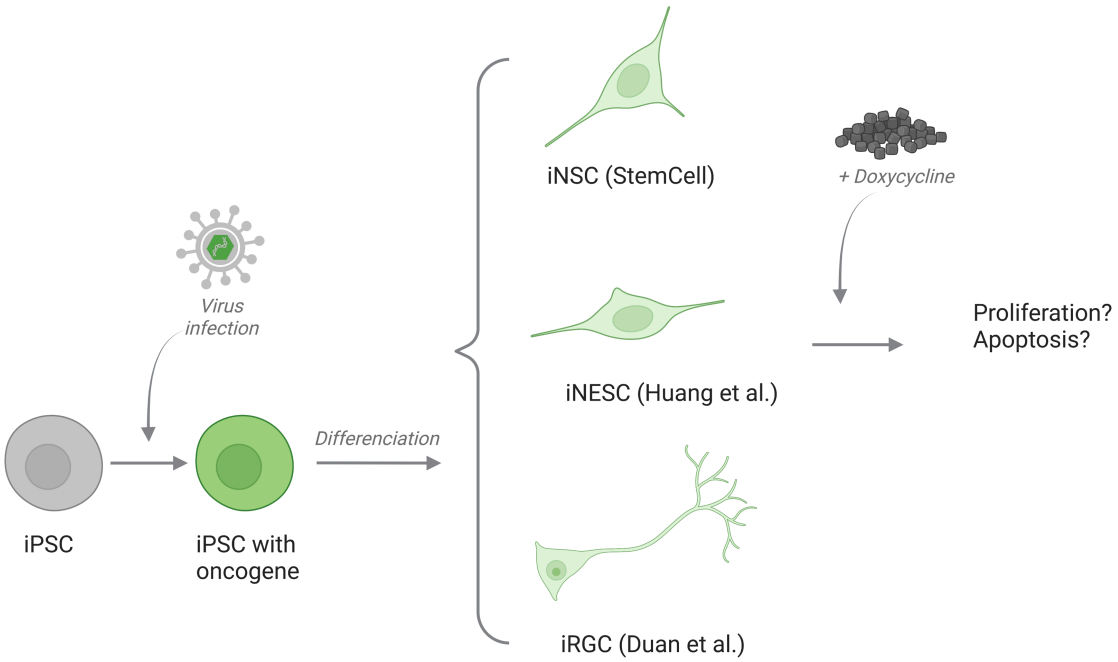

Figure 3-24 | Graphical illustration of the strategy to activate fusion gene expression in different neural progenitor cells.

After injecting the dox-inducible EWSR1-PLAGL1-containing iNSCs into mouse brains, I observed cell accumulation in the olfactory bulb and around hypothalamus (indicated by GFP-positive cells) in mice without dox diet (Figure 3-21a, b, c and d). It is possible that some of the inoculated cells migrated towards the olfactory bulb along the rostral migratory stream and some others were carried by the flow of cerebrospinal fluid to the third ventricular zone and resided around hypothalamus (Magnon et al., 2011).

Although *EWSR1-PLAGL1*-expressing (dox-induced) iNSCs formed a supratentorial brain tumor in mice upon dox-induction, the iNSCs without dox caused hydrocephalus in the brain as well, leading to a comparable overall survival. DNA methylation clustering showed a match to teratoma for iNSCs without dox, which is not astonishing since the pluripotent stem cells are able to give rise to tumor formation, particularly teratomas (Ben-David & Benvenisty, 2011; Hentze et al., 2009; McDonald et al., 2020). Several studies already proved that it is possible to generate NSCs through teratoma formation and the isolated NSCs have the potential to undergo a natural course of neural development (Hong et al., 2016; Kim et al., 2019). To avoid the formation of teratoma *in vivo*, potential strategies could be to utilize a different iPSC line or to titrate the number of injected cells (Lee et al., 2009).

In summary, I validated *EWSR1-PLAGL1* fusion breakpoint in NET_PLAGL1 cohort and generated supratentorial brain tumor expressing EWSR1-PLAGL1 fusion in mice using dox-inducible iPSC-derived iNSC xenograft technology. DNA methylation profiling showed high similarity of these tumors to ETMR, however, further molecular characterizations such as expression profiling need to be performed to depict the nature of generated PLAG1 fusion-driven mouse brain tumor.

Chapter 4

Murine model biobank for pediatric tumors based on DNA methylation profiling

4.1 Summary

Recent advances in molecular profiling methods led to the identification of multiple new molecularly defined tumor-types and -subtypes, distinguished by characteristic DNA methylation signatures. While the analysis of the human methylome using microarrays has become an affordable and routine method in many labs, this technology has not been available for murine samples until recently.

In the past 5 years, we have successfully generated a variety of mouse models for childhood tumors (e.g., brain tumors and sarcomas) using both, genetically engineered mouse models (GEMMs) as well as somatic gene transfer approaches. Most of these models faithfully reflect the human tumor counterpart at the histological level. It is also important to assess the molecular similarity across species. With the recently released Infinium Mouse Methylation BeadChip, we now set out using these models to generate a first DNA methylation-informed biobank for murine pediatric tumors.

I collected and profiled more than 80 mouse models (in total 315 samples) of pediatric tumors including gliomas, medulloblastomas, ependymomas and sarcomas, as well as 136 normal brain and muscle control tissues. DNA methylation-based clustering showed that samples from the same model clustered together. Primary tumors were also associated with their allograft models, confirming the stability and liability of *in vivo* passaging. The copy number variation of certain models recapitulated their human counterparts. One of the ultimate aims is to perform cross-species comparative analysis of established mouse models and the human counterparts, assessing how faithfully each models reflects the human situation, which is not part of the thesis. In addition, I will also analyze model-specific immune microenvironment and putative cells-of-origin, which is difficult in the human context due to the lack of material. I will correlate these to murine tumor samples and

thereby provide novel insights into tumor origins. In summary, this study will generate a validated biobank of murine models for pediatric cancers and provide a valuable resource for future developmental studies and preclinical trials.

4.2 Material comparison

Our lab has been working on mouse models for pediatric CNS tumors over many years and the list of established mouse models is constantly expanding. However, the available type of material is not unified: some are preserved as formalin-fixe paraffin-embedded (FFPE) blocks while the others are fresh-frozen (FrFr) tumor chunks.

The FFPE process is known to affect DNA integrity (Auerbach et al., 1977; Bonnet et al., 2018; Bresters et al., 1994; Feldman, 1973), limiting the use of techniques requiring high-quality DNA, such as Infinium Methylation microarrays. To overcome this limitation, I isolated the DNA from two samples of the same mouse tumor (in total 3 models): one underwent FFPE fixation and was stored at room temperature while the other sample was stored as FrFr tissue at -80°C. After DNA extraction, FFPE samples were subjected to an additional DNA restoration procedure. In a high-grade glioma (HGG) model and two ependymoma (EPN) models, the FFPE samples bundled together with their matched FrFr samples in an unsupervised clustering (Data processed by Martin Sill, Figure 4-1). This comparison was previously validated with human samples on the Infinium Human Methylation Microarray (Moran et al., 2014). Here we showed that the methylation signatures of FFPE samples are comparable to those from FrFr samples, which enabled us to analyze both types of materials on the Infinium Mouse Methylation array.

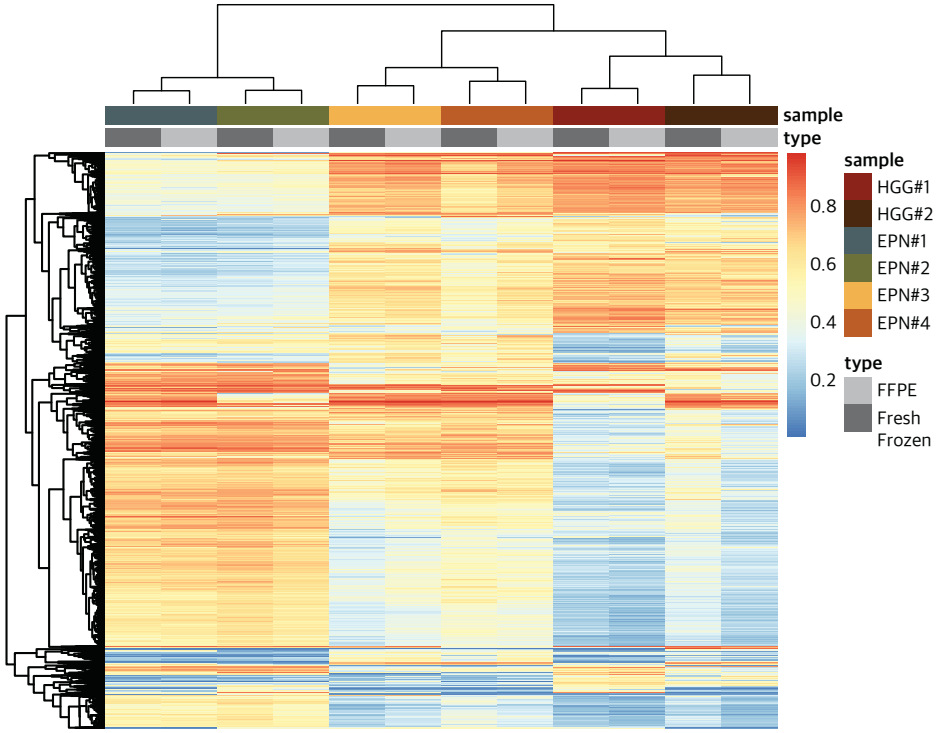

Figure 4-1 | FFPE and FrFr sample comparison

Unsupervised hierarchical clustering of the 10000 probes with highest standard deviation between the analyzed HGG model and two EPN models. In each case, signatures from FFPE and FrFr samples are comparable. Data processed by Martin Sill.

4.3 Biobank generation

Subsequently, I collected samples from models that colleagues and I generated over time. Up to this point, I profiled 315 samples including 276 samples from CNS tumors and 39 sarcoma samples (Table 4-1). These included electroporation-based models, RCAS models, GEMMs and allograft models. For each tumor entity, multiple subtypes were included (Table 4-1). Most models were analyzed as biological triplicates and some of them are, due to the missing material, only in duplicates.

	Tumor entity	Subtype number	Sample number
CNS tumors	High Grade Glioma	28	84
	Medulloblastoma	25	108
	Ependymoma	9	54
	Pilocytic Astrocytoma	2	5
	Other brain tumor	4	16
	NA	3	9
Sarcomas	Pleomorphic Rhabdomyosarcoma	5	13
	Synovial Sarcoma	3	7
	Other Sarcoma	6	16
	NA	1	3
	Total	**86**	**315**

Table 4-1 | Overview of profiled mouse models

DNA methylation is an epigenetic imprint which can be stably inherited across multiple cell divisions. During development and cell differentiation, DNA methylation is dynamic, but some DNA methylation patterns may be retained as a form of epigenetic memory (Kim & Costello, 2017). Methylome has already been used to identify the cellular origin of various cancers (Bormann et al., 2018; Servidei et al., 2021; Simon et al., 2022). To investigate the cellular origin of murine tumors, I isolated 130 normal brain tissue controls at different time points of brain development (P0, P7, P14, P21 and P28) from different locations in the brain (cerebral cortex, thalamus, brain stem and cerebellum) at which most brain tumors of our cohort occur (Table 4-2). The normal muscle control samples were kindly prepared by Roland Imle.

Controls	Sample number
CD1 normal brain	60*
Bl6 normal brain	60*
CD1 Adult NSC	1
CD1 CB NSC (P7)	3
CD1 GNP	6
Normal muscle	6

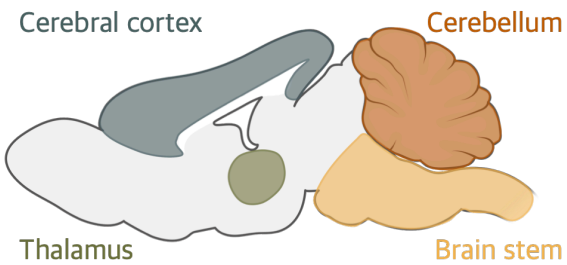

* P0, P7, P14, P21, P28 x triplicate
* Cerebral cortex, Thalamus, Brain Stem, Cerebellum

Table 4-2 | Overview of profiled control tissues

4.4 Clustering

After profiling collected samples on the Infinium Mouse Methylation Microarray, Martin helped me to process the data. The OpenSesame pipeline provided by Laird's lab was applied on the raw data (Zhou et al., 2018), which automatically filtered out poor performing probes. The standard deviation (SD) of each CpG probe across all samples was calculated, and a tSNE based on the top 10,000 probes with highest SD was generated (Figure 4-2).

The t-SNE illustrates the similarity between mouse models and normal tissue controls. Models from the same tumor entity cluster together, indicated by the color code on the right side of the figure. Synovial sarcoma models form a distinct cluster while the other sarcoma models mixed together. All available allografts from IUE-models (up to passage 3) cluster together with the original tumor for ST-EPN-ZFTA (Figure 4-2a) and for TFG-MET, Trp53 KO (Figure 4-2b). This showed the stability and liability of *in vivo* passaging of tumor cells. *In vitro* cultured ependymoma tumor cells from IUE-based mouse models up to passage 7 cluster together but not with the original tumor (Figure 4-2c). Interestingly, the normal brain controls displayed discrete clusters not only based on the brain location but also the mouse species (CD-1 vs. Bl6; Figure 4-2 circle vs. triangle). Overall, the results indicated that DNA methylation-based clusters can robustly separate different tumor entities and the mouse tumor cells retain their original DNA methylation pattern during *in vivo* passaging while these change when cultured *in vitro*.

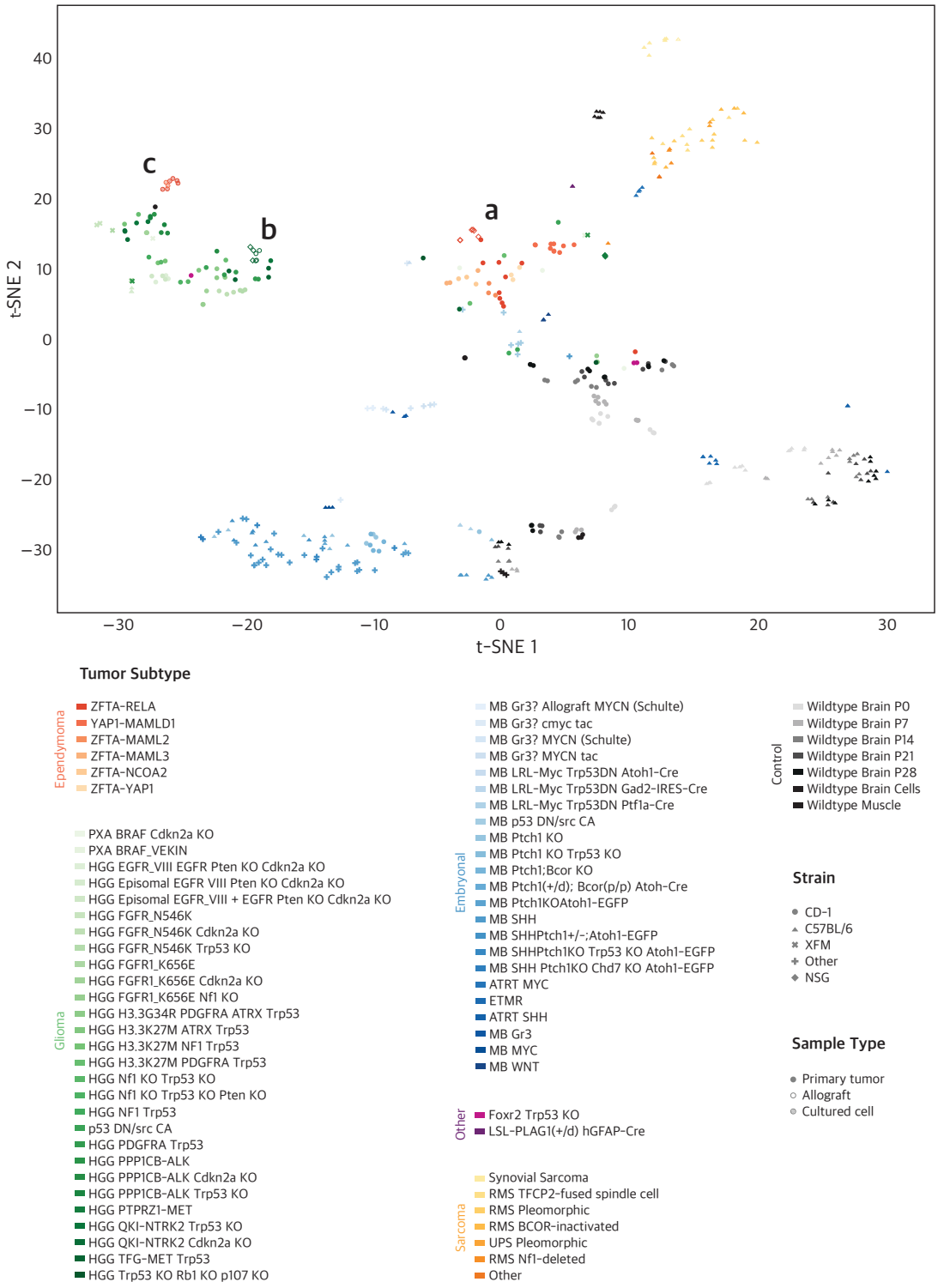

Figure 4-2 | t-SNE of all the mouse model samples and normal tissue controls

a, Allograft models from IUE-based ST-EPN-ZFTA mouse model. **b**, Allograft models from IUE-based TFG-MET mouse model with Trp53 KO. **c**, Cell cultures derived from IUE-based ST-EPN-ZFTA mouse model. Data processed by Martin Sill and illustrated by Stefanie Volz

4.5 Copy number variation

Since almost two decades, copy number variation (CNV) involving unbalanced rearrangements that change the composition of DNA, has been extensively studied and CNV can be associated with diseases (Levy et al., 2007; Redon et al., 2006). Recurrent CNVs continue to be described in different cancer types (Lee & Scherer, 2010). Therefore, it is essential to look into the CNV profiles of mouse models to investigate whether they recapitulate the pattern of their human counterparts.

In the IUE-based mouse models for ZFTA fusions, the CNV profile showed a relatively flat genome, which matched the patient data (Figure 4-3).

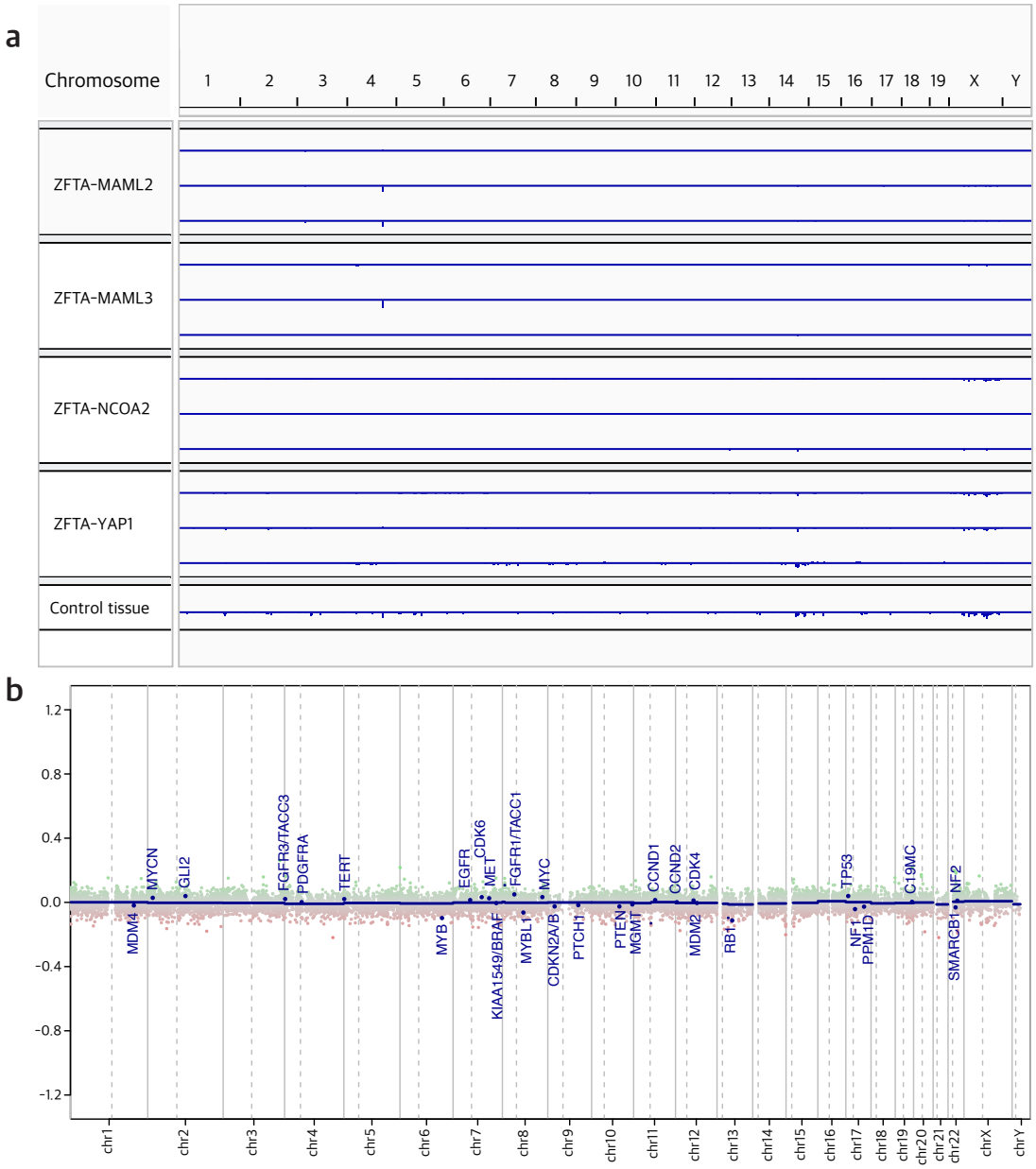

Figure 4-3 | Copy number profile of ZFTA fusion-driven samples

a, CNV from ZFTA fusion-driven mouse models. **b**, CNV from a ZFTA-MAML2-driven human tumor.

Various murine CNS tumors display an altered CNV pattern. For instance, one of the high-grade glioma models (PPP1CB-ALK; Trp53 KO) showed a loss of chromosome 4, which was identified in all three analyzed tumor samples (Figure 4-4). The murine chromosome 4 is syntenic to human chromosome 1p, which is frequently lost in human pediatric glioma.

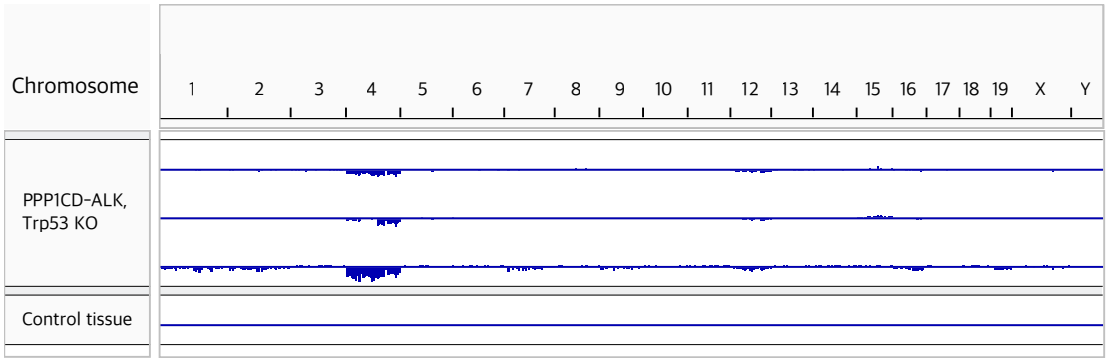

Figure 4-4 | Copy number profile of *PPP1CB-ALK* fusion-driven mouse models

Another high-grade glioma model with TFG-MET rearrangement recapitulated the human counterpart as well based on CNV profile. The profile indicated that all TFG-MET models harbor a gain of chromosome 11, which corresponded to human chromosome 17. This feature was also well preserved in the allograft models throughout 3 subsequent *in vivo* passages (Figure 4-5). In addition, allograft models also gained additional chromosome alterations which were not present in the primary tumor, such as loss of chromosome 16 (Figure 4-5).

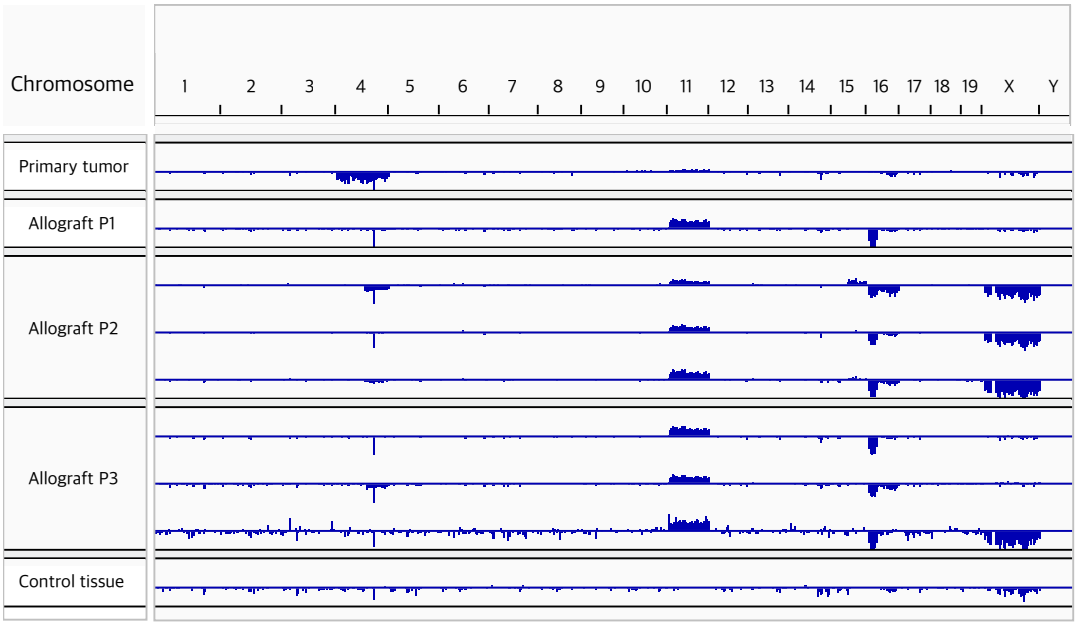

Figure 4-5 | Copy number profile of TFG-MET fusion-driven mouse models and their allografts up to passage 3

4.6 Discussion

Although mouse modelling is still indispensable for understanding tumor development and for preclinical drug studies, the similarity and faithfulness of murine models to the human disease have so far not been evaluated on a DNA-methylation level. Therefore, with the recently released mouse methylation microarray, we generated a mouse model biobank for pediatric tumors based on DNA methylation.

One of the ultimate goals was to implement the mouse samples into the existing human methylation classifier (Capper et al., 2018). Because of the pronounced species-related probes on the array, models always clustered with each other and separate from the human samples. Using orthologue filtering to narrow down to 1500 CpG sites, some models (e.g., medulloblastoma) clustered together with their human counterpart within a limited cohort size (Schoof et al., 2022). When enlarging the cohort, we again failed to circumvent the species effect. Alternative analysis methods need to be developed for this purpose.

Obvious separation of control samples from CD-1 and Bl6 mice was observed based on the DNA methylation clustering. Therefore, mouse strain difference needs to be taken into consideration for future analysis. For instance, while performing clustering of purified control cells with tumor cells for deciphering immune cell composition and cellular origin of the tumor, the strain must be matched.

Immune therapies are an attractive anti-cancer approach in addition to the conventional surgical intervention, chemotherapy, and radiotherapy that may be particularly effective to target diffusely-growing tumors (Hinrichs & Rosenberg, 2014; Quail & Joyce, 2013, 2017). A comprehensive study has analyzed the DNA methylation profile of a large pediatric brain tumor dataset to identify the main immune cell composition in pediatric CNS tumors using *in silico* deconvolution methods: CD4+/CD8+ T-cells, B-cells, Tregs, natural killer cells, eosinophils, neutrophils and monocytes (Yura Grabovska et al., 2020). To decipher the tumor immune microenvironment in the murine models, I will purify immune cell populations and use the derived methylation signatures to explore the model-specific immune microenvironment.

The cellular origin is a major factor to determine molecular types of the tumor (Alcantara Llaguno et al., 2015). Recent studies showed that tumors derived from distinct cell-of-origins demonstrated different behaviors in glioblastoma and Merkel cell carcinoma

models (Alcantara Llaguno et al., 2015; Gravemeyer et al., 2022). These findings suggest that the cellular origin essentially contributes to the development of tumor and highlights the importance of better comprehending the nature of cell-of-origin in tumors. In spite of the dynamic changes during tumor cell differentiation, DNA methylation patterns remain an epigenetic marker of cellular memory (Kim & Costello, 2017; Moran et al., 2016). Therefore, it is reasonable to explore the cellular origins of tumor based on DNA methylation profiles. To this end, I will purify and profile well-defined cell types such as NSCs, astrocytes, radial glial cells, granule neural progenitors and unipolar brush cells in order to correlate identified signatures to mouse tumor samples, thereby providing novel insights into tumor origins.

Chapter 5

Discussion, conclusions and future directions

5.1 Models for newly identified brain tumors

During my PhD studies, I validated new recurrent fusion genes discovered in pediatric supratentorial brain tumors: *ZFTA*- or *PLAGL1*-containing fusions. These two fusion partners are hallmarks of the relevant DNA methylation-based clusters and both contribute to the name of each cluster: supratentorial ependymoma *ZFTA* fusion-positive (ST-EPN-ZFTA) and neuroepithelial tumor *PLAGL1*-positive (NET_PLAGL1), respectively. I established mouse models for *ZFTA* fusion-driven tumors using *in utero* electroporation-based gene transfer technique and I employed a doxycycline-mediated fusion gene-expressing human iNSC xenograft to model *PLAGL1* fusion-driven tumors.

In the field of neuroscience, *in utero* electroporation (IUE) was first used to elucidate functions of genes and neural circuits during brain development (Saito, 2015). The highlight of this technique is that it allows to induce somatic gene transformations in a targeted area, which is particularly well suited to studying genes that are lethal while altered throughout the embryo during the development. Combining the IUE and the Tol2 transposon system, I expressed the *ZFTA* fusion genes constitutively in the NSCs located in cortical ventricular zone at E13.5 embryonic development stage, which subsequently leaded to tumor formation in cerebral cortex in mice. Alongside Tol2 system, I have successfully generated comparable *ZFTA-RELA*-positive brain tumors using another transposon system, Piggybac, which integrates specifically at TTAA tetranucleotides in the genome (Cary et al., 1989; Chen et al., 2020). This indicates the tumorigenesis of *ZFTA-RELA* is transposon-independent. On top of the stable expression of the genes of interest, Tet-On and Tet-Off system can also be combined to render the system inducible (Sato et al., 2013), which makes *in utero* electroporation a more powerful and versatile tool.

While modeling NET_PLAGL1 tumors, it was unsuccessful to induce tumors in mice via IUE at embryonic stage 13.5, 14.5 or 16.5 with *EWSR1-PLAGL1* fusion. The *EWSR1* gene has been intensively studied as a hallmark feature in the Ewing sarcoma field (Florencia

Cidre-Aranaz, 2021) and countless attempts and efforts have been made to generate Ewing sarcoma mouse models (Minas et al., 2017). Nevertheless, there was little progress regarding this topic. The most widely accepted leading cause is related to differences in GGAA microsatellites between organisms (Gangwal et al., 2008; Patel et al., 2012). Therefore, despite numerous advantages provided by the IUE technique, the species discrepancy remains the inevitable drawback. For this reason, I used human cells to surmount this barrier and obtained mouse tumors via orthotopic xenografting of iPSC-derived iNSCs carrying a doxycycline-induced *EWSR1-PLAGL1* fusion gene. Although the DNA methylation pattern of these tumors displayed strong iPSC signatures, expression profiles might circumvent this obstacle and show a similarity to the human tumor to some extent.

To obtain a more controlled experimental subject for pre-clinical drug treatment studies, I established allograft models for *ZFTA-RELA*-driven brain tumors. The first intention was to generate CD-1 syngeneic models however, the transplanted tumor cells did not survive probably due to the high polymorphism of the CD-1 mouse strain (Aldinger et al., 2009). Therefore, I used immunodeficient NSG mice as recipient resulting in tumor growth with 100% penetrance. Nonetheless, the lack of proper immune system might bias the result in case of high immune-infiltrative tumors. Establishing a syngeneic mouse model using an inbred strain such as C57BL/6 or BALB/c could overcome this restriction while the bottleneck becomes the primary tumor via IUE. Given the potential strain difference in tumor susceptibility, IUE might not induce tumors in C57BL/6 or BALB/c mice. Another technical constraint is the survival rate of embryos after suffering the electric pulses, especially with the inbred strains that usually have significantly smaller litter sizes. Instead of *in utero*, postnatal electroporation could largely increase the survival while more differentiated cells will be targeted as well (Dehay & Kennedy, 2007; Di Bella et al., 2021; Dwyer et al., 2016).

The allograft models demonstrated a substantial reduction in latency when increasing the passage number *in vivo*, as reported by other peers previously (Lampreht Tratar et al., 2018). Furthermore, according to the DNA methylation profiling, additional genomic alterations appeared during the passage. It was also reported that the blood-brain-barrier was disturbed in the intracranially injected mouse models due to the injury caused by the surgery (Leten et al., 2014). Therefore, when interpreting the outcome from the allograft models, we should take the above points into account. Since each allograft model behaves differently, it is hard to apply a general rule and standardize the protocol. Importantly, one must always confirm that the allograft still resembles the original tumor at histologic and molecular level before performing any preclinical study.

5.2 Cellular origin

Finding out the cellular origin of a tumor is beneficial for a variety of studies, including tumor modelling and targeted therapy. Numerous attempts have been carried out since decades to identify the cell-of-origin of tumors; several were successful, but some still remain debatable. It is therefore an urgent and important quest to develop a systematic method to identify the origin of a tumor.

Overexpression of *ZFTA* fusions using IUE *in vivo* gene transfer technology targeting NSCs located in the lateral ventricle that eventually gave rise to supratentorial ependymomas in mice proved that NSCs could be one of the candidates of cell-of-origin for supratentorial ependymomas, which is in line with the ependymoma formation using RCAS/N-TVA *in vivo* system (Ozawa et al., 2018).

A substantial number of studies showed that DNA methylation pattern preserves the epigenetic memory of the cells thus could potentially reflect the cellular origin (Kim & Costello, 2017; Moran et al., 2016). This is why we are trying to identify the cellular origin of the mouse tumor models based on DNA methylation profiling. Furthermore, with the development of iPSC-related technique, it is not unimaginable to generate a DNA methylation classifier with all known normal human cell types derived from iPSCs as reference. The ultimate goal would be to identify or at least to narrow down the potential cell-of-origin of a certain tumor by comparing DNA (deconvoluted) methylation patterns of the tumor and normal cells.

5.3 Future directions

While I established new mouse models and revealed important genes involved in ST-EPN-ZFTA, many pertinent questions remain. Discussed below are some that I consider most compelling in relation to my work.

5.3.1 Oncogenic driver dependency during tumor development?

I have demonstrated that the *ZFTA*-associated fusion genes are able to induce tumor formation without additional gene alterations which implied the decisive role of these fusion genes in tumor initiation. The follow-up interesting question would be whether the fusion

gene is required for the maintenance of tumor progression. A first step to answer this question would be to knock-out the fusion gene in all available ST-EPN-ZFTA models, including human and mouse cell lines, and assess the cell survival and/or proliferation. In addition, one could also generate an IUE mouse model in which the expression of the fusion gene can be manipulated via Tet-On/Tet-Off (Figure 5-1) or TAG protein degradation system (Nabet et al., 2018).

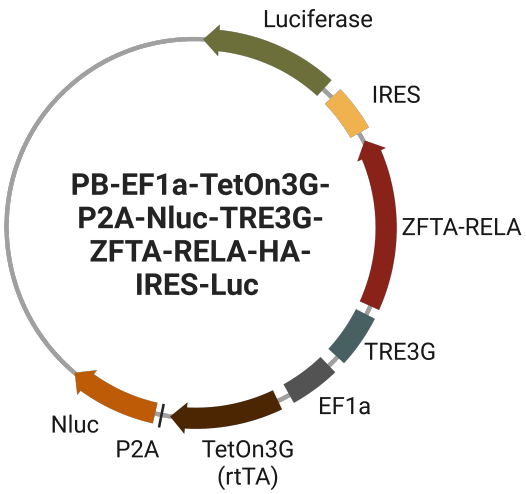

Figure 5-1 | Graphical illustration of Tet-On system

As mentioned in Chapter 2, based on IHC staining against HA-tagged fusion proteins, a portion of cell populations located in the tumor area did not seem to harbor the oncogenic driver. Another pertinent observation is that when culturing the IUE-based mouse tumor cells *in vitro*, in some cases they lost the fusion gene expression but kept proliferating intensively. It would be interesting to investigate whether these cells still form tumors in mice. Furthermore, sorting out the IUE-based tumor cells with or without fusion and subsequently transplant these orthotopically into mouse brains could provide further insights into the dependency of fusion proteins in tumor progression.

5.3.2 Co-factors of the fusion gene for transcription?

Given that 1) The discrepancy in the latency of IUE-based mouse models implies the variable transformation capacity of the *ZFTA* fusion genes; 2) the artificial ZFTA-VP64 or -EP300 did not induce tumor formation *in vivo*, I hypothesize that additional elements are implicated in the *ZFTA* fusion-mediated oncogene activation. The transcription factors exert

gene expression via specific assortment of mediators/co-factors which can alter transcription efficiency. I think it is beneficial to identify important co-factors of ZFTA fusions via, for instance, immunoprecipitation followed by mass spectrometry. This might provide new insights into the underlying mechanism of how ZFTA fusions activate oncogene expression. Further investigation might provide evidence which co-factors could be alternative therapeutic vulnerabilities.

5.3.3 Intercellular communication?

Over the past decade, the tumor microenvironment (TME) has been increasingly studied and was proven to functionally contribute to the hallmarks of cancer (Hanahan & Weinberg, 2011). In this complex TME network, how cells communicate and support each other remains the most important and interesting topic to explore. When performing co-staining against the proliferative marker Ki67 and HA-tag in *ZFTA-RELA* and *YAP1-MAMLD1*-driven mouse tumors, I found that the signal from these 2 markers did not overlap. This suggests that tumor cells communicate and sustain proliferative features via paracrine signaling. The aberrant expression of tyrosine kinase receptors EGFR, FGFR and EPHB2 provides strong supports for this hypothesis. The EPH/ephrin pathways can enhance malignant transformation in several tumors and it is also well established that the EPH/ephrin signals can promote tumor angiogenesis (Ahmadiankia, 2020; Ahmed & Bicknell, 2009). Although it has been shown a decade ago that overexpression of *EPHB2* in NSCs can drive brain tumor formation in mice, the role of EPH/ephrin signaling in EPN is still poorly understood (Johnson et al., 2010). Applying single-cell RNA-sequencing (scRNA-seq) on human tumors might help to uncover the intricate interactions between the EPN tumor cells and its TME. Indeed, a recent study using scRNA-seq revealed clear tumor heterogeneity in ST-EPN based on *in silico* analysis (Gojo et al., 2020). Further in-depth analyses and validations could help to explore more drugs targeting the paracrine signaling to diminish the support for cell proliferation.

Besides cell-cell contact, cells also communicate over secreted molecular factors through a highly complex system such as extracellular vesicles (EVs), among which exosomes are rising as novel intercellular messenger in both physiological and pathological conditions (Maia et al., 2018). Increasing evidence reinforced the key role of exosome in CNS tumor progression by providing an advantageous environment to promote tumor cell proliferation. Furthermore, tumor cells secrete exosomes in the TME to protect their proliferative feature by decreasing the inflammatory reaction thus suppressing the immune response (Harding et al., 2013; Maia et al., 2018). Recent studies illustrated that glioma cells

communicate via EV trafficking and glioma tumor cells secret a different repertoire of exosome content from the normal cells in TME which could influence malignant features of gliomas (Huang et al., 2022; Redzic et al., 2014; Skog et al., 2008; Tűzesi et al., 2017). Our lab has identified ST-EPN-ZFTA-specific EV populations using multi-omics data (Maass et al., 2022). However, further mechanistic investigations are needed to better understand the potential role of the EVs in cell-cell communication regarding the EPN therapeutic protocols.

5.3.4 Cancer stem cells?

A growing number of human tumors have been reported to comprise sub-populations with cancer stem cell (CSC) properties, functionally defined by their potent tumor-initiating capacities following serial transplantation into mice, which is the gold standard assay for CSCs. The presence of CSCs has been proved prospectively in various solid tumors including breast, colorectal and glioblastoma (Al-Hajj et al., 2003; O'Brien et al., 2007; Singh et al., 2004). Patients diagnosed with ST-EPN-ZFTA suffer tremendously from the relapses despite the surgical intervention and/or radiotherapy (Messahel et al., 2009), which gave a hint for the existence of persisting CSCs. The fact that the *ZFTA-RELA* fusion can generate allograft mouse models further corroborates that ST-EPN-ZFTA tumors contain CSCs as well. To be able to identify these CSCs is crucial for developing targeted therapies and increase the progression free survival of affected patients. Marking cells with uniquely distinguishable dyes or genetic elements has long been used for pinpointing their lineages. In recent years, the barcoding strategies have been harnessed in multiple model systems through a variety of forms (Alemany et al., 2018; Kalhor et al., 2018; McKenna et al., 2016). The Cre-recombinase-driven *Polylox* and the dox-inducible CRISPR/Cas9 barcoding system were established to trace the hematopoietic stem cell lineages in a physiological manner in mice (Bowling et al., 2020; Pei et al., 2019). Using these genetically engineered barcoded mice to generate *ZFTA* fusion-driven mice via *in-utero* electroporation followed by serial transplantation, it is conceivable to reveal the properties of CSCs in ST-EPN-ZFTA tumors.

5.3.5 Which cells support fusion positive cell growth?

Overexpression of *EWSR1-PLAGL1* fusion gene *in vivo* showed a completely different behavior from *in vitro* cultures. It is quite interesting to understand the underlying mechanism that triggered this opposite phenomenon. There must be additional signaling pathways being activated by the surrounding normal cells to stimulate the proliferative

feature of the fusion-containing cells. To identify the key factors/pathways, perhaps one simple way would be to co-culture the fusion-positive cells together with each known TME cells respectively, such as astrocytes, neurons and neural stem cells, or even combinations of several cell types. Once such proliferative phenotype is reproduced *in vitro*, multi-omics analysis of the cells as well as the supernatant could unveil the mystery of the behavior discrepancy, with the intention that one can mimic the *in vivo* environment in a dish to create a more reliable and less laborious model for brain tumor study. Moreover, in line with the important involvement of intercellular communication in EPN, finding out the supporting factors is imminent for developing further EPN treatment options.

One remaining puzzling piece is that *ZFTA-RELA* and *YAP1-MAMLD1* fusion did not induce tumors in human iNSCs and *ZFTA-RELA* even provoked apoptosis in this condition, while studies have illustrated that using mouse *Cdkn2a*$^{-/-}$ NSCs overexpressing *ZFTA-RELA* fusion rendered the cells malignant and formed brain tumors after orthotopic transplantation. Perhaps introducing a second hit such as *CDKN2A* KO could recover the proliferative feature of *ZFTA-RELA*-positive cells.

5.4 Concluding remarks

The studies described here provided representative mouse models for *C11orf95/ZFTA* fusion-driven tumors. Cross-species analyses identified *C11orf95/ZFTA*-specific oncogenic signaling pathways. Further *in vitro* and *in vivo* investigations validated *GLI2* as potential therapeutic vulnerability in these tumors. *C11orf95* is now officially designated as zinc finger translocation associated (*ZFTA*) by the HUGO Gene Nomenclature Committee. In addition, the WHO has accepted to name the group of supratentorial ependymoma carrying a fusion containing the *ZFTA* fusion gene Supratentorial ependymoma, ZFTA fusion-positive (ST-EPN-ZFTA). However, lots of obstacles emerged while modeling the *PLAGL1*-driven supratentorial brain tumors. Eventually, doxycycline-mediated *EWSR1-PLAGL1*-expressing human NSCs induced tumor formation after orthotopic transplantation *in vivo* but further effort still needs to be put on characterizing this tumor model at molecular level. Lack of tools to study the rare tumors is a general issue in the field thus it is urgent to expand the model repertoire for pediatric brain tumors. DNA methylation-based mouse model biobank could potentially provide a new platform to validate mouse models as well as to study the TME and the cellular origin of tumors, which is an exciting avenue in the near future.

Chapter 6

Materials and Methods

Parts of the written contents of the following chapter have been published in the research article "Cross-species Genomics Reveals Oncogenic Dependencies in ZFTA/C11orf95 Fusion–Positive Supratentorial Ependymomas" to Cancer Discovery in 2021. Contributions of authors other than myself are indicated.

6.1 Molecular biology methods

6.1.1 Plasmid cloning

Tol2-based overexpressing plasmids: The full or partial coding regions of human *ZFTA*, *RELA*, *MAML2*, *MAML3*, *NCOA2*, *EWSR1*, and *PLAGL1* cDNAs with a C-terminal HA tag were amplified by PCR and cloned into pT2K-IRES-Luc plasmid vectors using In-Fusion HD Cloning kit (Takara Bio). Dominant negative *Gli2* was amplified by RT-PCR on total RNA of mouse granular neural progenitor cells. pT2K plasmids were co-transfected with Tol2 transposase encoded in the pCAGGS plasmid. For the generation of *ZFTAΔZF1-RELA/MAML2/NCOA2* cDNA, a sequence of zinc finger domain was chosen based on UniProt prediction. The protein expression of all cloned overexpressing plasmids was confirmed by transient overexpression in HEK293T cells followed by protein extraction and Western blotting.

Dox-inducible shRNA plasmids: Human EPN cell line EP1NS was transduced with lentiviral pLKO-tet-on vector system (plasmid #21915, Addgene) containing a puromycin-resistance gene, and a tet-responsive element for dox-inducible expression of shRNA against GLI2 (shGLI2_1 and shGLI2_2) or a non-targeting control shRNA (shControl). The dox-inducible vectors were generated according to a publicly available protocol (Wee et al., 2008; Wiederschain et al., 2009). Lentiviral particles were generated in HEK293T cells. Virus-containing supernatant was collected to infect EP1NS cell line.

Dox inducible fusion expressing plasmids: HEK293T and EP1NS cells were transduced with the dox-inducible lentiviral vector system TLCV2 (plasmid #87360). The Cas9 sequence was replaced by EWSR1-PLAGL1, ZFTA-RELA or YAP1-MAMLD1 fusions using BshTI and BamHI cloning sites. Lentiviral particles were generated in HEK293T cells.

6.1.2 RNA Isolation and cDNA synthesis

Total RNA was extracted from cryo-preserved mouse tissues using a RNeasy Plus Mini Kit together with QIAshredder (QIAGEN) according to manufacturer's instructions and stored in -80 °C until use. cDNAs for downstream application were prepared using the SuperScript VILO cDNA Synthesis Kit (Invitrogen).

6.1.3 Quantitative RT-PCR

qRT-PCR mix was prepared following manufacturing protocol of Power SYBR Green PCR Master Mix (Applied Biosystems). qPCR was performed using the QuantStudio 5 RT-PCR system (Applied Biosystems). The cycling conditions used were 95 °C for 10 minutes and 40 cycles of 95 °C for 15s and 60 °C for 1 minutes following dissociation analysis. All qPCR reactions were done in triplicate and normalized to TBP mRNA levels.

6.1.4 Genomic DNA extraction

Genomic DNA extraction from fresh-frozen tumor chunk from the mouse models mentioned in Chapter 4 were performed using QIAamp DNA mini kit (#51304, QIAGEN) according to the manufacturer's instructions.

Maxwell RSC DNA FFPE kit (#AS1450, Promega) was used to extract genomic DNA from FFPE samples in Chapter 4. To extract tumor cells from the mouse brain embedded in paraffin block, I first cut the block with microtome into 10 mm thick slices and mount on glass slides. Then I used a scalpel to scratch off the area with tumor cells identified via H&E staining, and collect them into a 1.5 mL microcentrifuge tube. Maximum 2 mm^3 volume of tissue was collected per sample. Afterwards, according to the manufacturer's instruction, the samples were processed.

6.1.5 Western blotting

The protein expression of the plasmids used in this study was validated by western blotting according to the following procedures: HEK293T cells were transfected with the plasmids and harvested 48h after transfection. The cell pellets were lysed with RIPA buffer and 20 μg of the protein lysates were used for protein detection. Briefly, proteins were denatured for 5 minutes at 95 °C, loaded on NuPAGE Bis-Tris (#NP0301BOX, Invitrogen) and separated at 120 V for 2h. Proteins were transferred to methanol-activated PVDF membrane by tank electrotransfer in Towbin buffer for 1h at 110 V. Membrane was blocked with 5% skimmed milk in 0.5% Tween/TBS (TBST) for 1h at RT prior to overnight incubation with primary antibodies (section 7.3). After washing with TBST, membrane was incubated with secondary antibody for 1h at RT. The membrane was developed with either ECL (RPN2106, GE Lifesciences) or ECL Prime (RPN2232, GE Lifesciences) as recommended by the manufacturer followed by exposure to autoradiography films in a dark room.

6.1.6 CUT&RUN

CUT&RUN assay was performed as described in (Skene et al., 2018). Briefly, 0.5-1 million cells were captured with BioMagPlus Concanavalin A beads and incubated with primary antibody for 10-20 mins at room temperature. After washing away the EDTA in the buffer and unbound antibody with dig-wash buffer (20mM HEPES pH 7.5, 150mM NaCl, 0.5mM Spermidine, 1x Complete Protease Inhibitor EDTA-Free and 0.05% Digitonin), protein A-MNase was added and incubated for 10-20mins. The cells were washed again and placed in an ice-water pre-chilled metal block at least 5mins. $CaCl_2$ was added to the final concentration of 2 mM to activate protein A-MNase for 30mins on the ice-water chilled metal block. The reaction was stopped by addition of equal volume of 2XSTOP buffer (340 mM NaCl, 20mM EDTA, 4mM EGTA, 0.02% Digitonin, 5μL/ml RNase A, 50μg/ml glycogen and 2 pg/ml heterologous spike-in DNA). The protein-DNA complex was released and DNA was extracted with Gel and PCR Clean-up kit (Macherey-Nagel NucleoSpin®, cat. no.740609.250) or Phenol-chloroform-isoamyl alcohol precipitation (for small fragment DNA), followed by Qubit fluorometer and Agilent 4200 Tapestation quality and size distribution control. (Performed by Stephen Mack)

6.2 Cell biology methods

6.2.1 Immunohistochemistry staining

Brains with tumor from electroporated mice were dissected and fixed with formalin at 4 °C for minimum 24h up to 1 week. Fixed brain was placed in a tissue embedding cassette and dehydrate in the following solutions sequentially with indicated time.

Solution	Time x Number
70% Ethanol	30 min
80% Ethanol	30 min
90% Ethanol	4 h
100% Ethanol	10 h
100% Ethanol	7 h x 2
Xylene	4 h
Xylene	6 h x 2
Paraffin	6 h
Paraffin	4 h x 2

Dehydrated samples were then embedded in paraffin and cut into 5 µm-thick sections with microtome (Leica Biosystem). Sections were mounted on SuperFrost Plus adhesive microscope slides (Thermo) and dried overnight at 37 °C.

Before performing staining, FFPE samples were deparaffinized in the following solutions sequentially with indicated time.

Solution	Time x Number
Xylene	10 min x 2
100% Ethanol	2 min x 2
95% Ethanol	2 min
70% Ethanol	2 min
H_2O	Wash

Hematoxylin & Eosin staining: After deparaffinization, the sections were stained in hematoxylin solution for 2 min followed by washing with running tap water for 2 min. Then the samples were stained again with eosin solution for 2 min and quickly wash in water 10 times up and down.

DAB staining for Figure 2-5: After deparaffinization, the sections were pre-treated in citrate buffer at 100 ˚C for 30 minutes. Then the sections were incubated with anti-HA antibody (section 7.3) diluted with Dako REAL Antibody Diluent (Agilent #S2022) at room temperature (RT) overnight. DAB staining was performed the next day using SuperVision 2 HRP-polymer kit (DCS PD000POL) following the protocol provided by the manufacturer.

DAB staining for Figure 3-23: After deparaffinization, the sections were pre-treated in citrate buffer at 100 ˚C for 20 minutes. Then the sections were blocked with 10% normal donkey serum for 1 h and incubated with anti-HA or anti Ki67 antibody (section 7.3) at RT overnight. Next day, the sections were incubated with biotinylated secondary antibodies for 30 min and signals were amplified by a horseradish peroxidase system (ABC kit, Vector) followed by DAB staining (Nichirei N-Histofine® DAV-2V). Nuclei were counterstained with hematoxylin.

After staining, the sections were subjected to dehydration process again with the following steps and were mounted with cover media Eukitt® (Orsatec) followed by drying overnight under the chemical hood. Images were acquired with confocal microscopes (ZEISS Cell Observer) or Histoscanner.

Solution	**Time x Number**
70% Ethanol	1 min
95% Ethanol	1 min
100% Ethanol	1 min x 2
Xylene	2 min x 2

6.2.2 Immunofluorescence staining

HEK293T cells were cultured on glass coverslips one day before transfection. Plasmid constructs were transfected using Fugene® (Promega) following the instructions provided by manufacturer. 48h after transfection, cells were fixed with 4% paraformaldehyde for 20 minutes followed by 10 minutes permeabilization with Triton buffer (0.1% Triton in PBS). After washing with PBS two times, the primary antibody (section 7.3) was applied directly on the cells for 1 hour at RT. The antibody solution was removed by absorption with Whatman filter paper before washing the coverslips two times 5 minutes with PBS. The corresponding secondary antibody was applied subsequently, incubated for 30 minutes and three times washed for 5 minutes in PBS. Finally, cells were washed briefly in ddH_2O in order to remove salts and pure ethanol before they were mounted on

microscopy glass slides with Fluoromount-G™ containing 1 μg/mL DAPI (Southern biotech). Fluorescent images were captured using a confocal laser-scanning microscopy (LSM780 and 800, Zeiss; and SP5, Leica).

6.2.3 Cell proliferation assay

Infected EP1NS or iNSCs were selected with 1 or 5 μg/mL puromycin. The shRNA or fusion gene expression was achieved by adding a range of doxycycline concentration every 48h to the medium. For proliferation assay, 96h after dox administration, the cells were treated with EdU (final concentration: 10 μM) for 12h and subsequently harvested with Accutase solution. EdU-incorporated cells were labeled using a Click-iT EdU Alexa Fluor 647 Flow Cytometry Assay Kit (Life Technologies) according to the manufacturer's protocol. The cells were passed through a 35 μm cell strainer yielding a single cell suspension and analyzed by flow cytometry using a FACS Fortessa flow cytometer (BD Biosciences).

6.2.4 Apoptotic assay

For apoptosis assay, the infected cells were harvested 96h after dox treatment, and were subsequently washed twice with Cell Staining Buffer (BioLegend). Cells were then stained with Annexin V-APC and DAPI diluted in Annexin V Binding Buffer using Apoptosis Detection Kits (BioLegend) according to the manufacturer's protocol. Samples were analyzed by flow cytometry using a FACS Fortessa flow cytometer (BD Biosciences).

6.3 *In vitro* culture experiments

All cells were maintained in a humidified 5% CO_2 atmosphere at 37 °C and subcultured when cell confluency reached approximately 80%. Mycoplasma contamination was assessed periodically by GATC/Eurofins. To determine the exact cell number, 10μl of cell solution was mixed with 10μl of 0.4% TC10 trypan blue dye (BioRad). 10μl of the mixture was loaded into the counting chamber of dual-chamber slides (BioRad) and the viability and cell number were determined using TC20 Automated Cell Counter (BioRad).

6.3.1 Cell culture

HEK-293T (CRL-3216) cells were purchased from ATCC. HEK-293T cells were cultivated with Dulbecco's Modified Eagle Media (DMEM, Thermo Fisher) supplemented with heat-inactivated 10% fetal bovine serum (FBS, Thermo Fisher), 2 mM L-glutamine, 100 U/mL penicillin and 100 µg/mL streptomycin.

EP1NS cells were originally published in (Milde et al., 2011) and were cultured on Geltrex-coated plates in Neurobasal-A medium supplemented with 1µg/mL Heparin, 2mM L-Glutamine, Pen-Strep, 1 x B27, 10ng/mL bFGF and 20ng/mL EGF. Medium change was performed 2-3 times per week. While passage the cells, Accumax was used for detaching the cells from the matrix (5 minutes at 37 degrees).

Human iPSCs were cultured in mTeSR+ medium (StemCell Technologies). Once the hiPSCs reached an optimal density of 70% coverage, the cells were passaged and expanded. Cells were washed once with 1-2ml DPBS followed by the addition of 1ml enzyme-free passaging reagent ReLeSR™ (StemCell Technologies). ReLeSR™ was aspirated within 30 seconds, partially covering the cells with a thin film. To enable cell dissociation, the plate was incubated for 3 minutes at 37°C, 5% CO_2. After incubation, 1ml of mTeSR+ was added and the colonies were dissociated by firmly tapping on the side of the plate for 30-60 seconds. The broken-up colonies were collected in a 15ml canonical tube and flicked until the colonies became small (mean cell aggregate size 50-200µm). Cells were split up in an up to 1 : 50 ratio and seeded on Matrigel-coated plates at 37°C, 5% CO_2. After splitting, cells were maintained by daily media change.

6.3.2 Monolayer neural differentiation and NSC culture

Neural differentiation of hiPSC 771-3G NPCs was performed using STEMdiff™ Neural System (StemCell Technologies) according to both the manufacturer's protocol and a modified version of the commercial protocol, with the aim to generate forebrain-like NSCs. Briefly, iPSC lines were grown in mTeSR+ on Matrigel-coated 6-well plates until the day of differentiation. At the start of the induction protocol, the cells were washed once with 2 mL PBS and dissociated by adding 1 mL/well Accumax (Sigma) for 5 minutes at 37°C. The wells containing detached colonies were washed with 5 mL DMEM/F-12, collected into a 15 mL tube and centrifuged for 5 min at 300g. 1 x 10^6 single cells were then resuspended in 2 mL STEMdiff™ Neural Induction Medium (NIM) + SMADi on Matrigel-coated 6-well plates. To increase the survival rate of the cells, the media were supplemented with 10 µM Rho-

associated kinase inhibitor (ROCKi, Y-27632, Enzo) on the day of re-plating and passaging. Full media changes were carried out on the following three days. On the fourth day of the induction protocol, the cells were passaged using Accumax as described above and $1x10^6$ cells/well were plated on Matrigel-coated 6-well plates in NIM. After three passages, the cells were cultured in NSC Maintenance Medium (NSCMM) composed of DMEM/F12, GlutaMAX (1x), B27 supplement (1x), NEAA (0.5x), 5 ng/mL h-LIF, 1.5 μM CHIR99021, 2.5 μM SB525334, 40 ng/mL FGF2, and 40 ng/mL EGF, 2 μg/mL Heparin. The media was changed daily and after the cells reached the appropriate density.

6.3.3 Neon electroporation

Plasmid DNA mix was extracted from bacteria with EndoFree DNA extraction Maxi Kit (QIAGEN) and prepared for 10 μg/10^6 cells in high concentration. NSCs were cultured in NSCMM until 80-90% confluence and ready to be split. Single-cell suspension with a density of 10^6 cells/μL was prepared using Accumax (Sigma) as mentioned in 6.3.2. The electroporation followed the protocol provided by the manufacturer (Invitrogen Neon™ Transfection System, #MPK10096). In short, cells were resuspended in buffer R from the kit and mixed with the pre-prepared plasmid DNA mix. DNA-cell mix was transferred into the electrolyte buffer E2 with Neon™ pipette tip by fixing the pipette on the Neon™ station. The electroporation was applied via the Neon™ device according to the programs showed in the experiment. Electroporated cells were placed immediately on the Matrigel-coated plate. Medium was changed the next day. The transfection efficiency was analyzed based on GFP reporter by FACS Fortessa flow cytometer (BD Biosciences).

6.3.4 Liposome-based transfection

Liposomes-based transfection was realized using either Fugene® (Promega) or TransIT® (Mirus) according to the protocols provided by the manufacturer. Transfection reagent was warmed up to room temperature (RT) before use. For a 6-well plate format, 2 – 4 μg plasmid DNA was prepared in 400 μL OptiMEM® Reduced-Serum Medium (Gibco). Transfection reagent was added directly into the medium with a ratio of DNA(μg) : reagent(μL) = 1 : 3, vortexed well and incubated at RT for maximum 15 min. The mixture was added on top of the cells with a confluency of 60-70% without further mixing. Medium was changed the next day. The transfection efficiency was analyzed based on GFP reporter by FACS Fortessa flow cytometer (BD Biosciences).

6.3.5 Lentivirus production, concentration and quantification of titer

All the lentiviruses used in the thesis were produced using Fugene® liposome-based transfection on HEK293T cells with low passage number (less than passage 10). DNA mix for virus production was prepared as following: packaging plasmid (psPAX2, 2 μg) + envelop plasmid (pMD2.0, 2 μg) + lentiviral transfer plasmid (4 μg) for one 10 cm Petri dish. For virus production and concentration, the protocol below was used:

Timepoint	Procedures
Day 0	Seed 5 x 10^6 HEK293T cells in one 10 cm Petri dish
Day 1	Transfect DNA mix into cells using Fugene® liposome-based transfection
Day 2	Remove the medium and add 5mL fresh media
Day 4	Collect the supernatant containing viruses and centrifuge 5 min at 300 x g
	Pass the supernatant through 0.45 μm filter
	Add 3 volume of Lenti-X™ Concentrator (Clontech)
	Incubate at 4°C for 30 min and centrifuge 45 min at 1500 g
	Remove the supernatant and resuspend the pellet in 1/100th of the original volume with PBS

After the production and concentration, virus titer was determined directly on cells of target (EP1NS or iNSCs). Cells of target were seeded the day before virus concentration with 200K cells/well in 6-well plate. The concentrated viruses were added 10 μL to each well with a dilution of 1/10th, 1/100th,1/1000th, 1/10000th and undiluted. The media were changed freshly the next day and the tier was analyzed 2 days after based on GFP reporter by FACS Fortessa flow cytometer (BD Biosciences).

6.4 *In vivo* mouse experiments

CD-1 mice used for *in utero* electroporation were obtained from Charles River and housed in a vivarium with a 12h light/dark cycle with access to food and water ad libitum. The day of the plug and the birthdate are designated as embryonic day (E) 0.5 and postnatal day (P) 0, respectively. Allografting of IUE-based mouse tumor cells and engrafting of iPSC-derived cell suspensions were carried out in immundeficient NSG mice. NSG mice for transplantation as well as pregnant CD-1 mice for IUE were generated at the animal core facility at German Cancer Research Center and the vaginal plug date was recorded by the technicians. All animal experiments carried out during the thesis were conducted according

to the animal welfare regulations approved by the Animal Care and Use Committee of the National Institute of Neuroscience, NCNP in Japan (Approval number: 2019028R1) and the responsible authorities in Germany (Regierungspräsidium Karlsruhe, approval number: G-255/19, G-260/19, G-168/17 and G-75/20).

6.4.1 *In utero* electroporation

Before surgery, the injection needle was prepared using Borosilicate Glass Capillary, which was pulled on a micropipette puller with the following setting: heat = 560, pull = 150, velocity = 75, time = 250, and ground at an angle of 30 degree to make a sharp-angled tip allowing smooth injections into the developing brain through the uterus wall. The plasmid solution was prepared as follows: endotoxin-free DNA plasmid mixture was diluted with PBS into a final concentration of 1 µg/µL. 1 μL 1% filtered Fast Green solution was added per 20 μL plasmid solution for dying purpose. One day before the surgery, animals were provided with metamizol as pain killer in the drinking water at a concentration of 800 mg/kg/day. On the day of surgery, 20 minutes before starting the surgery, 5 mg/kg carprofen was injected to the dam subcutaneously. The surgery table and material were prepared as indicated in Figure 6-1 and cleaned with disinfectant to create an aseptic surgical environment.

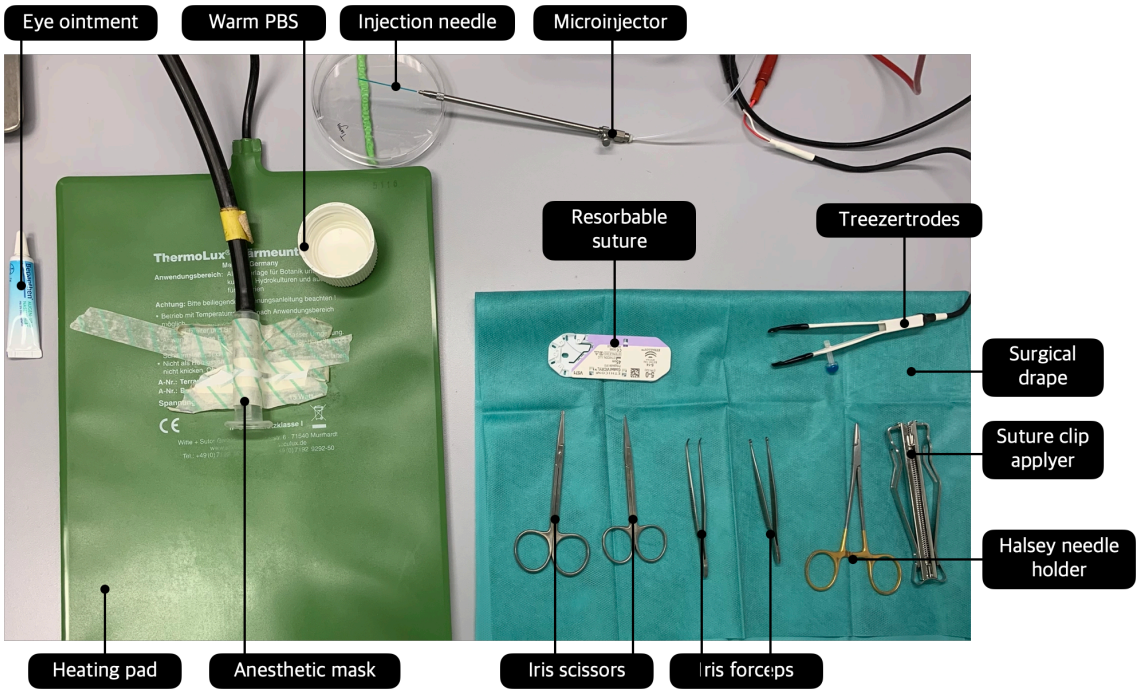

Figure 6-1 | Layout of surgery table prior to *in utero* electroporation

At E13.5, E14.5 or E16.5, the pregnant animals were anesthetized using 2%-2.5% isoflurane and fixed on a heating pad in dorsal decubitus (Figure 6-2a). The peritoneum fur was shaved and cleaned with skin disinfectant and 70% ethanol and eye ointment was applied to prevent corneal injury. A small skin incision of about 2.5 cm was made on the ventral side of the mouse followed by an incision of abdominal muscle (Figure 6-2b and c). The animal was then covered by a sterile gauze to reduce the risk of infection (Figure 6-2d). One side of uterine horn was gently retrieved and placed on the sterile gauze (Figure 6-2e). I injected approximately 1-2 μL of the plasmid solution into one side of the lateral ventricle of the brain (Figure 6-2f and g) and subsequently electroporated with 5 mm-diameter forceps-like electrodes (32 V, 50 ms-on, 450 ms-off, five pulses, (Figure 6-2h). During the surgery, warm PBS was dripped on the uterus to keep it hydrated. I placed back the manipulated uterus into the abdomen after all embryos, except the ones at the extremity, being injected and electroporated and same procedure was repeated for the other side of uterine horn. In the end, the peritoneum incision was sewed back using resorbable suture and the skin was closed by surgical clips (Figure 6-2i and j). The mouse was then placed back into a clean cage and carefully monitored for the next day. Mice received metamizol in the drinking water at the same concentration up to 2 days after the surgery.

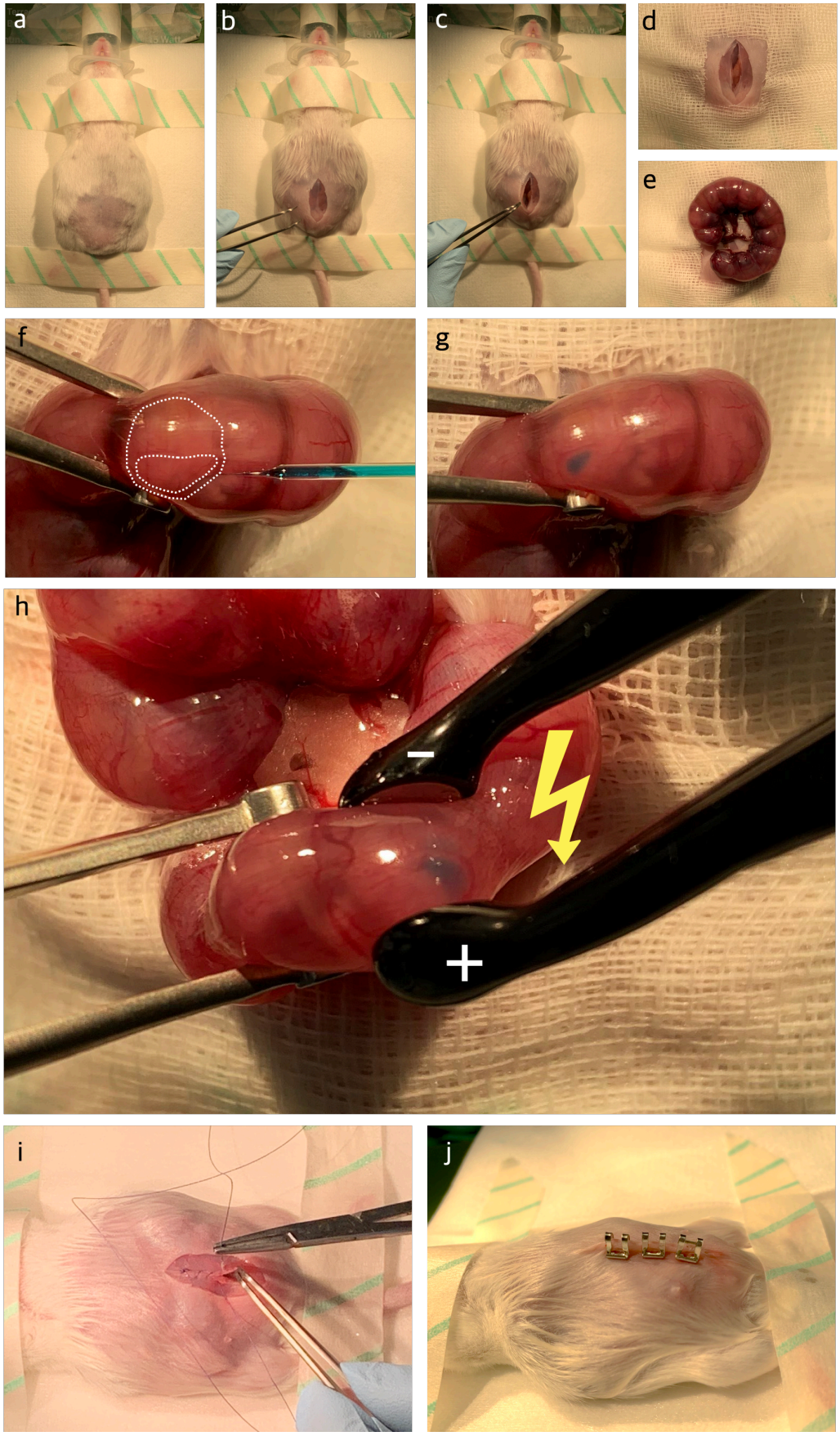
a
b
c
d
e
f
g
h
−
+
i
j

Figure 6-2 | Illustration of surgical procedures for *in utero* electroporation

a, Anesthetized dam was placed in dorsal decubitus on a heating pad and cleaned with disinfectant. **b**, A 2.5 cm skin incision was performed with sharp-end scissors. **c**, An incision of abdominal muscle was performed with blunt-end scissors. **d**, Sterile gauze was placed on the animal. **e**, Uterine horn was pulled out of the peritoneum and placed on the sterile gauze. **f**, Head of embryo (outer white dashed line) was fixed by ring-shaped iris forceps and the needle was inserted into the lateral ventricle (inner white dashed line). **g**, Plasmid mixture was injected into lateral ventricle using microinjector and visualized by Fast Green dye. **h**, Electric pules were applied via 5 mm-diameter forceps-like electrodes and the anode (+) was placed on the side of injection. **i**, Abdominal muscle was sewed using resorbable string with running suture. **j**, Skin was closed using surgical clips.

6.4.2 Intracranial injection

Cells for inoculation were harvested and dissociated using Accumax solution, washed with DMEM/12 and passed through a 40 mm cell strainer. Resulting single cell suspensions were pelleted for 5 minutes at 300 g and cells were resuspended in a small volume of complete NSCMM at a density of approximately 1 x 10^5 cell/µL. Analgesia was administered to female NSG mice (6-8 weeks) by subcutaneous injection of carprofen (5 mg/kg). After 20 minutes, animals were anaesthetized by isoflurane (1.5 - 2.5% (v/v)) and Puralube Vet Ointment sterile ocular lubricant (MWI Veterinary Supply) was applied to both eyes. After negative reflex testing (toe pinch), animals were fixated in a stereotactical frame and a 5 mm incision in the scalp was introduced. For local anesthesia, 0.25% bupivacaine was applied to the incision. A 18G cannula (diameter: 1.27 mm) was used to drill a small hole into the skull (location coordinates: 1 mm posterior to bregma; 1 mm to the left side of the midline; 1.5 mm deep). The Hamilton needle was then introduced into the brain and the cell suspension (4 µL media) was injected within a time frame of 2 minutes. The needle stayed in the tissue for another 2 minutes to avoid any reflux of the cell suspension. After slow removal of the needle the incision was closed by tissue adhesive. Only after recovery of the animal in a separate clean cage, was it placed back into the original cage. Operated animals were treated with carprofen subcutaneously (5 mg/kg) 20 minutes prior to the surgery. Mice implanted with human iPSC-derived iNSCs or IUE-derived mouse tumor cells were monitored regularly for signs of tumor formation, which can include distention of the calvarium, head tilt, reduced feeding, weight loss, dehydration, hunched posture, eye irritation, or poor grooming habits. In addition, tumor formation was regularly monitored by bioluminescence imaging of luciferase activity using an In Vivo Imaging System (c.f. section 6.4.3). Upon observation of symptoms, mice were euthanized, and tumor presence was confirmed visually during tissue resection. (Adapted from (Haag et al., 2021)

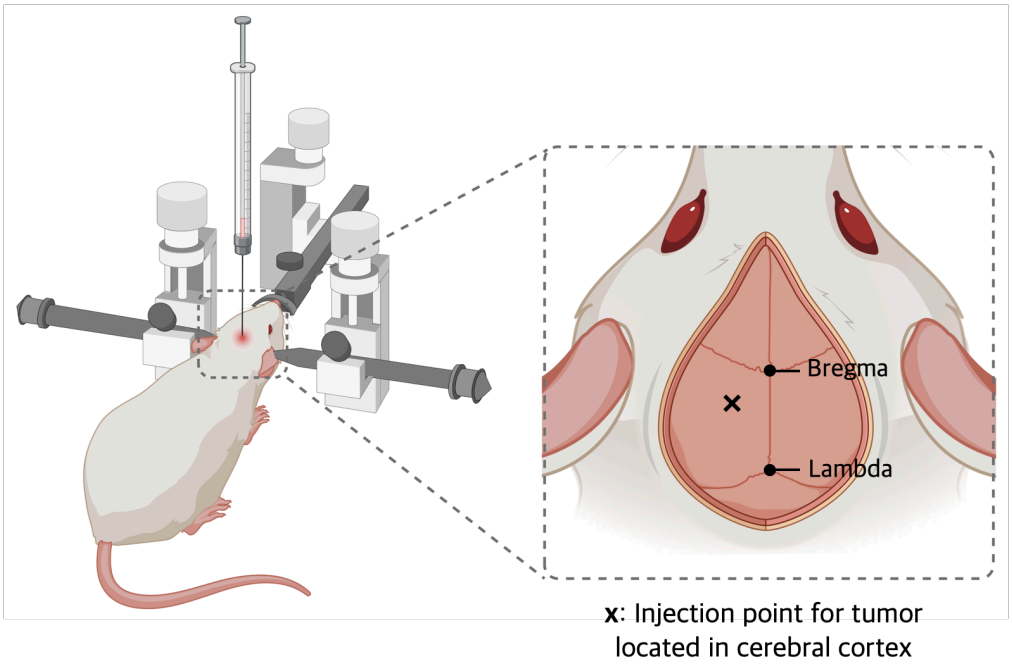

Figure 6-3 | Graphical illustration of stereotactic intracranial injection

The injection location: 1 mm posterior to bregma, 1 mm to the left side of the midline, 1.5 mm deep. Figure created with BioRender.com

6.4.3 In Vivo Imaging System (IVIS®)

For tumor formation analysis using IUE technology, electroporated animals were selected at postnatal day 7 (P7) by intraperitoneal (i.p.) injection of D-Luciferin (150 mg/kg) and subsequent bioluminescence imaging with IVIS Lumina LT Series III Caliper (Perkin Elmer). Mice without any bioluminescence signal at P7 were sacrificed immediately. Afterwards, tumor growth was monitored at P14, P21, P28 and every following 4 weeks by bioluminescence imaging until the mice reached endpoint criteria. For iNSC injected mice, bioluminescence imaging was carried out every 2 weeks starting from the day of dox treatment.

6.4.4 *In vivo* ATO treatment

A stock solution of 20 mg/mL ATO in 1 M NaOH was prepared. It was further diluted to 0.5 mg/mL ATO with PBS, and the solution was sterile-filtrated. The vehicle solution was prepared the same way but without ATO. When the bioluminescence signal of

the electroporated animals reached ca. 5 x 10^6 photo/second, the animals were allocated randomly to vehicle- and ATO-treatment group and treated five days per week either with 2.5 mg ATO/kg/day (i.p). or the equivalent volume of vehicle solution. Prior to the treatment, 20% mannitol in 0.9% saline was i.p injected into mice (5 mL/kg) to disrupt the blood–brain barrier. The mice were monitored daily for tumor-specific symptoms and euthanized when it exhibited neurological symptoms.

6.5 Data analyses

6.5.1 Tumor cross-species verification

The Affymetrix data cohorts were used for cross-species analysis. Human Affymterix data from corresponding study (Pajtler et al., 2015) was integrated from R2 system. The list of common mice-human gene orthologs from AGDEX Affymetrix reference (14635 genes in total) was integrated for gene probes selection in further comparison between human tumor and mouse model datasets. Initially differentially expressed orthologous genes between the ST-EPN-YAP1 and ST-EPN-RELA tumors starting from top 5000 most evident (min adjusted p-val < 0.0006) were applied as the target reference to confirm the model's correspondence based on unsupervised hierarchical clustering and principal component analysis as it was described previously (Pajtler et al., 2019). Further, in order to increase the specificity for ZFTA-driven effects, evident differentially expressed genes of ST-EPN-RELA tumors vs all other EPN groups were integrated for target candidate selection (n = 3825, min. adjusted p-val < 0.05). Differentially expressed genes between models were detected using limma R package (Ritchie et al., 2015) with adjusted p-val < 0.05.

For the gene ontology and pathway analysis the common orthologs between mouse models and human tumors were selected from differentially expressed genes specific for ST-EPN-RELA against all other EPN groups and for each ZFTA-driven model against MAMLD1-YAP1 control. Gene ontology analysis was performed using ClueGO tool (Bindea et al., 2009) by focusing the top 300 top evident genes. (Performed by Konstantin Okonechnikov)

6.5.2 Cut & Run and ChIP data processing

Paired-end reads were adapter and quality trimmed using Trimgalore (v0.6.5, default parameters, www.bioinformatics.babraham.ac.uk/projects/trim_galore) and aligned to mouse genome mm10 using Bowtie2 (v2.3.5.1, parameters: --local -D 20 -R 3 -N 0 -L 20 -i S,1,0.50 --no-unal --no-mixed --no-discordant --phred33 -I 10 -X 700). Duplicated reads were then marked and removed using picard MarkDuplicates (v2.21.1) (http://broadinstitute.github.io/picard/), and Samtools (v1.9), respectively with default parameters. For Rela and HA samples, only fragments of size less than 120bp were retained. Deeptools (v3.4.3) (Ramírez et al., 2016) was used to convert all the resulting BAM files to Bigwig format for visualization. MACS2 (v2.2.7.1) was used to call peaks, on the resulting BAM files, with a p-value threshold of 1e-3 (Zhang et al., 2008). A set of 6845 peaks were inferred in the HA CUT&RUN by overlapping the called peaks from the two independent mice using bedtools2. This set was further filtered to remove any overlaps with non-specific IgG peak signals (from both mice), resulting in 5608 peaks. The peaks were then annotated to nearest genomic features using *annotatePeaks.pl* from Homer (v4.11.1) (Heinz et al., 2010). (Performed by Stephen Mack)

6.5.3 Mouse DNA methylation array data processing

The Illumina Infinium Mouse Methylation BeadChip was used to obtain genome wide DNA from tumor and normal control tissues, according to the manufacturer's instructions (Illumina, San Diego, USA).

Data was generated at the Genomics and Proteomics Core Facility of the DKFZ (Heidelberg, Germany). DNA methylation data was generated from both fresh-frozen and formalin-fixed paraffin-embedded (FFPE) tissue samples. For most fresh-frozen samples, >500ng of DNA was used as input material. 250ng of DNA was used for most FFPE tissues. On-chip quality metrics of all samples were carefully controlled.

All computational analyses were performed in R version 4.1.1 (R Development Core Team, 2022). Raw signal intensities were obtained and preprocessed from IDAT-files using the sesame Bioconductor package version 1.10.5.

The beta methylation values have been filtered to the10,000 CpG probes with highest standard deviation across all samples in the cohort.

Non-linear dimension reduction of this filtered data set has been performed by applying t-distributed stochastic neighbor embedding using the implementation available in the R-package Rtsne version 0.16 with a perplexity parameter of 20 and 2500 iterations.

Copy number variation analysis has been performed by applying the functions available in the Bioconductor R-package sesame version 1.10.5. The functions originally only available for human DNA-methylation data have been slightly adapted to work with the mouse methylation array data. To this end gender specific reference data sets have been generated using 20 female and 20 male control tissue samples. (Performed by Martin Sill)

6.5.4 Statistical Analysis

The Kaplan-Meier-method was applied for survival analysis comparing the different fusion constructs and visualized using R version 3.6.1 (R Core Team, 2020) and the survival- and survminer-R packages (https://github.com/therneau/survival, https://github.com/kassambara/survminer). The Paired t test was used for EdU and Annexin V analysis in the shGLI2 experiment and visualized using GraphPad Prism.

Chapter 7

Appendix

7.1 List of plasmids used in the thesis

Plasmid ID	Details
pTZ38	pT2K-ZFTA-HA-IRES-Luc2
pTZ41	pT2K-ZFTA-MAML2-HA-IRES-Luc2
pTZ42	pT2K-ZFTA-MAML3-HA-IRES-Luc2
pTZ43	pT2K-ZFTA-NCOA2-HA-IRES-Luc2
pTZ44	pT2K-ZFTA-RELA-HA-IRES-Luc2
pTZ45	pT2K-ZFTA-SS18-HA-IRES-Luc2
pTZ46	pT2K-ZFTA-VP64-HA-IRES-Luc2
pTZ55	pT2K-ZFTA(ΔZF1)-MAML2-HA-IRES-Luc2
pTZ56	pT2K-ZFTA(ΔZF1)-NCOA2-HA-IRES-Luc2
pTZ57	pT2K-ZFTA(ΔZF1)-RELA-HA-IRES-Luc2
pTZ60	pT2K-ZFTA-RELA-HA-FLAG-dnGli2-IRES-Luc2
pTZ61	pT2K-ZFTA-RELA-HA-dnEphB2-FLAG-IRES-Luc2
pTZ65	pT2K-ZF1-p300-FLAG-IRES-Luc2
pTZ69	pT2K-YAP1-MAMLD1-HA-IRES-Luc2
pTZ74	pT2K-CAG-IRES-GreenFire
pTZ82	pT2K-ZFTA-RELA-HA-FLAG-dnLef1-IRES-Luc2
pTZ87	pT2K-EWSR1-PLAGL1-HA-IRES-Luc2
pTZ97	pLKO-Tet-On-shRNA-hGLI2-70
pTZ98	pLKO-Tet-On-shRNA-hGLI2-77
Addgene #98398	pLKO-Tet-On-shCtl
pTZ102	PB-ZFTA-RELA-HA-IRES-Luc2
pTZ115	pT2K-mEwsr1-PLAGL1-HA-Luc2
pTZ117	pT2K-EF1a-IRES-GreenFire
pTZ119	pT2K-EF1a-P2A-GreenFire
pTZ122	pT2K-PLAGL1-FOXO1-HA-IRES-Luc2
pTZ124	TLCV2-EWSR1-PLAGL1-HA-T2A-EGFP
pTZ125	TLCV2-ZFTA-RELA-HA-T2A-EGFP

pTZ126	TLCV2-YAP1-MAMLD1-HA-T2A-EGFP
pTZ127	PB-U6-sgGli2-CAG-Cas9-P2A-ZFTA-RELA-HA-IRES-Luc2
pTZ128	PB-U6-sgCtl-CAG-Cas9-P2A-ZFTA-RELA-HA-IRES-Luc2
SBI #TR0XX	pLenti-GreenFire
(Zuckermann et al., 2015)	pX330-sgRNA-Trp53
pKuZu-1H1	pCDH-CB-copGFP-T2A-puro-m
pKuZu-1G5	pCDH-CMV-copGFP-T2A-puro-m
pKuZu-1G8	pCDH-EF1-copGFP-T2A-Puro-m
pKuZu-1G7	pCDH-PGK-copGFP-T2A-puro-m
Addgene #12260	psPAX2
Addgene #12259	pMD2.G (VSV-G)

7.2 List of primers used in the thesis

Primer ID	Sequence	Note
TZ_pT2K-C11orf95_Fwd (3)	CATCATTTTGGCAAAGAATTCATGGAGCCCGGCGGGGAC	pTZ38 & pTZ41 cloning
TZ_C11orf95_MAML2_Rev (4)	AACCCTGGAGCTCCAGGATAGTCTGGCGCTC	
TZ_C11orf95_MAML2_Fwd (5)	TATCCTGGAGCTCCAGGGTTCCTTGAAAAGAAAAC	
TZ_C11orf95-MAML2-HA-Luc_Rev (70)	ATTGATCCCGCTCGAGTTAAGCATAGTCTGGTACATCGT	
TZ_4EP44_BP_Fwd (11)	CCTGATGGACTACGACGGC	ZFTA-MAML2 BP validation
TZ_4EP44_BP_Rev (12)	TTGGCTCATAGGCAAGGTCC	
TZ_7EP17_BP_Fwd (82)	CTGATGGACTACGACGGCAG	ZFTA-SS18 BP validation
TZ_7EP17_BP_Rev2 (90)	CTGGCCGTTCATCTGGTTCT	
9EP35_for	CCTGATGGACTACGACGGC	ZFTA-NCOA2 BP validation
9EP35_rev	GGTTTGGCAATAACCTGCCC	
TZ_pT2K-C11orf95_Fwd (3)	CATCATTTTGGCAAAGAATTCATGGAGCCCGGCGGGGAC	pTZ43 cloning
TZ_BPoligo_Fwd	GCTGCTACGGCCACGAGGGCTTCGGGCCGCCCGCCCCGGCGCCGCGTGACGGCGGCGATCTAGCTTTTAATAA	

TZ_BPoligo_Rev	TTATTAAAAGCTAGATCGCCGCCGTCACGCGGCGCCGGGGCGGGCGGCCCGAAGCCCTCGTGGCCGTAGCAGC	
TZ_NCOA2-HA-Luc_Rev (89)	ATTGATCCCGCTCGAGTTAAGCATAGTCTGGTACATCGTAAGGATAGCAATATTTCCGTG	
TZ_pT2K-C11orf95_Fwd (3)	CATCATTTTGGCAAAGAATTCATGGAGCCCGGCGGGGAC	pTZ45 cloning
TZ_SS18_fusion_Fwd (103)	TACAGGCCATGTCTTATGTTGGATGACAATAACC	
TZ_C11or95-SS18_Rev (104)	ACATAAGACATGGCCTGTAGGCGGGCGGCCCGAAGCCCTCGTGGCCGTAGCAGCG	
TZ_SS18-HA_Rev (105)	ATTGATCCCGCTCGAGTTAAGCATAGTCTGGTACATCGTAAGGATACTGCTGGTAATTTCCATACTG	
TZ_94684_BP_Fwd (110)	TACCTGATGGACTACGACGG	ZFTA-MAML3 BP validation
TZ_94684_BP_Rev (111)	TCTGCAAGGGCAAAGAAGGT	
TZ_pT2K-C11orf95_Fwd (3)	CATCATTTTGGCAAAGAATTCATGGAGCCCGGCGGGGAC	pTZ42 cloning
TZ_C11orf95-MAML3_Rev (123)	TCTCTTGTAGCTCCTCGTAGGCCTCCAGG	
TZ_C11orf95-MAML3_Fwd (124)	CTACGAGGAGCTACAAGAGACTGTGAAAAGGAAG	
TZ_MAML3-HA_Rev (125)	ATTGATCCCGCTCGAGTTAAGCATAGTCTGGTACATCGTAAGGATAGGGGTTACCAAACAATTCATCAAG	
TZ_pT2K-C11orf95_Fwd (3)	CATCATTTTGGCAAAGAATTCATGGAGCCCGGCGGGGAC	pTZ46 cloning
TZ_C11orf95-VP64_Rev (126)	CGGCAATTGGCTCCAGGATAGTCTGGCGCTC	
TZ_C11orf95-VP64_Fwd (127)	TATCCTGGAGCCAATTGCCGGATCCAAGG	
TZ_HA-IRES_Rev (128)	GCGGAATTGATCCCGCTCGAGCGAATTCCTACCGATTCAAGAAGC	
TZ_C11orf95delZF1_Rev	CCCGGGGACTGTGGTCGTGGTAGTAGCGCC	pTZ55, pTZ56, pTZ57 cloning
TZ_C11orf95delZF1_Fwd	CCACGACCACAGTCCCCGGGAGAAGGAA	
TZ_Gli2delC-Rev (138)	CGGAATTGATCCCGCTCGAGTCAGCTGGCCTCATTATCCCC	pTZ60, pTZ61, pTZ82 cloning
TZ_Flag-Gli2_Fwd1 (139)	TACAAAGACGATGACGATAAGGGATCCATGGAGACTTCTGCCCCAGC	
TZ_pT2K-Flag_Fwd2 (140)	ATCATTTTGGCAAAGAATTCATGGATTACAAAGACGATGACG	
TZ_HA-T2A_Rev (143)	CGCATGTTAGTAGACTTCCCCTGCCCTCGCCGGAGCCAGCATAGTCTGGTACATCG	
TZ_T2A-Flag_Fwd (144)	GGAAGTCTACTAACATGCGGGGACGTGGAGGAAAATCCCGGCCCAGATTACAAAGACGATGACG	
TZ_T2A-Ephb2_Fwd (158)	GGGAAGTCTACTAACATGCGGGGACGTGGAGGAAAATCCCGGCCCAATGGCCGTGCGCAGGCTG	

TZ_Ephb2-Flag_Rev (159)	CGGAATTGATCCCGCTCGAGTCACTTATCGTCATCGTCTTTGTAATCGGATCCGACACAGGAGATGTCAATTTCCTTG	
TZ_Flag-Lef1DN_Rev (174)	CCTGAGAGGAGGATCCCTTATCGTCATCGTCTTTG	
TZ_Flag-Lef1DN_Fwd (175)	TAAGGGATCCTCCTCTCAGGAGCCCTACCAC	
TZ_Lef1DN_Rev (176)	GCGGAATTGATCCCGCTCGAGTCAACAAGCTTCCATCTCCAGAAG	
TZ_GLI2-qPCR3_Fwd (164)	CCCCTACCGATTGACATGCG	qPCR for hGLI2
TZ_GLI2-qPCR3_Rev (165)	GAAAGCCGGATCAAGGAGATG	
TZ_C11-RELA-BP_Fwd (177)	GGGAGAAGGAAGTCATCAGCAAC	ZFTA-RELA Type 1 BP validation
TZ_C11-RELA-BP_Rev (178)	TGGTCCTGTGTAGCCATTGA	
TZ_EWSR1-PLAGL1_BP_Fwd (185)	GCCTCCCACTAGTTACCCA	EWSR1-PLAGL1 BP validation
TZ_EWSR1-PLAGL1_BP_Rev (186)	GCCATTTTGTTGGGGTCGTG	
TZ_EWSR1-PLAGL1_BP1_Fwd (211)	AGAGAACCGGAGCATGAGTG	
TZ_EWSR1-PLAGL1_BP1_Rev (212)	GGGCCAGGTGCCTCTTATAG	
TZ_PLAGL1-FOXO1_BP_Fwd (187)	TGAAAGAGAGCTTGCAGACC	PLAGL1-FOXO1 BP validation
TZ_PLAGL1-FOXO1_BP_Rev (188)	AGGAGATTTCCCGCTCTTGC	
TZ_hGLI2_shRNA70_Fwd (203)	CCGGGCTCTACTACTACGGCCAGATCTCGAGATCTGGCCGTAGTAGTAGAGCTTTTTG	pTZ97 cloning
TZ_hGLI2_shRNA70_Rev (204)	AATTCAAAAAGCTCTACTACTACGGCCAGATCTCGAGATCTGGCCGTAGTAGTAGAGC	
TZ_hGLI2_shRNA77_Fwd (205)	CCGGGTTCCTGAACATGATGACCTACTCGAGTAGGTCATCATGTTCAGGAACTTTTTG	pTZ98 cloning
TZ_hGLI2_shRNA77_Rev (206)	AATTCAAAAAGTTCCTGAACATGATGACCTACTCGAGTAGGTCATCATGTTCAGGAAC	
TZ_pGF1-PLAGL1_Fwd (224)	ATAGAAGATTCTAGAGCTAGCAAGCCCATGGCCACGTTCC	pTZ87 cloning
TZ_pGF1-PLAGL1-HA-Rev (225)	TCCCGCTCGAGATCTGAATTCTTAAGCATAGTCTGGTACATCGTAAGGATATCTGAATGCATGATGGAAATGAGGC	
TZ_pGF1-EWSR1_Fwd (226)	ATAGAAGATTCTAGAGCTAGCGAGAAAATGGCGTCCACGG	
TZ_pGF1-EWSR1Full_Rev (227)	TCCCGCTCGAGATCTGAATTCTTAAGCATAGTCTGGTACATCGTAAGGATAGTAGGGCCGATCTCTGCG	
TZ_pT2K-mEwsr1_Fwd (228)	CATCATTTTGGCAAAGAATTCGAGAAAATGGCGTCCACGG	pTZ115 cloning

TZ_mEwsr1-PLAGL1_Rev (229)	TAGCCATATGGGGTCCACCAGGCTTATTG	
TZ_mEwsr1-PLAGL1_Fwd (230)	TGGTGGACCCCATATGGCTACCCATTCTCCCCA	
TZ_HA-pT2K_Rev (231)	GCGGAATTGATCCCGCTCGAGTTAAGCATAGTCTGGTACATCGT	
TZ_EF1a-GF_Fwd (232)	GCCAGATGGGCCCTCGTCGACGGCTCCGGTGCCCGTCAG	pTZ117, pTZ119 cloning
TZ_EF1a-GF_Rev (233)	TCCCGCTCGAGATCTGAATTCGCTAGCTCTAGATCACGACACCTGAAATGGAAG	
TZ_EF1aCore-GF_Fwd (234)	ATGGGCCCTCGTCGACAAGGATCTGCGATCGCTCCG	
TZ_EF1aCore-GF_Rev (235)	CTCGAGATCTGAATTCGCTAGCTCTAGAGTAGGCGCCGGTCACAGC	
TZ_pT2K-GF_Fwd1 (236)	TTGAAACAAGCAGGGGATGTCGAAGAGAATCCCGGGCCAATGCCCGCCATGAAGATCG	
TZ_pT2K-GF_Rev (237)	CAGAGGGAAAAAGATCTGATATCTTACAATTTGGACTTTCCGCCC	
TZ_pT2K-PLAGL1_Fwd (243)	CATCATTTTGGCAAAGAATTAAGCCCATGGCCACGTTCCCCTGC	pTZ122 cloning
TZ_PLAGL1-FOXO1-BP_Rev (250)	GAATTGAATTCGAGGGGTGGAGGGAGGC	
TZ_PLAGL1-FOXO1-BP_Fwd (251)	CCACCCCTCGAATTCAATTCGTCATAATCTGTCCC	
TZ_FOXO1-HA_Rev (252)	AATTGATCCCGCTCGATTAAGCATAGTCTGGTACATCGTAAGGATAGCCTGACACCCAGC	
TZ_TLCV2-EWSR1_Fwd (244)	TACCGGTTCTAGAGCGCTGAGAAAATGGCGTCCACGGA	pTZ124 cloning
TZ_TLCV2-HA_Rev (245)	TGCCCTCTCCGGATCCAGCATAGTCTGGTACATCGT	
TZ_TLCV2-C11orf95_Fwd (246)	TACCGGTTCTAGAGCGCTGACCAATTCAGTCGACTGGATCC	pTZ125 cloning
TZ_TLCV2-HA_Rev (247)	TGCCCTCTCCGGATCCAGCGTAATCTGGAACATCGT	
TZ_TLCV2-YAP1_Fwd (248)	TACCGGTTCTAGAGCGCTCGGCAGAAGCCATGGATCC	pTZ126 cloning
TZ_TLCV2-HA_Rev (249)	TGCCCTCTCCGGATCCGGCATAGTCAGGCACG	

7.3 List of antibodies used for staining

Antibodies	Manufacturer	Catalog #	Application
Anti-HA-Tag (C29F4) Rabbit mAb	Cell Signaling	3724	IHC 1:500; IF 1:800; WB 1:1000
Anti-FLAG® M2 Mouse mAb	Sigma	F1804	WB 1:1000
Anti-β-Actin-HRP	abcam	ab49900	WB 1:10000
Anti-GAPDH Mouse mAb	Millipore	CB1001	WB 1:1000
Anti-Ki67 Rabbit polyAb	Abcam	ab15580	IHC 1:500
Anti-Ki67 Rat polyAb	BioLegend	652402	IF 1:500
Anti-Rabbit-HRP	Cell Signaling	7074	WB 1:3000
Anti-Mouse-HRP	Cell Signaling	7076	WB 1:3000
Anti-Rabbit-Alexa568	Invitrogen	A10042	IF 1:400
Anti-Rat-Alexa633	Invitrogen	A21094	IF 1:400

Chapter 8

Reference

Ahmadiankia, N. (2020). In vitro and in vivo studies of cancer cell behavior under nutrient deprivation. *Cell Biol Int*, *44*(8), 1588-1597. https://doi.org/10.1002/cbin.11368

Ahmed, Z., & Bicknell, R. (2009). Angiogenic signalling pathways. *Methods Mol Biol*, *467*, 3-24. https://doi.org/10.1007/978-1-59745-241-0_1

Al-Hajj, M., Wicha, M. S., Benito-Hernandez, A., Morrison, S. J., & Clarke, M. F. (2003). Prospective identification of tumorigenic breast cancer cells. *Proceedings of the National Academy of Sciences*, *100*(7), 3983-3988. https://doi.org/doi:10.1073/pnas.0530291100

Alcantara Llaguno, Sheila R., Wang, Z., Sun, D., Chen, J., Xu, J., Kim, E., Hatanpaa, Kimmo J., Raisanen, Jack M., Burns, Dennis K., Johnson, Jane E., & Parada, Luis F. (2015). Adult Lineage-Restricted CNS Progenitors Specify Distinct Glioblastoma Subtypes. *Cancer Cell*, *28*(4), 429-440. https://doi.org/10.1016/j.ccell.2015.09.007

Aldinger, K. A., Sokoloff, G., Rosenberg, D. M., Palmer, A. A., & Millen, K. J. (2009). Genetic Variation and Population Substructure in Outbred CD-1 Mice: Implications for Genome-Wide Association Studies. *PLoS One*, *4*(3), e4729. https://doi.org/10.1371/journal.pone.0004729

Alemany, A., Florescu, M., Baron, C. S., Peterson-Maduro, J., & van Oudenaarden, A. (2018). Whole-organism clone tracing using single-cell sequencing. *Nature*, *556*(7699), 108-112. https://doi.org/10.1038/nature25969

Anastasaki, C., Chatterjee, J., Cobb, O., Sanapala, S., Scheaffer, S. M., De Andrade Costa, A., Wilson, A. F., Kernan, C. M., Zafar, A. H., Ge, X., Garbow, J. R., Rodriguez, F. J., & Gutmann, D. H. (2022). Human induced pluripotent stem cell engineering establishes a humanized mouse platform for pediatric low-grade glioma modeling. *Acta Neuropathologica Communications*, *10*(1), 120. https://doi.org/10.1186/s40478-022-01428-2

Arabzade, A., Zhao, Y., Varadharajan, S., Chen, H.-C., Jessa, S., Rivas, B., Stuckert, A. J., Solis, M., Kardian, A., Tlais, D., Golbourn, B. J., Stanton, A.-C. J., Chan, Y. S., Olson, C., Karlin, K. L., Kong, K., Kupp, R., Hu, B., Injac, S. G., Ngo, M., Wang, P. R., De León, L. A., Sahm, F., Kawauchi, D., Pfister, S. M., Lin, C. Y., Hodges, H. C., Singh, I., Westbrook, T. F., Chintagumpala, M. M., Blaney, S. M., Parsons, D. W., Pajtler, K. W., Agnihotri, S., Gilbertson, R. J., Yi, J., Jabado, N., Kleinman, C. L., Bertrand, K. C., Deneen, B., & Mack, S. C. (2021). ZFTA–RELA Dictates Oncogenic Transcriptional Programs to Drive Aggressive Supratentorial Ependymoma. *Cancer Discovery*, *11*(9), 2200-2215. https://doi.org/10.1158/2159-8290.Cd-20-1066

Auerbach, C., Moutschen-Dahmen, M., & Moutschen, J. (1977). Genetic and cytogenetical effects of formaldehyde and related compounds. *Mutation Research/Reviews in Genetic Toxicology*, *39*(3), 317-361. https://doi.org/https://doi.org/10.1016/0165-1110(77)90011-2

Balciunas, D., Wangensteen, K. J., Wilber, A., Bell, J., Geurts, A., Sivasubbu, S., Wang, X., Hackett, P. B., Largaespada, D. A., McIvor, R. S., & Ekker, S. C. (2006). Harnessing a High Cargo-Capacity Transposon for Genetic Applications in Vertebrates. *PLOS Genetics*, *2*(11), e169. https://doi.org/10.1371/journal.pgen.0020169

Ballabio, C., Anderle, M., Gianesello, M., Lago, C., Miele, E., Cardano, M., Aiello, G., Piazza, S., Caron, D., Gianno, F., Ciolfi, A., Pedace, L., Mastronuzzi, A., Tartaglia, M., Locatelli, F., Ferretti, E., Giangaspero, F., & Tiberi, L. (2020). Modeling medulloblastoma in vivo and with human cerebellar organoids. *Nature Communications*, *11*(1), 583. https://doi.org/10.1038/s41467-019-13989-3

Barger, C. J., Branick, C., Chee, L., & Karpf, A. R. (2019). Pan-Cancer Analyses Reveal Genomic Features of FOXM1 Overexpression in Cancer. *Cancers (Basel)*, *11*(2). https://doi.org/10.3390/cancers11020251

Beerli, R. R., Segal, D. J., Dreier, B., & Barbas, C. F., 3rd. (1998). Toward controlling gene expression at will: specific regulation of the erbB-2/HER-2 promoter by using polydactyl zinc finger proteins

constructed from modular building blocks. *Proc Natl Acad Sci U S A*, *95*(25), 14628-14633. https://doi.org/10.1073/pnas.95.25.14628

Behjati, S., Gilbertson, R. J., & Pfister, S. M. (2021). Maturation Block in Childhood Cancer. *Cancer Discovery*, *11*(3), 542-544. https://doi.org/10.1158/2159-8290.Cd-20-0926

Ben-David, U., & Benvenisty, N. (2011). The tumorigenicity of human embryonic and induced pluripotent stem cells. *Nat Rev Cancer*, *11*(4), 268-277. https://doi.org/10.1038/nrc3034

Bencsik, R., Boto, P., Szabó, R. N., Toth, B. M., Simo, E., Bálint, B. L., & Szatmari, I. (2016). Improved transgene expression in doxycycline-inducible embryonic stem cells by repeated chemical selection or cell sorting. *Stem Cell Research*, *17*(2), 228-234. https://doi.org/https://doi.org/10.1016/j.scr.2016.08.014

Bez, A., Corsini, E., Curti, D., Biggiogera, M., Colombo, A., Nicosia, R. F., Pagano, S. F., & Parati, E. A. (2003). Neurosphere and neurosphere-forming cells: morphological and ultrastructural characterization. *Brain Res*, *993*(1-2), 18-29. https://doi.org/10.1016/j.brainres.2003.08.061

Bindea, G., Mlecnik, B., Hackl, H., Charoentong, P., Tosolini, M., Kirilovsky, A., Fridman, W.-H., Pagès, F., Trajanoski, Z., & Galon, J. (2009). ClueGO: a Cytoscape plug-in to decipher functionally grouped gene ontology and pathway annotation networks. *Bioinformatics*, *25*(8), 1091-1093. https://doi.org/10.1093/bioinformatics/btp101

Bird, A. (2002). DNA methylation patterns and epigenetic memory. *Genes Dev*, *16*(1), 6-21. https://doi.org/10.1101/gad.947102

Birey, F., Andersen, J., Makinson, C. D., Islam, S., Wei, W., Huber, N., Fan, H. C., Metzler, K. R. C., Panagiotakos, G., Thom, N., O'Rourke, N. A., Steinmetz, L. M., Bernstein, J. A., Hallmayer, J., Huguenard, J. R., & Paşca, S. P. (2017). Assembly of functionally integrated human forebrain spheroids. *Nature*, *545*(7652), 54-59. https://doi.org/10.1038/nature22330

Bonnet, E., Moutet, M.-L., Baulard, C., Bacq-Daian, D., Sandron, F., Mesrob, L., Fin, B., Delépine, M., Palomares, M.-A., Jubin, C., Blanché, H., Meyer, V., Boland, A., Olaso, R., & Deleuze, J.-F. (2018). Performance comparison of three DNA extraction kits on human whole-exome data from formalin-fixed paraffin-embedded normal and tumor samples. *PLoS One*, *13*(4), e0195471. https://doi.org/10.1371/journal.pone.0195471

Bormann, F., Rodríguez-Paredes, M., Lasitschka, F., Edelmann, D., Musch, T., Benner, A., Bergman, Y., Dieter, S. M., Ball, C. R., Glimm, H., Linhart, H. G., & Lyko, F. (2018). Cell-of-Origin DNA Methylation Signatures Are Maintained during Colorectal Carcinogenesis. *Cell Reports*, *23*(11), 3407-3418. https://doi.org/https://doi.org/10.1016/j.celrep.2018.05.045

Borrell, V., Yoshimura, Y., & Callaway, E. M. (2005). Targeted gene delivery to telencephalic inhibitory neurons by directional in utero electroporation. *J Neurosci Methods*, *143*(2), 151-158. https://doi.org/10.1016/j.jneumeth.2004.09.027

Bowling, S., Sritharan, D., Osorio, F. G., Nguyen, M., Cheung, P., Rodriguez-Fraticelli, A., Patel, S., Yuan, W. C., Fujiwara, Y., Li, B. E., Orkin, S. H., Hormoz, S., & Camargo, F. D. (2020). An Engineered CRISPR-Cas9 Mouse Line for Simultaneous Readout of Lineage Histories and Gene Expression Profiles in Single Cells. *Cell*, *181*(6), 1410-1422.e1427. https://doi.org/10.1016/j.cell.2020.04.048

Brantley-Sieders, D. M., Jiang, A., Sarma, K., Badu-Nkansah, A., Walter, D. L., Shyr, Y., & Chen, J. (2011). Eph/Ephrin Profiling in Human Breast Cancer Reveals Significant Associations between Expression Level and Clinical Outcome. *PLoS One*, *6*(9), e24426. https://doi.org/10.1371/journal.pone.0024426

Brat, D. J., Aldape, K., Colman, H., Figrarella-Branger, D., Fuller, G. N., Giannini, C., Holland, E. C., Jenkins, R. B., Kleinschmidt-DeMasters, B., Komori, T., Kros, J. M., Louis, D. N., McLean, C., Perry, A., Reifenberger, G., Sarkar, C., Stupp, R., van den Bent, M. J., von Deimling, A., & Weller, M. (2020). cIMPACT-NOW update 5: recommended grading criteria and terminologies for IDH-mutant astrocytomas. *Acta Neuropathol*, *139*(3), 603-608. https://doi.org/10.1007/s00401-020-02127-9

Brat, D. J., Aldape, K., Colman, H., Holland, E. C., Louis, D. N., Jenkins, R. B., Kleinschmidt-DeMasters, B. K., Perry, A., Reifenberger, G., Stupp, R., von Deimling, A., & Weller, M. (2018). cIMPACT-NOW update 3: recommended diagnostic criteria for "Diffuse astrocytic glioma, IDH-wildtype, with molecular features of glioblastoma, WHO grade IV". *Acta Neuropathol*, *136*(5), 805-810. https://doi.org/10.1007/s00401-018-1913-0

Bresters, D., Schipper, M. E. I., Reesink, H. W., Boeser-Nunnink, B. D. M., & Cuypers, H. T. M. (1994). The duration of fixation influences the yield of HCV cDNA-PCR products from formalin-fixed, paraffin-embedded liver tissue. *Journal of Virological Methods*, *48*(2), 267-272. https://doi.org/https://doi.org/10.1016/0166-0934(94)90125-2

Bushweller, J. H. (2019). Targeting transcription factors in cancer — from undruggable to reality. *Nature Reviews Cancer*, *19*(11), 611-624. https://doi.org/10.1038/s41568-019-0196-7

Campbell, K., & Götz, M. (2002). Radial glia: multi-purpose cells for vertebrate brain development. *Trends Neurosci*, *25*(5), 235-238. https://doi.org/10.1016/s0166-2236(02)02156-2

Capper, D., Jones, D. T. W., Sill, M., Hovestadt, V., Schrimpf, D., Sturm, D., Koelsche, C., Sahm, F., Chavez, L., Reuss, D. E., Kratz, A., Wefers, A. K., Huang, K., Pajtler, K. W., Schweizer, L., Stichel, D., Olar, A., Engel, N. W., Lindenberg, K., Harter, P. N., Braczynski, A. K., Plate, K. H., Dohmen, H., Garvalov, B. K., Coras, R., Hölsken, A., Hewer, E., Bewerunge-Hudler, M., Schick, M., Fischer, R., Beschorner, R., Schittenhelm, J., Staszewski, O., Wani, K., Varlet, P., Pages, M., Temming, P., Lohmann, D., Selt, F., Witt, H., Milde, T., Witt, O., Aronica, E., Giangaspero, F., Rushing, E., Scheurlen, W., Geisenberger, C., Rodriguez, F. J., Becker, A., Preusser, M., Haberler, C., Bjerkvig, R., Cryan, J., Farrell, M., Deckert, M., Hench, J., Frank, S., Serrano, J., Kannan, K., Tsirigos, A., Brück, W., Hofer, S., Brehmer, S., Seiz-Rosenhagen, M., Hänggi, D., Hans, V., Rozsnoki, S., Hansford, J. R., Kohlhof, P., Kristensen, B. W., Lechner, M., Lopes, B., Mawrin, C., Ketter, R., Kulozik, A., Khatib, Z., Heppner, F., Koch, A., Jouvet, A., Keohane, C., Mühleisen, H., Mueller, W., Pohl, U., Prinz, M., Benner, A., Zapatka, M., Gottardo, N. G., Driever, P. H., Kramm, C. M., Müller, H. L., Rutkowski, S., von Hoff, K., Frühwald, M. C., Gnekow, A., Fleischhack, G., Tippelt, S., Calaminus, G., Monoranu, C.-M., Perry, A., Jones, C., Jacques, T. S., Radlwimmer, B., Gessi, M., Pietsch, T., Schramm, J., Schackert, G., Westphal, M., Reifenberger, G., Wesseling, P., Weller, M., Collins, V. P., Blümcke, I., Bendszus, M., Debus, J., Huang, A., Jabado, N., Northcott, P. A., Paulus, W., Gajjar, A., Robinson, G. W., Taylor, M. D., Jaunmuktane, Z., Ryzhova, M., Platten, M., Unterberg, A., Wick, W., Karajannis, M. A., Mittelbronn, M., Acker, T., Hartmann, C., Aldape, K., Schüller, U., Buslei, R., Lichter, P., Kool, M., Herold-Mende, C., Ellison, D. W., Hasselblatt, M., Snuderl, M., Brandner, S., Korshunov, A., von Deimling, A., & Pfister, S. M. (2018). DNA methylation-based classification of central nervous system tumours. *Nature*, *555*(7697), 469-474. https://doi.org/10.1038/nature26000

Caragher, S., Chalmers, A. J., & Gomez-Roman, N. (2019). Glioblastoma's Next Top Model: Novel Culture Systems for Brain Cancer Radiotherapy Research. *Cancers (Basel)*, *11*(1). https://doi.org/10.3390/cancers11010044

Cary, L. C., Goebel, M., Corsaro, B. G., Wang, H. G., Rosen, E., & Fraser, M. J. (1989). Transposon mutagenesis of baculoviruses: analysis of Trichoplusia ni transposon IFP2 insertions within the FP-locus of nuclear polyhedrosis viruses. *Virology*, *172*(1), 156-169. https://doi.org/10.1016/0042-6822(89)90117-7

Chambers, I., Colby, D., Robertson, M., Nichols, J., Lee, S., Tweedie, S., & Smith, A. (2003). Functional expression cloning of Nanog, a pluripotency sustaining factor in embryonic stem cells. *Cell*, *113*(5), 643-655. https://doi.org/10.1016/s0092-8674(03)00392-1

Chan, E. T., Quon, G. T., Chua, G., Babak, T., Trochesset, M., Zirngibl, R. A., Aubin, J., Ratcliffe, M. J., Wilde, A., Brudno, M., Morris, Q. D., & Hughes, T. R. (2009). Conservation of core gene expression in vertebrate tissues. *J Biol*, *8*(3), 33. https://doi.org/10.1186/jbiol130

Chen, Q., Luo, W., Veach, R. A., Hickman, A. B., Wilson, M. H., & Dyda, F. (2020). Structural basis of seamless excision and specific targeting by piggyBac transposase. *Nat Commun*, *11*(1), 3446. https://doi.org/10.1038/s41467-020-17128-1

Chiu, S. T., Chang, K. J., Ting, C. H., Shen, H. C., Li, H., & Hsieh, F. J. (2009). Over-expression of EphB3 enhances cell-cell contacts and suppresses tumor growth in HT-29 human colon cancer cells. *Carcinogenesis*, *30*(9), 1475-1486. https://doi.org/10.1093/carcin/bgp133

Chow, R. D., Guzman, C. D., Wang, G., Schmidt, F., Youngblood, M. W., Ye, L., Errami, Y., Dong, M. B., Martinez, M. A., Zhang, S., Renauer, P., Bilguvar, K., Gunel, M., Sharp, P. A., Zhang, F., Platt, R. J., & Chen, S. (2017). AAV-mediated direct in vivo CRISPR screen identifies functional suppressors in glioblastoma. *Nat Neurosci*, *20*(10), 1329-1341. https://doi.org/10.1038/nn.4620

Chung, S., Andersson, T., Sonntag, K. C., Björklund, L., Isacson, O., & Kim, K. S. (2002). Analysis of different promoter systems for efficient transgene expression in mouse embryonic stem cell lines. *Stem Cells*, *20*(2), 139-145. https://doi.org/10.1634/stemcells.20-2-139

Cunningham, R. M., Walton, M. A., & Carter, P. M. (2018). The Major Causes of Death in Children and Adolescents in the United States. *New England Journal of Medicine*, *379*(25), 2468-2475. https://doi.org/10.1056/NEJMsr1804754

Curtin, S. C., Minino, A. M., & Anderson, R. N. (2016). Declines in Cancer Death Rates Among Children and Adolescents in the United States, 1999-2014. *NCHS Data Brief*(257), 1-8.

Cutler, D. J., Zwick, M. E., Carrasquillo, M. M., Yohn, C. T., Tobin, K. P., Kashuk, C., Mathews, D. J., Shah, N. A., Eichler, E. E., Warrington, J. A., & Chakravarti, A. (2001). High-throughput variation

detection and genotyping using microarrays. *Genome Res*, *11*(11), 1913-1925. https://doi.org/10.1101/gr.197201

Dahlstrand, J., Lardelli, M., & Lendahl, U. (1995). Nestin mRNA expression correlates with the central nervous system progenitor cell state in many, but not all, regions of developing central nervous system. *Brain Res Dev Brain Res*, *84*(1), 109-129. https://doi.org/10.1016/0165-3806(94)00162-s

Danjo, T., Eiraku, M., Muguruma, K., Watanabe, K., Kawada, M., Yanagawa, Y., Rubenstein, J. L., & Sasai, Y. (2011). Subregional specification of embryonic stem cell-derived ventral telencephalic tissues by timed and combinatory treatment with extrinsic signals. *J Neurosci*, *31*(5), 1919-1933. https://doi.org/10.1523/jneurosci.5128-10.2011

David Gordon, N. J. S. (2009). *Neural Cell Transplantation - Methods and Protocols*. Humana Totowa, NJ. https://doi.org/https://doi.org/10.1007/978-1-60327-931-4

Day, C.-P., Carter, J., Bonomi, C., Hollingshead, M., & Merlino, G. (2012). Preclinical therapeutic response of residual metastatic disease is distinct from its primary tumor of origin. *International Journal of Cancer*, *130*(1), 190-199. https://doi.org/https://doi.org/10.1002/ijc.25978

Day, C.-P., Merlino, G., & Van Dyke, T. (2015). Preclinical Mouse Cancer Models: A Maze of Opportunities and Challenges. *Cell*, *163*(1), 39-53. https://doi.org/https://doi.org/10.1016/j.cell.2015.08.068

De, B., Khakoo, Y., Souweidane, M. M., Dunkel, I. J., Patel, S. H., Gilheeney, S. W., De Braganca, K. C., Karajannis, M. A., & Wolden, S. L. (2018). Patterns of relapse for children with localized intracranial ependymoma. *J Neurooncol*, *138*(2), 435-445. https://doi.org/10.1007/s11060-018-2815-7

Dehay, C., & Kennedy, H. (2007). Cell-cycle control and cortical development. *Nature Reviews Neuroscience*, *8*(6), 438-450. https://doi.org/10.1038/nrn2097

Dennler, S., André, J., Verrecchia, F., & Mauviel, A. (2009). Cloning of the human GLI2 Promoter: transcriptional activation by transforming growth factor-beta via SMAD3/beta-catenin cooperation. *J Biol Chem*, *284*(46), 31523-31531. https://doi.org/10.1074/jbc.M109.059964

Devarakonda, S., Morgensztern, D., & Govindan, R. (2015). Genomic alterations in lung adenocarcinoma. *Lancet Oncol*, *16*(7), e342-351. https://doi.org/10.1016/s1470-2045(15)00077-7

Di Bella, D. J., Habibi, E., Stickels, R. R., Scalia, G., Brown, J., Yadollahpour, P., Yang, S. M., Abbate, C., Biancalani, T., Macosko, E. Z., Chen, F., Regev, A., & Arlotta, P. (2021). Molecular logic of cellular diversification in the mouse cerebral cortex. *Nature*, *595*(7868), 554-559. https://doi.org/10.1038/s41586-021-03670-5

Di Lullo, E., & Kriegstein, A. R. (2017). The use of brain organoids to investigate neural development and disease. *Nature Reviews Neuroscience*, *18*(10), 573-584. https://doi.org/10.1038/nrn.2017.107

Ding, Y. Q., Yin, J., Kania, A., Zhao, Z. Q., Johnson, R. L., & Chen, Z. F. (2004). Lmx1b controls the differentiation and migration of the superficial dorsal horn neurons of the spinal cord. *Development*, *131*(15), 3693-3703. https://doi.org/10.1242/dev.01250

Dobson, T. H. W., & Gopalakrishnan, V. (2018). Preclinical Models of Pediatric Brain Tumors-Forging Ahead. *Bioengineering (Basel)*, *5*(4). https://doi.org/10.3390/bioengineering5040081

Douvaras, P., Wang, J., Zimmer, M., Hanchuk, S., O'Bara, M. A., Sadiq, S., Sim, F. J., Goldman, J., & Fossati, V. (2014). Efficient generation of myelinating oligodendrocytes from primary progressive multiple sclerosis patients by induced pluripotent stem cells. *Stem Cell Reports*, *3*(2), 250-259. https://doi.org/10.1016/j.stemcr.2014.06.012

Downing, J. R., Head, D. R., Parham, D. M., Douglass, E. C., Hulshof, M. G., Link, M. P., Motroni, T. A., Grier, H. E., Curcio-Brint, A. M., & Shapiro, D. N. (1993). Detection of the (11;22)(q24;q12) translocation of Ewing's sarcoma and peripheral neuroectodermal tumor by reverse transcription polymerase chain reaction. *Am J Pathol*, *143*(5), 1294-1300.

Duan, L., Peng, C. Y., Pan, L., & Kessler, J. A. (2015). Human pluripotent stem cell-derived radial glia recapitulate developmental events and provide real-time access to cortical neurons and astrocytes. *Stem Cells Transl Med*, *4*(5), 437-447. https://doi.org/10.5966/sctm.2014-0137

Dwyer, N. D., Chen, B., Chou, S.-J., Hippenmeyer, S., Nguyen, L., & Ghashghaei, H. T. (2016). Neural Stem Cells to Cerebral Cortex: Emerging Mechanisms Regulating Progenitor Behavior and Productivity. *The Journal of Neuroscience*, *36*(45), 11394-11401. https://doi.org/10.1523/jneurosci.2359-16.2016

Eckner, R., Ewen, M. E., Newsome, D., Gerdes, M., DeCaprio, J. A., Lawrence, J. B., & Livingston, D. M. (1994). Molecular cloning and functional analysis of the adenovirus E1A-associated 300-kD protein (p300) reveals a protein with properties of a transcriptional adaptor. *Genes Dev*, *8*(8), 869-884. https://doi.org/10.1101/gad.8.8.869

Eiraku, M., & Sasai, Y. (2012). Self-formation of layered neural structures in three-dimensional culture of ES cells. *Curr Opin Neurobiol*, *22*(5), 768-777. https://doi.org/10.1016/j.conb.2012.02.005

Ellison, D. W., Aldape, K. D., Capper, D., Fouladi, M., Gilbert, M. R., Gilbertson, R. J., Hawkins, C., Merchant, T. E., Pajtler, K., Venneti, S., & Louis, D. N. (2020). cIMPACT-NOW update 7: advancing the molecular classification of ependymal tumors. *Brain Pathol*, *30*(5), 863-866. https://doi.org/10.1111/bpa.12866

Ellison, D. W., Hawkins, C., Jones, D. T. W., Onar-Thomas, A., Pfister, S. M., Reifenberger, G., & Louis, D. N. (2019). cIMPACT-NOW update 4: diffuse gliomas characterized by MYB, MYBL1, or FGFR1 alterations or BRAF(V600E) mutation. *Acta Neuropathol*, *137*(4), 683-687. https://doi.org/10.1007/s00401-019-01987-0

Ellison, D. W., Kocak, M., Figarella-Branger, D., Felice, G., Catherine, G., Pietsch, T., Frappaz, D., Massimino, M., Grill, J., Boyett, J. M., & Grundy, R. G. (2011). Histopathological grading of pediatric ependymoma: reproducibility and clinical relevance in European trial cohorts. *J Negat Results Biomed*, *10*, 7. https://doi.org/10.1186/1477-5751-10-7

Feldman, M. Y. (1973). Reactions of Nucleic Acids and NucleoDroteins with Formaldehyde11Translated by A. L. Pumpiansky, Moscow. In J. N. Davidson & W. E. Cohn (Eds.), *Progress in Nucleic Acid Research and Molecular Biology* (Vol. 13, pp. 1-49). Academic Press. https://doi.org/https://doi.org/10.1016/S0079-6603(08)60099-9

Fernandez, A. F., Assenov, Y., Martin-Subero, J. I., Balint, B., Siebert, R., Taniguchi, H., Yamamoto, H., Hidalgo, M., Tan, A. C., Galm, O., Ferrer, I., Sanchez-Cespedes, M., Villanueva, A., Carmona, J., Sanchez-Mut, J. V., Berdasco, M., Moreno, V., Capella, G., Monk, D., Ballestar, E., Ropero, S., Martinez, R., Sanchez-Carbayo, M., Prosper, F., Agirre, X., Fraga, M. F., Graña, O., Perez-Jurado, L., Mora, J., Puig, S., Prat, J., Badimon, L., Puca, A. A., Meltzer, S. J., Lengauer, T., Bridgewater, J., Bock, C., & Esteller, M. (2012). A DNA methylation fingerprint of 1628 human samples. *Genome Res*, *22*(2), 407-419. https://doi.org/10.1101/gr.119867.110

Fiebig, H. H., Schuchhardt, C., Henss, H., Fiedler, L., & Löhr, G. W. (1984). Comparison of tumor response in nude mice and in the patients. *Behring Inst Mitt*(74), 343-352.

Florencia Cidre-Aranaz, T. G. P. G. (2021). *Ewing Sarcoma - Methods and Protocols*. Humana New York, NY. https://doi.org/https://doi.org/10.1007/978-1-0716-1020-6

Fraser, M. J., Ciszczon, T., Elick, T., & Bauser, C. (1996). Precise excision of TTAA-specific lepidopteran transposons piggyBac (IFP2) and tagalong (TFP3) from the baculovirus genome in cell lines from two species of Lepidoptera. *Insect Mol Biol*, *5*(2), 141-151. https://doi.org/10.1111/j.1365-2583.1996.tb00048.x

Friedman, H. S., Burger, P. C., Bigner, S. H., Trojanowski, J. Q., Brodeur, G. M., He, X. M., Wikstrand, C. J., Kurtzberg, J., Berens, M. E., Halperin, E. C., & et al. (1988). Phenotypic and genotypic analysis of a human medulloblastoma cell line and transplantable xenograft (D341 Med) demonstrating amplification of c-myc. *Am J Pathol*, *130*(3), 472-484.

Friedman, H. S., Burger, P. C., Bigner, S. H., Trojanowski, J. Q., Wikstrand, C. J., Halperin, E. C., & Bigner, D. D. (1985). Establishment and characterization of the human medulloblastoma cell line and transplantable xenograft D283 Med. *J Neuropathol Exp Neurol*, *44*(6), 592-605. https://doi.org/10.1097/00005072-198511000-00005

Fu, D. Y., Wang, Z. M., Wang, B. L., Chen, L., Yang, W. T., Shen, Z. Z., Huang, W., & Shao, Z. M. (2010). Frequent epigenetic inactivation of the receptor tyrosine kinase EphA5 by promoter methylation in human breast cancer. *Hum Pathol*, *41*(1), 48-58. https://doi.org/10.1016/j.humpath.2009.06.007

Gainor, J. F., Varghese, A. M., Ou, S. H., Kabraji, S., Awad, M. M., Katayama, R., Pawlak, A., Mino-Kenudson, M., Yeap, B. Y., Riely, G. J., Iafrate, A. J., Arcila, M. E., Ladanyi, M., Engelman, J. A., Dias-Santagata, D., & Shaw, A. T. (2013). ALK rearrangements are mutually exclusive with mutations in EGFR or KRAS: an analysis of 1,683 patients with non-small cell lung cancer. *Clin Cancer Res*, *19*(15), 4273-4281. https://doi.org/10.1158/1078-0432.Ccr-13-0318

Gangwal, K., Sankar, S., Hollenhorst, P. C., Kinsey, M., Haroldsen, S. C., Shah, A. A., Boucher, K. M., Watkins, W. S., Jorde, L. B., Graves, B. J., & Lessnick, S. L. (2008). Microsatellites as EWS/FLI response elements in Ewing's sarcoma. *Proceedings of the National Academy of Sciences*, *105*(29), 10149-10154. https://doi.org/doi:10.1073/pnas.0801073105

Garraway, L. A., & Lander, E. S. (2013). Lessons from the cancer genome. *Cell*, *153*(1), 17-37. https://doi.org/10.1016/j.cell.2013.03.002

Ghasemi, D. R., Sill, M., Okonechnikov, K., Korshunov, A., Yip, S., Schutz, P. W., Scheie, D., Kruse, A., Harter, P. N., Kastelan, M., Wagner, M., Hartmann, C., Benzel, J., Maass, K. K., Khasraw, M., Strater, R., Thomas, C., Paulus, W., Kratz, C. P., Witt, H., Kawauchi, D., Herold-Mende, C., Sahm, F., Brandner, S., Kool, M., Jones, D. T. W., von Deimling, A., Pfister, S. M., Reuss, D. E., & Pajtler, K. W. (2019). MYCN amplification drives an aggressive form of spinal ependymoma. *Acta Neuropathol*, *138*(6), 1075-1089. https://doi.org/10.1007/s00401-019-02056-2

Gojo, J., Englinger, B., Jiang, L., Hübner, J. M., Shaw, M. L., Hack, O. A., Madlener, S., Kirchhofer, D., Liu, I., Pyrdol, J., Hovestadt, V., Mazzola, E., Mathewson, N. D., Trissal, M., Lötsch, D., Dorfer, C., Haberler, C., Halfmann, A., Mayr, L., Peyrl, A., Geyeregger, R., Schwalm, B., Mauermann, M., Pajtler, K. W., Milde, T., Shore, M. E., Geduldig, J. E., Pelton, K., Czech, T., Ashenberg, O., Wucherpfennig, K. W., Rozenblatt-Rosen, O., Alexandrescu, S., Ligon, K. L., Pfister, S. M., Regev, A., Slavc, I., Berger, W., Suvà, M. L., Kool, M., & Filbin, M. G. (2020). Single-Cell RNA-Seq Reveals Cellular Hierarchies and Impaired Developmental Trajectories in Pediatric Ependymoma. *Cancer Cell*, *38*(1), 44-59.e49. https://doi.org/https://doi.org/10.1016/j.ccell.2020.06.004

Goodspeed, A., Heiser, L. M., Gray, J. W., & Costello, J. C. (2016). Tumor-Derived Cell Lines as Molecular Models of Cancer Pharmacogenomics. *Mol Cancer Res*, *14*(1), 3-13. https://doi.org/10.1158/1541-7786.Mcr-15-0189

Grabovska, Y., Mackay, A., O'Hare, P., Crosier, S., Finetti, M., Schwalbe, E. C., Pickles, J. C., Fairchild, A. R., Avery, A., Cockle, J., Hill, R., Lindsey, J., Hicks, D., Kristiansen, M., Chalker, J., Anderson, J., Hargrave, D., Jacques, T. S., Straathof, K., Bailey, S., Jones, C., Clifford, S. C., & Williamson, D. (2020). Pediatric pan-central nervous system tumor analysis of immune-cell infiltration identifies correlates of antitumor immunity. *Nat Commun*, *11*(1), 4324. https://doi.org/10.1038/s41467-020-18070-y

Grabovska, Y., Mackay, A., O'Hare, P., Crosier, S., Finetti, M., Schwalbe, E. C., Pickles, J. C., Fairchild, A. R., Avery, A., Cockle, J., Hill, R., Lindsey, J., Hicks, D., Kristiansen, M., Chalker, J., Anderson, J., Hargrave, D., Jacques, T. S., Straathof, K., Bailey, S., Jones, C., Clifford, S. C., & Williamson, D. (2020). Pediatric pan-central nervous system tumor analysis of immune-cell infiltration identifies correlates of antitumor immunity. *Nature Communications*, *11*(1), 4324. https://doi.org/10.1038/s41467-020-18070-y

Grabundzija, I., Irgang, M., Mátés, L., Belay, E., Matrai, J., Gogol-Döring, A., Kawakami, K., Chen, W., Ruiz, P., Chuah, M. K., VandenDriessche, T., Izsvák, Z., & Ivics, Z. (2010). Comparative analysis of transposable element vector systems in human cells. *Mol Ther*, *18*(6), 1200-1209. https://doi.org/10.1038/mt.2010.47

Gravemeyer, J., Spassova, I., Verhaegen, M. E., Dlugosz, A. A., Hoffmann, D., Lange, A., & Becker, J. C. (2022). DNA-methylation patterns imply a common cellular origin of virus- and UV-associated Merkel cell carcinoma. *Oncogene*, *41*(1), 37-45. https://doi.org/10.1038/s41388-021-02064-1

Gröbner, S. N., Worst, B. C., Weischenfeldt, J., Buchhalter, I., Kleinheinz, K., Rudneva, V. A., Johann, P. D., Balasubramanian, G. P., Segura-Wang, M., Brabetz, S., Bender, S., Hutter, B., Sturm, D., Pfaff, E., Hübschmann, D., Zipprich, G., Heinold, M., Eils, J., Lawerenz, C., Erkek, S., Lambo, S., Waszak, S., Blattmann, C., Borkhardt, A., Kuhlen, M., Eggert, A., Fulda, S., Gessler, M., Wegert, J., Kappler, R., Baumhoer, D., Burdach, S., Kirschner-Schwabe, R., Kontny, U., Kulozik, A. E., Lohmann, D., Hettmer, S., Eckert, C., Bielack, S., Nathrath, M., Niemeyer, C., Richter, G. H., Schulte, J., Siebert, R., Westermann, F., Molenaar, J. J., Vassal, G., Witt, H., Lichter, P., Weber, U., Eils, R., Korshunov, A., Witt, O., Pfister, S., Reifenberger, G., Felsberg, J., von Kalle, C., Schmidt, M., Bartholomä, C., Taylor, M., Pfister, S., Jones, D., Lichter, P., Jäger, N., Buchhalter, I., Korbel, J., Stütz, A., Rausch, T., Radlwimmer, B., Yaspo, M.-L., Lehrach, H., Warnatz, H.-J., Landgraf, P., Borkhardt, A., Brors, B., Zapatka, M., Eils, R., Eils, R., Eils, J., Lawerenz, C., Siebert, R., Wagner, S., Haake, A., Richter, J., Richter, G., Eils, R., Lawerenz, C., Eils, J., Kerssemakers, J., Jaeger-Schmidt, C., Scholz, I., Bergmann, A. K., Borst, C., Burkhardt, B., Claviez, A., Dreyling, M., Eberth, S., Einsele, H., Frickhofen, N., Haas, S., Hansmann, M.-L., Karsch, D., Kneba, M., Lisfeld, J., Mantovani-Löffler, L., Rohde, M., Ott, G., Stadler, C., Staib, P., Stilgenbauer, S., Trümper, L., Zenz, T., Hansmann, M.-L., Kube, D., Küppers, R., Weniger, M., Hummel, M., Klapper, W., Kostezka, U., Lenze, D., Möller, P., Rosenwald, A., Ott, G., Szczepanowski, M., Ammerpohl, O., Aukema, S. M., Binder, V., Borkhardt, A., Haake, A., Hoell, J. I., Leich, E., Lichter, P., López, C., Nagel, I., Pischimariov, J., Radlwimmer, B., Richter, J., Rosenstiel, P., Rosenwald, A., Schilhabel, M., Schreiber, S., Vater, I., Wagener, R., Siebert, R., Bernhart, S. H., Binder, H., Brors, B., Doose, G., Eils, R., Hoffmann, S., Hopp, L., Hübschmann, D., Kleinheinz, K., Kretzmer, H., Kreuz, M., Korbel, J., Langenberger, D., Loeffler, M., Rosolowski, M., Schlesner, M., Stadler, P. F., Sungalee, S., Burkhardt, B., Kratz, C. P., Witt, O., van Tilburg, C. M., Kramm, C. M., Fleischhack, G., Dirksen, U., Rutkowski, S., Frühwald, M., von Hoff, K., Wolf, S., Klingebiel, T., Koscielniak, E., Landgraf, P., Koster, J., Resnick, A. C., Zhang, J., Liu, Y., Zhou, X., Waanders, A. J., Zwijnenburg, D. A., Raman, P., Brors, B., Weber, U. D., Northcott, P. A., Pajtler, K. W., Kool, M., Piro, R. M., Korbel, J. O., Schlesner, M., Eils, R., Jones, D. T.

W., Lichter, P., Chavez, L., Zapatka, M., Pfister, S. M., Project, I. P.-S., & Project, I. M.-S. (2018). The landscape of genomic alterations across childhood cancers. *Nature*, *555*(7696), 321-327. https://doi.org/10.1038/nature25480

Gronych, J., Korshunov, A., Bageritz, J., Milde, T., Jugold, M., Hambardzumyan, D., Remke, M., Hartmann, C., Witt, H., Jones, D. T. W., Witt, O., Heiland, S., Bendszus, M., Holland, E. C., Pfister, S., & Lichter, P. (2011). An activated mutant BRAF kinase domain is sufficient to induce pilocytic astrocytoma in mice. *The Journal of Clinical Investigation*, *121*(4), 1344-1348. https://doi.org/10.1172/JCI44656

Gucciardo, E., Sugiyama, N., & Lehti, K. (2014). Eph- and ephrin-dependent mechanisms in tumor and stem cell dynamics. *Cell Mol Life Sci*, *71*(19), 3685-3710. https://doi.org/10.1007/s00018-014-1633-0

Guo, H., Miao, H., Gerber, L., Singh, J., Denning, M. F., Gilliam, A. C., & Wang, B. (2006). Disruption of EphA2 receptor tyrosine kinase leads to increased susceptibility to carcinogenesis in mouse skin. *Cancer Res*, *66*(14), 7050-7058. https://doi.org/10.1158/0008-5472.Can-06-0004

Guttridge, D. C., Albanese, C., Reuther, J. Y., Pestell, R. G., & Baldwin, A. S., Jr. (1999). NF-kappaB controls cell growth and differentiation through transcriptional regulation of cyclin D1. *Mol Cell Biol*, *19*(8), 5785-5799. https://doi.org/10.1128/mcb.19.8.5785

Haag, D., Mack, N., Benites Goncalves da Silva, P., Statz, B., Clark, J., Tanabe, K., Sharma, T., Jäger, N., Jones, D. T. W., Kawauchi, D., Wernig, M., & Pfister, S. M. (2021). H3.3-K27M drives neural stem cell-specific gliomagenesis in a human iPSC-derived model. *Cancer Cell*, *39*(3), 407-422.e413. https://doi.org/10.1016/j.ccell.2021.01.005

Hanahan, D., & Weinberg, R. A. (2000). The hallmarks of cancer. *Cell*, *100*(1), 57-70. https://doi.org/10.1016/s0092-8674(00)81683-9

Hanahan, D., & Weinberg, R. A. (2011). Hallmarks of cancer: the next generation. *Cell*, *144*(5), 646-674. https://doi.org/10.1016/j.cell.2011.02.013

Harding, C. V., Heuser, J. E., & Stahl, P. D. (2013). Exosomes: looking back three decades and into the future. *J Cell Biol*, *200*(4), 367-371. https://doi.org/10.1083/jcb.201212113

Hastings, J. W. (1996). Chemistries and colors of bioluminescent reactions: a review. *Gene*, *173*(1 Spec No), 5-11. https://doi.org/10.1016/0378-1119(95)00676-1

Heinz, S., Benner, C., Spann, N., Bertolino, E., Lin, Y. C., Laslo, P., Cheng, J. X., Murre, C., Singh, H., & Glass, C. K. (2010). Simple combinations of lineage-determining transcription factors prime cis-regulatory elements required for macrophage and B cell identities. *Mol Cell*, *38*(4), 576-589. https://doi.org/10.1016/j.molcel.2010.05.004

Hemmati, H. D., Nakano, I., Lazareff, J. A., Masterman-Smith, M., Geschwind, D. H., Bronner-Fraser, M., & Kornblum, H. I. (2003). Cancerous stem cells can arise from pediatric brain tumors. *Proc Natl Acad Sci U S A*, *100*(25), 15178-15183. https://doi.org/10.1073/pnas.2036535100

Hentze, H., Soong, P. L., Wang, S. T., Phillips, B. W., Putti, T. C., & Dunn, N. R. (2009). Teratoma formation by human embryonic stem cells: evaluation of essential parameters for future safety studies. *Stem Cell Res*, *2*(3), 198-210. https://doi.org/10.1016/j.scr.2009.02.002

Herath, N. I., Doecke, J., Spanevello, M. D., Leggett, B. A., & Boyd, A. W. (2009). Epigenetic silencing of EphA1 expression in colorectal cancer is correlated with poor survival. *Br J Cancer*, *100*(7), 1095-1102. https://doi.org/10.1038/sj.bjc.6604970

Herbst, F., Ball, C. R., Tuorto, F., Nowrouzi, A., Wang, W., Zavidij, O., Dieter, S. M., Fessler, S., van der Hoeven, F., Kloz, U., Lyko, F., Schmidt, M., von Kalle, C., & Glimm, H. (2012). Extensive methylation of promoter sequences silences lentiviral transgene expression during stem cell differentiation in vivo. *Mol Ther*, *20*(5), 1014-1021. https://doi.org/10.1038/mt.2012.46

Hermans, E., & Hulleman, E. (2019). Patient-Derived Orthotopic Xenograft Models of Pediatric Brain Tumors: In a Mature Phase or Still in Its Infancy? *Front Oncol*, *9*, 1418. https://doi.org/10.3389/fonc.2019.01418

Heuer, G. G., Jackson, E. M., Magge, S. N., & Storm, P. B. (2007). Surgical management of pediatric brain tumors. *Expert Rev Anticancer Ther*, *7*(12 Suppl), S61-68. https://doi.org/10.1586/14737140.7.12s.S61

Heydt, C., Wölwer, C. B., Velazquez Camacho, O., Wagener-Ryczek, S., Pappesch, R., Siemanowski, J., Rehker, J., Haller, F., Agaimy, A., Worm, K., Herold, T., Pfarr, N., Weichert, W., Kirchner, T., Jung, A., Kumbrink, J., Goering, W., Esposito, I., Buettner, R., Hillmer, A. M., & Merkelbach-Bruse, S. (2021). Detection of gene fusions using targeted next-generation sequencing: a comparative evaluation. *BMC Medical Genomics*, *14*(1), 62. https://doi.org/10.1186/s12920-021-00909-y

Heyer, J., Kwong, L. N., Lowe, S. W., & Chin, L. (2010). Non-germline genetically engineered mouse models for translational cancer research. *Nature Reviews Cancer*, *10*(7), 470-480. https://doi.org/10.1038/nrc2877

Hickman, D. L., Johnson, J., Vemulapalli, T. H., Crisler, J. R., & Shepherd, R. (2017). Commonly Used Animal Models. *Principles of Animal Research for Graduate and Undergraduate Students*, 25.

Hinrichs, C. S., & Rosenberg, S. A. (2014). Exploiting the curative potential of adoptive T-cell therapy for cancer. *Immunol Rev*, *257*(1), 56-71. https://doi.org/10.1111/imr.12132

Hinz, M., Krappmann, D., Eichten, A., Heder, A., Scheidereit, C., & Strauss, M. (1999). NF-kappaB function in growth control: regulation of cyclin D1 expression and G0/G1-to-S-phase transition. *Mol Cell Biol*, *19*(4), 2690-2698. https://doi.org/10.1128/mcb.19.4.2690

Hong, M., Tao, S., Zhang, L., Diao, L.-T., Huang, X., Huang, S., Xie, S.-J., Xiao, Z.-D., & Zhang, H. (2020). RNA sequencing: new technologies and applications in cancer research. *Journal of Hematology & Oncology*, *13*(1), 166. https://doi.org/10.1186/s13045-020-01005-x

Hong, Y. J., & Do, J. T. (2019). Neural Lineage Differentiation From Pluripotent Stem Cells to Mimic Human Brain Tissues [Review]. *Frontiers in Bioengineering and Biotechnology*, *7*. https://doi.org/10.3389/fbioe.2019.00400

Hong, Y. J., Kim, J. S., Choi, H. W., Song, H., Park, C., & Do, J. T. (2016). In Vivo Generation of Neural Stem Cells Through Teratoma Formation. *Stem Cells and Development*, *25*(17), 1311-1317. https://doi.org/10.1089/scd.2016.0124

Houghton, J. A., Houghton, P. J., & Green, A. A. (1982). Chemotherapy of childhood rhabdomyosarcomas growing as xenografts in immune-deprived mice. *Cancer Res*, *42*(2), 535-539.

Houghton, P. J., Morton, C. L., Tucker, C., Payne, D., Favours, E., Cole, C., Gorlick, R., Kolb, E. A., Zhang, W., Lock, R., Carol, H., Tajbakhsh, M., Reynolds, C. P., Maris, J. M., Courtright, J., Keir, S. T., Friedman, H. S., Stopford, C., Zeidner, J., Wu, J., Liu, T., Billups, C. A., Khan, J., Ansher, S., Zhang, J., & Smith, M. A. (2007). The pediatric preclinical testing program: description of models and early testing results. *Pediatr Blood Cancer*, *49*(7), 928-940. https://doi.org/10.1002/pbc.21078

Hovestadt, V., Jones, D. T. W., Picelli, S., Wang, W., Kool, M., Northcott, P. A., Sultan, M., Stachurski, K., Ryzhova, M., Warnatz, H.-J., Ralser, M., Brun, S., Bunt, J., Jäger, N., Kleinheinz, K., Erkek, S., Weber, U. D., Bartholomae, C. C., von Kalle, C., Lawerenz, C., Eils, J., Koster, J., Versteeg, R., Milde, T., Witt, O., Schmidt, S., Wolf, S., Pietsch, T., Rutkowski, S., Scheurlen, W., Taylor, M. D., Brors, B., Felsberg, J., Reifenberger, G., Borkhardt, A., Lehrach, H., Wechsler-Reya, R. J., Eils, R., Yaspo, M.-L., Landgraf, P., Korshunov, A., Zapatka, M., Radlwimmer, B., Pfister, S. M., & Lichter, P. (2014). Decoding the regulatory landscape of medulloblastoma using DNA methylation sequencing. *Nature*, *510*(7506), 537-541. https://doi.org/10.1038/nature13268

Hovestadt, V., Remke, M., Kool, M., Pietsch, T., Northcott, P. A., Fischer, R., Cavalli, F. M., Ramaswamy, V., Zapatka, M., Reifenberger, G., Rutkowski, S., Schick, M., Bewerunge-Hudler, M., Korshunov, A., Lichter, P., Taylor, M. D., Pfister, S. M., & Jones, D. T. (2013). Robust molecular subgrouping and copy-number profiling of medulloblastoma from small amounts of archival tumour material using high-density DNA methylation arrays. *Acta Neuropathol*, *125*(6), 913-916. https://doi.org/10.1007/s00401-013-1126-5

Howlader N, N. A., Krapcho M, Miller D, Brest A, Yu M, Ruhl J, Tatalovich Z, Mariotto A, Lewis DR, Chen HS, Feuer EJ, Cronin KA (eds). (2021). SEER Cancer Statistics Review, 1975-2018.

Huang, M., Tailor, J., Zhen, Q., Gillmor, A. H., Miller, M. L., Weishaupt, H., Chen, J., Zheng, T., Nash, E. K., McHenry, L. K., An, Z., Ye, F., Takashima, Y., Clarke, J., Ayetey, H., Cavalli, F. M. G., Luu, B., Moriarity, B. S., Ilkhanizadeh, S., Chavez, L., Yu, C., Kurian, K. M., Magnaldo, T., Sevenet, N., Koch, P., Pollard, S. M., Dirks, P., Snyder, M. P., Largaespada, D. A., Cho, Y. J., Phillips, J. J., Swartling, F. J., Morrissy, A. S., Kool, M., Pfister, S. M., Taylor, M. D., Smith, A., & Weiss, W. A. (2019). Engineering Genetic Predisposition in Human Neuroepithelial Stem Cells Recapitulates Medulloblastoma Tumorigenesis. *Cell Stem Cell*, *25*(3), 433-446.e437. https://doi.org/10.1016/j.stem.2019.05.013

Huang, Z., Keramat, S., Izadirad, M., Chen, Z. S., & Soukhtanloo, M. (2022). The Potential Role of Exosomes in the Treatment of Brain Tumors, Recent Updates and Advances. *Front Oncol*, *12*, 869929. https://doi.org/10.3389/fonc.2022.869929

Hubert, C. G., Rivera, M., Spangler, L. C., Wu, Q., Mack, S. C., Prager, B. C., Couce, M., McLendon, R. E., Sloan, A. E., & Rich, J. N. (2016). A Three-Dimensional Organoid Culture System Derived from Human Glioblastomas Recapitulates the Hypoxic Gradients and Cancer Stem Cell Heterogeneity of Tumors Found In Vivo. *Cancer Res*, *76*(8), 2465-2477. https://doi.org/10.1158/0008-5472.Can-15-2402

Hum, N. R., Sebastian, A., Gilmore, S. F., He, W., Martin, K. A., Hinckley, A., Dubbin, K. R., Moya, M. L., Wheeler, E. K., Coleman, M. A., & Loots, G. G. (2020). Comparative Molecular Analysis of Cancer Behavior Cultured In Vitro, In Vivo, and Ex Vivo. *Cancers (Basel)*, *12*(3). https://doi.org/10.3390/cancers12030690

Huszthy, P. C., Daphu, I., Niclou, S. P., Stieber, D., Nigro, J. M., Sakariassen, P., Miletic, H., Thorsen, F., & Bjerkvig, R. (2012). In vivo models of primary brain tumors: pitfalls and perspectives. *Neuro Oncol*, *14*(8), 979-993. https://doi.org/10.1093/neuonc/nos135

Ivanov, D. P., Coyle, B., Walker, D. A., & Grabowska, A. M. (2016). In vitro models of medulloblastoma: Choosing the right tool for the job. *Journal of Biotechnology*, *236*, 10-25. https://doi.org/https://doi.org/10.1016/j.jbiotec.2016.07.028

Ivics, Z., Hackett, P. B., Plasterk, R. H., & Izsvák, Z. (1997). Molecular reconstruction of Sleeping Beauty, a Tc1-like transposon from fish, and its transposition in human cells. *Cell*, *91*(4), 501-510. https://doi.org/10.1016/s0092-8674(00)80436-5

Ivics, Z., Izsvak, Z., Minter, A., & Hackett, P. B. (1996). Identification of functional domains and evolution of Tc1-like transposable elements. *Proc Natl Acad Sci U S A*, *93*(10), 5008-5013. https://doi.org/10.1073/pnas.93.10.5008

Jacobsen, P. F., Jenkyn, D. J., & Papadimitriou, J. M. (1985). Establishment of a human medulloblastoma cell line and its heterotransplantation into nude mice. *J Neuropathol Exp Neurol*, *44*(5), 472-485. https://doi.org/10.1097/00005072-198509000-00003

Janes, P. W., Griesshaber, B., Atapattu, L., Nievergall, E., Hii, L. L., Mensinga, A., Chheang, C., Day, B. W., Boyd, A. W., Bastiaens, P. I., Jørgensen, C., Pawson, T., & Lackmann, M. (2011). Eph receptor function is modulated by heterooligomerization of A and B type Eph receptors. *Journal of Cell Biology*, *195*(6), 1033-1045. https://doi.org/10.1083/jcb.201104037

Jarmalaite, S., Laurinaviciene, A., Tverkuviene, J., Kalinauskaite, N., Petroska, D., Böhling, T., & Husgafvel-Pursiainen, K. (2011). Tumor suppressor gene ZAC/PLAGL1: altered expression and loss of the nonimprinted allele in pheochromocytomas. *Cancer Genet*, *204*(7), 398-404. https://doi.org/10.1016/j.cancergen.2011.07.002

Jemal, A., Ward, E. M., Johnson, C. J., Cronin, K. A., Ma, J., Ryerson, B., Mariotto, A., Lake, A. J., Wilson, R., Sherman, R. L., Anderson, R. N., Henley, S. J., Kohler, B. A., Penberthy, L., Feuer, E. J., & Weir, H. K. (2017). Annual Report to the Nation on the Status of Cancer, 1975-2014, Featuring Survival. *J Natl Cancer Inst*, *109*(9). https://doi.org/10.1093/jnci/djx030

Jinek, M., Chylinski, K., Fonfara, I., Hauer, M., Doudna, J. A., & Charpentier, E. (2012). A Programmable Dual-RNA–Guided DNA Endonuclease in Adaptive Bacterial Immunity. *Science*, *337*(6096), 816-821. https://doi.org/doi:10.1126/science.1225829

Jo, J., Xiao, Y., Sun, A. X., Cukuroglu, E., Tran, H. D., Göke, J., Tan, Z. Y., Saw, T. Y., Tan, C. P., Lokman, H., Lee, Y., Kim, D., Ko, H. S., Kim, S. O., Park, J. H., Cho, N. J., Hyde, T. M., Kleinman, J. E., Shin, J. H., Weinberger, D. R., Tan, E. K., Je, H. S., & Ng, H. H. (2016). Midbrain-like Organoids from Human Pluripotent Stem Cells Contain Functional Dopaminergic and Neuromelanin-Producing Neurons. *Cell Stem Cell*, *19*(2), 248-257. https://doi.org/10.1016/j.stem.2016.07.005

Johann, P. D., Erkek, S., Zapatka, M., Kerl, K., Buchhalter, I., Hovestadt, V., Jones, D. T. W., Sturm, D., Hermann, C., Segura Wang, M., Korshunov, A., Rhyzova, M., Gröbner, S., Brabetz, S., Chavez, L., Bens, S., Gröschel, S., Kratochwil, F., Wittmann, A., Sieber, L., Geörg, C., Wolf, S., Beck, K., Oyen, F., Capper, D., van Sluis, P., Volckmann, R., Koster, J., Versteeg, R., von Deimling, A., Milde, T., Witt, O., Kulozik, A. E., Ebinger, M., Shalaby, T., Grotzer, M., Sumerauer, D., Zamecnik, J., Mora, J., Jabado, N., Taylor, M. D., Huang, A., Aronica, E., Bertoni, A., Radlwimmer, B., Pietsch, T., Schüller, U., Schneppenheim, R., Northcott, P. A., Korbel, J. O., Siebert, R., Frühwald, M. C., Lichter, P., Eils, R., Gajjar, A., Hasselblatt, M., Pfister, S. M., & Kool, M. (2016). Atypical Teratoid/Rhabdoid Tumors Are Comprised of Three Epigenetic Subgroups with Distinct Enhancer Landscapes. *Cancer Cell*, *29*(3), 379-393. https://doi.org/10.1016/j.ccell.2016.02.001

Johnson, R. A., Wright, K. D., Poppleton, H., Mohankumar, K. M., Finkelstein, D., Pounds, S. B., Rand, V., Leary, S. E., White, E., Eden, C., Hogg, T., Northcott, P., Mack, S., Neale, G., Wang, Y. D., Coyle, B., Atkinson, J., DeWire, M., Kranenburg, T. A., Gillespie, Y., Allen, J. C., Merchant, T., Boop, F. A., Sanford, R. A., Gajjar, A., Ellison, D. W., Taylor, M. D., Grundy, R. G., & Gilbertson, R. J. (2010). Cross-species genomics matches driver mutations and cell compartments to model ependymoma. *Nature*, *466*(7306), 632-636. https://doi.org/10.1038/nature09173

Jones, C., Perryman, L., & Hargrave, D. (2012). Paediatric and adult malignant glioma: close relatives or distant cousins? *Nature Reviews Clinical Oncology*, *9*(7), 400-413. https://doi.org/10.1038/nrclinonc.2012.87

Jørgensen, C., Sherman, A., Chen, G. I., Pasculescu, A., Poliakov, A., Hsiung, M., Larsen, B., Wilkinson, D. G., Linding, R., & Pawson, T. (2009). Cell-specific information processing in segregating populations of Eph receptor ephrin-expressing cells. *Science*, *326*(5959), 1502-1509. https://doi.org/10.1126/science.1176615

Kadoshima, T., Sakaguchi, H., Nakano, T., Soen, M., Ando, S., Eiraku, M., & Sasai, Y. (2013). Self-organization of axial polarity, inside-out layer pattern, and species-specific progenitor dynamics in human ES cell-derived neocortex. *Proc Natl Acad Sci U S A*, *110*(50), 20284-20289. https://doi.org/10.1073/pnas.1315710110

Kalhor, R., Kalhor, K., Mejia, L., Leeper, K., Graveline, A., Mali, P., & Church, G. M. (2018). Developmental barcoding of whole mouse via homing CRISPR. *Science*, *361*(6405). https://doi.org/10.1126/science.aat9804

Kantarjian, H. M., O'Brien, S., Cortes, J., Giles, F. J., Faderl, S., Issa, J.-P., Garcia-Manero, G., Rios, M. B., Shan, J., Andreeff, M., Keating, M., & Talpaz, M. (2003). Results of decitabine (5-aza-2'deoxycytidine) therapy in 130 patients with chronic myelogenous leukemia. *Cancer*, *98*(3), 522-528. https://doi.org/https://doi.org/10.1002/cncr.11543

Kasper, M., Schnidar, H., Neill, G. W., Hanneder, M., Klingler, S., Blaas, L., Schmid, C., Hauser-Kronberger, C., Regl, G., Philpott, M. P., & Aberger, F. (2006). Selective modulation of Hedgehog/GLI target gene expression by epidermal growth factor signaling in human keratinocytes. *Mol Cell Biol*, *26*(16), 6283-6298. https://doi.org/10.1128/mcb.02317-05

Katrin Scheinemann, E. B. (2015). *Pediatric Neuro-oncology*. Springer New York, NY.

Kawauchi, D., Ogg, R. J., Liu, L., Shih, D. J. H., Finkelstein, D., Murphy, B. L., Rehg, J. E., Korshunov, A., Calabrese, C., Zindy, F., Phoenix, T., Kawaguchi, Y., Gronych, J., Gilbertson, R. J., Lichter, P., Gajjar, A., Kool, M., Northcott, P. A., Pfister, S. M., & Roussel, M. F. (2017). Novel MYC-driven medulloblastoma models from multiple embryonic cerebellar cells. *Oncogene*, *36*(37), 5231-5242. https://doi.org/10.1038/onc.2017.110

Kawauchi, D., Taniguchi, H., Watanabe, H., Saito, T., & Murakami, F. (2006). Direct visualization of nucleogenesis by precerebellar neurons: involvement of ventricle-directed, radial fibre-associated migration. *Development*, *133*(6), 1113-1123. https://doi.org/10.1242/dev.02283

Keck, M.-K., Sill, M., Wittmann, A., Joshi, P., Stichel, D., Beck, P., Okonechnikow, K., Sievers, P., Wefers, A. K., Roncaroli, F., Avula, S., McCabe, M. G., Hayden, J. T., Wesseling, P., Øra, I., Nistér, M., Kranendonk, M. E. G., Tops, B. B. J., Zapotocky, M., Zamecnik, J., Vasiljevic, A., Fenouil, T., Meyronet, D., von Hoff, K., Schüller, U., Loiseau, H., Figarella-Branger, D., Kramm, C. M., Sturm, D., Scheie, D., Rauramaa, T., Pesola, J., Gojo, J., Haberler, C., Brandner, S., Jacques, T., Sexton Oates, A., Saffery, R., Koscielniak, E., Baker, S. J., Yip, S., Snuderl, M., Ud Din, N., Samuel, D., Schramm, K., Blattner-Johnson, M., Selt, F., Ecker, J., Milde, T., von Deimling, A., Korshunov, A., Perry, A., Pfister, S. M., Sahm, F., Solomon, D. A., & Jones, D. T. W. (2023). Amplification of the PLAG-family genes—PLAGL1 and PLAGL2—is a key feature of the novel tumor type CNS embryonal tumor with PLAGL amplification. *Acta Neuropathologica*, *145*(1), 49-69. https://doi.org/10.1007/s00401-022-02516-2

Keles, G. E., Berger, M. S., Srinivasan, J., Kolstoe, D. D., Bobola, M. S., & Silber, J. R. (1995). Establishment and characterization of four human medulloblastoma-derived cell lines. *Oncol Res*, *7*(10-11), 493-503.

Kijima, N., & Kanemura, Y. (2016). Molecular Classification of Medulloblastoma. *Neurol Med Chir (Tokyo)*, *56*(11), 687-697. https://doi.org/10.2176/nmc.ra.2016-0016

Kilday, J. P., Rahman, R., Dyer, S., Ridley, L., Lowe, J., Coyle, B., & Grundy, R. (2009). Pediatric ependymoma: biological perspectives. *Mol Cancer Res*, *7*(6), 765-786. https://doi.org/10.1158/1541-7786.Mcr-08-0584

Kim, H., Kim, M., Im, S. K., & Fang, S. (2018). Mouse Cre-LoxP system: general principles to determine tissue-specific roles of target genes. *Lab Anim Res*, *34*(4), 147-159. https://doi.org/10.5625/lar.2018.34.4.147

Kim, K., Higashi, M., Fumino, S., & Tajiri, T. (2019). Derivation of neural stem cells from human teratomas. *Stem Cell Res*, *41*, 101633. https://doi.org/10.1016/j.scr.2019.101633

Kim, M., & Costello, J. (2017). DNA methylation: an epigenetic mark of cellular memory. *Experimental & Molecular Medicine*, *49*(4), e322-e322. https://doi.org/10.1038/emm.2017.10

Koelsche, C., Hovestadt, V., Jones, D. T., Capper, D., Sturm, D., Sahm, F., Schrimpf, D., Adeberg, S., Böhmer, K., Hagenlocher, C., Mechtersheimer, G., Kohlhof, P., Mühleisen, H., Beschorner, R., Hartmann, C., Braczynski, A. K., Mittelbronn, M., Buslei, R., Becker, A., Grote, A., Urbach, H., Staszewski, O., Prinz, M.,

Hewer, E., Pfister, S. M., von Deimling, A., & Reuss, D. E. (2015). Melanotic tumors of the nervous system are characterized by distinct mutational, chromosomal and epigenomic profiles. *Brain Pathol*, *25*(2), 202-208. https://doi.org/10.1111/bpa.12228

Koga, A., Inagaki, H., Bessho, Y., & Hori, H. (1995). Insertion of a novel transposable element in the tyrosinase gene is responsible for an albino mutation in the medaka fish, Oryzias latipes. *Mol Gen Genet*, *249*(4), 400-405. https://doi.org/10.1007/bf00287101

Koga, A., Suzuki, M., Inagaki, H., Bessho, Y., & Hori, H. (1996). Transposable element in fish. *Nature*, *383*(6595), 30. https://doi.org/10.1038/383030a0

Koller, B. H., Hagemann, L. J., Doetschman, T., Hagaman, J. R., Huang, S., Williams, P. J., First, N. L., Maeda, N., & Smithies, O. (1989). Germ-line transmission of a planned alteration made in a hypoxanthine phosphoribosyltransferase gene by homologous recombination in embryonic stem cells. *Proc Natl Acad Sci U S A*, *86*(22), 8927-8931. https://doi.org/10.1073/pnas.86.22.8927

Kool, M., Koster, J., Bunt, J., Hasselt, N. E., Lakeman, A., van Sluis, P., Troost, D., Meeteren, N. S., Caron, H. N., Cloos, J., Mrsić, A., Ylstra, B., Grajkowska, W., Hartmann, W., Pietsch, T., Ellison, D., Clifford, S. C., & Versteeg, R. (2008). Integrated genomics identifies five medulloblastoma subtypes with distinct genetic profiles, pathway signatures and clinicopathological features. *PLoS One*, *3*(8), e3088. https://doi.org/10.1371/journal.pone.0003088

Korshunov, A., Capper, D., Reuss, D., Schrimpf, D., Ryzhova, M., Hovestadt, V., Sturm, D., Meyer, J., Jones, C., Zheludkova, O., Kumirova, E., Golanov, A., Kool, M., Schüller, U., Mittelbronn, M., Hasselblatt, M., Schittenhelm, J., Reifenberger, G., Herold-Mende, C., Lichter, P., von Deimling, A., Pfister, S. M., & Jones, D. T. (2016). Histologically distinct neuroepithelial tumors with histone 3 G34 mutation are molecularly similar and comprise a single nosologic entity. *Acta Neuropathol*, *131*(1), 137-146. https://doi.org/10.1007/s00401-015-1493-1

Korshunov, A., Sturm, D., Ryzhova, M., Hovestadt, V., Gessi, M., Jones, D. T., Remke, M., Northcott, P., Perry, A., Picard, D., Rosenblum, M., Antonelli, M., Aronica, E., Schüller, U., Hasselblatt, M., Woehrer, A., Zheludkova, O., Kumirova, E., Puget, S., Taylor, M. D., Giangaspero, F., Peter Collins, V., von Deimling, A., Lichter, P., Huang, A., Pietsch, T., Pfister, S. M., & Kool, M. (2014). Embryonal tumor with abundant neuropil and true rosettes (ETANTR), ependymoblastoma, and medulloepithelioma share molecular similarity and comprise a single clinicopathological entity. *Acta Neuropathol*, *128*(2), 279-289. https://doi.org/10.1007/s00401-013-1228-0

Kosugi, S., Hasebe, M., Entani, T., Takayama, S., Tomita, M., & Yanagawa, H. (2008). Design of peptide inhibitors for the importin alpha/beta nuclear import pathway by activity-based profiling. *Chem Biol*, *15*(9), 940-949. https://doi.org/10.1016/j.chembiol.2008.07.019

Kosugi, S., Hasebe, M., Matsumura, N., Takashima, H., Miyamoto-Sato, E., Tomita, M., & Yanagawa, H. (2009). Six classes of nuclear localization signals specific to different binding grooves of importin alpha. *J Biol Chem*, *284*(1), 478-485. https://doi.org/10.1074/jbc.M807017200

Kosugi, S., Hasebe, M., Tomita, M., & Yanagawa, H. (2009). Systematic identification of cell cycle-dependent yeast nucleocytoplasmic shuttling proteins by prediction of composite motifs. *Proc Natl Acad Sci U S A*, *106*(25), 10171-10176. https://doi.org/10.1073/pnas.0900604106

Kowalczyk, A. E., Krazinski, B. E., Godlewski, J., Kiewisz, J., Kwiatkowski, P., Sliwinska-Jewsiewicka, A., Kiezun, J., Wierzbicki, P. M., Bodek, G., Sulik, M., & Kmiec, Z. (2015). Altered expression of the PLAGL1 (ZAC1/LOT1) gene in colorectal cancer: Correlations to the clinicopathological parameters. *Int J Oncol*, *47*(3), 951-962. https://doi.org/10.3892/ijo.2015.3067

Krencik, R., & Zhang, S. C. (2011). Directed differentiation of functional astroglial subtypes from human pluripotent stem cells. *Nat Protoc*, *6*(11), 1710-1717. https://doi.org/10.1038/nprot.2011.405

Kuang, S. Q., Bai, H., Fang, Z. H., Lopez, G., Yang, H., Tong, W., Wang, Z. Z., & Garcia-Manero, G. (2010). Aberrant DNA methylation and epigenetic inactivation of Eph receptor tyrosine kinases and ephrin ligands in acute lymphoblastic leukemia. *Blood*, *115*(12), 2412-2419. https://doi.org/10.1182/blood-2009-05-222208

Kupp, R., Ruff, L., Terranova, S., Nathan, E., Ballereau, S., Stark, R., Sekhar Reddy Chilamakuri, C., Hoffmann, N., Wickham-Rahrmann, K., Widdess, M., Arabzade, A., Zhao, Y., Varadharajan, S., Zheng, T., Murugesan, M. K., Pfister, S. M., Kawauchi, D., Pajtler, K. W., Deneen, B., Mack, S. C., Masih, K. E., Gryder, B. E., Khan, J., & Gilbertson, R. J. (2021). ZFTA-translocations constitute ependymoma chromatin remodeling and transcription factors. *Cancer Discovery*, candisc.1052.2020. https://doi.org/10.1158/2159-8290.Cd-20-1052

Lambert, S. R., Witt, H., Hovestadt, V., Zucknick, M., Kool, M., Pearson, D. M., Korshunov, A., Ryzhova, M., Ichimura, K., Jabado, N., Fontebasso, A. M., Lichter, P., Pfister, S. M., Collins, V. P., & Jones,

D. T. (2013). Differential expression and methylation of brain developmental genes define location-specific subsets of pilocytic astrocytoma. *Acta Neuropathol*, *126*(2), 291-301. https://doi.org/10.1007/s00401-013-1124-7

Lampreht Tratar, U., Horvat, S., & Cemazar, M. (2018). Transgenic Mouse Models in Cancer Research. *Front Oncol*, *8*, 268. https://doi.org/10.3389/fonc.2018.00268

Lancaster, M. A., Renner, M., Martin, C. A., Wenzel, D., Bicknell, L. S., Hurles, M. E., Homfray, T., Penninger, J. M., Jackson, A. P., & Knoblich, J. A. (2013). Cerebral organoids model human brain development and microcephaly. *Nature*, *501*(7467), 373-379. https://doi.org/10.1038/nature12517

Lander, E. S., Linton, L. M., Birren, B., Nusbaum, C., Zody, M. C., Baldwin, J., Devon, K., Dewar, K., Doyle, M., FitzHugh, W., Funke, R., Gage, D., Harris, K., Heaford, A., Howland, J., Kann, L., Lehoczky, J., LeVine, R., McEwan, P., McKernan, K., Meldrim, J., Mesirov, J. P., Miranda, C., Morris, W., Naylor, J., Raymond, C., Rosetti, M., Santos, R., Sheridan, A., Sougnez, C., Stange-Thomann, Y., Stojanovic, N., Subramanian, A., Wyman, D., Rogers, J., Sulston, J., Ainscough, R., Beck, S., Bentley, D., Burton, J., Clee, C., Carter, N., Coulson, A., Deadman, R., Deloukas, P., Dunham, A., Dunham, I., Durbin, R., French, L., Grafham, D., Gregory, S., Hubbard, T., Humphray, S., Hunt, A., Jones, M., Lloyd, C., McMurray, A., Matthews, L., Mercer, S., Milne, S., Mullikin, J. C., Mungall, A., Plumb, R., Ross, M., Shownkeen, R., Sims, S., Waterston, R. H., Wilson, R. K., Hillier, L. W., McPherson, J. D., Marra, M. A., Mardis, E. R., Fulton, L. A., Chinwalla, A. T., Pepin, K. H., Gish, W. R., Chissoe, S. L., Wendl, M. C., Delehaunty, K. D., Miner, T. L., Delehaunty, A., Kramer, J. B., Cook, L. L., Fulton, R. S., Johnson, D. L., Minx, P. J., Clifton, S. W., Hawkins, T., Branscomb, E., Predki, P., Richardson, P., Wenning, S., Slezak, T., Doggett, N., Cheng, J. F., Olsen, A., Lucas, S., Elkin, C., Uberbacher, E., Frazier, M., Gibbs, R. A., Muzny, D. M., Scherer, S. E., Bouck, J. B., Sodergren, E. J., Worley, K. C., Rives, C. M., Gorrell, J. H., Metzker, M. L., Naylor, S. L., Kucherlapati, R. S., Nelson, D. L., Weinstock, G. M., Sakaki, Y., Fujiyama, A., Hattori, M., Yada, T., Toyoda, A., Itoh, T., Kawagoe, C., Watanabe, H., Totoki, Y., Taylor, T., Weissenbach, J., Heilig, R., Saurin, W., Artiguenave, F., Brottier, P., Bruls, T., Pelletier, E., Robert, C., Wincker, P., Smith, D. R., Doucette-Stamm, L., Rubenfield, M., Weinstock, K., Lee, H. M., Dubois, J., Rosenthal, A., Platzer, M., Nyakatura, G., Taudien, S., Rump, A., Yang, H., Yu, J., Wang, J., Huang, G., Gu, J., Hood, L., Rowen, L., Madan, A., Qin, S., Davis, R. W., Federspiel, N. A., Abola, A. P., Proctor, M. J., Myers, R. M., Schmutz, J., Dickson, M., Grimwood, J., Cox, D. R., Olson, M. V., Kaul, R., Raymond, C., Shimizu, N., Kawasaki, K., Minoshima, S., Evans, G. A., Athanasiou, M., Schultz, R., Roe, B. A., Chen, F., Pan, H., Ramser, J., Lehrach, H., Reinhardt, R., McCombie, W. R., de la Bastide, M., Dedhia, N., Blöcker, H., Hornischer, K., Nordsiek, G., Agarwala, R., Aravind, L., Bailey, J. A., Bateman, A., Batzoglou, S., Birney, E., Bork, P., Brown, D. G., Burge, C. B., Cerutti, L., Chen, H. C., Church, D., Clamp, M., Copley, R. R., Doerks, T., Eddy, S. R., Eichler, E. E., Furey, T. S., Galagan, J., Gilbert, J. G., Harmon, C., Hayashizaki, Y., Haussler, D., Hermjakob, H., Hokamp, K., Jang, W., Johnson, L. S., Jones, T. A., Kasif, S., Kaspryzk, A., Kennedy, S., Kent, W. J., Kitts, P., Koonin, E. V., Korf, I., Kulp, D., Lancet, D., Lowe, T. M., McLysaght, A., Mikkelsen, T., Moran, J. V., Mulder, N., Pollara, V. J., Ponting, C. P., Schuler, G., Schultz, J., Slater, G., Smit, A. F., Stupka, E., Szustakowki, J., Thierry-Mieg, D., Thierry-Mieg, J., Wagner, L., Wallis, J., Wheeler, R., Williams, A., Wolf, Y. I., Wolfe, K. H., Yang, S. P., Yeh, R. F., Collins, F., Guyer, M. S., Peterson, J., Felsenfeld, A., Wetterstrand, K. A., Patrinos, A., Morgan, M. J., de Jong, P., Catanese, J. J., Osoegawa, K., Shizuya, H., Choi, S., Chen, Y. J., & Szustakowki, J. (2001). Initial sequencing and analysis of the human genome. *Nature*, *409*(6822), 860-921. https://doi.org/10.1038/35057062

Ledur, P. F., Onzi, G. R., Zong, H., & Lenz, G. (2017). Culture conditions defining glioblastoma cells behavior: what is the impact for novel discoveries? *Oncotarget*, *8*(40), 69185-69197. https://doi.org/10.18632/oncotarget.20193

Lee, A. S., Tang, C., Cao, F., Xie, X., van der Bogt, K., Hwang, A., Connolly, A. J., Robbins, R. C., & Wu, J. C. (2009). Effects of cell number on teratoma formation by human embryonic stem cells. *Cell Cycle*, *8*(16), 2608-2612. https://doi.org/10.4161/cc.8.16.9353

Lee, C., & Scherer, S. W. (2010). The clinical context of copy number variation in the human genome. *Expert Rev Mol Med*, *12*, e8. https://doi.org/10.1017/s1462399410001390

Lee, J., Kotliarova, S., Kotliarov, Y., Li, A., Su, Q., Donin, N. M., Pastorino, S., Purow, B. W., Christopher, N., Zhang, W., Park, J. K., & Fine, H. A. (2006). Tumor stem cells derived from glioblastomas cultured in bFGF and EGF more closely mirror the phenotype and genotype of primary tumors than do serum-cultured cell lines. *Cancer Cell*, *9*(5), 391-403. https://doi.org/10.1016/j.ccr.2006.03.030

Lemeta, S., Jarmalaite, S., Pylkkänen, L., Böhling, T., & Husgafvel-Pursiainen, K. (2007). Preferential loss of the nonimprinted allele for the ZAC1 tumor suppressor gene in human capillary hemangioblastoma. *J Neuropathol Exp Neurol*, *66*(9), 860-867. https://doi.org/10.1097/nen.0b013e318149ee64

Leten, C., Struys, T., Dresselaers, T., & Himmelreich, U. (2014). In vivo and ex vivo assessment of the blood brain barrier integrity in different glioblastoma animal models. *Journal of Neuro-Oncology*, *119*(2), 297-306. https://doi.org/10.1007/s11060-014-1514-2

Levy, S., Sutton, G., Ng, P. C., Feuk, L., Halpern, A. L., Walenz, B. P., Axelrod, N., Huang, J., Kirkness, E. F., Denisov, G., Lin, Y., MacDonald, J. R., Pang, A. W., Shago, M., Stockwell, T. B., Tsiamouri, A., Bafna, V., Bansal, V., Kravitz, S. A., Busam, D. A., Beeson, K. Y., McIntosh, T. C., Remington, K. A., Abril, J. F., Gill, J., Borman, J., Rogers, Y. H., Frazier, M. E., Scherer, S. W., Strausberg, R. L., & Venter, J. C. (2007). The diploid genome sequence of an individual human. *PLoS Biol*, *5*(10), e254. https://doi.org/10.1371/journal.pbio.0050254

Li, A. P. (2005). Preclinical in vitro screening assays for drug-like properties. *Drug Discov Today Technol*, *2*(2), 179-185. https://doi.org/10.1016/j.ddtec.2005.05.024

Li, Z., & Langhans, S. A. (2021). In Vivo and Ex Vivo Pediatric Brain Tumor Models: An Overview [Review]. *Frontiers in Oncology*, *11*. https://doi.org/10.3389/fonc.2021.620831

Liao, B. Y., & Zhang, J. (2006). Evolutionary conservation of expression profiles between human and mouse orthologous genes. *Mol Biol Evol*, *23*(3), 530-540. https://doi.org/10.1093/molbev/msj054

Lilienblum, W., Dekant, W., Foth, H., Gebel, T., Hengstler, J. G., Kahl, R., Kramer, P. J., Schweinfurth, H., & Wollin, K. M. (2008). Alternative methods to safety studies in experimental animals: role in the risk assessment of chemicals under the new European Chemicals Legislation (REACH). *Arch Toxicol*, *82*(4), 211-236. https://doi.org/10.1007/s00204-008-0279-9

Lin, G. L., & Monje, M. (2017). A Protocol for Rapid Post-mortem Cell Culture of Diffuse Intrinsic Pontine Glioma (DIPG). *J Vis Exp*(121). https://doi.org/10.3791/55360

Linkous, A., Balamatsias, D., Snuderl, M., Edwards, L., Miyaguchi, K., Milner, T., Reich, B., Cohen-Gould, L., Storaska, A., Nakayama, Y., Schenkein, E., Singhania, R., Cirigliano, S., Magdeldin, T., Lin, Y., Nanjangud, G., Chadalavada, K., Pisapia, D., Liston, C., & Fine, H. A. (2019). Modeling Patient-Derived Glioblastoma with Cerebral Organoids. *Cell Rep*, *26*(12), 3203-3211.e3205. https://doi.org/10.1016/j.celrep.2019.02.063

Lipshutz, R. J., Fodor, S. P., Gingeras, T. R., & Lockhart, D. J. (1999). High density synthetic oligonucleotide arrays. *Nat Genet*, *21*(1 Suppl), 20-24. https://doi.org/10.1038/4447

Lister, R., Pelizzola, M., Dowen, R. H., Hawkins, R. D., Hon, G., Tonti-Filippini, J., Nery, J. R., Lee, L., Ye, Z., Ngo, Q.-M., Edsall, L., Antosiewicz-Bourget, J., Stewart, R., Ruotti, V., Millar, A. H., Thomson, J. A., Ren, B., & Ecker, J. R. (2009). Human DNA methylomes at base resolution show widespread epigenomic differences. *Nature*, *462*(7271), 315-322. https://doi.org/10.1038/nature08514

Lockhart, D. J., Dong, H., Byrne, M. C., Follettie, M. T., Gallo, M. V., Chee, M. S., Mittmann, M., Wang, C., Kobayashi, M., Horton, H., & Brown, E. L. (1996). Expression monitoring by hybridization to high-density oligonucleotide arrays. *Nat Biotechnol*, *14*(13), 1675-1680. https://doi.org/10.1038/nbt1296-1675

Louis, D. N., Aldape, K., Brat, D. J., Capper, D., Ellison, D. W., Hawkins, C., Paulus, W., Perry, A., Reifenberger, G., Figarella-Branger, D., Wesseling, P., Batchelor, T. T., Gregory Cairncross, J., Pfister, S. M., Rutkowski, S., Weller, M., Wick, W., & von Deimling, A. (2017). cIMPACT-NOW (the consortium to inform molecular and practical approaches to CNS tumor taxonomy): a new initiative in advancing nervous system tumor classification. *Brain Pathol*, *27*(6), 851-852. https://doi.org/10.1111/bpa.12457

Louis, D. N., Ellison, D. W., Brat, D. J., Aldape, K., Capper, D., Hawkins, C., Paulus, W., Perry, A., Reifenberger, G., Figarella-Branger, D., von Deimling, A., & Wesseling, P. (2019). cIMPACT-NOW: a practical summary of diagnostic points from Round 1 updates. *Brain Pathol*, *29*(4), 469-472. https://doi.org/10.1111/bpa.12732

Louis, D. N., Ohgaki, H., Wiestler, O. D., Cavenee, W. K., Burger, P. C., Jouvet, A., Scheithauer, B. W., & Kleihues, P. (2007). The 2007 WHO classification of tumours of the central nervous system. *Acta Neuropathol*, *114*(2), 97-109. https://doi.org/10.1007/s00401-007-0243-4

Louis, D. N., Perry, A., Reifenberger, G., von Deimling, A., Figarella-Branger, D., Cavenee, W. K., Ohgaki, H., Wiestler, O. D., Kleihues, P., & Ellison, D. W. (2016). The 2016 World Health Organization Classification of Tumors of the Central Nervous System: a summary. *Acta Neuropathologica*, *131*(6), 803-820. https://doi.org/10.1007/s00401-016-1545-1

Louis, D. N., Perry, A., Wesseling, P., Brat, D. J., Cree, I. A., Figarella-Branger, D., Hawkins, C., Ng, H. K., Pfister, S. M., Reifenberger, G., Soffietti, R., von Deimling, A., & Ellison, D. W. (2021). The 2021 WHO Classification of Tumors of the Central Nervous System: a summary. *Neuro-Oncology*, *23*(8), 1231-1251. https://doi.org/10.1093/neuonc/noab106

Louis, D. N., Wesseling, P., Aldape, K., Brat, D. J., Capper, D., Cree, I. A., Eberhart, C., Figarella-Branger, D., Fouladi, M., Fuller, G. N., Giannini, C., Haberler, C., Hawkins, C., Komori, T., Kros, J. M., Ng, H. K., Orr, B. A., Park, S. H., Paulus, W., Perry, A., Pietsch, T., Reifenberger, G., Rosenblum, M., Rous, B.,

Sahm, F., Sarkar, C., Solomon, D. A., Tabori, U., van den Bent, M. J., von Deimling, A., Weller, M., White, V. A., & Ellison, D. W. (2020). cIMPACT-NOW update 6: new entity and diagnostic principle recommendations of the cIMPACT-Utrecht meeting on future CNS tumor classification and grading. *Brain Pathol*, *30*(4), 844-856. https://doi.org/10.1111/bpa.12832

Louis, D. N., Wesseling, P., Paulus, W., Giannini, C., Batchelor, T. T., Cairncross, J. G., Capper, D., Figarella-Branger, D., Lopes, M. B., Wick, W., & van den Bent, M. (2018). cIMPACT-NOW update 1: Not Otherwise Specified (NOS) and Not Elsewhere Classified (NEC). *Acta Neuropathol*, *135*(3), 481-484. https://doi.org/10.1007/s00401-018-1808-0

Lovett, M. L., Nieland, T. J. F., Dingle, Y. L., & Kaplan, D. L. (2020). Innovations in 3-Dimensional Tissue Models of Human Brain Physiology and Diseases. *Adv Funct Mater*, *30*(44). https://doi.org/10.1002/adfm.201909146

Ma, X., Liu, Y., Liu, Y., Alexandrov, L. B., Edmonson, M. N., Gawad, C., Zhou, X., Li, Y., Rusch, M. C., Easton, J., Huether, R., Gonzalez-Pena, V., Wilkinson, M. R., Hermida, L. C., Davis, S., Sioson, E., Pounds, S., Cao, X., Ries, R. E., Wang, Z., Chen, X., Dong, L., Diskin, S. J., Smith, M. A., Guidry Auvil, J. M., Meltzer, P. S., Lau, C. C., Perlman, E. J., Maris, J. M., Meshinchi, S., Hunger, S. P., Gerhard, D. S., & Zhang, J. (2018). Pan-cancer genome and transcriptome analyses of 1,699 paediatric leukaemias and solid tumours. *Nature*, *555*(7696), 371-376. https://doi.org/10.1038/nature25795

Maass, K. K., Roosen, M. M., Mueller, T., Senfter, D., Benzel, J., Wedig, T., Kalxsdorf, M., Krijgsveld, J., Pfister, S. M., & Pajtler, K. W. (2022). EPEN-28. Oncogenic dependency of pediatric ependymomas on extracellular vesicle pathways. *Neuro-Oncology*, *24*(Supplement_1), i45-i45. https://doi.org/10.1093/neuonc/noac079.164

Mack, S. C., Pajtler, K. W., Chavez, L., Okonechnikov, K., Bertrand, K. C., Wang, X., Erkek, S., Federation, A., Song, A., Lee, C., Wang, X., McDonald, L., Morrow, J. J., Saiakhova, A., Sin-Chan, P., Wu, Q., Michaelraj, K. A., Miller, T. E., Hubert, C. G., Ryzhova, M., Garzia, L., Donovan, L., Dombrowski, S., Factor, D. C., Luu, B., Valentim, C. L. L., Gimple, R. C., Morton, A., Kim, L., Prager, B. C., Lee, J. J. Y., Wu, X., Zuccaro, J., Thompson, Y., Holgado, B. L., Reimand, J., Ke, S. Q., Tropper, A., Lai, S., Vijayarajah, S., Doan, S., Mahadev, V., Minan, A. F., Grobner, S. N., Lienhard, M., Zapatka, M., Huang, Z., Aldape, K. D., Carcaboso, A. M., Houghton, P. J., Keir, S. T., Milde, T., Witt, H., Li, Y., Li, C. J., Bian, X. W., Jones, D. T. W., Scott, I., Singh, S. K., Huang, A., Dirks, P. B., Bouffet, E., Bradner, J. E., Ramaswamy, V., Jabado, N., Rutka, J. T., Northcott, P. A., Lupien, M., Lichter, P., Korshunov, A., Scacheri, P. C., Pfister, S. M., Kool, M., Taylor, M. D., & Rich, J. N. (2018). Therapeutic targeting of ependymoma as informed by oncogenic enhancer profiling. *Nature*, *553*(7686), 101-105. https://doi.org/10.1038/nature25169

Mack, S. C., Witt, H., Piro, R. M., Gu, L., Zuyderduyn, S., Stütz, A. M., Wang, X., Gallo, M., Garzia, L., Zayne, K., Zhang, X., Ramaswamy, V., Jäger, N., Jones, D. T., Sill, M., Pugh, T. J., Ryzhova, M., Wani, K. M., Shih, D. J., Head, R., Remke, M., Bailey, S. D., Zichner, T., Faria, C. C., Barszczyk, M., Stark, S., Seker-Cin, H., Hutter, S., Johann, P., Bender, S., Hovestadt, V., Tzaridis, T., Dubuc, A. M., Northcott, P. A., Peacock, J., Bertrand, K. C., Agnihotri, S., Cavalli, F. M., Clarke, I., Nethery-Brokx, K., Creasy, C. L., Verma, S. K., Koster, J., Wu, X., Yao, Y., Milde, T., Sin-Chan, P., Zuccaro, J., Lau, L., Pereira, S., Castelo-Branco, P., Hirst, M., Marra, M. A., Roberts, S. S., Fults, D., Massimi, L., Cho, Y. J., Van Meter, T., Grajkowska, W., Lach, B., Kulozik, A. E., von Deimling, A., Witt, O., Scherer, S. W., Fan, X., Muraszko, K. M., Kool, M., Pomeroy, S. L., Gupta, N., Phillips, J., Huang, A., Tabori, U., Hawkins, C., Malkin, D., Kongkham, P. N., Weiss, W. A., Jabado, N., Rutka, J. T., Bouffet, E., Korbel, J. O., Lupien, M., Aldape, K. D., Bader, G. D., Eils, R., Lichter, P., Dirks, P. B., Pfister, S. M., Korshunov, A., & Taylor, M. D. (2014). Epigenomic alterations define lethal CIMP-positive ependymomas of infancy. *Nature*, *506*(7489), 445-450. https://doi.org/10.1038/nature13108

Magnon, C., Lucas, D., & Frenette, P. S. (2011). Trafficking of Stem Cells. In M.-D. Filippi & H. Geiger (Eds.), *Stem Cell Migration: Methods and Protocols* (pp. 3-24). Humana Press. https://doi.org/10.1007/978-1-61779-145-1_1

Maia, J., Caja, S., Strano Moraes, M. C., Couto, N., & Costa-Silva, B. (2018). Exosome-Based Cell-Cell Communication in the Tumor Microenvironment. *Front Cell Dev Biol*, *6*, 18. https://doi.org/10.3389/fcell.2018.00018

Mak, I. W., Evaniew, N., & Ghert, M. (2014). Lost in translation: animal models and clinical trials in cancer treatment. *Am J Transl Res*, *6*(2), 114-118.

Malgulwar, P. B., Nambirajan, A., Pathak, P., Faruq, M., Rajeshwari, M., Singh, M., Suri, V., Sarkar, C., & Sharma, M. C. (2018). C11orf95-RELA fusions and upregulated NF-KB signalling characterise a subset of aggressive supratentorial ependymomas that express L1CAM and nestin. *J Neurooncol*, *138*(1), 29-39. https://doi.org/10.1007/s11060-018-2767-y

Mariani, M. R., Carpaneto, E. M., Ulivi, M., Allfrey, V. G., & Boffa, L. C. (2003). Correlation between butyrate-induced histone hyperacetylation turn-over and c-myc expression. *The Journal of Steroid*

Biochemistry and Molecular Biology, *86*(2), 167-171. https://doi.org/https://doi.org/10.1016/S0960-0760(03)00267-X

Marinoff, A. E., Ma, C., Guo, D., Snuderl, M., Wright, K. D., Manley, P. E., Al-Sayegh, H., Sinai, C. E., Ullrich, N. J., Marcus, K., Haas-Kogan, D., Goumnerova, L., London, W. B., Kieran, M. W., Chi, S. N., Fangusaro, J., & Bandopadhayay, P. (2017). Rethinking childhood ependymoma: a retrospective, multi-center analysis reveals poor long-term overall survival. *J Neurooncol*, *135*(1), 201-211. https://doi.org/10.1007/s11060-017-2568-8

Mattern, J., Bak, M., Hahn, E. W., & Volm, M. (1988). Human tumor xenografts as model for drug testing. *Cancer Metastasis Rev*, *7*(3), 263-284. https://doi.org/10.1007/bf00047755

McCleary-Wheeler, A. L. (2014). From Normal Development to Disease: The Biochemistry and Regulation of GLI2. *Medical Epigenetics*, *2*(1), 1-19. https://doi.org/10.1159/000358364

McDonald, D., Wu, Y., Dailamy, A., Tat, J., Parekh, U., Zhao, D., Hu, M., Tipps, A., Zhang, K., & Mali, P. (2020). Defining the Teratoma as a Model for Multi-lineage Human Development. *Cell*, *183*(5), 1402-1419.e1418. https://doi.org/10.1016/j.cell.2020.10.018

McKenna, A., Findlay, G. M., Gagnon, J. A., Horwitz, M. S., Schier, A. F., & Shendure, J. (2016). Whole-organism lineage tracing by combinatorial and cumulative genome editing. *Science*, *353*(6298), aaf7907. https://doi.org/10.1126/science.aaf7907

McPherson, A., Hormozdiari, F., Zayed, A., Giuliany, R., Ha, G., Sun, M. G., Griffith, M., Heravi Moussavi, A., Senz, J., Melnyk, N., Pacheco, M., Marra, M. A., Hirst, M., Nielsen, T. O., Sahinalp, S. C., Huntsman, D., & Shah, S. P. (2011). deFuse: an algorithm for gene fusion discovery in tumor RNA-Seq data. *PLoS Comput Biol*, *7*(5), e1001138. https://doi.org/10.1371/journal.pcbi.1001138

Merchant, T. E., Li, C., Xiong, X., Kun, L. E., Boop, F. A., & Sanford, R. A. (2009). Conformal radiotherapy after surgery for paediatric ependymoma: a prospective study. *Lancet Oncol*, *10*(3), 258-266. https://doi.org/10.1016/s1470-2045(08)70342-5

Messahel, B., Ashley, S., Saran, F., Ellison, D., Ironside, J., Phipps, K., Cox, T., Chong, W. K., Robinson, K., Picton, S., Pinkerton, C. R., Mallucci, C., Macarthur, D., Jaspan, T., Michalski, A., & Grundy, R. G. (2009). Relapsed intracranial ependymoma in children in the UK: Patterns of relapse, survival and therapeutic outcome. *European Journal of Cancer*, *45*(10), 1815-1823. https://doi.org/10.1016/j.ejca.2009.03.018

Meyer, G. (2007). Genetic control of neuronal migrations in human cortical development. *Adv Anat Embryol Cell Biol*, *189*, 1 p preceding 1, 1-111.

Miao, H., Li, D. Q., Mukherjee, A., Guo, H., Petty, A., Cutter, J., Basilion, J. P., Sedor, J., Wu, J., Danielpour, D., Sloan, A. E., Cohen, M. L., & Wang, B. (2009). EphA2 mediates ligand-dependent inhibition and ligand-independent promotion of cell migration and invasion via a reciprocal regulatory loop with Akt. *Cancer Cell*, *16*(1), 9-20. https://doi.org/10.1016/j.ccr.2009.04.009

Milde, T., Kleber, S., Korshunov, A., Witt, H., Hielscher, T., Koch, P., Kopp, H.-G., Jugold, M., Deubzer, H. E., Oehme, I., Lodrini, M., Gröne, H.-J., Benner, A., Brüstle, O., Gilbertson, R. J., von Deimling, A., Kulozik, A. E., Pfister, S. M., Martin-Villalba, A., & Witt, O. (2011). A novel human high-risk ependymoma stem cell model reveals the differentiation-inducing potential of the histone deacetylase inhibitor Vorinostat. *Acta Neuropathologica*, *122*(5), 637. https://doi.org/10.1007/s00401-011-0866-3

Miller, J. A., Horvath, S., & Geschwind, D. H. (2010). Divergence of human and mouse brain transcriptome highlights Alzheimer disease pathways. *Proc Natl Acad Sci U S A*, *107*(28), 12698-12703. https://doi.org/10.1073/pnas.0914257107

Minas, T. Z., Surdez, D., Javaheri, T., Tanaka, M., Howarth, M., Kang, H. J., Han, J., Han, Z. Y., Sax, B., Kream, B. E., Hong, S. H., Çelik, H., Tirode, F., Tuckermann, J., Toretsky, J. A., Kenner, L., Kovar, H., Lee, S., Sweet-Cordero, E. A., Nakamura, T., Moriggl, R., Delattre, O., & Üren, A. (2017). Combined experience of six independent laboratories attempting to create an Ewing sarcoma mouse model. *Oncotarget*, *8*(21), 34141-34163. https://doi.org/10.18632/oncotarget.9388

Mitsui, K., Tokuzawa, Y., Itoh, H., Segawa, K., Murakami, M., Takahashi, K., Maruyama, M., Maeda, M., & Yamanaka, S. (2003). The homeoprotein Nanog is required for maintenance of pluripotency in mouse epiblast and ES cells. *Cell*, *113*(5), 631-642. https://doi.org/10.1016/s0092-8674(03)00393-3

Mizutani, K., & Saito, T. (2005). Progenitors resume generating neurons after temporary inhibition of neurogenesis by Notch activation in the mammalian cerebral cortex. *Development*, *132*(6), 1295-1304. https://doi.org/10.1242/dev.01693

Monaco, G., van Dam, S., Casal Novo Ribeiro, J. L., Larbi, A., & de Magalhães, J. P. (2015). A comparison of human and mouse gene co-expression networks reveals conservation and divergence at the tissue, pathway and disease levels. *BMC Evol Biol*, *15*, 259. https://doi.org/10.1186/s12862-015-0534-7

Monzel, A. S., Smits, L. M., Hemmer, K., Hachi, S., Moreno, E. L., van Wuellen, T., Jarazo, J., Walter, J., Brüggemann, I., Boussaad, I., Berger, E., Fleming, R. M. T., Bolognin, S., & Schwamborn, J. C. (2017). Derivation of Human Midbrain-Specific Organoids from Neuroepithelial Stem Cells. *Stem Cell Reports*, *8*(5), 1144-1154. https://doi.org/10.1016/j.stemcr.2017.03.010

Moran, S., Martínez-Cardús, A., Sayols, S., Musulén, E., Balañá, C., Estival-Gonzalez, A., Moutinho, C., Heyn, H., Diaz-Lagares, A., de Moura, M. C., Stella, G. M., Comoglio, P. M., Ruiz-Miró, M., Matias-Guiu, X., Pazo-Cid, R., Antón, A., Lopez-Lopez, R., Soler, G., Longo, F., Guerra, I., Fernandez, S., Assenov, Y., Plass, C., Morales, R., Carles, J., Bowtell, D., Mileshkin, L., Sia, D., Tothill, R., Tabernero, J., Llovet, J. M., & Esteller, M. (2016). Epigenetic profiling to classify cancer of unknown primary: a multicentre, retrospective analysis. *Lancet Oncol*, *17*(10), 1386-1395. https://doi.org/10.1016/s1470-2045(16)30297-2

Moran, S., Vizoso, M., Martinez-Cardús, A., Gomez, A., Matías-Guiu, X., Chiavenna, S. M., Fernandez, A. G., & Esteller, M. (2014). Validation of DNA methylation profiling in formalin-fixed paraffin-embedded samples using the Infinium HumanMethylation450 Microarray. *Epigenetics*, *9*(6), 829-833. https://doi.org/10.4161/epi.28790

Morfouace, M., Nimmervoll, B., Boulos, N., Patel, Y. T., Shelat, A., Freeman, B. B., 3rd, Robinson, G. W., Wright, K., Gajjar, A., Stewart, C. F., Gilbertson, R. J., & Roussel, M. F. (2016). Preclinical studies of 5-fluoro-2'-deoxycytidine and tetrahydrouridine in pediatric brain tumors. *J Neurooncol*, *126*(2), 225-234. https://doi.org/10.1007/s11060-015-1965-0

Morshead, C. M., Reynolds, B. A., Craig, C. G., McBurney, M. W., Staines, W. A., Morassutti, D., Weiss, S., & van der Kooy, D. (1994). Neural stem cells in the adult mammalian forebrain: a relatively quiescent subpopulation of subependymal cells. *Neuron*, *13*(5), 1071-1082. https://doi.org/10.1016/0896-6273(94)90046-9

Mortazavi, A., Williams, B. A., McCue, K., Schaeffer, L., & Wold, B. (2008). Mapping and quantifying mammalian transcriptomes by RNA-Seq. *Nat Methods*, *5*(7), 621-628. https://doi.org/10.1038/nmeth.1226

Mou, H., Kennedy, Z., Anderson, D. G., Yin, H., & Xue, W. (2015). Precision cancer mouse models through genome editing with CRISPR-Cas9. *Genome Med*, *7*(1), 53. https://doi.org/10.1186/s13073-015-0178-7

Muguruma, K., Nishiyama, A., Kawakami, H., Hashimoto, K., & Sasai, Y. (2015). Self-organization of polarized cerebellar tissue in 3D culture of human pluripotent stem cells. *Cell Rep*, *10*(4), 537-550. https://doi.org/10.1016/j.celrep.2014.12.051

Muguruma, K., Nishiyama, A., Ono, Y., Miyawaki, H., Mizuhara, E., Hori, S., Kakizuka, A., Obata, K., Yanagawa, Y., Hirano, T., & Sasai, Y. (2010). Ontogeny-recapitulating generation and tissue integration of ES cell-derived Purkinje cells. *Nat Neurosci*, *13*(10), 1171-1180. https://doi.org/10.1038/nn.2638

Mullard, A. (2016). Parsing clinical success rates. *Nature Reviews Drug Discovery*, *15*(7), 447-447. https://doi.org/10.1038/nrd.2016.136

Nabet, B., Roberts, J. M., Buckley, D. L., Paulk, J., Dastjerdi, S., Yang, A., Leggett, A. L., Erb, M. A., Lawlor, M. A., Souza, A., Scott, T. G., Vittori, S., Perry, J. A., Qi, J., Winter, G. E., Wong, K. K., Gray, N. S., & Bradner, J. E. (2018). The dTAG system for immediate and target-specific protein degradation. *Nat Chem Biol*, *14*(5), 431-441. https://doi.org/10.1038/s41589-018-0021-8

Neely, J. E., Ballard, E. T., Britt, A. L., & Workman, L. (1983). Characteristics of 85 Pediatric Tumors Heterotransplanted into Nude Mice. *Pathobiology*, *51*(4), 217-227. https://doi.org/10.1159/000163194

Neumann, J. E., Swartling, F. J., & Schüller, U. (2017). Medulloblastoma: experimental models and reality. *Acta Neuropathol*, *134*(5), 679-689. https://doi.org/10.1007/s00401-017-1753-3

Neumann, J. E., Wefers, A. K., Lambo, S., Bianchi, E., Bockstaller, M., Dorostkar, M. M., Meister, V., Schindler, P., Korshunov, A., von Hoff, K., Nowak, J., Warmuth-Metz, M., Schneider, M. R., Renner-Muller, I., Merk, D. J., Shakarami, M., Sharma, T., Chavez, L., Glass, R., Chan, J. A., Taketo, M. M., Neumann, P., Kool, M., & Schuller, U. (2017). A mouse model for embryonal tumors with multilayered rosettes uncovers the therapeutic potential of Sonic-hedgehog inhibitors. *Nat Med*, *23*(10), 1191-1202. https://doi.org/10.1038/nm.4402

Ng, H. H., & Surani, M. A. (2011). The transcriptional and signalling networks of pluripotency. *Nat Cell Biol*, *13*(5), 490-496. https://doi.org/10.1038/ncb0511-490

Ni, J., Clark, K. J., Fahrenkrug, S. C., & Ekker, S. C. (2008). Transposon tools hopping in vertebrates. *Brief Funct Genomic Proteomic*, *7*(6), 444-453. https://doi.org/10.1093/bfgp/eln049

Niclou, S. P., Danzeisen, C., Eikesdal, H. P., Wiig, H., Brons, N. H., Poli, A. M., Svendsen, A., Torsvik, A., Enger, P., Terzis, J. A., & Bjerkvig, R. (2008). A novel eGFP-expressing immunodeficient mouse model to study tumor-host interactions. *Faseb j*, *22*(9), 3120-3128. https://doi.org/10.1096/fj.08-109611

Noblitt, L. W., Bangari, D. S., Shukla, S., Knapp, D. W., Mohammed, S., Kinch, M. S., & Mittal, S. K. (2004). Decreased tumorigenic potential of EphA2-overexpressing breast cancer cells following treatment with adenoviral vectors that express EphrinA1. *Cancer Gene Ther*, *11*(11), 757-766. https://doi.org/10.1038/sj.cgt.7700761

Noren, N. K., Foos, G., Hauser, C. A., & Pasquale, E. B. (2006). The EphB4 receptor suppresses breast cancer cell tumorigenicity through an Abl-Crk pathway. *Nat Cell Biol*, *8*(8), 815-825. https://doi.org/10.1038/ncb1438

Norrman, K., Fischer, Y., Bonnamy, B., Wolfhagen Sand, F., Ravassard, P., & Semb, H. (2010). Quantitative Comparison of Constitutive Promoters in Human ES cells. *PLoS One*, *5*(8), e12413. https://doi.org/10.1371/journal.pone.0012413

O'Brien, C. A., Pollett, A., Gallinger, S., & Dick, J. E. (2007). A human colon cancer cell capable of initiating tumour growth in immunodeficient mice. *Nature*, *445*(7123), 106-110. https://doi.org/10.1038/nature05372

Ogawa, J., Pao, G. M., Shokhirev, M. N., & Verma, I. M. (2018). Glioblastoma Model Using Human Cerebral Organoids. *Cell Rep*, *23*(4), 1220-1229. https://doi.org/10.1016/j.celrep.2018.03.105

Okonechnikov, K., Imai-Matsushima, A., Paul, L., Seitz, A., Meyer, T. F., & Garcia-Alcalde, F. (2016). InFusion: advancing discovery of fusion genes and chimeric transcripts from deep RNA-sequencing data. *PLoS One*, *11*(12), e0167417.

Orsulic, S. (2002). An RCAS-TVA-based approach to designer mouse models. *Mamm Genome*, *13*(10), 543-547. https://doi.org/10.1007/s00335-002-4003-4

Ostrom, Q. T., Cioffi, G., Waite, K., Kruchko, C., & Barnholtz-Sloan, J. S. (2021). CBTRUS Statistical Report: Primary Brain and Other Central Nervous System Tumors Diagnosed in the United States in 2014-2018. *Neuro Oncol*, *23*(12 Suppl 2), iii1-iii105. https://doi.org/10.1093/neuonc/noab200

Ostrom, Q. T., de Blank, P. M., Kruchko, C., Petersen, C. M., Liao, P., Finlay, J. L., Stearns, D. S., Wolff, J. E., Wolinsky, Y., Letterio, J. J., & Barnholtz-Sloan, J. S. (2015). Alex's Lemonade Stand Foundation Infant and Childhood Primary Brain and Central Nervous System Tumors Diagnosed in the United States in 2007-2011. *Neuro Oncol*, *16 Suppl 10*(Suppl 10), x1-x36. https://doi.org/10.1093/neuonc/nou327

Ostrom, Q. T., Price, M., Neff, C., Cioffi, G., Waite, K. A., Kruchko, C., & Barnholtz-Sloan, J. S. (2022). CBTRUS Statistical Report: Primary Brain and Other Central Nervous System Tumors Diagnosed in the United States in 2015-2019. *Neuro Oncol*, *24*(Suppl 5), v1-v95. https://doi.org/10.1093/neuonc/noac202

Ozawa, T., Arora, S., Szulzewsky, F., Juric-Sekhar, G., Miyajima, Y., Bolouri, H., Yasui, Y., Barber, J., Kupp, R., Dalton, J., Jones, T. S., Nakada, M., Kumabe, T., Ellison, D. W., Gilbertson, R. J., & Holland, E. C. (2018). A De Novo Mouse Model of C11orf95-RELA Fusion-Driven Ependymoma Identifies Driver Functions in Addition to NF-kappaB. *Cell Rep*, *23*(13), 3787-3797. https://doi.org/10.1016/j.celrep.2018.04.099

Pajtler, K. W., Wei, Y., Okonechnikov, K., Silva, P. B. G., Vouri, M., Zhang, L., Brabetz, S., Sieber, L., Gulley, M., Mauermann, M., Wedig, T., Mack, N., Imamura Kawasawa, Y., Sharma, T., Zuckermann, M., Andreiuolo, F., Holland, E., Maass, K., Korkel-Qu, H., Liu, H. K., Sahm, F., Capper, D., Bunt, J., Richards, L. J., Jones, D. T. W., Korshunov, A., Chavez, L., Lichter, P., Hoshino, M., Pfister, S. M., Kool, M., Li, W., & Kawauchi, D. (2019). YAP1 subgroup supratentorial ependymoma requires TEAD and nuclear factor I-mediated transcriptional programmes for tumorigenesis. *Nat Commun*, *10*(1), 3914. https://doi.org/10.1038/s41467-019-11884-5

Pajtler, K. W., Witt, H., Sill, M., Jones, D. T., Hovestadt, V., Kratochwil, F., Wani, K., Tatevossian, R., Punchihewa, C., Johann, P., Reimand, J., Warnatz, H. J., Ryzhova, M., Mack, S., Ramaswamy, V., Capper, D., Schweizer, L., Sieber, L., Wittmann, A., Huang, Z., van Sluis, P., Volckmann, R., Koster, J., Versteeg, R., Fults, D., Toledano, H., Avigad, S., Hoffman, L. M., Donson, A. M., Foreman, N., Hewer, E., Zitterbart, K., Gilbert, M., Armstrong, T. S., Gupta, N., Allen, J. C., Karajannis, M. A., Zagzag, D., Hasselblatt, M., Kulozik, A. E., Witt, O., Collins, V. P., von Hoff, K., Rutkowski, S., Pietsch, T., Bader, G., Yaspo, M. L., von Deimling, A., Lichter, P., Taylor, M. D., Gilbertson, R., Ellison, D. W., Aldape, K., Korshunov, A., Kool, M., & Pfister, S. M. (2015). Molecular Classification of Ependymal Tumors across All CNS Compartments, Histopathological Grades, and Age Groups. *Cancer Cell*, *27*(5), 728-743. https://doi.org/10.1016/j.ccell.2015.04.002

Palm, T., Bolognin, S., Meiser, J., Nickels, S., Träger, C., Meilenbrock, R.-L., Brockhaus, J., Schreitmüller, M., Missler, M., & Schwamborn, J. C. (2015). Rapid and robust generation of long-term self-renewing human neural stem cells with the ability to generate mature astroglia. *Scientific Reports*, *5*(1), 16321. https://doi.org/10.1038/srep16321

Pardridge, W. M. (2002). William Pardridge discusses the lack of BBB research. Interview by Rebecca N. Lawrence. *Drug Discov Today*, *7*(4), 223-226. https://doi.org/10.1016/s1359-6446(02)02195-5

Parker, M., Mohankumar, K. M., Punchihewa, C., Weinlich, R., Dalton, J. D., Li, Y., Lee, R., Tatevossian, R. G., Phoenix, T. N., Thiruvenkatam, R., White, E., Tang, B., Orisme, W., Gupta, K., Rusch, M., Chen, X., Li, Y., Nagahawhatte, P., Hedlund, E., Finkelstein, D., Wu, G., Shurtleff, S., Easton, J., Boggs, K., Yergeau, D., Vadodaria, B., Mulder, H. L., Becksfort, J., Gupta, P., Huether, R., Ma, J., Song, G., Gajjar, A., Merchant, T., Boop, F., Smith, A. A., Ding, L., Lu, C., Ochoa, K., Zhao, D., Fulton, R. S., Fulton, L. L., Mardis, E. R., Wilson, R. K., Downing, J. R., Green, D. R., Zhang, J., Ellison, D. W., & Gilbertson, R. J. (2014). C11orf95-RELA fusions drive oncogenic NF-kappaB signalling in ependymoma. *Nature*, *506*(7489), 451-455. https://doi.org/10.1038/nature13109

Patel, N., Black, J., Chen, X., Marcondes, A. M., Grady, W. M., Lawlor, E. R., & Borinstein, S. C. (2012). DNA methylation and gene expression profiling of ewing sarcoma primary tumors reveal genes that are potential targets of epigenetic inactivation. *Sarcoma*, *2012*, 498472. https://doi.org/10.1155/2012/498472

Pei, W., Wang, X., Rössler, J., Feyerabend, T. B., Höfer, T., & Rodewald, H.-R. (2019). Using Cre-recombinase-driven Polylox barcoding for in vivo fate mapping in mice. *Nature Protocols*, *14*(6), 1820-1840. https://doi.org/10.1038/s41596-019-0163-5

Perrin, S. (2014). Preclinical research: Make mouse studies work. *Nature*, *507*(7493), 423-425. https://doi.org/10.1038/507423a

Pfister, S. M., Reyes-Múgica, M., Chan, J. K. C., Hasle, H., Lazar, A. J., Rossi, S., Ferrari, A., Jarzembowski, J. A., Pritchard-Jones, K., Hill, D. A., Jacques, T. S., Wesseling, P., López Terrada, D. H., von Deimling, A., Kratz, C. P., Cree, I. A., & Alaggio, R. (2022). A Summary of the Inaugural WHO Classification of Pediatric Tumors: Transitioning from the Optical into the Molecular Era. *Cancer Discovery*, *12*(2), 331-355. https://doi.org/10.1158/2159-8290.Cd-21-1094

Pietsch, T., Scharmann, T., Fonatsch, C., Schmidt, D., Ockler, R., Freihoff, D., Albrecht, S., Wiestler, O. D., Zeltzer, P., & Riehm, H. (1994). Characterization of five new cell lines derived from human primitive neuroectodermal tumors of the central nervous system. *Cancer Res*, *54*(12), 3278-3287.

Pollack, I. F., Agnihotri, S., & Broniscer, A. (2019). Childhood brain tumors: current management, biological insights, and future directions: JNSPG 75th Anniversary Invited Review Article. *Journal of Neurosurgery: Pediatrics PED*, *23*(3), 261-273. https://doi.org/10.3171/2018.10.Peds18377

Polli, J. E. (2008). In vitro studies are sometimes better than conventional human pharmacokinetic in vivo studies in assessing bioequivalence of immediate-release solid oral dosage forms. *Aaps j*, *10*(2), 289-299. https://doi.org/10.1208/s12248-008-9027-6

Qian, X., Nguyen, H. N., Song, M. M., Hadiono, C., Ogden, S. C., Hammack, C., Yao, B., Hamersky, G. R., Jacob, F., Zhong, C., Yoon, K. J., Jeang, W., Lin, L., Li, Y., Thakor, J., Berg, D. A., Zhang, C., Kang, E., Chickering, M., Nauen, D., Ho, C. Y., Wen, Z., Christian, K. M., Shi, P. Y., Maher, B. J., Wu, H., Jin, P., Tang, H., Song, H., & Ming, G. L. (2016). Brain-Region-Specific Organoids Using Mini-bioreactors for Modeling ZIKV Exposure. *Cell*, *165*(5), 1238-1254. https://doi.org/10.1016/j.cell.2016.04.032

Quail, D. F., & Joyce, J. A. (2013). Microenvironmental regulation of tumor progression and metastasis. *Nat Med*, *19*(11), 1423-1437. https://doi.org/10.1038/nm.3394

Quail, D. F., & Joyce, J. A. (2017). The Microenvironmental Landscape of Brain Tumors. *Cancer Cell*, *31*(3), 326-341. https://doi.org/10.1016/j.ccell.2017.02.009

Ramírez, F., Ryan, D. P., Grüning, B., Bhardwaj, V., Kilpert, F., Richter, A. S., Heyne, S., Dündar, F., & Manke, T. (2016). deepTools2: a next generation web server for deep-sequencing data analysis. *Nucleic Acids Research*, *44*(W1), W160-W165. https://doi.org/10.1093/nar/gkw257

Redon, R., Ishikawa, S., Fitch, K. R., Feuk, L., Perry, G. H., Andrews, T. D., Fiegler, H., Shapero, M. H., Carson, A. R., Chen, W., Cho, E. K., Dallaire, S., Freeman, J. L., González, J. R., Gratacòs, M., Huang, J., Kalaitzopoulos, D., Komura, D., MacDonald, J. R., Marshall, C. R., Mei, R., Montgomery, L., Nishimura, K., Okamura, K., Shen, F., Somerville, M. J., Tchinda, J., Valsesia, A., Woodwark, C., Yang, F., Zhang, J., Zerjal, T., Zhang, J., Armengol, L., Conrad, D. F., Estivill, X., Tyler-Smith, C., Carter, N. P., Aburatani, H., Lee, C., Jones, K. W., Scherer, S. W., & Hurles, M. E. (2006). Global variation in copy number in the human genome. *Nature*, *444*(7118), 444-454. https://doi.org/10.1038/nature05329

Redzic, J. S., Ung, T. H., & Graner, M. W. (2014). Glioblastoma extracellular vesicles: reservoirs of potential biomarkers. *Pharmgenomics Pers Med*, *7*, 65-77. https://doi.org/10.2147/pgpm.S39768

Reuss, D. E., Kratz, A., Sahm, F., Capper, D., Schrimpf, D., Koelsche, C., Hovestadt, V., Bewerunge-Hudler, M., Jones, D. T., Schittenhelm, J., Mittelbronn, M., Rushing, E., Simon, M., Westphal, M., Unterberg, A., Platten, M., Paulus, W., Reifenberger, G., Tonn, J. C., Aldape, K., Pfister, S. M., Korshunov, A., Weller, M., Herold-Mende, C., Wick, W., Brandner, S., & von Deimling, A. (2015). Adult IDH wild type astrocytomas biologically and clinically resolve into other tumor entities. *Acta Neuropathol*, *130*(3), 407-417. https://doi.org/10.1007/s00401-015-1454-8

Reynolds, B. A., & Weiss, S. (1992). Generation of neurons and astrocytes from isolated cells of the adult mammalian central nervous system. *Science*, *255*(5052), 1707-1710. https://doi.org/10.1126/science.1553558

Riggi, N., Knoechel, B., Gillespie, S. M., Rheinbay, E., Boulay, G., Suva, M. L., Rossetti, N. E., Boonseng, W. E., Oksuz, O., Cook, E. B., Formey, A., Patel, A., Gymrek, M., Thapar, V., Deshpande, V., Ting, D. T., Hornicek, F. J., Nielsen, G. P., Stamenkovic, I., Aryee, M. J., Bernstein, B. E., & Rivera, M. N. (2014). EWS-FLI1 utilizes divergent chromatin remodeling mechanisms to directly activate or repress enhancer elements in Ewing sarcoma. *Cancer Cell*, *26*(5), 668-681. https://doi.org/10.1016/j.ccell.2014.10.004

Ritchie, M. E., Phipson, B., Wu, D., Hu, Y., Law, C. W., Shi, W., & Smyth, G. K. (2015). limma powers differential expression analyses for RNA-sequencing and microarray studies. *Nucleic Acids Research*, *43*(7), e47-e47. https://doi.org/10.1093/nar/gkv007

Robertson, F. L., Marqués-Torrejón, M. A., Morrison, G. M., & Pollard, S. M. (2019). Experimental models and tools to tackle glioblastoma. *Dis Model Mech*, *12*(9). https://doi.org/10.1242/dmm.040386

Roosen, M., Odé, Z., Bunt, J., & Kool, M. (2022). The oncogenic fusion landscape in pediatric CNS neoplasms. *Acta Neuropathologica*, *143*(4), 427-451. https://doi.org/10.1007/s00401-022-02405-8

Rowley, J. D. (1973). Letter: A new consistent chromosomal abnormality in chronic myelogenous leukaemia identified by quinacrine fluorescence and Giemsa staining. *Nature*, *243*(5405), 290-293. https://doi.org/10.1038/243290a0

Rubinstein, L. V., Shoemaker, R. H., Paull, K. D., Simon, R. M., Tosini, S., Skehan, P., Scudiero, D. A., Monks, A., & Boyd, M. R. (1990). Comparison of in vitro anticancer-drug-screening data generated with a tetrazolium assay versus a protein assay against a diverse panel of human tumor cell lines. *J Natl Cancer Inst*, *82*(13), 1113-1118. https://doi.org/10.1093/jnci/82.13.1113

Saba, R., Johnson, J. E., & Saito, T. (2005). Commissural neuron identity is specified by a homeodomain protein, Mbh1, that is directly downstream of Math1. *Development*, *132*(9), 2147-2155. https://doi.org/10.1242/dev.01781

Saba, R., Nakatsuji, N., & Saito, T. (2003). Mammalian BarH1 confers commissural neuron identity on dorsal cells in the spinal cord. *J Neurosci*, *23*(6), 1987-1991. https://doi.org/10.1523/jneurosci.23-06-01987.2003

Saito, T. (2006). In vivo electroporation in the embryonic mouse central nervous system. *Nat Protoc*, *1*(3), 1552-1558. https://doi.org/10.1038/nprot.2006.276

Saito, T. (2010). Embryonic in vivo electroporation in the mouse. *Methods Enzymol*, *477*, 37-50. https://doi.org/10.1016/s0076-6879(10)77003-8

Saito, T. (2015). *Electroporation Methods in Neuroscience*. Humana New York, NY

.

Saito, T., & Nakatsuji, N. (2001). Efficient gene transfer into the embryonic mouse brain using in vivo electroporation. *Dev Biol*, *240*(1), 237-246. https://doi.org/10.1006/dbio.2001.0439

Sakaguchi, H., Kadoshima, T., Soen, M., Narii, N., Ishida, Y., Ohgushi, M., Takahashi, J., Eiraku, M., & Sasai, Y. (2015). Generation of functional hippocampal neurons from self-organizing human embryonic stem cell-derived dorsomedial telencephalic tissue. *Nature Communications*, *6*(1), 8896. https://doi.org/10.1038/ncomms9896

Sandén, E. (2016). Experimental models of pediatric brain tumors. Establishment, immunophenotyping and clinical implications. Lund University].

Sandoval-Villegas, N., Nurieva, W., Amberger, M., & Ivics, Z. (2021). Contemporary Transposon Tools: A Review and Guide through Mechanisms and Applications of Sleeping Beauty, piggyBac and Tol2 for Genome Engineering. *International Journal of Molecular Sciences*, *22*(10), 5084. https://www.mdpi.com/1422-0067/22/10/5084

Sansom, S. N., Griffiths, D. S., Faedo, A., Kleinjan, D. J., Ruan, Y., Smith, J., van Heyningen, V., Rubenstein, J. L., & Livesey, F. J. (2009). The level of the transcription factor Pax6 is essential for controlling the balance between neural stem cell self-renewal and neurogenesis. *PLoS Genet*, *5*(6), e1000511. https://doi.org/10.1371/journal.pgen.1000511

Sarkaria, J. N., Hu, L. S., Parney, I. F., Pafundi, D. H., Brinkmann, D. H., Laack, N. N., Giannini, C., Burns, T. C., Kizilbash, S. H., Laramy, J. K., Swanson, K. R., Kaufmann, T. J., Brown, P. D., Agar, N. Y. R., Galanis, E., Buckner, J. C., & Elmquist, W. F. (2018). Is the blood-brain barrier really disrupted in all glioblastomas? A critical assessment of existing clinical data. *Neuro Oncol*, *20*(2), 184-191. https://doi.org/10.1093/neuonc/nox175

Sato, T., Muroyama, Y., & Saito, T. (2013). Inducible gene expression in postmitotic neurons by an in vivo electroporation-based tetracycline system. *J Neurosci Methods*, *214*(2), 170-176. https://doi.org/10.1016/j.jneumeth.2013.01.014

Sboner, A., Habegger, L., Pflueger, D., Terry, S., Chen, D. Z., Rozowsky, J. S., Tewari, A. K., Kitabayashi, N., Moss, B. J., Chee, M. S., Demichelis, F., Rubin, M. A., & Gerstein, M. B. (2010). FusionSeq: a modular framework for finding gene fusions by analyzing paired-end RNA-sequencing data. *Genome Biol*, *11*(10), R104. https://doi.org/10.1186/gb-2010-11-10-r104

Schnidar, H., Eberl, M., Klingler, S., Mangelberger, D., Kasper, M., Hauser-Kronberger, C., Regl, G., Kroismayr, R., Moriggl, R., Sibilia, M., & Aberger, F. (2009). Epidermal growth factor receptor signaling synergizes with Hedgehog/GLI in oncogenic transformation via activation of the MEK/ERK/JUN pathway. *Cancer Res*, *69*(4), 1284-1292. https://doi.org/10.1158/0008-5472.Can-08-2331

Schoof, M., Spohn, M., Dorostkar, M., Neyazi, S., Bockmayr, M., Swartling, F., Kawauchi, D., Gilbertson, R., Taylor, J., Pei, Y., Glass, R., Cheng, J., Galarza, N. M., Hench, J., Herms, J., Jurmeister, P., Schweizer, L., Capper, D., Harter, P., Thomas, C., Hasselblatt, M., Blattner-Johnson, M., Jones, D., Frank, S., Kerl, K., & Schüller, U. (2022). PATH-04. Array-based global DNA Methylation profiling of mouse brain tumors allows comparison to human tumors. *Neuro-Oncology*, *24*(Supplement_1), i158-i159. https://doi.org/10.1093/neuonc/noac079.588

Schuller, U., Heine, V. M., Mao, J., Kho, A. T., Dillon, A. K., Han, Y. G., Huillard, E., Sun, T., Ligon, A. H., Qian, Y., Ma, Q., Alvarez-Buylla, A., McMahon, A. P., Rowitch, D. H., & Ligon, K. L. (2008). Acquisition of granule neuron precursor identity is a critical determinant of progenitor cell competence to form Shh-induced medulloblastoma. *Cancer Cell*, *14*(2), 123-134. https://doi.org/10.1016/j.ccr.2008.07.005

Schüller, U., Heine, V. M., Mao, J., Kho, A. T., Dillon, A. K., Han, Y. G., Huillard, E., Sun, T., Ligon, A. H., Qian, Y., Ma, Q., Alvarez-Buylla, A., McMahon, A. P., Rowitch, D. H., & Ligon, K. L. (2008). Acquisition of granule neuron precursor identity is a critical determinant of progenitor cell competence to form Shh-induced medulloblastoma. *Cancer Cell*, *14*(2), 123-134. https://doi.org/10.1016/j.ccr.2008.07.005

Seligman, A. M., Shear, M. J., & Alexander, L. (1939). Studies in Carcinogenesis: VIII. Experimental Production of Brain Tumors in Mice with Methylcholanthrene1. *The American Journal of Cancer*, *37*(3), 364-395. https://doi.org/10.1158/ajc.1939.364

Sengupta, S., Sobo, M., Lee, K., Senthil Kumar, S., White, A. R., Mender, I., Fuller, C., Chow, L. M. L., Fouladi, M., Shay, J. W., & Drissi, R. (2018). Induced Telomere Damage to Treat Telomerase Expressing Therapy-Resistant Pediatric Brain Tumors. *Mol Cancer Ther*, *17*(7), 1504-1514. https://doi.org/10.1158/1535-7163.Mct-17-0792

Servidei, T., Lucchetti, D., Navarra, P., Sgambato, A., Riccardi, R., & Ruggiero, A. (2021). Cell-of-Origin and Genetic, Epigenetic, and Microenvironmental Factors Contribute to the Intra-Tumoral Heterogeneity of Pediatric Intracranial Ependymoma. *Cancers (Basel)*, *13*(23). https://doi.org/10.3390/cancers13236100

Sewing, A. C. P., Lagerweij, T., van Vuurden, D. G., Meel, M. H., Veringa, S. J. E., Carcaboso, A. M., Gaillard, P. J., Peter Vandertop, W., Wesseling, P., Noske, D., Kaspers, G. J. L., & Hulleman, E. (2017). Preclinical evaluation of convection-enhanced delivery of liposomal doxorubicin to treat pediatric diffuse intrinsic pontine glioma and thalamic high-grade glioma. *J Neurosurg Pediatr*, *19*(5), 518-530. https://doi.org/10.3171/2016.9.Peds16152

Shagin, D. A., Barsova, E. V., Yanushevich, Y. G., Fradkov, A. F., Lukyanov, K. A., Labas, Y. A., Semenova, T. N., Ugalde, J. A., Meyers, A., Nunez, J. M., Widder, E. A., Lukyanov, S. A., & Matz, M. V. (2004). GFP-like proteins as ubiquitous metazoan superfamily: evolution of functional features and structural complexity. *Mol Biol Evol*, *21*(5), 841-850. https://doi.org/10.1093/molbev/msh079

Siegel, R. L., Miller, K. D., Fuchs, H. E., & Jemal, A. (2021). Cancer Statistics, 2021. *CA Cancer J Clin*, *71*(1), 7-33. https://doi.org/10.3322/caac.21654

Siegel, R. L., Miller, K. D., & Jemal, A. (2020). Cancer statistics, 2020. *CA: A Cancer Journal for Clinicians*, *70*(1), 7-30. https://doi.org/https://doi.org/10.3322/caac.21590

Sievers, P., Henneken, S. C., Blume, C., Sill, M., Schrimpf, D., Stichel, D., Okonechnikov, K., Reuss, D. E., Benzel, J., Maaß, K. K., Kool, M., Sturm, D., Zheng, T., Ghasemi, D. R., Kohlhof-Meinecke, P., Cruz, O., Suñol, M., Lavarino, C., Ruf, V., Boldt, H. B., Pagès, M., Pouget, C., Schweizer, L., Kranendonk, M. E. G., Akhtar, N., Bunkowski, S., Stadelmann, C., Schüller, U., Mueller, W. C., Dohmen, H., Acker, T., Harter, P. N., Mawrin, C., Beschorner, R., Brandner, S., Snuderl, M., Abdullaev, Z., Aldape, K., Gilbert, M. R., Armstrong, T. S., Ellison, D. W., Capper, D., Ichimura, K., Reifenberger, G., Grundy, R. G., Jabado, N., Krskova, L., Zapotocky, M., Vicha, A., Varlet, P., Wesseling, P., Rutkowski, S., Korshunov, A., Wick, W., Pfister, S. M., Jones, D. T. W., von Deimling, A., Pajtler, K. W., & Sahm, F. (2021). Recurrent fusions in PLAGL1 define a distinct subset of pediatric-type supratentorial neuroepithelial tumors. *Acta Neuropathol*, *142*(5), 827-839. https://doi.org/10.1007/s00401-021-02356-6

Simeonova, I., & Huillard, E. (2014). In vivo models of brain tumors: roles of genetically engineered mouse models in understanding tumor biology and use in preclinical studies. *Cell Mol Life Sci*, *71*(20), 4007-4026. https://doi.org/10.1007/s00018-014-1675-3

Simon, T., Riemer, P., Jarosch, A., Detjen, K., Di Domenico, A., Bormann, F., Menne, A., Khouja, S., Monjé, N., Childs, L. H., Lenze, D., Leser, U., Rossner, F., Morkel, M., Blüthgen, N., Pavel, M., Horst, D., Capper, D., Marinoni, I., Perren, A., Mamlouk, S., & Sers, C. (2022). DNA methylation reveals distinct cells of origin for pancreatic neuroendocrine carcinomas and pancreatic neuroendocrine tumors. *Genome Medicine*, *14*(1), 24. https://doi.org/10.1186/s13073-022-01018-w

Singh, S. K., Clarke, I. D., Terasaki, M., Bonn, V. E., Hawkins, C., Squire, J., & Dirks, P. B. (2003). Identification of a cancer stem cell in human brain tumors. *Cancer Res*, *63*(18), 5821-5828.

Singh, S. K., Hawkins, C., Clarke, I. D., Squire, J. A., Bayani, J., Hide, T., Henkelman, R. M., Cusimano, M. D., & Dirks, P. B. (2004). Identification of human brain tumour initiating cells. *Nature*, *432*(7015), 396-401. https://doi.org/10.1038/nature03128

Skene, P. J., Henikoff, J. G., & Henikoff, S. (2018). Targeted in situ genome-wide profiling with high efficiency for low cell numbers. *Nature Protocols*, *13*(5), 1006-1019. https://doi.org/10.1038/nprot.2018.015

Skog, J., Würdinger, T., van Rijn, S., Meijer, D. H., Gainche, L., Sena-Esteves, M., Curry, W. T., Jr., Carter, B. S., Krichevsky, A. M., & Breakefield, X. O. (2008). Glioblastoma microvesicles transport RNA and proteins that promote tumour growth and provide diagnostic biomarkers. *Nat Cell Biol*, *10*(12), 1470-1476. https://doi.org/10.1038/ncb1800

Smith, C. L., Blake, J. A., Kadin, J. A., Richardson, J. E., Bult, C. J., & Group, t. M. G. D. (2017). Mouse Genome Database (MGD)-2018: knowledgebase for the laboratory mouse. *Nucleic Acids Research*, *46*(D1), D836-D842. https://doi.org/10.1093/nar/gkx1006

Solomon, M. J., Larsen, P. L., & Varshavsky, A. (1988). Mapping protein-DNA interactions in vivo with formaldehyde: evidence that histone H4 is retained on a highly transcribed gene. *Cell*, *53*(6), 937-947. https://doi.org/10.1016/s0092-8674(88)90469-2

Sreedharan, S., Maturi, N. P., Xie, Y., Sundström, A., Jarvius, M., Libard, S., Alafuzoff, I., Weishaupt, H., Fryknäs, M., Larsson, R., Swartling, F. J., & Uhrbom, L. (2017). Mouse Models of Pediatric Supratentorial High-grade Glioma Reveal How Cell-of-Origin Influences Tumor Development and Phenotype. *Cancer Res*, *77*(3), 802-812. https://doi.org/10.1158/0008-5472.Can-16-2482

Stamatovic, S. M., Johnson, A. M., Keep, R. F., & Andjelkovic, A. V. (2016). Junctional proteins of the blood-brain barrier: New insights into function and dysfunction. *Tissue Barriers*, *4*(1), e1154641. https://doi.org/10.1080/21688370.2016.1154641

Staynov, D. Z., & Crane-Robinson, C. (1988). Footprinting of linker histones H5 and H1 on the nucleosome. *EMBO J*, *7*(12), 3685-3691. https://doi.org/10.1002/j.1460-2075.1988.tb03250.x

Stiles, J., & Jernigan, T. L. (2010). The basics of brain development. *Neuropsychol Rev*, *20*(4), 327-348. https://doi.org/10.1007/s11065-010-9148-4

Stratton, M. R., Campbell, P. J., & Futreal, P. A. (2009). The cancer genome. *Nature*, *458*(7239), 719-724. https://doi.org/10.1038/nature07943

Sturm, D., Orr, B. A., Toprak, U. H., Hovestadt, V., Jones, D. T. W., Capper, D., Sill, M., Buchhalter, I., Northcott, P. A., Leis, I., Ryzhova, M., Koelsche, C., Pfaff, E., Allen, S. J., Balasubramanian, G., Worst, B. C., Pajtler, K. W., Brabetz, S., Johann, P. D., Sahm, F., Reimand, J., Mackay, A., Carvalho, D. M., Remke, M., Phillips, J. J., Perry, A., Cowdrey, C., Drissi, R., Fouladi, M., Giangaspero, F., Łastowska, M., Grajkowska, W., Scheurlen, W., Pietsch, T., Hagel, C., Gojo, J., Lötsch, D., Berger, W., Slavc, I., Haberler, C., Jouvet, A., Holm, S., Hofer, S., Prinz, M., Keohane, C., Fried, I., Mawrin, C., Scheie, D., Mobley, B. C., Schniederjan, M.

J., Santi, M., Buccoliero, A. M., Dahiya, S., Kramm, C. M., von Bueren, A. O., von Hoff, K., Rutkowski, S., Herold-Mende, C., Frühwald, M. C., Milde, T., Hasselblatt, M., Wesseling, P., Rößler, J., Schüller, U., Ebinger, M., Schittenhelm, J., Frank, S., Grobholz, R., Vajtai, I., Hans, V., Schneppenheim, R., Zitterbart, K., Collins, V. P., Aronica, E., Varlet, P., Puget, S., Dufour, C., Grill, J., Figarella-Branger, D., Wolter, M., Schuhmann, M. U., Shalaby, T., Grotzer, M., van Meter, T., Monoranu, C. M., Felsberg, J., Reifenberger, G., Snuderl, M., Forrester, L. A., Koster, J., Versteeg, R., Volckmann, R., van Sluis, P., Wolf, S., Mikkelsen, T., Gajjar, A., Aldape, K., Moore, A. S., Taylor, M. D., Jones, C., Jabado, N., Karajannis, M. A., Eils, R., Schlesner, M., Lichter, P., von Deimling, A., Pfister, S. M., Ellison, D. W., Korshunov, A., & Kool, M. (2016). New Brain Tumor Entities Emerge from Molecular Classification of CNS-PNETs. *Cell*, *164*(5), 1060-1072. https://doi.org/10.1016/j.cell.2016.01.015

Sturm, D., Witt, H., Hovestadt, V., Khuong-Quang, D. A., Jones, D. T., Konermann, C., Pfaff, E., Tönjes, M., Sill, M., Bender, S., Kool, M., Zapatka, M., Becker, N., Zucknick, M., Hielscher, T., Liu, X. Y., Fontebasso, A. M., Ryzhova, M., Albrecht, S., Jacob, K., Wolter, M., Ebinger, M., Schuhmann, M. U., van Meter, T., Frühwald, M. C., Hauch, H., Pekrun, A., Radlwimmer, B., Niehues, T., von Komorowski, G., Dürken, M., Kulozik, A. E., Madden, J., Donson, A., Foreman, N. K., Drissi, R., Fouladi, M., Scheurlen, W., von Deimling, A., Monoranu, C., Roggendorf, W., Herold-Mende, C., Unterberg, A., Kramm, C. M., Felsberg, J., Hartmann, C., Wiestler, B., Wick, W., Milde, T., Witt, O., Lindroth, A. M., Schwartzentruber, J., Faury, D., Fleming, A., Zakrzewska, M., Liberski, P. P., Zakrzewski, K., Hauser, P., Garami, M., Klekner, A., Bognar, L., Morrissy, S., Cavalli, F., Taylor, M. D., van Sluis, P., Koster, J., Versteeg, R., Volckmann, R., Mikkelsen, T., Aldape, K., Reifenberger, G., Collins, V. P., Majewski, J., Korshunov, A., Lichter, P., Plass, C., Jabado, N., & Pfister, S. M. (2012). Hotspot mutations in H3F3A and IDH1 define distinct epigenetic and biological subgroups of glioblastoma. *Cancer Cell*, *22*(4), 425-437. https://doi.org/10.1016/j.ccr.2012.08.024

Suga, H., Kadoshima, T., Minaguchi, M., Ohgushi, M., Soen, M., Nakano, T., Takata, N., Wataya, T., Muguruma, K., Miyoshi, H., Yonemura, S., Oiso, Y., & Sasai, Y. (2011). Self-formation of functional adenohypophysis in three-dimensional culture. *Nature*, *480*(7375), 57-62. https://doi.org/10.1038/nature10637

Sugai, K., Fukuzawa, R., Shofuda, T., Fukusumi, H., Kawabata, S., Nishiyama, Y., Higuchi, Y., Kawai, K., Isoda, M., Kanematsu, D., Hashimoto-Tamaoki, T., Kohyama, J., Iwanami, A., Suemizu, H., Ikeda, E., Matsumoto, M., Kanemura, Y., Nakamura, M., & Okano, H. (2016). Pathological classification of human iPSC-derived neural stem/progenitor cells towards safety assessment of transplantation therapy for CNS diseases. *Molecular Brain*, *9*(1), 85. https://doi.org/10.1186/s13041-016-0265-8

Sun, X.-Y., Ju, X.-C., Li, Y., Zeng, P.-M., Wu, J., Zhou, Y.-Y., Shen, L.-B., Dong, J., Chen, Y.-J., & Luo, Z.-G. (2022). Generation of vascularized brain organoids to study neurovascular interactions. *Elife*, *11*, e76707. https://doi.org/10.7554/eLife.76707

Suslov, O. N., Kukekov, V. G., Ignatova, T. N., & Steindler, D. A. (2002). Neural stem cell heterogeneity demonstrated by molecular phenotyping of clonal neurospheres. *Proc Natl Acad Sci U S A*, *99*(22), 14506-14511. https://doi.org/10.1073/pnas.212525299

Sweeney, M. D., Kisler, K., Montagne, A., Toga, A. W., & Zlokovic, B. V. (2018). The role of brain vasculature in neurodegenerative disorders. *Nature Neuroscience*, *21*(10), 1318-1331. https://doi.org/10.1038/s41593-018-0234-x

Tabata, H., & Nakajima, K. (2001). Efficient in utero gene transfer system to the developing mouse brain using electroporation: visualization of neuronal migration in the developing cortex. *Neuroscience*, *103*(4), 865-872. https://doi.org/10.1016/s0306-4522(01)00016-1

Tanaka, M., Yamazaki, Y., Kanno, Y., Igarashi, K., Aisaki, K., Kanno, J., & Nakamura, T. (2014). Ewing's sarcoma precursors are highly enriched in embryonic osteochondrogenic progenitors. *J Clin Invest*, *124*(7), 3061-3074. https://doi.org/10.1172/jci72399

Taylor, M. D., Poppleton, H., Fuller, C., Su, X., Liu, Y., Jensen, P., Magdaleno, S., Dalton, J., Calabrese, C., Board, J., Macdonald, T., Rutka, J., Guha, A., Gajjar, A., Curran, T., & Gilbertson, R. J. (2005). Radial glia cells are candidate stem cells of ependymoma. *Cancer Cell*, *8*(4), 323-335. https://doi.org/10.1016/j.ccr.2005.09.001

Teng, L., Nakada, M., Furuyama, N., Sabit, H., Furuta, T., Hayashi, Y., Takino, T., Dong, Y., Sato, H., Sai, Y., Miyamoto, K., Berens, M. E., Zhao, S. G., & Hamada, J. (2013). Ligand-dependent EphB1 signaling suppresses glioma invasion and correlates with patient survival. *Neuro Oncol*, *15*(12), 1710-1720. https://doi.org/10.1093/neuonc/not128

Thomas, C., Sill, M., Ruland, V., Witten, A., Hartung, S., Kordes, U., Jeibmann, A., Beschorner, R., Keyvani, K., Bergmann, M., Mittelbronn, M., Pietsch, T., Felsberg, J., Monoranu, C. M., Varlet, P., Hauser, P., Olar, A., Grundy, R. G., Wolff, J. E., Korshunov, A., Jones, D. T., Bewerunge-Hudler, M., Hovestadt, V., von Deimling, A., Pfister, S. M., Paulus, W., Capper, D., & Hasselblatt, M. (2016). Methylation profiling of

choroid plexus tumors reveals 3 clinically distinct subgroups. *Neuro Oncol*, *18*(6), 790-796. https://doi.org/10.1093/neuonc/nov322

Thompson, S., Clarke, A. R., Pow, A. M., Hooper, M. L., & Melton, D. W. (1989). Germ line transmission and expression of a corrected HPRT gene produced by gene targeting in embryonic stem cells. *Cell*, *56*(2), 313-321. https://doi.org/10.1016/0092-8674(89)90905-7

Tűzesi, Á., Kling, T., Wenger, A., Lunavat, T. R., Jang, S. C., Rydenhag, B., Lötvall, J., Pollard, S. M., Danielsson, A., & Carén, H. (2017). Pediatric brain tumor cells release exosomes with a miRNA repertoire that differs from exosomes secreted by normal cells. *Oncotarget*, *8*(52), 90164-90175. https://doi.org/10.18632/oncotarget.21621

Uhrig, S., Ellermann, J., Walther, T., Burkhardt, P., Fröhlich, M., Hutter, B., Toprak, U. H., Neumann, O., Stenzinger, A., Scholl, C., Fröhling, S., & Brors, B. (2021). Accurate and efficient detection of gene fusions from RNA sequencing data. *Genome Res*, *31*(3), 448-460. https://doi.org/10.1101/gr.257246.119

van den Bent, M. J. (2010). Interobserver variation of the histopathological diagnosis in clinical trials on glioma: a clinician's perspective. *Acta Neuropathol*, *120*(3), 297-304. https://doi.org/10.1007/s00401-010-0725-7

Vega-Benedetti, A. F., Saucedo, C., Zavattari, P., Vanni, R., Zugaza, J. L., & Parada, L. A. (2017). PLAGL1: an important player in diverse pathological processes. *J Appl Genet*, *58*(1), 71-78. https://doi.org/10.1007/s13353-016-0355-4

Venter, J. C., Adams, M. D., Myers, E. W., Li, P. W., Mural, R. J., Sutton, G. G., Smith, H. O., Yandell, M., Evans, C. A., Holt, R. A., Gocayne, J. D., Amanatides, P., Ballew, R. M., Huson, D. H., Wortman, J. R., Zhang, Q., Kodira, C. D., Zheng, X. H., Chen, L., Skupski, M., Subramanian, G., Thomas, P. D., Zhang, J., Gabor Miklos, G. L., Nelson, C., Broder, S., Clark, A. G., Nadeau, J., McKusick, V. A., Zinder, N., Levine, A. J., Roberts, R. J., Simon, M., Slayman, C., Hunkapiller, M., Bolanos, R., Delcher, A., Dew, I., Fasulo, D., Flanigan, M., Florea, L., Halpern, A., Hannenhalli, S., Kravitz, S., Levy, S., Mobarry, C., Reinert, K., Remington, K., Abu-Threideh, J., Beasley, E., Biddick, K., Bonazzi, V., Brandon, R., Cargill, M., Chandramouliswaran, I., Charlab, R., Chaturvedi, K., Deng, Z., Di Francesco, V., Dunn, P., Eilbeck, K., Evangelista, C., Gabrielian, A. E., Gan, W., Ge, W., Gong, F., Gu, Z., Guan, P., Heiman, T. J., Higgins, M. E., Ji, R. R., Ke, Z., Ketchum, K. A., Lai, Z., Lei, Y., Li, Z., Li, J., Liang, Y., Lin, X., Lu, F., Merkulov, G. V., Milshina, N., Moore, H. M., Naik, A. K., Narayan, V. A., Neelam, B., Nusskern, D., Rusch, D. B., Salzberg, S., Shao, W., Shue, B., Sun, J., Wang, Z., Wang, A., Wang, X., Wang, J., Wei, M., Wides, R., Xiao, C., Yan, C., Yao, A., Ye, J., Zhan, M., Zhang, W., Zhang, H., Zhao, Q., Zheng, L., Zhong, F., Zhong, W., Zhu, S., Zhao, S., Gilbert, D., Baumhueter, S., Spier, G., Carter, C., Cravchik, A., Woodage, T., Ali, F., An, H., Awe, A., Baldwin, D., Baden, H., Barnstead, M., Barrow, I., Beeson, K., Busam, D., Carver, A., Center, A., Cheng, M. L., Curry, L., Danaher, S., Davenport, L., Desilets, R., Dietz, S., Dodson, K., Doup, L., Ferriera, S., Garg, N., Gluecksmann, A., Hart, B., Haynes, J., Haynes, C., Heiner, C., Hladun, S., Hostin, D., Houck, J., Howland, T., Ibegwam, C., Johnson, J., Kalush, F., Kline, L., Koduru, S., Love, A., Mann, F., May, D., McCawley, S., McIntosh, T., McMullen, I., Moy, M., Moy, L., Murphy, B., Nelson, K., Pfannkoch, C., Pratts, E., Puri, V., Qureshi, H., Reardon, M., Rodriguez, R., Rogers, Y. H., Romblad, D., Ruhfel, B., Scott, R., Sitter, C., Smallwood, M., Stewart, E., Strong, R., Suh, E., Thomas, R., Tint, N. N., Tse, S., Vech, C., Wang, G., Wetter, J., Williams, S., Williams, M., Windsor, S., Winn-Deen, E., Wolfe, K., Zaveri, J., Zaveri, K., Abril, J. F., Guigó, R., Campbell, M. J., Sjolander, K. V., Karlak, B., Kejariwal, A., Mi, H., Lazareva, B., Hatton, T., Narechania, A., Diemer, K., Muruganujan, A., Guo, N., Sato, S., Bafna, V., Istrail, S., Lippert, R., Schwartz, R., Walenz, B., Yooseph, S., Allen, D., Basu, A., Baxendale, J., Blick, L., Caminha, M., Carnes-Stine, J., Caulk, P., Chiang, Y. H., Coyne, M., Dahlke, C., Deslattes Mays, A., Dombroski, M., Donnelly, M., Ely, D., Esparham, S., Fosler, C., Gire, H., Glanowski, S., Glasser, K., Glodek, A., Gorokhov, M., Graham, K., Gropman, B., Harris, M., Heil, J., Henderson, S., Hoover, J., Jennings, D., Jordan, C., Jordan, J., Kasha, J., Kagan, L., Kraft, C., Levitsky, A., Lewis, M., Liu, X., Lopez, J., Ma, D., Majoros, W., McDaniel, J., Murphy, S., Newman, M., Nguyen, T., Nguyen, N., Nodell, M., Pan, S., Peck, J., Peterson, M., Rowe, W., Sanders, R., Scott, J., Simpson, M., Smith, T., Sprague, A., Stockwell, T., Turner, R., Venter, E., Wang, M., Wen, M., Wu, D., Wu, M., Xia, A., Zandieh, A., & Zhu, X. (2001). The sequence of the human genome. *Science*, *291*(5507), 1304-1351. https://doi.org/10.1126/science.1058040

von Werder, A., Seidler, B., Schmid, R. M., Schneider, G., & Saur, D. (2012). Production of avian retroviruses and tissue-specific somatic retroviral gene transfer in vivo using the RCAS/TVA system. *Nature Protocols*, *7*(6), 1167-1183. https://doi.org/10.1038/nprot.2012.060

Wang, D., Coscoy, L., Zylberberg, M., Avila, P. C., Boushey, H. A., Ganem, D., & DeRisi, J. L. (2002). Microarray-based detection and genotyping of viral pathogens. *Proc Natl Acad Sci U S A*, *99*(24), 15687-15692. https://doi.org/10.1073/pnas.242579699

Wang, G. Y., So, P.-L., Wang, L., Libove, E., Wang, J., & Epstein, E. H. (2011). Establishment of Murine Basal Cell Carcinoma Allografts: A Potential Model for Preclinical Drug Testing and for Molecular Analysis. *Journal of Investigative Dermatology*, *131*(11), 2298-2305. https://doi.org/https://doi.org/10.1038/jid.2011.204

Ward, E., DeSantis, C., Robbins, A., Kohler, B., & Jemal, A. (2014). Childhood and adolescent cancer statistics, 2014. *CA: A Cancer Journal for Clinicians*, *64*(2), 83-103. https://doi.org/https://doi.org/10.3322/caac.21219

Wasson, J. C., Saylors, R. L., 3rd, Zeltzer, P., Friedman, H. S., Bigner, S. H., Burger, P. C., Bigner, D. D., Look, A. T., Douglass, E. C., & Brodeur, G. M. (1990). Oncogene amplification in pediatric brain tumors. *Cancer Res*, *50*(10), 2987-2990.

Waterston, R. H., Lindblad-Toh, K., Birney, E., Rogers, J., Abril, J. F., Agarwal, P., Agarwala, R., Ainscough, R., Alexandersson, M., An, P., Antonarakis, S. E., Attwood, J., Baertsch, R., Bailey, J., Barlow, K., Beck, S., Berry, E., Birren, B., Bloom, T., Bork, P., Botcherby, M., Bray, N., Brent, M. R., Brown, D. G., Brown, S. D., Bult, C., Burton, J., Butler, J., Campbell, R. D., Carninci, P., Cawley, S., Chiaromonte, F., Chinwalla, A. T., Church, D. M., Clamp, M., Clee, C., Collins, F. S., Cook, L. L., Copley, R. R., Coulson, A., Couronne, O., Cuff, J., Curwen, V., Cutts, T., Daly, M., David, R., Davies, J., Delehaunty, K. D., Deri, J., Dermitzakis, E. T., Dewey, C., Dickens, N. J., Diekhans, M., Dodge, S., Dubchak, I., Dunn, D. M., Eddy, S. R., Elnitski, L., Emes, R. D., Eswara, P., Eyras, E., Felsenfeld, A., Fewell, G. A., Flicek, P., Foley, K., Frankel, W. N., Fulton, L. A., Fulton, R. S., Furey, T. S., Gage, D., Gibbs, R. A., Glusman, G., Gnerre, S., Goldman, N., Goodstadt, L., Grafham, D., Graves, T. A., Green, E. D., Gregory, S., Guigó, R., Guyer, M., Hardison, R. C., Haussler, D., Hayashizaki, Y., Hillier, L. W., Hinrichs, A., Hlavina, W., Holzer, T., Hsu, F., Hua, A., Hubbard, T., Hunt, A., Jackson, I., Jaffe, D. B., Johnson, L. S., Jones, M., Jones, T. A., Joy, A., Kamal, M., Karlsson, E. K., Karolchik, D., Kasprzyk, A., Kawai, J., Keibler, E., Kells, C., Kent, W. J., Kirby, A., Kolbe, D. L., Korf, I., Kucherlapati, R. S., Kulbokas, E. J., Kulp, D., Landers, T., Leger, J. P., Leonard, S., Letunic, I., Levine, R., Li, J., Li, M., Lloyd, C., Lucas, S., Ma, B., Maglott, D. R., Mardis, E. R., Matthews, L., Mauceli, E., Mayer, J. H., McCarthy, M., McCombie, W. R., McLaren, S., McLay, K., McPherson, J. D., Meldrim, J., Meredith, B., Mesirov, J. P., Miller, W., Miner, T. L., Mongin, E., Montgomery, K. T., Morgan, M., Mott, R., Mullikin, J. C., Muzny, D. M., Nash, W. E., Nelson, J. O., Nhan, M. N., Nicol, R., Ning, Z., Nusbaum, C., O'Connor, M. J., Okazaki, Y., Oliver, K., Overton-Larty, E., Pachter, L., Parra, G., Pepin, K. H., Peterson, J., Pevzner, P., Plumb, R., Pohl, C. S., Poliakov, A., Ponce, T. C., Ponting, C. P., Potter, S., Quail, M., Reymond, A., Roe, B. A., Roskin, K. M., Rubin, E. M., Rust, A. G., Santos, R., Sapojnikov, V., Schultz, B., Schultz, J., Schwartz, M. S., Schwartz, S., Scott, C., Seaman, S., Searle, S., Sharpe, T., Sheridan, A., Shownkeen, R., Sims, S., Singer, J. B., Slater, G., Smit, A., Smith, D. R., Spencer, B., Stabenau, A., Stange-Thomann, N., Sugnet, C., Suyama, M., Tesler, G., Thompson, J., Torrents, D., Trevaskis, E., Tromp, J., Ucla, C., Ureta-Vidal, A., Vinson, J. P., Von Niederhausern, A. C., Wade, C. M., Wall, M., Weber, R. J., Weiss, R. B., Wendl, M. C., West, A. P., Wetterstrand, K., Wheeler, R., Whelan, S., Wierzbowski, J., Willey, D., Williams, S., Wilson, R. K., Winter, E., Worley, K. C., Wyman, D., Yang, S., Yang, S. P., Zdobnov, E. M., Zody, M. C., & Lander, E. S. (2002). Initial sequencing and comparative analysis of the mouse genome. *Nature*, *420*(6915), 520-562. https://doi.org/10.1038/nature01262

Weber, J., & Rad, R. (2019). Engineering CRISPR mouse models of cancer. *Curr Opin Genet Dev*, *54*, 88-96. https://doi.org/10.1016/j.gde.2019.04.001

Wee, S., Wiederschain, D., Maira, S. M., Loo, A., Miller, C., deBeaumont, R., Stegmeier, F., Yao, Y. M., & Lengauer, C. (2008). PTEN-deficient cancers depend on PIK3CB. *Proc Natl Acad Sci U S A*, *105*(35), 13057-13062. https://doi.org/10.1073/pnas.0802655105

Wenger, A., Larsson, S., Danielsson, A., Elbæk, K. J., Kettunen, P., Tisell, M., Sabel, M., Lannering, B., Nordborg, C., Schepke, E., & Carén, H. (2017). Stem cell cultures derived from pediatric brain tumors accurately model the originating tumors. *Oncotarget*, *8*(12), 18626-18639. https://doi.org/10.18632/oncotarget.14826

Wichterle, H., Lieberam, I., Porter, J. A., & Jessell, T. M. (2002). Directed differentiation of embryonic stem cells into motor neurons. *Cell*, *110*(3), 385-397. https://doi.org/10.1016/s0092-8674(02)00835-8

Widera, D., Mikenberg, I., Elvers, M., Kaltschmidt, C., & Kaltschmidt, B. (2006). Tumor necrosis factor alpha triggers proliferation of adult neural stem cells via IKK/NF-kappaB signaling. *BMC Neurosci*, *7*, 64. https://doi.org/10.1186/1471-2202-7-64

Wiederschain, D., Wee, S., Chen, L., Loo, A., Yang, G., Huang, A., Chen, Y., Caponigro, G., Yao, Y. M., Lengauer, C., Sellers, W. R., & Benson, J. D. (2009). Single-vector inducible lentiviral RNAi system for oncology target validation. *Cell Cycle*, *8*(3), 498-504. https://doi.org/10.4161/cc.8.3.7701

Wienke, J., Dierselhuis, M. P., Tytgat, G. A. M., Künkele, A., Nierkens, S., & Molenaar, J. J. (2021). The immune landscape of neuroblastoma: Challenges and opportunities for novel therapeutic strategies in pediatric oncology. *Eur J Cancer*, *144*, 123-150. https://doi.org/10.1016/j.ejca.2020.11.014

Wimmer, R. A., Leopoldi, A., Aichinger, M., Kerjaschki, D., & Penninger, J. M. (2019). Generation of blood vessel organoids from human pluripotent stem cells. *Nat Protoc*, *14*(11), 3082-3100. https://doi.org/10.1038/s41596-019-0213-z

Witt, H., Mack, S. C., Ryzhova, M., Bender, S., Sill, M., Isserlin, R., Benner, A., Hielscher, T., Milde, T., Remke, M., Jones, D. T., Northcott, P. A., Garzia, L., Bertrand, K. C., Wittmann, A., Yao, Y., Roberts, S. S., Massimi, L., Van Meter, T., Weiss, W. A., Gupta, N., Grajkowska, W., Lach, B., Cho, Y. J., von Deimling, A., Kulozik, A. E., Witt, O., Bader, G. D., Hawkins, C. E., Tabori, U., Guha, A., Rutka, J. T., Lichter, P., Korshunov, A., Taylor, M. D., & Pfister, S. M. (2011). Delineation of two clinically and molecularly distinct subgroups of posterior fossa ependymoma. *Cancer Cell*, *20*(2), 143-157. https://doi.org/10.1016/j.ccr.2011.07.007

Wong, C. H., Siah, K. W., & Lo, A. W. (2018). Estimation of clinical trial success rates and related parameters. *Biostatistics*, *20*(2), 273-286. https://doi.org/10.1093/biostatistics/kxx069

Wong, D. W., Leung, E. L., So, K. K., Tam, I. Y., Sihoe, A. D., Cheng, L. C., Ho, K. K., Au, J. S., Chung, L. P., & Pik Wong, M. (2009). The EML4-ALK fusion gene is involved in various histologic types of lung cancers from nonsmokers with wild-type EGFR and KRAS. *Cancer*, *115*(8), 1723-1733. https://doi.org/10.1002/cncr.24181

Wouters, O. J., McKee, M., & Luyten, J. (2020). Estimated Research and Development Investment Needed to Bring a New Medicine to Market, 2009-2018. *JAMA*, *323*(9), 844-853. https://doi.org/10.1001/jama.2020.1166

Wu, C. C., Beird, H. C., Andrew Livingston, J., Advani, S., Mitra, A., Cao, S., Reuben, A., Ingram, D., Wang, W. L., Ju, Z., Hong Leung, C., Lin, H., Zheng, Y., Roszik, J., Wang, W., Patel, S., Benjamin, R. S., Somaiah, N., Conley, A. P., Mills, G. B., Hwu, P., Gorlick, R., Lazar, A., Daw, N. C., Lewis, V., & Futreal, P. A. (2020). Immuno-genomic landscape of osteosarcoma. *Nat Commun*, *11*(1), 1008. https://doi.org/10.1038/s41467-020-14646-w

Wu, L., Sun, T., Kobayashi, K., Gao, P., & Griffin, J. D. (2002). Identification of a family of mastermind-like transcriptional coactivators for mammalian notch receptors. *Mol Cell Biol*, *22*(21), 7688-7700. https://doi.org/10.1128/mcb.22.21.7688-7700.2002

Wykosky, J., Gibo, D. M., Stanton, C., & Debinski, W. (2005). EphA2 as a novel molecular marker and target in glioblastoma multiforme. *Mol Cancer Res*, *3*(10), 541-551. https://doi.org/10.1158/1541-7786.Mcr-05-0056

Wykosky, J., Palma, E., Gibo, D. M., Ringler, S., Turner, C. P., & Debinski, W. (2008). Soluble monomeric EphrinA1 is released from tumor cells and is a functional ligand for the EphA2 receptor. *Oncogene*, *27*(58), 7260-7273. https://doi.org/10.1038/onc.2008.328

Xia, X., Zhang, Y., Zieth, C. R., & Zhang, S. C. (2007). Transgenes delivered by lentiviral vector are suppressed in human embryonic stem cells in a promoter-dependent manner. *Stem Cells Dev*, *16*(1), 167-176. https://doi.org/10.1089/scd.2006.0057

Xiao, W., Sohrabi, A., & Seidlits, S. K. (2017). Integrating the glioblastoma microenvironment into engineered experimental models. *Future Sci OA*, *3*(3), Fso189. https://doi.org/10.4155/fsoa-2016-0094

Xu, J., Erdreich-Epstein, A., Gonzalez-Gomez, I., Melendez, E. Y., Smbatyan, G., Moats, R. A., Rosol, M., Biegel, J. A., & Reynolds, C. P. (2012). Novel cell lines established from pediatric brain tumors. *J Neurooncol*, *107*(2), 269-280. https://doi.org/10.1007/s11060-011-0756-5

Xu, J., Erdreich-Epstein, A., Gonzalez-Gomez, I., Melendez, E. Y., Smbatyan, G., Moats, R. A., Rosol, M., Biegel, J. A., & Reynolds, C. P. (2012). Novel cell lines established from pediatric brain tumors. *Journal of Neuro-Oncology*, *107*(2), 269-280. https://doi.org/10.1007/s11060-011-0756-5

Xu, J., Margol, A., Asgharzadeh, S., & Erdreich-Epstein, A. (2015). Pediatric Brain Tumor Cell Lines. *Journal of Cellular Biochemistry*, *116*(2), 218-224. https://doi.org/https://doi.org/10.1002/jcb.24976

Yachnis, A. T., Neubauer, D., & Muir, D. (1998). Characterization of a primary central nervous system atypical teratoid/rhabdoid tumor and derivative cell line: immunophenotype and neoplastic properties. *J Neuropathol Exp Neurol*, *57*(10), 961-971. https://doi.org/10.1097/00005072-199810000-00008

Yan, P. S., Chen, C. M., Shi, H., Rahmatpanah, F., Wei, S. H., Caldwell, C. W., & Huang, T. H. (2001). Dissecting complex epigenetic alterations in breast cancer using CpG island microarrays. *Cancer Res*, *61*(23), 8375-8380.

Yang, H., Wang, H., & Jaenisch, R. (2014). Generating genetically modified mice using CRISPR/Cas-mediated genome engineering. *Nat Protoc*, *9*(8), 1956-1968. https://doi.org/10.1038/nprot.2014.134

Yang, Z. J., Ellis, T., Markant, S. L., Read, T. A., Kessler, J. D., Bourboulas, M., Schüller, U., Machold, R., Fishell, G., Rowitch, D. H., Wainwright, B. J., & Wechsler-Reya, R. J. (2008). Medulloblastoma can be initiated by deletion of Patched in lineage-restricted progenitors or stem cells. *Cancer Cell*, *14*(2), 135-145. https://doi.org/10.1016/j.ccr.2008.07.003

Young, K. M., Bartlett, P. F., & Coulson, E. J. (2006). Neural progenitor number is regulated by nuclear factor-kappaB p65 and p50 subunit-dependent proliferation rather than cell survival. *J Neurosci Res*, *83*(1), 39-49. https://doi.org/10.1002/jnr.20702

Zarzosa, P., Navarro, N., Giralt, I., Molist, C., Almazán-Moga, A., Vidal, I., Soriano, A., Segura, M. F., Hladun, R., Villanueva, A., Gallego, S., & Roma, J. (2017). Patient-derived xenografts for childhood solid tumors: a valuable tool to test new drugs and personalize treatments. *Clin Transl Oncol*, *19*(1), 44-50. https://doi.org/10.1007/s12094-016-1557-2

Zhang, H., Su, B., Jiao, L., Xu, Z. H., Zhang, C. J., Nie, J., Gao, M. L., Zhang, Y. V., & Jin, Z. B. (2021). Transplantation of GMP-grade human iPSC-derived retinal pigment epithelial cells in rodent model: the first pre-clinical study for safety and efficacy in China. *Ann Transl Med*, *9*(3), 245. https://doi.org/10.21037/atm-20-4707

Zhang, Y., Liu, T., Meyer, C. A., Eeckhoute, J., Johnson, D. S., Bernstein, B. E., Nusbaum, C., Myers, R. M., Brown, M., Li, W., & Liu, X. S. (2008). Model-based Analysis of ChIP-Seq (MACS). *Genome Biology*, *9*(9), R137. https://doi.org/10.1186/gb-2008-9-9-r137

Zheng, T., Ghasemi, D. R., Okonechnikov, K., Korshunov, A., Sill, M., Hübner, J.-M., Maaß, K. K., Snuderl, M., Gojo, J., Schüller, U., Gerber, N. U., Hernáiz-Driever, P., Milde, T., Sturm, D., Chapman, R., Grundy, R. G., von Deimling, A., Jones, D. T. W., Kool, M., Pfister, S. M., Sahm, F., Kawauchi, D., & Pajtler, K. W. (2020). EPEN-18. CROSS-SPECIES GENOMICS IDENTIFIES GLI2 AS AN ONCOGENE OF C11orf95 FUSION-POSITIVE SUPRATENTORIAL EPENDYMOMA. *Neuro-Oncology*, *22*(Supplement_3), iii311-iii311. https://doi.org/10.1093/neuonc/noaa222.156

Zheng, T., Ghasemi, D. R., Okonechnikov, K., Korshunov, A., Sill, M., Maass, K. K., Benites Goncalves da Silva, P., Ryzhova, M., Gojo, J., Stichel, D., Arabzade, A., Kupp, R., Benzel, J., Taya, S., Adachi, T., Shiraishi, R., Gerber, N. U., Sturm, D., Ecker, J., Sievers, P., Selt, F., Chapman, R., Haberler, C., Figarella-Branger, D., Reifenberger, G., Fleischhack, G., Rutkowski, S., Donson, A. M., Ramaswamy, V., Capper, D., Ellison, D. W., Herold-Mende, C. C., Schuller, U., Brandner, S., Hernaiz Driever, P., Kros, J. M., Snuderl, M., Milde, T., Grundy, R. G., Hoshino, M., Mack, S. C., Gilbertson, R. J., Jones, D. T. W., Kool, M., von Deimling, A., Pfister, S. M., Sahm, F., Kawauchi, D., & Pajtler, K. W. (2021). Cross-species genomics reveals oncogenic dependencies in ZFTA/C11orf95 fusion-positive supratentorial ependymomas. *Cancer Discovery*, candisc.0963.2020. https://doi.org/10.1158/2159-8290.Cd-20-0963

Zheng, T., Sill, M., Imle, R., Shiraishi, R., Wang, W., Morcavallo, A., Chesler, L., Kawauchi, D., Ayrault, O., Pavlo, L., Pfister, S. M., Kutscher, L. M., Banito, A., Jones, D. W., Pajtler, K. W., & Zuckermann, M. (2022). MODL-07. DNA methylation-based biobank of murine models for pediatric tumors. *Neuro-Oncology*, *24*(Supplement_1), i169-i170. https://doi.org/10.1093/neuonc/noac079.630

Zhou, W., Triche, T. J., Jr, Laird, P. W., & Shen, H. (2018). SeSAMe: reducing artifactual detection of DNA methylation by Infinium BeadChips in genomic deletions. *Nucleic Acids Research*, *46*(20), e123-e123. https://doi.org/10.1093/nar/gky691

Zhou, Z., Luther, N., Singh, R., Boockvar, J. A., Souweidane, M. M., & Greenfield, J. P. (2017). Glioblastoma spheroids produce infiltrative gliomas in the rat brainstem. *Childs Nerv Syst*, *33*(3), 437-446. https://doi.org/10.1007/s00381-017-3344-y

Zuckermann, M. (2016). Development and application of approaches that facilitate somatic gene transfer of "CRISPR nucleases" to target candidate tumor suppressor genes in the murine brain Ruperto-Carola University of Heidelberg].

Zuckermann, M., Hovestadt, V., Knobbe-Thomsen, C. B., Zapatka, M., Northcott, P. A., Schramm, K., Belic, J., Jones, D. T., Tschida, B., Moriarity, B., Largaespada, D., Roussel, M. F., Korshunov, A., Reifenberger, G., Pfister, S. M., Lichter, P., Kawauchi, D., & Gronych, J. (2015). Somatic CRISPR/Cas9-mediated tumour suppressor disruption enables versatile brain tumour modelling. *Nat Commun*, *6*, 7391. https://doi.org/10.1038/ncomms8391